



UNIVERSITAT
POLITÈCNICA
DE VALÈNCIA

Departamento de Máquinas y Motores Térmicos

DOCTORAL THESIS:

**“Synthesis of the 1D modelling of
turbochargers and its effects on
engine performance prediction”**

Presented by: MR. ARTEM DOMBROVSKY
Supervised by: DR. FRANCISCO JOSÉ ARNAU MARTÍNEZ

in fulfillment of the requisites for the degree of

Doctor of Philosophy

Valencia, April 2017

PhD. Thesis

“Synthesis of the 1D modelling of turbochargers and its effects on engine performance prediction”

AUTHORS

Presented by: MR. ARTEM DOMBROVSKY

Supervised by: DR. FRANCISCO JOSÉ ARNAU MARTÍNEZ

DEFENSE COMMITTEE

Chairman: DR. JOSÉ MANUEL LUJÁN MARTÍNEZ

Secretary: DR. OCTAVIO ARMAS VERGEL

Member: DR. SAM AKEHURST

Valencia, April 2017

Synthesis of the 1D modelling of turbochargers and its effects on engine performance prediction

Artem Dombrovsky

Abstract

Low fuel consumption is one of the main requirements for current internal combustion engines for passenger car applications. One of the most used strategies to achieve this goal is to use downsized engines (smaller engines while maintaining power) which implies the usage of turbochargers. The coupling between both machines (the turbocharger and the internal combustion engines) presents many difficulties due to the different nature between turbomachines and reciprocating machines. These difficulties make the optimal design of the turbocharged internal combustion engines a complicated issue.

In this thesis a strong effort has been made to improve the global understanding of different physical phenomena occurring in turbochargers and in turbocharged engines. The work has been focused on the 1D modelling of the phenomena since 1D tools currently play a major role in the engine design process. Both experimental and modelling efforts have been made to understand the heat transfer and gas flow processes in turbochargers. Previously to the experimental analysis a literature review has been made in which the state of the art of heat transfer and gas flow modelling in turbochargers have been analysed.

The experimental effort of the thesis has been focused on measuring different turbochargers in the gas stand and the engine test bench. In the first case, the gas stand, a more controlled environment, has been used to perform tests at different conditions. Hot tests with insulated and not insulated turbochargers have been made to characterise the external heat transfer. Moreover, adiabatic tests have been made to compare the effect of the heat transfer on different turbocharger variables and for the validation of the turbine gas flow models. In the engine test bench full and partial load tests have been made for model validation purposes.

For the models development task, the work has been divided in heat flow models and gas flow models. In the first case, a general heat transfer model for turbochargers has been proposed based on the measured turbochargers and data available from previous works of the literature. This model includes a procedure of conductive conductances estimation, internal and external convection correlations and radiation estimation procedure. In the case of the gas flow modelling, an extended model for VGT performance maps extrapolation for both the efficiency and the mass flow has been developed as well as a model for discharge coefficient prediction in valves for two stage turbochargers.

Finally, the models have been fully validated coupling them with a 1D modelling software simulating both the gas stand and the whole engine. On the one hand, the results of the validation show that compressor and turbine outlet temperature prediction is highly improved using the developed models. This result proves that the turbocharger heat transfer phenomena are important not only for partial load and transient simulation but also in full loads. On the other hand, the VGT extrapolation model accuracy is high even at off-design conditions.

Resumen

El bajo consumo de combustible es uno de los principales requerimientos de los motores de combustión interna actuales para aplicaciones de coches de pasajeros. Una de las estrategias más usadas para conseguir ese fin es el uso de motores "*downsized*" (motores más pequeños con la misma potencia) lo que implica el uso de turbocompresores. El acoplamiento entre ambas máquinas (el turbocompresor y el motor de combustión alternativo) presenta muchas dificultades debido a la diferente naturaleza entre las turbomáquinas y las máquinas alternativas. Estas dificultades convierten el diseño óptimo de los motores de combustión interna sobrealimentados en un asunto complicado.

En esta tesis se ha realizado un importante esfuerzo para mejorar el entendimiento global de los diferentes fenómenos físicos que ocurren en los turbocompresores y en los motores sobrealimentados. El trabajo se ha centrado en el modelado 1D de los fenómenos puesto que las herramientas 1D juegan actualmente un papel principal en el proceso de diseño del motor. Se han realizado tanto esfuerzos experimentales como de modelado para el entendimiento de los procesos de transmisión de calor y de flujo de gases en turbocompresores. Previamente al análisis experimental se ha realizado una revisión de la literatura disponible en la que se ha analizado el estado del arte del modelado de transmisión de calor y flujo de gases en turbocompresores.

El esfuerzo experimental de la tesis se ha centrado en la medida de diferentes turbocompresores en el banco de gas y en el banco motor. En el primer caso, se ha utilizado el banco de gas, un ambiente más controlado, para realizar ensayos en diferentes condiciones. Se han realizado ensayos calientes con y sin aislamiento del turbocompresor para caracterizar el flujo de calor externo. Además, se han realizado ensayos adiabáticos para comparar el efecto de la transmisión de calor sobre diferentes variables del turbocompresor y para la validación de los modelos de flujo de gases de la turbina. En el banco motor se han realizado ensayos a plena carga y a cargas parciales para usarlos en la validación.

Para la tarea del desarrollo de los modelos, el trabajo se dividió en modelos de flujo de calor y modelos de flujo de gases. En el primer caso, se ha propuesto un modelo general de transmisión de calor para turbocompresores basado en los turbocompresores medidos y en datos disponibles de trabajos previos de la literatura. Este modelo incluye un procedimiento para la estimación de las conductancias conductivas, correlaciones de convección interna y externa y un procedimiento de estimación de la radiación. En el caso del modelado de flujo de gases, se ha desarrollado un modelo extendido para la extrapolación de mapas de funcionamiento de TGV tanto para el rendimiento como para el gasto másico además del modelo de predicción de coeficientes de descarga en válvulas de turbocompresores de doble etapa.

Finalmente, los modelos han sido completamente validados con su acoplamiento a un software de modelado 1D simulando tanto el banco de

turbos como el motor completo. Por un lado, los resultados de la validación señalan que la predicción de las temperaturas de salida de compresor y turbina mejora notablemente usando los modelos desarrollados. Este resultado demuestra que los fenómenos de transmisión de calor son importantes no sólo en simulaciones de cargas parciales y de transitorios sino también en plenas cargas. Por otro lado, la precisión del modelo de extrapolación de TGV es alta incluso en condiciones fuera de diseño.

Resum

El baix consum de combustible és un dels principals requeriments dels motors de combustió interna actuals per a aplicacions de cotxes de passatgers. Una de les estratègies més usades per a aconseguir eixe fi és l'ús de motors "*downsized*" (motors més xicotets amb la mateixa potència) el que implica l'ús de turbocompressors. L'adaptament entre ambdues màquines (el turbocompressor i el motor de combustió alternatiu) presenta moltes dificultats degut a la diferent naturalesa entre les turbomàquines i les màquines alternatives. Estes dificultats convertixen el disseny òptim dels motors de combustió interna sobrealimentats en un assumpte complicat.

En esta tesi s'ha realitzat un important esforç per a millorar l'enteniment global dels diferents fenòmens físics que ocorren en els turbocompressors i en els motors sobrealimentats. El treball s'ha centrat en el modelatge 1D dels fenòmens ja que les ferramentes 1D juguen actualment un paper principal en el procés de disseny del motor. S'han realitzat tant esforços experimentals com de modelatge per a l'enteniment dels processos de transmissió de calor i de flux de gasos en turbocompressors. Prèviament a l'anàlisi experimental s'ha realitzat una revisió de la literatura disponible en què s'ha analitzat l'estat de l'art del modelatge de transmissió de calor i flux de gasos en turbocompressors.

L'esforç experimental de la tesi s'ha centrat en la mesura de diferents turbocompressors en el banc de gas i en el banc motor. En el primer cas, s'ha utilitzat el banc de gas, un ambient més controlat, per a realitzar assajos en diferents condicions. S'han realitzat assajos calents amb i sense aïllament del turbocompressor per a caracteritzar el flux de calor extern. A més, s'han realitzat assajos adiabàtics per a comparar l'efecte de la transmissió de calor sobre diferents variables del turbocompressor i per a la validació dels models de flux de gasos de la turbina. En el banc motor s'han realitzat assajos a plena càrrega i a càrregues parcials per a usar-los en la validació.

Per a la tasca del desenvolupament dels models, el treball es va dividir en models de flux de calor i models de flux de gasos. En el primer cas, s'ha proposat un model general de transmissió de calor per a turbocompressors basat en els turbocompressors mesurats i en dades disponibles de treballs previs de la literatura. Este model inclou un procediment per a l'estimació de les conductàncies conductives, correlacions de convecció interna i externa i un procediment d'estimació de la radiació. En el cas del modelatge de flux de gasos, s'ha desenvolupat un model estés per a l'extrapolació de mapes de funcionament de TGV tant per al rendiment com per al gasto màssic a més del model de predicció de coeficients de descàrrega en vàlvules de turbocompressors de doble etapa.

Finalment, els models han sigut completament validats amb el seu adaptament a un software de modelatge 1D simulant tant el banc de turbos com el motor complet. D'una banda, els resultats de la validació assenyalen que la predicció de les temperatures d'eixida de compressor i turbina millora notablement usant els models desenrotllats. Este resultat

demostra que els fenòmens de transmissió de calor són importants no sols en simulacions de càrregues parcials i de transitoris sinó també en plenes càrregues. D'altra banda, la precisió del model d'extrapolació de TGV és alta inclús en condicions fora de disseny.

List of publications

The following papers form the basis of this thesis:

- “External heat losses in small turbochargers: Model and experiments” by Payri, Olmeda, Arnau, Dombrovsky, and Smith [1].
- “Analysis and Methodology to Characterize Heat Transfer Phenomena in Automotive Turbochargers” by Serrano, Olmeda, Arnau, Dombrovsky, and Smith [2].
- “Methodology to Characterize Heat Transfer Phenomena in Small Automotive Turbochargers: Experiments and Modelling Based Analysis” by Serrano, Olmeda, Arnau, Dombrovsky, and Smith [3].
- “Turbocharger heat transfer and mechanical losses influence in predicting engines performance by using one-dimensional simulation codes” by Serrano, Olmeda, Arnau, Dombrovsky, and Smith [4].
- “Development and validation of a radial turbine efficiency and mass flow model at design and off-design conditions” by Serrano, Arnau, García-Cuevas, Dombrovsky, and Tartoussi [5].
- “General Procedure for the Determination of Heat Transfer Properties in Small Automotive Turbochargers” by Serrano, Olmeda, Arnau, and Dombrovsky [6].
- “A comprehensive experimental procedure for turbochargers performance characterization” by Desantes, Galindo, Serrano, and Dombrovsky [7].

Division of work between authors

These publications have been done in collaboration with other researchers, being the authors’ signatures in order of seniority. The respondent performed the experimental measurements, models setup and results post-processing. Methodologies, models development and results discussions were done in collaboration with the rest of co-authors.

Other publications

The following is a list of other publications in which the author of this thesis has been involved during the research leading to the present work. Although not directly present in this document, they have provided a deeper insight in the behaviour of automotive turbochargers.

-
- “Development of a high temperature turbocharger for heavy duty applications” by Sullivan, Brown, Eastwood, Green, Dombrovsky, and Arnau [8].

Acknowledgements

First of all I would like to thank all the members of CMT-Motores Térmicos for providing me the tools and the environment to complete this work. This acknowledgement extends to all the students, technicians, researchers, professor and administration staff. I dedicate a special mention to the supervisor of this work, Dr. Francisco Arnau, for his help and insight into the most difficult topics of this work. I also would like to thank Prof. José Ramón Serrano for his continuous guidance throughout these years. I have learned a lot from him. I would also express my gratitude to Dr. Pablo Olmeda for his good advice and his help. My gratitude also goes to the technicians Valentín Ucedo, Miguel Ortiz and Jose "the lathe man" for their great job in test bench assembling and testing. The goodness of the experimental results is all their merit. I would also like to thank all the master students that contributed to keep this work going: Vincenzo, Quentin, Valentin, Adrián, Julian, Arnau, Álex, Luis Domingo, Davide, Diego, Pau and Jesús Mario. Specially I express my gratitude to Luis Miguel for his constant and unconditional computing assistance and to Miguel Reyes for his help during my first steps in the department. I would also want to thank my officemates Lele, Javi, Enrique, Lukas and Ricardo for creating an excellent working atmosphere.

Eventually, I would like to thank my parents and my brother for being there my whole life. It would have been impossible to accomplish the work without their support. I also feel indebted to my old friends Sergio, Guille, Pablo and Juanma and the new ones Julián, Pablo and Dani for tolerating my continuous weird thoughts.

And of course, I owe a lot to my partner, Maggie, who helped me to discover myself and be the best version of myself.

Contents

Contents	xi
List of Figures	xiii
List of Tables	xviii
Nomenclature	xix
1 Introduction	1
1.1 Motivations	2
1.2 Objectives	6
1.3 Methodology	6
1.4 References	10
2 Bibliographical Survey	13
2.1 Introduction	15
2.2 Heat transfer modelling in turbochargers	15
2.3 Turbine maps extrapolation methods	32
2.4 Waste-Gate Discharge coefficient characterisation	35
2.5 References	38
3 Experimental Analysis	49
3.1 Introduction	51
3.2 Themohydraulic test bench	52
3.3 Gas stand	55
3.4 Engine test bench	77
3.5 References	84
4 Theoretical development of turbocharger model	87
4.1 Introduction	89
4.2 Heat flow models	89
4.3 Gas flow models	113
4.4 References	131

5	Models Validation	135
5.1	Introduction	138
5.2	Experimental analysis and validation	138
5.3	Model validation in gas stand conditions	150
5.4	Model validation in engine conditions	156
5.5	References	186
6	Conclusions and Future Works	189
6.1	Introduction	190
6.2	Main contributions	190
6.3	Future works	194
6.4	References	195
	Bibliography	197

List of Figures

1.1	Number of registered vehicles worldwide	2
1.2	Comparison of altitude effect on bmep between naturally aspirated and turbocharged engines	3
1.3	Outline of the dissertation	9
2.1	Turbine casing: inner and outer wall temperature difference in three different locations [37]	17
2.2	Compressor isentropic efficiency with different turbine inlet temperatures and rotational speeds [39]	17
2.3	(a) Compressor enthalpy-entropy chart (b) Turbine enthalpy-entropy chart	20
2.4	Compression and expansion process according to [44]	21
2.5	Compressor performance map with differences between adiabatic and diabatic compressor efficiency [50]	23
2.6	Heat correction factor for compressor efficiency [50]	24
2.7	Resistances for turbocharger heat transfer model [63]	26
2.8	Temperature and mass flow effects on the time constant τ [74]	28
2.9	Temperature gradients in the turbine wheel [78]	29
2.10	Steady state CHT calculations at full load: external and internal surface temperatures [81]	30
2.11	Turbine heat divided by turbine mechanical power on an engine operation map [19]	31
2.12	Compressor efficiency compared to model efficiency for different assumed percentages of heat transfer before compression [85]	32
2.13	Unsteady turbine model with six rotor entries [103]	35
2.14	Schematic of a regulated two stage turbocharging system [109]	36
2.15	Effect of the obstacle disturbance on the discharge coefficient [113]	37
3.1	Turbocharger geometry simplification	52
3.2	Thermohydraulic test bench layout	54
3.3	Gas stand layout	56
3.4	Gas stand layout	57
3.5	Detail of wall thermocouple installation	60
3.6	Wall thermocouples installed on a turbocharger	61
3.7	Two stage turbocharging system installed in the test bench.	63
3.8	Measured and interpolated mass flow on LPT map	65
3.9	Schematic of thermocouples installation and fluids distribution in the LPC	67
3.10	Location of the drills for thermocouples installation in LPC volute	68

LIST OF FIGURES

3.11	Measured points for convection correlations characterization	69
3.12	Comparison of pressure ratio measured at hot insulated conditions versus measurements at adiabatic conditions. Turbocharger without water cooling (T#2)	71
3.13	Comparison of compressor efficiency measured at hot insulated conditions versus efficiency measured at adiabatic conditions. Water-cooled turbocharger (T#1)	72
3.14	Comparison of compressor efficiency measured at hot insulated conditions versus efficiency measured at adiabatic conditions. Non water-cooled turbocharger (T#2)	73
3.15	Comparison of hot insulated measurements of turbine mass flow with adiabatic measurements (T#2)	74
3.16	Comparison of hot insulated measured TDE with adiabatic measurements (T#2)	75
3.17	Comparison of hot insulated measured ETE with adiabatic measurements (T#2)	76
3.18	Comparison of hot insulated measured ETE/TDE with adiabatic measurements (T#2)	76
3.19	Layout of the engine test cell	78
3.20	Flow coefficients of the intake and exhaust valves	81
3.21	RoHR during acceleration for T#1 (left) and T#2 (right)	82
3.22	In-cylinder conditions at EVO for T#1 (left) and T#2 (right)	82
3.23	Engine torque at steady conditions. Left: T#1, Right: T#2	83
3.24	Compressor outlet conditions. Left: T#1, Right: T#2	83
3.25	Turbine inlet conditions. Left: T#1, Right: T#2	84
3.26	Turbocharger speed. Left: T#1, Right: T#2	84
4.1	Lumped heat transfer model	90
4.2	GAS/T fitting	92
4.3	H ₂ /O fitting	92
4.4	H ₂ /W fitting	93
4.5	$Nu_{C/W}$ modelling results	95
4.6	$Q_{C/W}$ modelling results	95
4.7	Schematic of sensors location on the compressor	96
4.8	Thermal network of the cooled compressor	97
4.9	$Q_{C/AIR}$ modelling results	97
4.10	Simplification of turbocharger geometry	99
4.11	Capacitance fitting for each turbocharger	110
4.12	Nodes equivalent width	111
4.13	Conductive conductances fitting for each turbocharger	112

4.14	(a) Reduction of a radial turbine to an equivalent nozzle and stations distribution. (b) Measured ratio of pressure drop in the rotor to total pressure drop in the turbine ('d') in the VGT map [27] of T#6	114
4.15	(a) Geometrical relations of a VGT stator vanes (b) Linear relations between stator vanes angle and VGT opening	115
4.16	Reduced mass flow coefficients dependence with VGT position (a, c and e) and final fitted coefficients (b, d and f)	120
4.17	Difference between fitted and geometrical z_3^{geom} coefficient (a) and modelled 'z' versus fitted 'z' (b)	123
4.18	Procedure for mass flow parameter and efficiency extrapolation . . .	125
4.19	Real mass flow against theoretical mass flow for by-pass valve	127
4.20	Average C_D versus average by-pass valve polynomial fitting	128
4.21	Modelled by-pass valve mass flow against theoretical mass flow . . .	128
4.22	Averaged waste-gate valve C_D against by-pass valve position	129
4.23	Modelled discharge coefficient of the waste-gate valve	130
4.24	Modelled waste-gate valve mass flow against theoretical mass flow .	130
5.1	Comparison between measured external heat transfers and model prediction	139
5.2	Difference, in dimensionless form, between measured external heat transfer and model results	140
5.3	Comparison between external heat transfers: adjusted external model and unbalance method	141
5.4	Comparison between external heat transfers: adjusted external model and unbalance method in engine	141
5.5	Importance of modelled external heat fluxes compared to turbine enthalpy drop	142
5.6	Analysis of modelled external heat transfer in turbine side	143
5.7	Analysis of modeled external heat transfer in compressor side	144
5.8	Fitted equivalent area and reduced mass flow for T#1 (a) and for T#2 (b) and measured versus modelled A_{Neq} (c)	146
5.9	Root mean square error of efficiency fitting for the different turbochargers	147
5.10	Efficiency extrapolation in blade to jet speed ratio for different VGT positions of T#6, T#1 and T#2 (dots correspond to experimental data and solid lines to model results)	148
5.11	Reduced mass flow rate extrapolation results where extreme rotational speeds were fully extrapolated (dots correspond to experimental data and solid lines to model results)	149
5.12	Efficiency extrapolation results for T#6 checking model capabilities at high blade to jet speed ratio (dots correspond to experimental data and solid lines to model results)	150

LIST OF FIGURES

5.13	Modelling procedure	151
5.14	GT-POWER™ model of turbocharger test bench	152
5.15	Turbine (a) and compressor (b) outlet temperatures for T#2	153
5.16	Turbine (a) and compressor (b) outlet temperatures for T#1	154
5.17	Turbine (a) and compressor (b) outlet temperatures for T#1 using re-elaborated correlations	155
5.18	Transient evolution compressor and turbine outlet temperatures for T#1	155
5.19	Engine Model in GT-POWER™	157
5.20	In-cylinder pressure and temperature for T#1 at 2500 rpm and full load (2.0 litres engine)	157
5.21	In-cylinder pressure and temperature at EVO for T#1 (2.0 litres engine)	158
5.22	Engine variables T#1. Actual 2.0 litres engine	159
5.23	Engine variables T#2. Emulated 1.6 litres engine	159
5.24	T#1 Compressor pressure ratio and temperature increment	160
5.25	T#2 Compressor pressure ratio and temperature increment	160
5.26	T#1 Turbine pressure ratio and temperature drop	162
5.27	T#2 Turbine pressure ratio and temperature drop	162
5.28	T#1 and T#2 turbocharger speed	164
5.29	T#1 and T#2 compressor efficiency	165
5.30	T#1 and T#2 turbine efficiency	166
5.31	T#1 and T#2 turbocharger efficiency	167
5.32	T#1 and T#2 heat power balance	168
5.33	T#1 and T#2 mechanical power balance	169
5.34	Modelled against measured torque for T#1 and T#2	172
5.35	Modelled against measured air mass flow for T#1 and T#2	173
5.36	Compressor pressure ratio and temperature increment for T#1	175
5.37	Compressor pressure ratio and temperature increment for T#2	176
5.38	Turbine pressure ratio and temperature drop for T#1	177
5.39	Turbine pressure ratio and temperature drop for T#2	178
5.40	Turbocharger speed for T#1 and T#2	179
5.41	Nodes temperatures for T#1	180
5.42	Nodes temperatures for T#2	180
5.43	Correlation between engine VGT position signal and real VGT dis- placement	181
5.44	Torque during tip in and tip out tests for T#1 at 1500 rpm	183
5.45	Torque during tip in and tip out tests for T#2 at 1000 rpm	183
5.46	Air mass during tip in and tip out tests for T#1 at 2000 rpm	184
5.47	Air mass during tip in and tip out tests for T#2 at 1600 rpm	184
5.48	Compressor outlet temperature during tip in and tip out tests for T#1 at 1500 rpm	185

5.49 Compressor outlet temperature during tip in and tip out tests for
T#2 at 1600 rpm 185

5.50 Turbine outlet temperature during tip in and tip out tests for T#1 at
1250 rpm 186

5.51 Turbine outlet temperature during tip in and tip out tests for T#2 at
2400 rpm 186

List of Tables

3.1	Turbochargers characteristics (a sketch of geometrical acronyms is shown in Figure 3.1)	53
3.2	Accuracies of measurement sensors	56
3.3	Temperature differences in adiabatic tests	62
3.4	Test campaign for valves characterisation at full load points	64
3.5	Test campaign for valves characterisation outside of full load points .	65
3.6	Geometrical area of the fully open valves (in mm ²)	66
3.7	Water correlation test campaign	70
3.8	Main characteristics of the employed engine	79
4.1	View factor equations	104
4.2	View factor equations	105
4.3	Turbocharger material data	108
4.4	Capacitance fitting constants values	110
4.5	Coefficient 'a' values	119
4.6	Efficiency coefficients average and standard deviation	124
5.1	Emissivity values for turbocharger zones	139

Nomenclature

\dot{h}	Specific enthalpy flow	K	Conductance
\dot{m}	Mass flow rate	K	Efficiency equation coefficient
\dot{m}_{red}	Reduced mass flow rate	K	Turbocharger speed constant
\dot{Q}	Heat flux	L	Length
\dot{W}'	Mechanical and heat power	N	Turbocharger speed
\dot{W}	Power	n	Number of measurements
A	Area	n	Rotational speed
a	Rotor discharge coefficient	n_b	Number of blades
b	Reduced mass flow fitting coefficient	n_{red}	Reduced rotational speed
C	Capacitance	p	Pressure
c	Reduced mass flow fitting coefficient	R	Perfect gas constant
C_D	Discharge coefficient	r	Radius
c_p	Specific heat capacity at constant pressure	s	Specific entropy
c_{ss}	Isentropic jet velocity	sd	Standard deviation
D	Diameter	sp	Spacing between stator blades
d	Reduced mass flow fitting coefficient	T	Temperature
h	Convective coefficient	t	Blades and/or channel width
		u	Blade tip speed
		u	Standard deviation

LIST OF TABLES

v	Absolute velocity	Δ	Increment or drop
w	Relative velocity	δ	Angle between consecutive stator blades
F	View factor	ϵ	Emissivity
Gr	Grasshof number	η	Efficiency
Nu	Nusselt number	γ	Specific heat capacities ratio
Pr	Prandtl number	κ	Conductivity
Ra	Rayleigh number	μ	dynamic viscosity
Re	Reynolds number	ν	Kinematic viscosity
BSFC	Brake specific fuel consumption	ϕ	Diameter
CFD	Computational fluid dynamics	Π	Pressure ratio
COT	Compressor outlet temperature	ρ	Density
ECU	Engine control unit	σ	Blade to jet speed ratio
EGR	Exhaust gas recirculation	σ	Steffan-Boltzman constant
ETE	Effective turbine efficiency	θ	Tangential velocity component
EVO	Exhaust valve opening	φ	Angle of the stator vanes
FGT	Fixed geometry turbine	Overbar and others	
ICE	Internal combustion engine	-	Average value
LUM	Look up map model	*	Reduced or corrected quantity
TOT	Turbine outlet temperature	Subscripts	
VGT	Variable geometry turbine	0	Turbine inlet station
Greek Symbols		1	Stator inlet station
α	Absolute velocity angle	2	Stator outlet station
α	Percentage	2'	Stator throat station
β	Relative velocity angle		

<i>2a</i>	Stator vanes axis of rotation station	<i>Neq</i>	Refers to equivalent nozzle
<i>3</i>	Rotor inlet station	<i>oil</i>	Oil
<i>4</i>	Rotor outlet station	<i>r</i>	Refers to radiation
<i>a, adiab.</i>	Adiabatic conditions	<i>red</i>	Refers to reduced variables
<i>air</i>	Air	<i>s</i>	Isentropic conditions and Stator
<i>amb</i>	Refers to ambient	<i>s</i>	Shield
<i>C</i>	Compressor node	<i>T</i>	Refers to turbine
<i>c</i>	Refers to compressor	<i>t</i>	Total conditions
<i>CF</i>	Forced convection	<i>TE</i>	Distance between stator blades axis of rotation and trailing edge
<i>CN</i>	Natural / Free convection	<i>TG</i>	Refers to turbocharger
<i>diab.</i>	Diabatic conditions	<i>th</i>	Refers to throat
<i>eff</i>	Effective	<i>ts</i>	Total to static
<i>ext</i>	Refers to external surface	<i>unb</i>	Unbalance
<i>gas</i>	Gas	<i>W</i>	Water node
<i>geom</i>	Refers to geometry	<i>w</i>	Refers to wall temperature
<i>H</i>	Refers to housing		
<i>H1</i>	Refers to housing node close to turbine		
<i>H2</i>	Refers to central housing node		
<i>H3</i>	Refers to housing node close to compressor		
<i>i, j, k, n</i>	Generic element		
<i>lat</i>	Refers to lateral surface		
<i>mech</i>	Refers to mechanical losses		
<i>metal</i>	Refers to metal angle		

Introduction

Contents

1.1	Motivations	2
1.2	Objectives	6
1.3	Methodology	6
1.4	References	10

Figures

1.1	Number of registered vehicles worldwide	2
1.2	Comparison of altitude effect on bmep between naturally aspirated and turbocharged engines	3
1.3	Outline of the dissertation	9

1.1 Motivations

The first patent of an internal combustion engine (ICE) dates from 1876 [9]. After more than a century it is still the main source of propulsion for transportation worldwide. The number of vehicles in developed countries is growing [10] as it is shown in Figure 1.1. In some developed countries, as the United States, there are 797 motor vehicles per one thousand people. In business terms, ICE top six manufacturers had a global revenue of 1067 USD billions in 2014. Furthermore, the vehicle industry has a prominent position in worldwide economy with many interactions between manufacturers, governments, suppliers and clients [11]. Consequently, it is justified in modern societies to devote time and resources to the development and improvement of ICE technology and the good use of it, facing environmental and social problems that arise from car usage. It is even more justified if it is considered that this technology will still be in use while new alternatives like electric vehicles are under development [12].

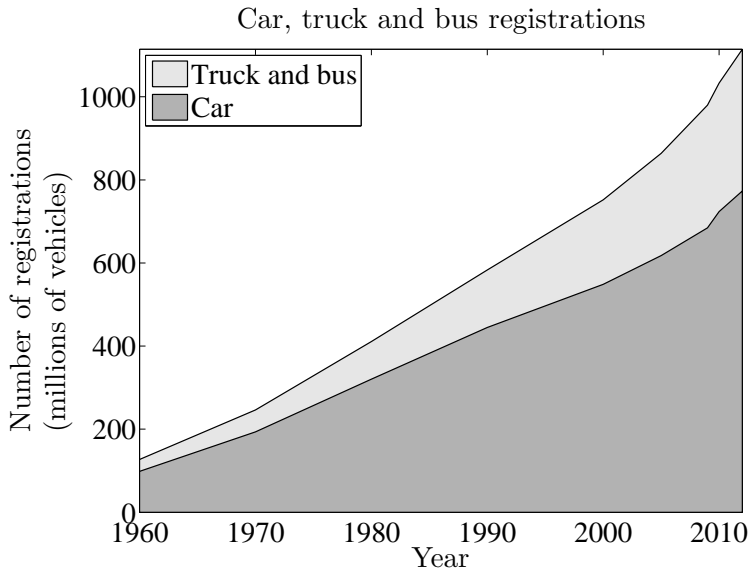


Figure 1.1: Number of registered vehicles worldwide

New concepts have appeared throughout the years to increase the power and the efficiency of the ICE. One of this concepts is turbocharging. The coupling of a turbocharger to the engine provides an effective way to increase output power by increasing air density inside the cylinder. Equation 1.1 in which four-stroke engine effective power is shown depicts that solution. Among the variables appearing in Equation 1.1 the air density can be easily increased by using a turbocharger or a supercharger. The difference between these two devices lies in

the fact that the energy used to drive the compressor that increases air density at the intake comes from different sources. In the case of the turbocharger it comes from a turbine that extracts energy from engine exhaust gases and in the case of the supercharger the power to move the compressor is extracted from engine crankshaft.

$$P = \frac{\eta_{vol}\rho_a V_{sw} N \eta_f Q_f}{2} \left(\frac{1}{AFR} \right) \quad (1.1)$$

The first use of turbocharging in an ICE appeared in 1917 for aviation engines so, in the same way as for ICE technology, the idea of turbocharging is not novel. As it can be observed in Figure 1.2 engine bmep and thus effective power decrease as altitude increases due to lower density. For that reason, early aviation engines required means to increase effective power. By using a turbocharger it is possible to increase the power and fly at a higher service ceiling with the same power as naturally aspirated engine as shown by the grey curve in Figure 1.2. One of the first uses of turbocharging for ground transport was on truck engines as more power and torque are required for that application. Truck and heavy duty engines manufacturers started using turbocharging around 1954 and its use continues today, improving the performance of both the ICE and the turbocharger [13].

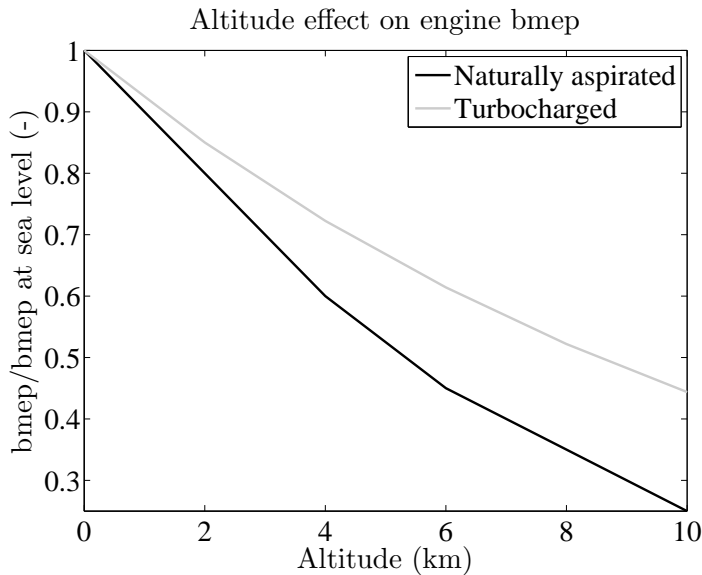


Figure 1.2: Comparison of altitude effect on bmep between naturally aspirated and turbocharged engines

In the last years, strict emissions regulations impulsed ICE design in a different direction where pollutants reduction became the main design issue. ICE application on passenger cars suffered the most severe restrictions as their pollution affects heavily inhabited zones. The strict European regulation [14] concerning passenger car emissions is a proof of this trend. Moreover, energy usage had become an important issue worldwide promoting energy harvesting and saving technologies [15]. Related with that an increased engine efficiency can contribute to energy waste reduction and consequently to fuel savings. This fact can help to extend the time available for finding alternative solutions to fossil fuels. In this global framework ICE manufacturers for passenger car applications devote more resources to engine research and design improvement focusing on these two problems.

One of the main techniques to reduce carbon dioxide emissions and reduce fuel consumption is using downsized engines. An important effort from both industry and engine research facilities is focused on this solution, proved by global projects like the one developed in [16]. In the last years downsizing has been heavily used in passenger car engines. Downsizing consist in the reduction of engine swept volume keeping the same power as the higher volume engine i.e increasing engine specific power. The power increment needed to match the smaller volume engine power to the bigger engine is achieved by means of turbocharging. The advantage of this approach is the effective efficiency increment compared to a naturally aspirated engine of higher volume. As the efficiency is higher, the emissions of carbon dioxide are lower as both are directly related by the combustion process. In Equation 1.2 the expression for effective engine efficiency is provided. For a given indicated power, indicated efficiency is the same in both the naturally aspirated and the turbocharged engines. However, a much higher bmep will be achieved in the turbocharged engine for the same power due to higher cylinder pressures. Nevertheless, the sum of terms pmep + fmep + amep will not suffer a considerable increase. The mean effective pressure of auxiliary systems (amep) is similar in both engines as exhaust gas turbocharging is used, so no power is extracted from the crankshaft. Pumping losses mean effective pressure (pmep) can increase in the case of a turbocharged engine but not to a high extent as the back-pressure due to the turbine is compensated by the higher pressure at the intake provided by the compressor. Friction mean effective pressure (fmep) may slightly increase in turbocharged engine due to the larger dimension of bearings because of the increased cylinder pressure. However, as this increment is much lower than the bmep increment, the turbocharged engine efficiency will be higher according to Equation 1.2.

$$\eta_e = \eta_i \cdot \eta_m = \eta_i \cdot \frac{\text{bmep}}{\text{bmep} + \text{pmep} + \text{fmep} + \text{amep}} \quad (1.2)$$

In this framework, turbocharging has become a key technology for this application as it is one of the best ways of achieving same effective power in the downsized engine. However, the coupling between the ICE and the turbocharger presents several difficulties [17]. The problem is inherent to the way in which each machine works. While an ICE is an alternative machine that works with pulsating flow, a turbocharger is a continuous flow machine. Several studies as the one presented in [18] show the effects of pulsating flow on turbocharger behaviour. Other aspects of the modelling of turbocharger and engine coupling like heat transfer [19] or partial admission [20] are at high discussion in nowadays research as it can be deduced from the recent papers published about these issues.

Engine research has usually been focused in two complementary aspects: experimentation and modelling. While experiments in engine test rigs provide a way of measuring variables in real conditions, modelling provides a tool for the prediction of engine behaviour, reducing additional experimental costs. Both approaches are used in a combined way since modelling requires experimental data for validation and calibration while experimentation benefits from modelling due to the reduction of the number of tests. In ICE modelling field 1D modelling tools are widely used in industry and research [21]. In these tools fluid dynamics equations are simplified to a one-dimensional case using different discretization schemes to compute gas properties in the different cells. That way flow items like pipes can be calculated. The processes occurring in other engine systems like the combustion in a cylinder are calculated based on experimental information.

The research in this field is focused mainly on the independent modelling of the turbocharger or the engine. Little research has been done concerning the effects of turbocharging modelling on engine performance modelling. This probably occurs due to the fact that generally engine manufacturers and turbocharger manufacturers are different companies and the communication of important information is uncommon between them. However, advanced turbocharger modelling is an important tool to improve ICE design in order to fulfil current emission regulation and engine performance goals. The effect of the different turbocharger models like the heat transfer model on engine performance modelling must be analysed to characterise the real impact on predictions.

At CMT-Motores Térmicos of Universitat Politècnica de València several dissertations have been performed concerning turbocharging models and experimentation. The thesis of Tiseira [22] deals with compressor surge problem from both modelling and experimental points of view. Cervelló [23] developed a testing methodology for turbochargers that have been extensively used afterwards. Fajardo [24] centred his studies on a 3D modelling of turbocharger turbines. Using a similar approach, Navarro [25] studied compressor acoustic

problem. Reyes-Belmonte [26] centred his efforts on improving and developing a methodology to account heat transfer in turbochargers. Finally, García-Cuevas [27] developed an improved model for turbine simulation using a quasi 2D approach. In this framework, the current dissertation provides an improvement of some of the models previously developed focusing mainly on the models that can enhance engine simulation using commercial 1D tools like GT-POWER™. Moreover, as it has been stated previously, the effect of these turbocharger models on whole-engine models is studied in depth.

1.2 Objectives

The main objective of this PhD dissertation is to offer a global approach to turbocharger advanced modelling and show its impact on engine performance prediction when using a 1D whole engine model. Several tasks must be performed prior to accomplishing the main objective. These tasks correspond to a generalisation of turbocharger 1D submodels and are listed below:

- Experimental analysis of the variables affected by heat transfer phenomena in turbochargers in both the gas stand and the engine test bench.
- Development of a general methodology to characterise heat transfer phenomena in turbochargers taking into account convective, conductive and radiative heat transfer modes.
- Development of a map extrapolation tool for VGTs and fixed geometry turbines for both the reduced mass flow and the total to static efficiency.
- Development of a methodology to characterise wastegate discharge coefficient for fixed geometry turbines.
- Integration of turbocharger submodels into a whole engine model for validation.

After the fulfilment of these tasks the main objective can be achieved. This will be done by studying the effect of turbocharger modelling on a whole engine model performance predictions at different engine operating conditions. Full loads, partial loads and tip in and tip out cases will be discussed separately and compared to experimental results performed in an engine test bench.

1.3 Methodology

In this dissertation a refined approach regarding turbocharger 1D modelling that considers the effect on whole engine models was developed starting from

previous works. For that purpose, several turbocharger modelling problems have been studied providing a clear methodology for accounting different aspects like heat transfer, map extrapolation and wastegate discharge coefficient calculation. The validation of the different models has been done using experimental data from both the gas stand and the engine test bench. This approach results in the work being divided into two complementary parts, in the same way as it is done in engine design process.

Focusing on the objectives of the dissertation, the experimental part is conceived as a way to provide valuable inputs to build the models. Moreover, it will give insight into the turbocharger parameters that are strongly affected by different phenomena like heat transfer. In that way, the experimental work has been divided in heat transfer characterisation, discharge coefficient measurement in wastegated turbines and adiabatic map characterization for turbine map extrapolation tools. A deep analysis of the obtained results has also been performed in the different experimental parts.

For heat transfer characterisation, several testing methodologies have been used in order to isolate the different heat transfer modes so they can be studied independently. Conductive heat transfer has been characterised in the thermohydraulic test bench before the tests in the gas stand, using the methodology described in [28]. Turbocharger wall temperature measurements are necessary and were redundantly measured. Gas stand offers the most controlled environment for turbochargers testing, what makes possible the development of models from reliable data. Different heat transfer paths in the turbocharger were measured using the turbocharger itself as a heat transfer sensor since the conductive conductances have been characterised in the thermohydraulic bench. However, actual turbocharger operating conditions at higher temperatures are better reproduced in an engine test bench. For that reason, engine test bench experimental results have been analysed and used for validation in the thesis. External and internal heat transfer were distinguished in order to build an external heat transfer model in this work.

The adjusted and validated external heat transfer model has been used to perform an analysis of the different heat flows, showing that the most important external heat fluxes come from the turbine external surface, due to its higher temperature and big areas. External heat fluxes at the central housing are negligible compared to the turbine enthalpy drop. In compressor side, external heat flow can be reversed, i.e. it can be lost or absorbed depending on the running conditions. In this way, the most important seems to be the heat radiated by the turbine side but the other paths cannot be neglected.

For the discharge coefficients characterisation, the testing methodology was focused on mass flow measurement through the wastegate during turbocharger operation. An indirect approach was used, in which the whole turbocharger system was tested at the same time in a gas stand. For the adiabatic map

characterisation, the focus of the tests was on the correct measurement of turbine adiabatic efficiency achieved by minimising heat transfer fluxes along the turbocharger using the approach detailed in [29].

From the modelling point of view, several turbocharger models to account for different aspects have been developed in the thesis. In the first place, a general methodology to account for heat transfer phenomena in turbochargers has been developed. This methodology helps to save experimental costs of turbocharger heat transfer characterisation. As it will be proved by a 1D whole engine model, turbocharger heat transfer phenomena play an important role in whole engine simulations. The results of the simulations will show much better predictions in turbine outlet temperature compared to the original model without heat transfer modelling. Compressor outlet temperature prediction will be slightly improved, as well. It will be also proved for both variables that the precision of the generic methodology is similar to the precision given by specific correlations based on empirical data of a given turbocharger. In that way, experimental characterisation of the turbocharger in several test rigs can be avoided without losing precision in compressor and turbine outlet temperature prediction.

In the second place, a turbine map extrapolation model has been developed which is crucial in whole engine simulations since the pulsating flow makes the turbine work outside of its design conditions. The model shows good agreement with the experimental data even when it is calibrated with a very limited set of data. In this model both mass flow and efficiency can be extrapolated beyond typical turbine map measured range in whatever variable, i.e. VGT position, reduced speed and blade to jet speed ratio. In the case of wastegated turbines, wastegate valve discharge coefficient has been modelled in a mathematical way. The error in mass flow prediction using this procedure is small if compared with the experimental results.

Finally, after the theoretical development of the different turbocharger models they were integrated in a GT-POWER™ model by means of an external library. GT-POWER™ were used since it is widely used in industry and research although the developed models can be coupled and used in any other 1D modelling environment. After the integration in GT-POWER™, the models were validated against experimental data. Several simulations have been performed to show the effect of the different models on the prediction of several engine variables. The heat transfer model has been studied using a whole engine model in both transient and steady conditions. The wastegate discharge coefficient model has been studied in a two stage turbocharger gas stand model. Finally, the turbine map extrapolation model was studied in a single stage turbocharger gas stand model.

Contrary to the general view that heat transfer phenomena occurring in turbochargers are only important at partial loads and transient engine evolutions, in this work, it will be demonstrated that full load operating points are also

affected by these phenomena. The compressor and turbine outlet temperatures are important variables to be predicted at these operating points. The importance is in inter-cooler design (or combustion process), after-treatment, exhaust energy recovery and two stage turbocharging modelling and design because accurately predicted boundary conditions can be used in each case.

The work will also show that turbo speed prediction is not affected by heat transfer when hot turbocharger maps in which compressor and turbine have been measured at the same time are used.

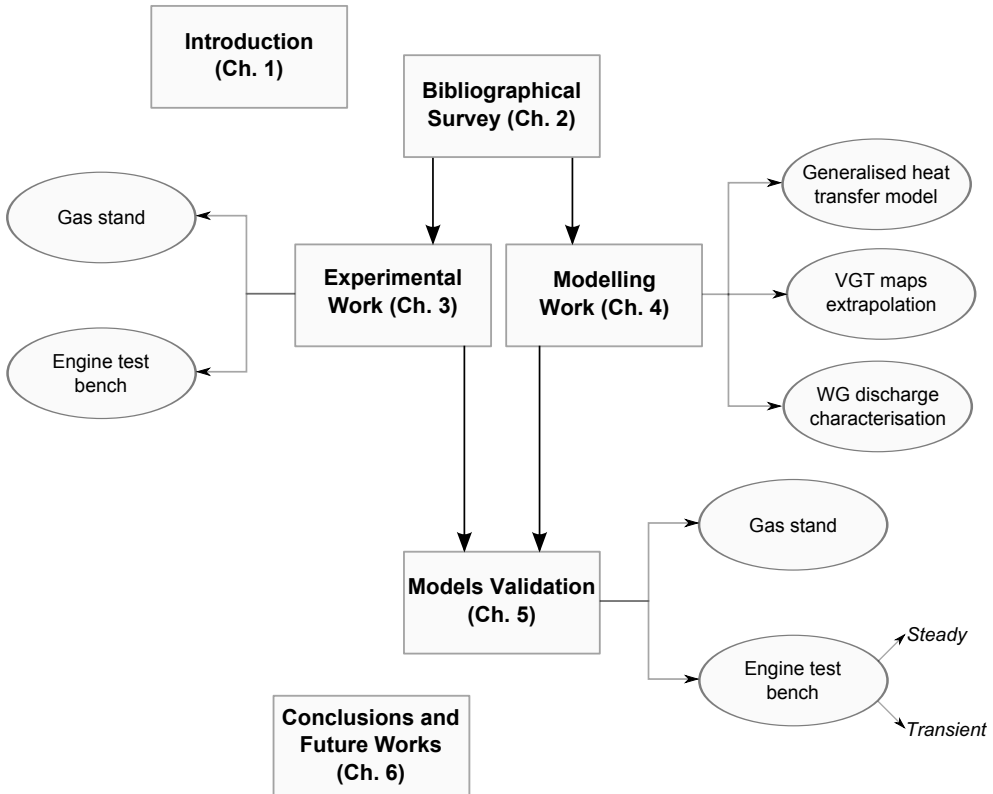


Figure 1.3: Outline of the dissertation

In Figure 1.3 an outline of the dissertation is presented including chapters' distribution. As it can be observed in Figure 1.3, the whole dissertation represents a full cycle of experimentation, modelling and validation as it is customary in engine design and research. In that way, after the current introduction and a deep review of the available research on the different subjects of study, each chapter corresponds to one step of this cycle.

Chapter 1 sets the motivation of the research, the primary objectives that

have been achieved during the development of the thesis work and the methodology employed to achieve these objectives.

Chapter 2 provides a deep insight into the available research regarding the different parts of the dissertation. Different heat transfer models will be discussed with focus on 1D models, empirical models and CFD models. The influence of these models on engine performance prediction will also be discussed. Regarding turbine maps extrapolation, several models available on the literature will be discussed stating their advantages and disadvantages. These models are based on empirical, mean line or CFD approaches. Finally, the flow thorough an orifice will be studied showing available research regarding wastegate discharge coefficient determination.

Chapter 3 will provide a description of the experimental work in both the gas stand and the engine test bench. The focus will be on test methodology, on the results and on the analysis of these results. This analysis will provide insight into the effects of turbocharger phenomena on the performance variables of both the engine and the turbocharger.

Chapter 4 is dedicated to the development of the modelling part of the dissertation. In this chapter, the underlying theory of the models is described as well as model integration in a commercial 1D software. The different turbocharger models and their effect on engine performance prediction will be discussed. This includes a generalised heat transfer model composed by internal convection, conduction and external heat transfer, a turbine performance map extrapolation model for both the reduced mass flow and the efficiency and wastegate discharge coefficient modelling.

Chapter 5 deals with the validation of the models developed in the previous chapter using the gas stand and the whole engine models in a 1D gas dynamic software. In the whole engine model case both steady and transient simulations will be studied. Different turbochargers that have not been used in the model development phase will be used in this validation stage.

Finally, chapter 6 gives an insight of the main contributions of the work performed in the thesis as well as a list of possible future works that fell beyond the scope of this work.

1.4 References

- [9] T. Suzuki. *Romance of engines*. Ed. by Warrendale: Society of Automotive Engineers. Society of Automotive Engineers, 1997 (cit. on p. 2).
- [10] D. Sperling and D. Gordon. *Two Billion Cars: Driving Toward Sustainability*. Ed. by Oxford University Press. Oxford University Press, 2009 (cit. on p. 2).

-
- [11] T. Sturgeon, J. Van Biesebroeck, and G. Gereffi. “Value chains, networks and clusters: reframing the global automotive industry”. In: *Journal of Economic Geography* 8 (2008), pp. 297–321 (cit. on p. 2).
- [12] World Energy Council. *Global Transport Scenarios 2050*. Tech. rep. WEC London, 2011 (cit. on p. 2).
- [13] J. Hartman. *Turbocharging Performance Handbook*. Ed. by Motorbooks. Motorbooks, 2007 (cit. on p. 3).
- [14] Official Journal of the European Union. *REGULATION (EC) No 715/2007 OF THE EUROPEAN PARLIAMENT AND OF THE COUNCIL of 20 June 2007 on type approval of motor vehicles with respect to emissions from light passenger and commercial vehicles (Euro 5 and Euro 6) and on access to vehicle repair and maintenance information*. 2007 (cit. on p. 4).
- [15] A. M. Omer. “Energy, environment and sustainable development”. In: *Renewable and Sustainable Energy Reviews* 12.9 (2008), pp. 2265–2300. DOI: 10.1016/j.rser.2007.05.001 (cit. on p. 4).
- [16] Turner, J., Popplewell, A., Patel, R., Johnson, T. et al. “Ultra Boost for Economy: Extending the Limits of Extreme Engine Downsizing”. In: *SAE Int. J. Engines* 7.1 (2014). DOI: 10.4271/2014-01-1185 (cit. on p. 4).
- [17] N. Baines. *Intake Boosting*. Encyclopedia of Automotive Engineering. John Wiley & Sons, Ltd., 2014. DOI: 10.1002/9781118354179.auto126 (cit. on p. 5).
- [18] M. Padzillah, S. Rajoo, and R. Martinez-Botas. “Influence of speed and frequency towards the automotive turbocharger turbine performance under pulsating flow conditions”. In: *Energy Conversion and Management* 80 (2014), pp. 416–428. DOI: 10.1016/j.enconman.2014.01.047 (cit. on pp. 5, 35).
- [19] R. Burke, C. Vagg, D. Chalet, and P. Chesse. “Heat transfer in turbocharger turbines under steady, pulsating and transient conditions”. In: *International Journal of Heat and Fluid Flow* 52 (2015), pp. 185–197. DOI: 10.1016/j.ijheatfluidflow.2015.01.004 (cit. on pp. 5, 31).
- [20] M. Chiong, S. Rajoo, R. Martinez-Botas, and A. Costall. “Engine turbocharger performance prediction: One-dimensional modeling of a twin entry turbine”. In: *Energy Conversion and Management* 57 (2012), pp. 68–78. DOI: 10.1016/j.enconman.2011.12.001 (cit. on p. 5).

- [21] M. Barratta and E. Spessa. *Numerical Simulation Techniques for the Prediction of Fluid-Dynamics, Combustion and Performance in IC Engines Fuelled by CNG*. Computational Simulations and Applications, InTech, Dr. Zhu Jianping (Ed.), 2011. DOI: 10.5772/25081 (cit. on pp. 5, 15).
- [22] Andrés Omar Tiseira. “Caracterización experimental y modelado de bombeo en compresores centrífugos de sobrealimentación”. PhD thesis. Universitat Poliècnica de València, 2008 (cit. on p. 5).
- [23] Carmen Cervelló Romero. “Contribución a la caracterización experimental y al modelado de turbinas de geometría variable en grupos de sobrealimentación”. PhD thesis. Universitat Poliècnica de València, 2004 (cit. on p. 5).
- [24] P. Fajardo. “Methodology for the Numerical Characterization of a Radial Turbine under Steady and Pulsating Flow”. PhD thesis. Universitat Poliècnica de València, 2012 (cit. on p. 5).
- [25] R. Navarro. “A numerical approach for predicting flow-induced acoustics at near-stall conditions in an automotive turbocharger compressor”. PhD thesis. Universitat Poliècnica de València, 2014 (cit. on p. 5).
- [26] Miguel Ángel Reyes-Belmonte. “Contribution to the Experimental Characterization and 1-D Modelling of Turbochargers for IC Engines”. PhD thesis. Universitat Poliècnica de València, 2013 (cit. on pp. 6, 26, 51, 52, 60, 66, 89, 91, 94, 98, 114, 145, 151, 153, 190).
- [27] Luis Miguel García-Cuevas González. “Experiments and Modelling of Automotive Turbochargers under Unsteady Conditions”. PhD thesis. Universitat Poliècnica de València, 2014 (cit. on pp. 6, 62, 113, 114, 118).
- [28] J. Serrano, P. Olmeda, A. Páez, and F. Vidal. “An experimental procedure to determine heat transfer properties of turbochargers”. In: *Measurement Science and Technology* 21.3 (2010). DOI: 10.1088/0957-0233/21/3/035109 (cit. on pp. 7, 27, 52, 54, 89).
- [29] J. R. Serrano, P. Olmeda, A. Tiseira, L. M. García-Cuevas, and A. Lefebvre. “Theoretical and experimental study of mechanical losses in automotive turbochargers”. In: *Energy* 55 (2013), pp. 888–898. DOI: 10.1016/j.energy.2013.04.042 (cit. on pp. 8, 27).

Bibliographical Survey

Contents

2.1	Introduction	15
2.2	Heat transfer modelling in turbochargers	15
	One dimensional models	18
	Empirical models	27
	CFD models	28
	Heat transfer models influence on engine performance calculation	30
2.3	Turbine maps extrapolation methods	32
	Empirical models	33
	Mean line models	34
	CFD models	35
2.4	Waste-Gate Discharge coefficient characterisation	35
2.5	References	38

Figures

2.1	Turbine casing: inner and outer wall temperature difference in three different locations [37]	17
2.2	Compressor isentropic efficiency with different turbine inlet temperatures and rotational speeds [39]	17
2.3	(a) Compressor enthalpy-entropy chart (b) Turbine enthalpy-entropy chart	20
2.4	Compression and expansion process according to [44]	21
2.5	Compressor performance map with differences between adiabatic and diabatic compressor efficiency [50]	23

2.6	Heat correction factor for compressor efficiency [50]	24
2.7	Resistances for turbocharger heat transfer model [63]	26
2.8	Temperature and mass flow effects on the time constant τ [74] . .	28
2.9	Temperature gradients in the turbine wheel [78]	29
2.10	Steady state CHT calculations at full load: external and internal surface temperatures [81]	30
2.11	Turbine heat divided by turbine mechanical power on an engine operation map [19]	31
2.12	Compressor efficiency compared to model efficiency for different assumed percentages of heat transfer before compression [85] . . .	32
2.13	Unsteady turbine model with six rotor entries [103]	35
2.14	Schematic of a regulated two stage turbocharging system [109] . .	36
2.15	Effect of the obstacle disturbance on the discharge coefficient [113]	37

2.1 Introduction

The usage of turbochargers has evolved throughout the last years. Improvements regarding the operation of turbochargers are currently under development on diesel and gasoline automotive engines. The improvements are focused on several topics of engine and turbocharging matching. Some of them are related with heat transfer modelling in order to take into account these phenomena in one dimensional models. Furthermore, the effect of these phenomena on turbocharger and engine performance has also been studied in the last years by the scientific community. Several approaches have been developed to account for heat transfer phenomena in turbochargers ranging from lumped-mass modelling to complex computational calculations. In order to improve turbine design and modelling a lot of research effort was also devoted in the last years to turbine map extrapolation techniques. Several approaches were used regarding this topic, ranging between empirical models and CFD approaches. Another interesting topic related with the contents of current thesis is the discharge coefficient modelling of the different valves used in turbocharging. This topic is acquiring a lot of attention in the last years as two stage turbocharging solution makes use of several by-pass valves. In this chapter a comprehensive literature review regarding the different topics of the thesis is presented.

Several aspects of current turbocharging research regarding compressor map extrapolation and surge detection as well as pulsating flow effects are left aside in this chapter as they are not clearly related to the thesis.

2.2 Heat transfer modelling in turbochargers

Traditionally, turbochargers behaviour has been modelled neglecting heat transfer phenomena [21, 30], specially when a whole-engine 1D simulation of transient gasoline cycles was carried out [31, 32]. However, in the last decade several authors pointed the importance of considering heat transfer phenomena in turbochargers to improve models prediction capabilities in terms of precision and robustness. Previously to those claims, the effect of heat transfer on efficiency measurements in turbocharger hot gas stands has already been considered by [33]. This author pointed out that the measured efficiency in both compressor and turbine is different from adiabatic efficiency in the case of hot gas flowing through the turbine. The reason of this behaviour is the difficulty of measuring the fluid temperature difference due to pure compression or expansion, decoupled from possible heat fluxes [2]. These heat fluxes cannot be neglected for many turbochargers and engine operative points. Even in axial compressors the effect of heat transfer on the efficiency is important [34]. Therefore, the heat transfer phenomena in map measurement affect turbocharger and engine

1D modelling [35] as compressor and turbine efficiencies are used to compute properly the outlet temperatures and the powers of both machines. Compressor outlet temperature prediction is crucial in setting correct boundary conditions for the intercooler and combustion chamber. Turbine outlet temperature prediction is important in increasing the accuracy of after treatment modelling and in improving the prediction of the available energy for a second turbine. Furthermore, it is also important for modelling exhaust energy recovery systems. Finally, accurate power output calculation is necessary to calculate turbocharger speed which affects to overall turbocharger performance.

In order to show the importance of heat transfer phenomena in turbocharger modelling different approaches and studies have been performed. Experimental studies of the phenomena, both in a gas stand [36] and in an engine test bench [37] have been published. The gas stand tests decouple the turbocharger phenomena from the ones associated to the engine. The engine test bench experiments represent the closest approximation to real vehicle operation conditions. The work performed in [37] reveal that turbine and compressor temperatures are not uniform during engine operation. Furthermore, Figure 2.1 shows that there is an important difference between inner and outer walls of the turbocharger at three different locations. The 'external' location corresponds to casing temperature measurement on the opposite side to the engine, the 'engine' locations corresponds to the point of the casing that faces the engine directly and 'top' is located between 'engine' and 'external'. Aghaali et al. [38] also made an important effort in analysing different heat transfer conditions in the turbocharger on engine operation.

Furthermore, theoretical studies [39] showed that isentropic efficiency definition is insufficient to correctly asses the heat transfer in compressors spinning at low speeds. The reason reported by these authors is that the denominator of isentropic efficiency definition, shown in Equation 2.1 is not equal to the shaft power for diabatic flows. In this case the temperature rise of the denominator is composed of shaft power and heat addition due to heat transfer effects.

$$\eta_s = \frac{T_{2s} - T_1}{T_2 - T_1} \quad (2.1)$$

In Figure 2.2 it can be observed that the effect of turbine inlet temperature on compressor efficiency is more important at low and medium rotational speeds. The drop in efficiency is clear when the turbine inlet temperature is increasing.

The authors propose to use the polytropic efficiency definition adding a heat transfer component as shown in Equation 2.2, where η_p is the polytropic efficiency, η_{pq} the diabatic polytropic efficiency, q_{12} the specific heat transfer in

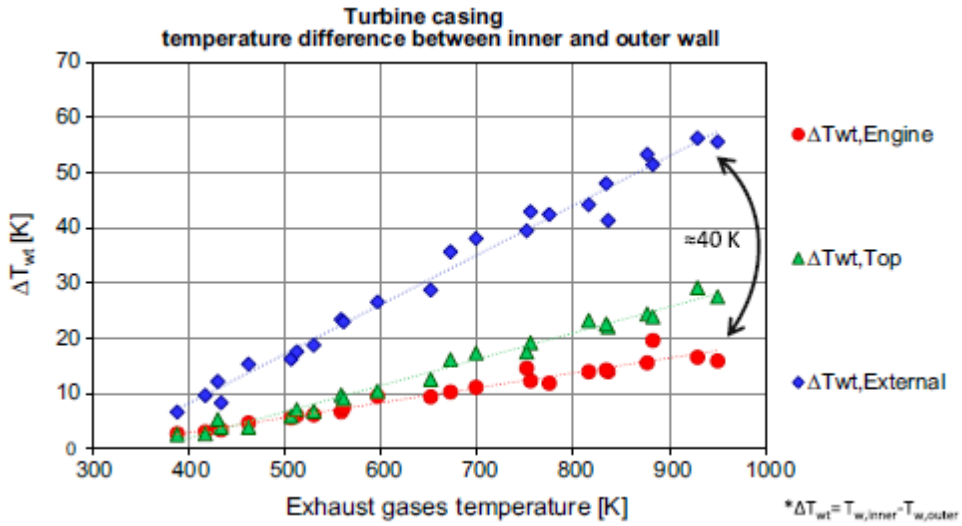


Figure 2.1: Turbine casing: inner and outer wall temperature difference in three different locations [37]

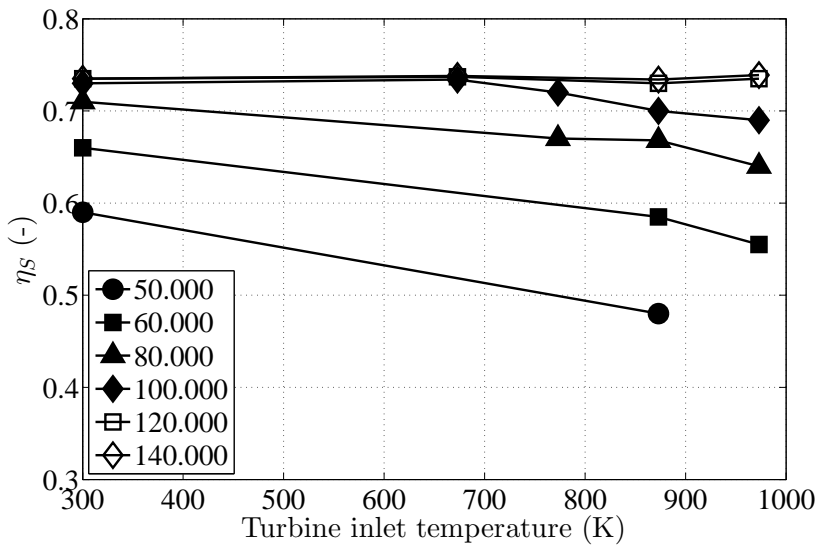


Figure 2.2: Compressor isentropic efficiency with different turbine inlet temperatures and rotational speeds [39]

the compressor and y_{12} the specific polytropic head rise in the compressor.

$$\eta_p = \frac{1}{\frac{1}{\eta_{pq}} - \frac{q_{12}}{y_{12}}} \tag{2.2}$$

Shaaban and Seume [40] developed and confirmed experimentally the theory that compressor non-adiabatic performance is dominated by the compressor heat number, defined in Equation 2.3, and peripheral Mach number. The deviation from adiabatic performance increases with the decreasing of peripheral Mach number due to the relative decrement of aerodynamic work compared to the amount of heat transfer. The effect of the compressor heat number has the inverse trend. High values of the compressor heat number correspond to higher deviations between non-adiabatic and adiabatic compressor performances. The reason for this behaviour can be inferred from Equation 2.3. Higher compressor heat transfer, q_C , result in high compressor heat numbers and thus in higher non-adiabatic performance of the compressor.

$$\zeta_{h,C} = \frac{q_C}{c_{p,air} T_{1t}} \quad (2.3)$$

Diango et al. [41] have considered heat transfer in turbochargers and micro gas turbine using an exergetic analysis. This analysis allows a detailed calculation of losses in the turbocharger, distinguishing heat transfer from shaft power. The same authors have also demonstrated in [42] that internal and heat transfer in small gas turbines introduces a drop in their performance. The adiabaticity assumption in this type of machines and in turbochargers leads to inaccurate results. Furthermore, the insulation of the turbine results in a higher drop in performance compared to non-insulated case.

All these studies show that the importance of heat transfer phenomena in the overall power exchange inside the turbocharger can be significant at low and medium turbocharger speeds. In the next subsections the different approaches in the literature to take into account these phenomena in turbocharger modelling will be described. Additionally, studies reflecting the impact of heat transfer models in engine performance will be discussed in a separate subsection.

One dimensional models

Turbocharger heat transfer models based on a 1D approach study the compression and expansion processes in compressor and turbines from a thermodynamic point of view. In this analysis the difference between isentropic adiabatic and diabatic processes is highlighted. The characterization of these processes is made by measuring performance maps of compressor and turbine in a gas stand. The traditional approach in 1D models of turbocharged reciprocating engines has always been the usage of these maps measured in hot conditions [30]. Thus, with a given gas conditions at the inlet of the turbomachine, the outlet conditions are easily obtained using the measured efficiency and pressure ratio provided by the map.

The gas stand measured variables necessary to characterise a performance map include compressor and turbine inlet and outlet temperatures, pressures and mass flows, as well as turbocharger shaft speed. Performance maps are composed of four main parameters: reduced or corrected mass flow (equation 2.4), reduced or corrected shaft speed (equation 2.5), total to static or total to total pressure ratio (equation 2.6) and total to static or total to total efficiency (equation 2.7).

$$\dot{m}_t^{red} = \frac{\dot{m}_t \cdot \sqrt{T_{3t}}}{p_{3t}}; \quad \dot{m}_c^* = \frac{\dot{m}_c \cdot \sqrt{T_{1t}/T_{ref}}}{p_{1t}/p_{ref}} \quad (2.4)$$

$$N_t^{red} = \frac{N}{\sqrt{T_{3t}}}; \quad N_c^* = \frac{N}{\sqrt{T_{1t}/T_{ref}}} \quad (2.5)$$

$$\pi_t^{t/s} = \frac{p_{3t}}{p_4}; \quad \pi_c^{t/t} = \frac{p_{2t}}{p_{1t}} \quad (2.6)$$

$$\eta_t^{t/s} = \frac{1 - T_4/T_{3t}}{1 - (1/\pi_t^{t/s})^{\frac{\gamma-1}{\gamma}}}; \quad \eta_c^{t/t} = \frac{(\pi_c^{t/t})^{\frac{\gamma-1}{\gamma}} - 1}{T_{2t}/T_{1t} - 1} \quad (2.7)$$

In these equations the standard definitions for compressor and turbine have been chosen in terms of reduced or corrected parameters. As it can be observed in the equations, in reduced and corrected mass flow and speed definitions inlet pressure and temperature are included, making the maps useful for comparison even when inlet conditions are different to the measured in the gas stand. Those parameters are highly useful as they relate the different conditions that can appear in both compressor and turbine. For instance, for a given reduced mass flow and reduced speed there is only one efficiency and one pressure ratio possible value. Furthermore, the maps reveal zones of optimal operation, where the efficiency of the turbomachine is higher and zones of undesired operation as, for instance, surge zone in the compressor.

The measurement of the maps in the gas stand can be done using different approaches. The main two approaches are hot and cold tests. In hot tests the turbine inlet temperature is high (similar to the exhaust gases temperature of the engine) while in cold tests the temperature is kept at lower levels, usually below 130°C.

In the first approach the efficiency values of compressor and turbine are affected by heat transfer phenomena occurring during the tests due to the high temperature differences. In Figures 2.3a and 2.3b it can be observed that the evolution in the enthalpy-entropy chart is different in both cases. Following the ideas of [43] some heat is added or subtracted in the process. This heat changes the temperature at the outlet of the compressor or at the inlet of the turbine so it is different from the corresponding adiabatic evolution. Thus, the efficiency

computed from equation 2.7 would be different from pure adiabatic efficiency of the turbomachine. In the cold tests the measured efficiencies are less affected by heat transfer effects and are closer to the adiabatic definition.

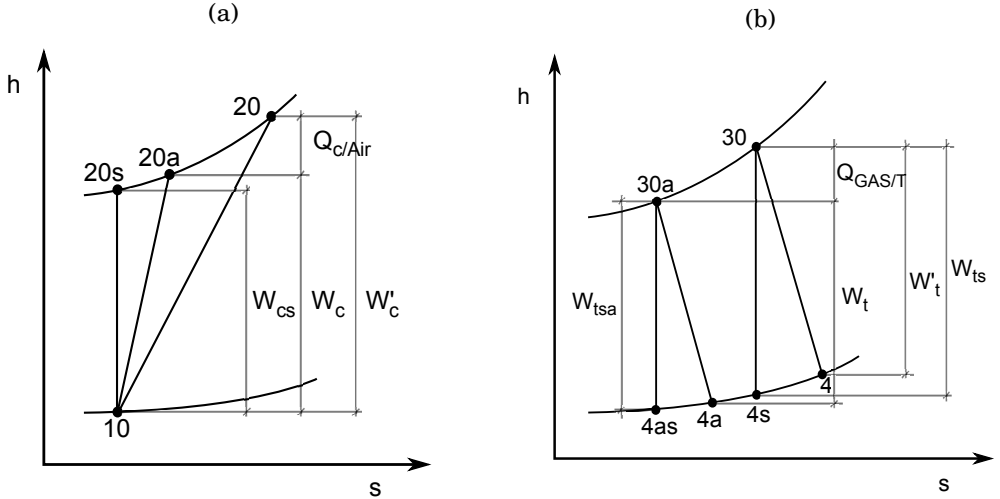


Figure 2.3: (a) Compressor enthalpy-entropy chart (b) Turbine enthalpy-entropy chart

Sidorow et al. [44] have proposed a three stage division of the compression and expansion processes as shown in Figure 2.4. In their proposal heat is extracted or added before the adiabatic compression or expansion and after it.

Several definitions of turbine efficiency in hot conditions have been used in the literature. Turbine efficiency can be defined based on the isentropic power of the turbine or isentropic power of the compressor. In the last case, mechanical losses are taken into account in the definition. In Equation 2.8 the first definition is shown, called turbine diabatic efficiency (TDE) as in a general case of hot gases it corresponds to a diabatic evolution. In Equation 2.9 effective turbine efficiency is presented. This definition is also called map efficiency as it is normally used by turbocharger manufacturers in the performance map that they supply with the product. This definition is affected by both the heat transfer to the compressor and turbocharger friction losses as demonstrated in [45].

$$TDE = \frac{T_{30a} - T_{4a}}{T_{30a} - T_{4as}} = \frac{\dot{W}_t}{\dot{W}_{tsa}} \quad (2.8)$$

$$ETE = \eta_{t,map} = \frac{\dot{m}_c \cdot c_{p,c} \cdot (T_{20} - T_{10})}{\dot{m}_t \cdot c_{p,t} \cdot (T_{30} - T_{4s})} = \frac{\dot{W}_c + \dot{Q}_{C/Air}}{\dot{W}_{ts}} \quad (2.9)$$

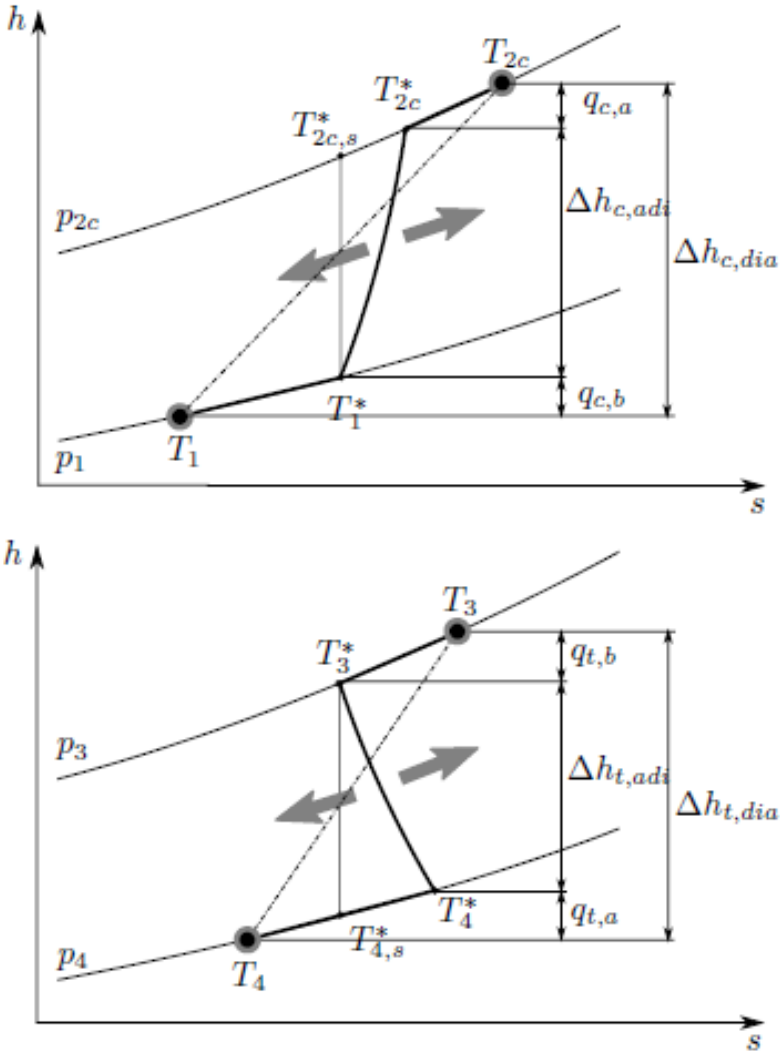


Figure 2.4: Compression and expansion process according to [44]

For the compressor the definition of efficiencies in adiabatic and in hot (diabatic) maps are presented in Equations 2.10 and 2.11, where the temperature definitions are shown in Figure 2.3a.

$$\eta_{c,adiab.} = \frac{T_{20s} - T_{10}}{T_{20a} - T_{10}} = \frac{\dot{W}_{cs}}{\dot{W}_c} \quad (2.10)$$

$$\eta_{c,dia.} = \frac{T_{20s} - T_{10}}{T_{20} - T_{10}} = \frac{\dot{W}_{cs}}{\dot{W}'_c} = \frac{\dot{W}_{cs}}{\dot{W}_c + \dot{Q}_{C/Air}} \quad (2.11)$$

Furthermore, according to [46] the effect of non-adiabatic turbocharger operation impacts on the prediction of the performances of the bearings.

The efficiency values are crucial for correct outlet temperatures computation. Therefore, it is important to consider if cold or hot maps must be used for better prediction. Furthermore, the different ways of defining turbine efficiency must be also taken into account. The standard approach is to use hot maps because the temperatures in the engine are similar to those in the gas stand so measured efficiencies will give more accurate values of outlet temperature for the same conditions. However, in present thesis it will be proven that turbine outlet temperature prediction accuracy is low using hot maps at similar conditions without heat transfer model. If a cold map is used the prediction will be worse as the temperatures in the gas stand are much lower than those in the engine. However, if different engine conditions are to be modelled such as partial loads and transients (which are actually important for normative driving cycles) the hot map approach might yield worse results in terms of precision due to lower temperatures in the engine. It is possible to use cold maps for such conditions when the temperatures in the engine are similar to those in cold maps but it could be difficult to find reasonable similarities.

To overcome these problems different approaches have been proposed to take into account the type of map used in the models and the temperature conditions during map measurement. Heat transfer phenomena must be studied and taken into account for this purpose in 1D simulations.

Experiments in gas stand as performed by [47] have been used to evaluate the effect of turbine inlet temperature and mass flow on turbine and compressor casings temperature. The authors concluded that the influence of turbine inlet temperature on turbine casing maximum temperature is nearly linear. The effect of increasing turbine mass flow is reflected in the increment of compressor casing temperature due to the increment of compressor pressure ratio.

Lüddecke et al. [48] have performed an extensive experimental study in a gas stand showing the important impact of turbine inlet temperature in compressor and turbine efficiencies. The effect of water cooling temperature has been also studied in [48] showing higher compressor efficiencies in the case of lower water cooling temperatures. External radiation measured using thermal imaging shows higher bearing housing temperatures in the case of higher turbine inlet temperature. Finally, this study proposed a methodology of measuring a wider turbine map range by using different turbine inlet temperatures. In that way for lower temperatures the expansion ratios will be higher for the same reduced speed. The conclusions of a more recent study made by Marelli et al. [49] are similar. In both papers simple correction models for compressor efficiency have been proposed. However, neither of them quantified the heat transfer in the different turbocharger elements.

Schinnerl et al. [50] have also performed and extensive experimental cam-

paigned to study the effect of heat transfer on compressor and turbine performance. In Figure 2.5 it can be observed that the effect of heat transfer on compressor efficiency is higher in the low and medium turbocharger speed range. This impact is also correlated with the coolant temperature as shown in Figure 2.6 where the coefficient of Equation 2.12 is plotted against the corrected mass flow. The values of f_q higher than unity indicate that the compressor is losing heat to the central housing, thus increasing the value of the measured efficiency. Lower values than unity mean that the compressor is receiving heat what gives lower measured efficiency. As it can be observed in Figure 2.6 when the coolant is at lower temperature compressor measured efficiency will be higher and when the coolant temperature is high the measured efficiency will be lower. Finally, in [50] it is also reported that a significant improvement in turbine outlet temperature prediction can be achieved with a calculation of more accurate values of turbine isentropic efficiency using a heat transfer model.

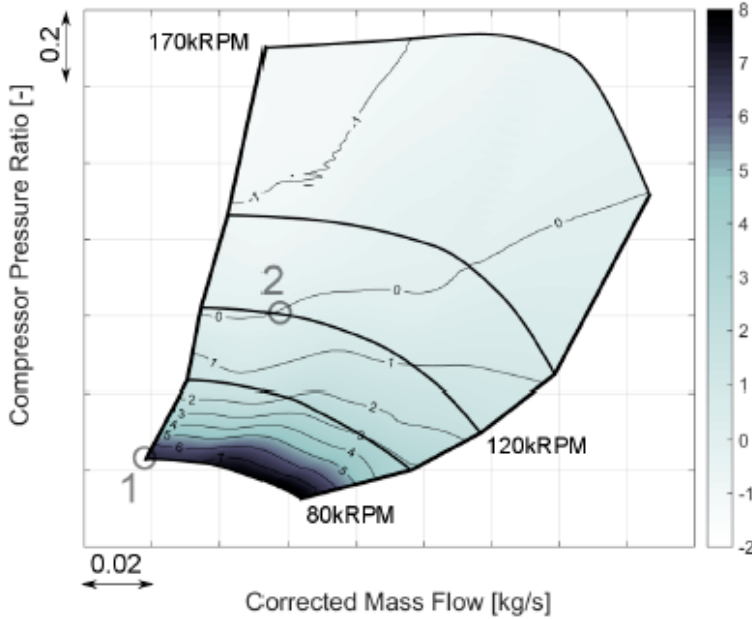


Figure 2.5: Compressor performance map with differences between adiabatic and diabatic compressor efficiency [50]

$$f_q = \frac{\Delta h_{dia,c} - q_{c,a} - q_{c,b}}{\Delta h_{dia,c}} \quad (2.12)$$

In Muqeem et al. review work [51] it is stated that turbine non-adiabatic operation can increase turbo lag. The reason is the inaccurate prediction of

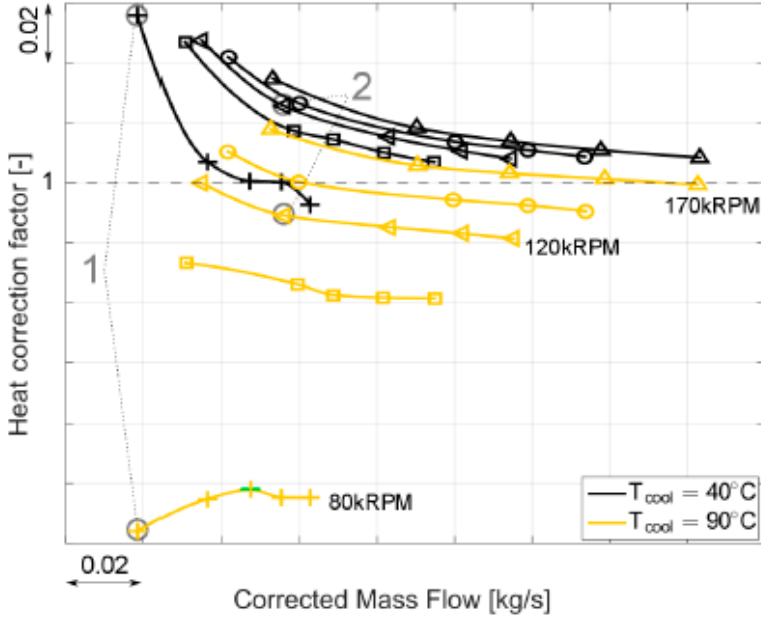


Figure 2.6: Heat correction factor for compressor efficiency [50]

compressor and turbine power without heat transfer model what can increase the denominator of Equation 2.13.

$$\Delta t = I_{rotor} \int_{\omega_1}^{\omega_2} \frac{\omega d\omega}{\dot{W}_T - \dot{W}_C} \quad (2.13)$$

Shaaban and Seume [52] have studied the effect of turbocharger heat transfer on internal combustion engine volumetric efficiency. It is stated in their study that at part loads a decrease of 4% in volumetric efficiency can be expected at medium turbocharger rotational speeds.

Other authors [53] showed that manufacturers maps must be modified in diesel engines simulation codes in order to take into account heat transfer effects. The authors have proposed a very simple heat transfer model taking into account the turbine inlet temperature to correct compressor manufacturers map. Even with the simple model proposed an improvement in compressor outlet temperature prediction was detected.

A similar kind of models can also be based on tests in engine rigs [54]. From those tests a 1-D heat transfer model was developed in [37].

Aghaali et al. [55] studied the effect of heat transfer at different engine load points. The experiments show the effects of different variables on heat transfer phenomena. According to this work, the temperature of turbocharger

working fluids is affected by the turbine and compressor performance and the temperature of the walls.

Bohn et al. [56, 57] have studied turbocharger heat transfer using a conjugate 3D model. They found that at low Reynolds numbers in the compressor the compressed air is heated by the heat flux coming from the turbine. If the Reynolds number is high the air is heated by compression and this heat goes to the casing.

In [58] a conjugate CFD heat transfer model has been used in conjunction with a 1D model. The 3D model was used to estimate a value of the wetted compressor area before and after compression. The authors used this estimation in 1D simulations concluding that the difference between this approach and considering heat transfer only after the compression process is only of one percentage point in outlet temperature prediction. This conclusion clearly validates the simplifications given in Figures 2.3a and 2.3b where the addition or subtraction of heat in the compressor is considered only after the compression process.

Models based on calibrated coefficients to provide an estimation of heat transfer or adiabatic efficiency are widely used. The authors of [48] have proposed a method based on water cooling to correct the measurements of turbine efficiency taking into account heat transfer. This model takes into account only conduction inside of the turbocharger, not considering external heat transfer between the test cell and the turbocharger. Two coefficients were calibrated in this model offering precise results.

Some authors use calibration coefficients for engine models [59, 55]. They conducted a test campaign at different engine loads [60] to build a heat transfer model in GT-POWER™. In the first place, efficiency multipliers were used proving difficult the proper calculation of turbine outlet conditions using only the multipliers. For that reason, an improved model is proposed in which a heat sink and a heat source are used in the compressor and turbine, respectively. In a different study of the same authors [38] a model to include external heat transfer is included, taking into account both external convection and radiation. Several methods have been compared to compute Nusselt numbers for convective heat transfer based on previous studies of the literature. Finally the authors propose a correlation that better fits their experiments which has been made at a wide range of external heat transfer conditions.

Shaaban et al. [61] developed a special software capable of simulating the turbocharger performance taking into account the heat transfer in compressor and turbine. The software implements a model developed on physically based regression equations.

Another approaches used in the literature are the lumped capacitance models. For that purpose the turbocharger is divided in several nodes and the interactions between different fluids and the metal nodes are considered. In

Figure 2.7 this kind of model is shown. It is necessary to provide a way to compute all the heat flows considered. This can be done by using gas stand experiments to fit standard convective correlations as done in [62], [63] and [64]. More considerations must be taken into account to compute the heat flows between the metal nodes like the metal conductances between the nodes. These models also give the possibility to consider thermal inertia and thus model transient behaviour of the turbocharger regarding heat transfer.

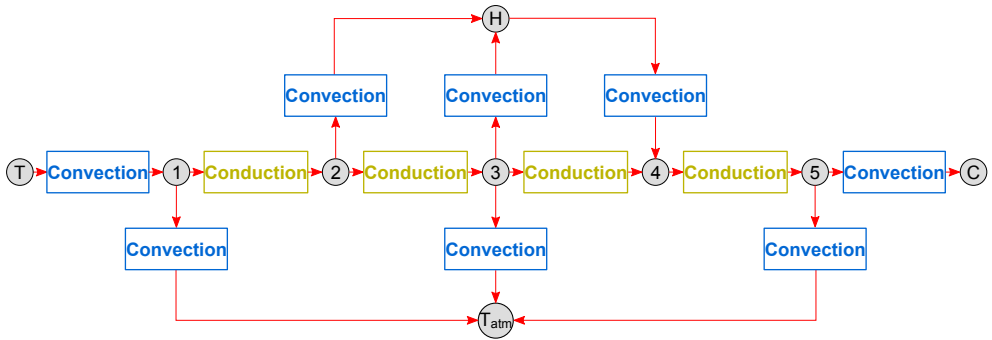


Figure 2.7: Resistances for turbocharger heat transfer model [63]

The convective heat transfer is calculated in these studies by using correlations of the form shown in Equation 2.14. It is a conventional approach in the study of convective heat transfer [65].

$$Nu = a \cdot Re^b \cdot Pr^c \quad (2.14)$$

Serrano et al. [66] propose general coefficients for the convective heat transfer correlations for the different fluids. In order to take into account the variation of Nusselt number depending on different turbine conditions new terms can be added to Equation 2.14. Some authors like Lavagnoli et al. [67] have reported different Nusselt numbers in axial turbines depending on circumferential position. This fact can be extrapolated to radial turbocharger turbines as shown in previous studies made by Reyes [26]. Taking into account these previous works special care must be taken in modelling the convective heat transfer of variable geometry turbines.

Authors like [68] have performed a sensitivity study of the heat transfer model parameters in this kind of approach. The results show that the influence is low on gas temperature prediction but high on housing temperatures prediction.

The procedure detailed in [69] is similar to the previously described one. In this study, the authors separated the different heat transfer phenomena that occur in the turbocharger. Heat transfer by conduction among the metal nodes is studied independently of the convection with the different fluids using the

procedure detailed in [28]. The convective heat transfer has been studied in gas stand using different type of tests taking special care with measurement uncertainty with the procedures described in [70]. The external heat transfer has also been studied in [1] using a simplified geometry for the turbocharger. The proposed model has been built using experimental results from the gas stand and the engine test bench.

Other authors like [71] have found that convective correlations coefficients on three different turbochargers have similar values for internal convection. However, external free convection coefficients proved to be dependant on turbocharger model.

The results found in previous studies suggest that convective correlations of the form proposed in Equation 2.14 can be used consistently on different turbochargers for internal heat transfer modelling. However, special care must be taken on modelling external heat transfer to provide general results applicable to different turbocharger models. According to Shaaban [72] the external heat transfer can represent up to 70% of the total heat transfer of the turbine at low rotational speeds.

In [73] engine transient behaviour has been modelled using a lumped model considering only turbine and compressor casings. The results reported in this study show an important improvement in predicting turbine outlet temperature in engine transient conditions even with high inaccuracies in predicting metal temperatures. The approach used in this study, as well as in the previous lumped approaches needs an adiabatic map to provide proper results.

Turbocharger heat transfer also has an impact on mechanical losses computation as it affects to oil outlet temperature. For that reason in order to decouple heat transfer and friction losses even in almost adiabatic measurements it is necessary to take into account the heat transfer as it was done in [29]. In that study a mechanical losses model is proposed based on the simplification of the Navier-Stokes equations applied to the thrust and journal bearings of a turbocharger. In order to fit the model adiabatic measurements are needed so the oil temperature increment is due only to friction losses power.

Empirical models

Empirical models for turbochargers heat transfer consist on adjusting coefficients of mathematical expressions to experimental results. The adjusted equations can be used later for different conditions to the studied experimentally.

An example of pure empirical approach can be found in Tadesse et al. [74]. These authors have tested a turbocharger turbine in fast transient evolutions measuring temperatures at different volute radial positions. This transient

behaviour has been modelled using a first order differential equation (equation 2.15) in which the time constant τ is adjusted for each test.

$$\pm \tau \frac{dT}{dt} = T \quad (2.15)$$

It can be concluded that the variation of turbine inlet temperature does not affect the time constant. However an important impact of the turbine mass flow was observed. In Figure 2.8 the time constant for each test is represented for four different thermocouple positions represented by 'MP' in the legend. Four turbine inlet temperatures have been tested represented by different colours in Figure 2.8. It can be observed that there is a clear decreasing trend with increasing mass flow for all thermocouple positions. The impact of the different turbine inlet temperatures is negligible on the adjusted time constant in all the cases.

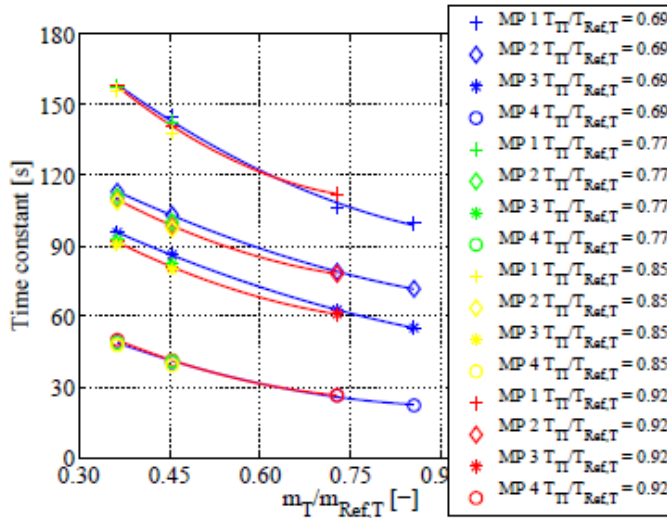


Figure 2.8: Temperature and mass flow effects on the time constant τ [74]

The results of this empirical model can be used as boundary conditions for conjugate heat transfer calculations or for thermal stress analysis of turbine wheel and case.

CFD models

Some authors [75] have performed CFD (Computational Fluid Dynamics) studies in order to better understand the heat transfer phenomena in turbochargers and their implications. In the simulations done by Hellstrom et al. [76] it was

found that the shaft speed is not affected by the heat transfer in the turbine. These numerical studies also show the relevant heat transfer paths and their magnitude.

The complex power exchange network during turbocharger acceleration can be found in [77]. The authors performed CFD calculation of the whole turbocharger. The most important heat paths according to this study are: turbine housing to ambient, turbine housing to bearing housing, bearing housing to coolant, bearing housing to compressor housing and compressor housing to charge air.

Diefenthal et al. in [78] and [79] have performed a numerical CFD study in order to gain knowledge of the transient temperature distribution in the turbine wheel. In Figure 2.9 the temperature gradients in the turbine wheel are shown. It is clear that non-adiabatic behaviour is expected in this case.

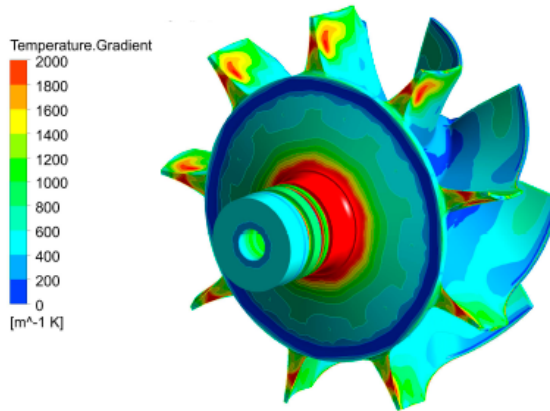


Figure 2.9: Temperature gradients in the turbine wheel [78]

Gu et al. [80] have performed numerical simulations and found that the external heat transfer has an important impact on a centrifugal compressor performance. They also found that the internal heat transfer in the compressor is dominated by the shroud surface.

Heuer et al. [81] have calculated the external temperature of turbine housing using a conjugate heat transfer numerical simulation. The results for turbochargers with integrated engine manifold are shown in Figure 2.10. It can be observed that turbine housing wall temperature is mostly uniform for two different twin entry designs.

Verstraete et al. [82] have performed a conjugate heat transfer calculation in a micro gas turbine composed of radial compressor and turbine. The main conclusion of their study is that the heat transfer in diffuser and nozzle is the

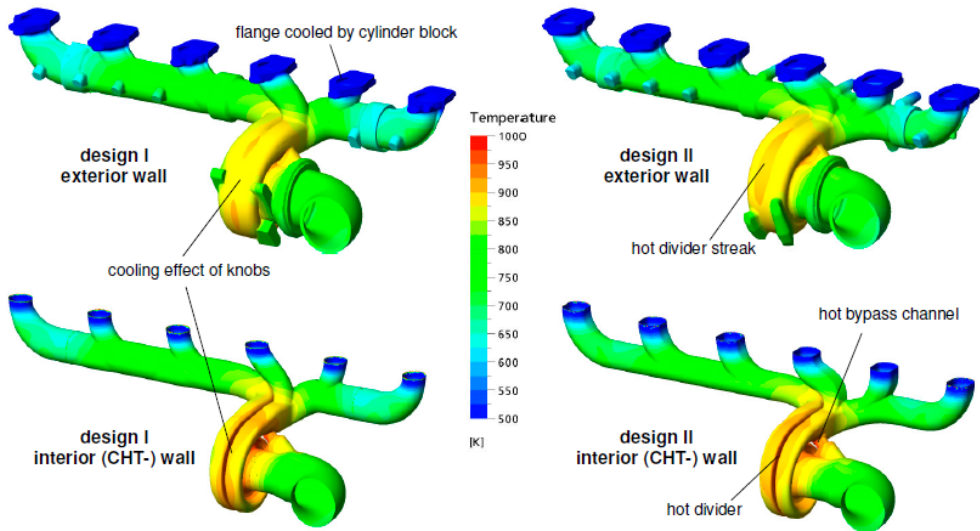


Figure 2.10: Steady state CHT calculations at full load: external and internal surface temperatures [81]

main contribution to the total heat transfer. It depends on both solid and fluid conductivities with a major role of the fluid one.

Yamagata et al. [83] have performed a three dimensional heat transfer calculation on a high pressure ratio compressor. They concluded that the heat inflow in the compressor comes from the hot back plate. They also reported that the metal temperatures are proportional to the compressor outlet temperature. They found that the effect of turbine inlet and oil temperatures in compressor performance is lower than expected what implies that the oil is removing most of the heat that goes from turbine to compressor.

Heat transfer models influence on engine performance calculation

The influence of turbocharger heat transfer and mechanical losses models on engine performance prediction is not clear. It is widely accepted that the influence of heat transfer and mechanical losses models is important at part loads and at transient operation [55].

Some authors have performed experimental measurements in gas stand concluding that the effect of turbocharger heat transfer is irrelevant compared to turbocharger mechanical power at high engine loads [84]. Other authors [54] have measured turbocharger performance in an engine test bench concluding

that at high engine speeds and loads the deviation between adiabatic and non-adiabatic compressor efficiency is small.

However, more recent studies [19] show that heat transfer in the turbine always represent an important part of its enthalpy change, being more relevant in the low torque region. In Figure 2.11 the ratio of turbine heat power to total turbine enthalpy drop is represented on an engine map. It can be observed that even at high engine speeds and loads turbine heat represents 40% of the mechanical power. In the low load and low speed area the ratio is close to 0.9 meaning that heat transfer in the turbine must be considered for correct prediction in the models. The conclusion of this study is that for precise temperature prediction even at high engine speeds and loads heat transfer must be taken into account.

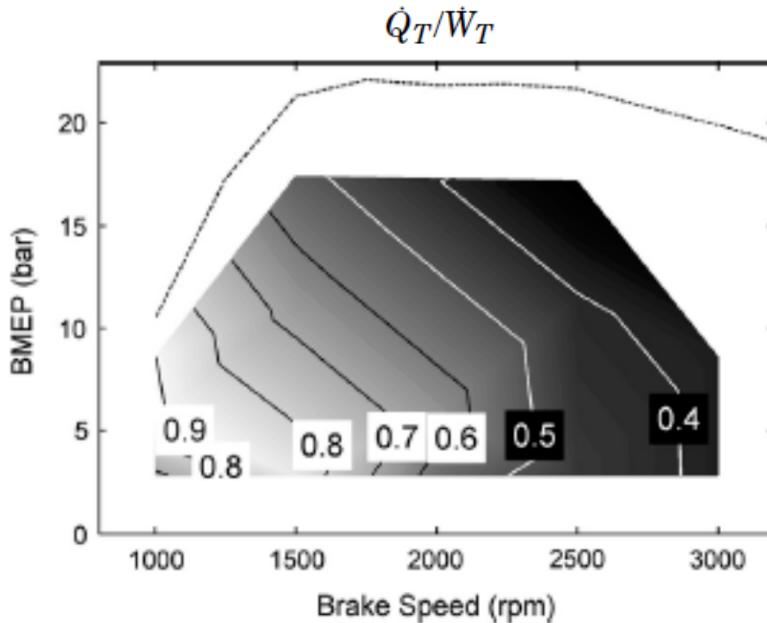


Figure 2.11: Turbine heat divided by turbine mechanical power on an engine operation map [19]

In another recent study [85] it has been pointed out that at higher powers the distribution of heat transfer during compression process has important effects. These authors propose the usage of α_A , defined in equation 2.16 as the quotient between the compressor area before the compression process and the total compressor area. In Figure 2.12 it can be observed that for different percentages of this coefficient the efficiency of the compressor can vary up to 5 percentage points at high turbocharger speeds.

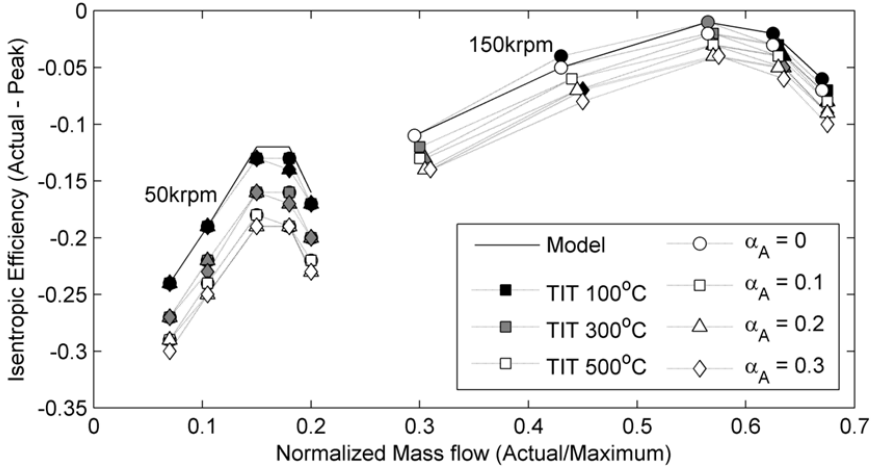


Figure 2.12: Compressor efficiency compared to model efficiency for different assumed percentages of heat transfer before compression [85]

$$\alpha_A = \frac{A_b}{A_T} \quad (2.16)$$

2.3 Turbine maps extrapolation methods

As it is shown in [30], during engine transient and partial load design conditions for the ICE the turbocharger turbine works at off-design conditions. In these off-design conditions the turbine works at high blade to jet speed ratios (σ) or low pressure ratios and low power outputs as shown in [86] due to turbocharger wheel inertia and pulsating flow in the exhaust of the ICE. Traditional measurements of turbine maps in gas stands are unable to capture this behaviour [87]. Only a narrow turbine map range is provided by manufacturers as a standard practice. Turbine maps are necessary when using 1D or 0D modelling tools to predict the whole engine behaviour. Turbocharged ICE designers must rely on map extrapolation tools when predicting engine performance outside of turbine design operative conditions [88].

As any extrapolation tool, the extrapolation models have always faced an important validation problem. The validity of the modelling can be checked for the measured conditions but not in the outside area, where it is really interesting to use the model. To overcome this problem, special tests in a gas stand can be used in which the turbine is measured outside of its design range, at extremely

high BSR [89]. This new approach provides wider BSR range than using a closed circuit in the compressor to extended the operational range of the turbine [90].

Empirical models

Empirical models use pure polynomial expression in which several coefficients are fitted using measured data. These models are simple but have inaccuracy problems if the extrapolated turbocharger is very different from the used for the fitting. To solve that problem semi-empirical models have also been developed. In those models turbomachinery principles equations are used and fitting coefficients are added to model certain aspects that can only be assessed experimentally. These models are generally more robust the pure empirical ones.

In the last years, several proposals have appeared in the literature regarding this topic. Some of them are based on pure theoretical approaches [91]. A comprehensive study of the different losses in stator and rotor have been considered in this work. A procedure to compute the performance parameters of nozzled and nozzleless turbines is also presented in [91]. The parameters of losses models have not been proved to be general on a wide range of turbine sizes or VGT positions.

Baines [92] also presents a model based on the characterisation of different losses such as passage losses or tip clearance losses also considered by Dambach et al. [93]. Nevertheless no general procedure for coefficients fitting or a comprehensive model validation at highly off-design conditions have been reported in this studies.

Other models are based on physical considerations but use empirical parameters for fitting stator outlet flow angles, without a clear correlation against physical values of average flow angles [94]. Furthermore, the model proposed in [94] relies on tangent functions, which are mathematically unstable during fitting procedures using numerical methods. Moreover, the model shown in [94] was only validated for blade to jet speed ratio extrapolation, not for turbocharger speed or VGT position extrapolation.

Other models are purely empirical and use the information of the map to fit coefficients as has been done in [95] for SI and DI engines control as shown in equation 2.17, where c and k are the fitting coefficients of the reduced mass flow. A similar approach has been used in [96] for automotive engines simulation, also with a control oriented objective.

$$m_{red} = c \sqrt{1 - \pi_t^k} \quad (2.17)$$

In [97] a Taylor series expansion is used to develop a model able of predicting mass flow parameter of radial turbines. Seven coefficients of equation 2.18 must

be calibrated in order to use the model, where z is defined in equation 2.19.

$$\phi^2 = \begin{cases} a_0 + a_1 z^5 \left(1 - \pi_t^{\frac{1-k}{k}}\right) + a_2 n_t^2 z^5 + a_3 z^5 \ln \pi_t + a_4 n_t^2 z^4 \left(1 - \pi_t^{\frac{1-k}{k}}\right) + \\ a_5 z^5 \left(1 - \pi_t^{\frac{1-k}{k}}\right) \ln z + a_6 n_t^2 z^5 \ln z + a_7 n_t^4 z^4, \pi_t \leq 3.5 \\ \phi^2 [\pi_t = 3.5, n_t = \max(n_t) \text{ at } \pi_t = 3.5], \text{ otherwise} \end{cases} \quad (2.18)$$

$$z = 1 - 1.357 \times 10^{-12} D_1^2 \left(\frac{M}{\varphi \cos \alpha_1}\right)^2 n_t^2 \quad (2.19)$$

Bozza et al. [98] have developed a 1D model based on the complex 3D turbine geometry to simulate automotive turbochargers. An optimization code is used to calibrate the 17 (19 in VGT case) different coefficients of the proposed model using only a limited set of turbine performance points. This model provides good accuracy in predicting turbine mass flow and adiabatic efficiency.

Sieros et al. [99] have proposed a quadratic polynomial in turbine expansion ratio and reduced speed to determine the reduced mass flow of jet engine turbines as shown in equation 2.20.

$$m_{red} = a_0 + a_1 \pi_t + a_2 N_{red} + a_3 \pi_t N_{red} + a_4 \pi_t^2 + a_5 N_{red}^2 \quad (2.20)$$

Zhugue et al. [100] have developed one-dimensional models for compressor and turbine. These models make possible the prediction of turbocharger performance with the possibility of extrapolating turbocharger performance maps.

A review of the advantages and disadvantages of each kind of model has been performed in [101]. In this work the authors implemented and compared different literature models for a given turbocharger.

Mean line models

Mean line modelling consists on assuming that there is a mean streamline through the stage of a turbomachine whose conditions are an average of the passage conditions [102].

Mean line models are used for simulating pulsating flow conditions, requiring different modelling approaches similar to the proposed in [103], where meanline and one-dimensional models are integrated as shown in Figure 2.13. In [104] non-adiabatic pressure loss boundary is used as an alternative to the integration of the mean line model. These models allow the prediction of the performance parameters of the turbine that are used in the one-dimensional models. Another interesting application of these tools is the fast evaluation of turbine capabilities in design process as performed in [105].

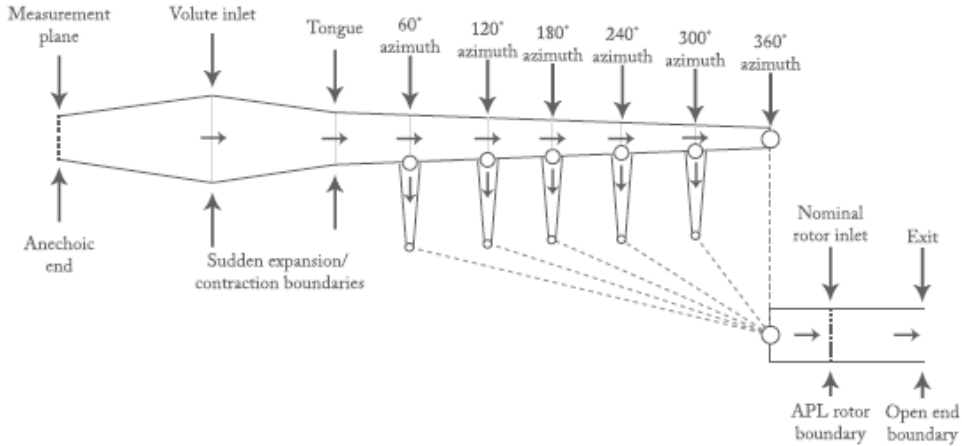


Figure 2.13: Unsteady turbine model with six rotor entries [103]

CFD models

CFD models for turbine design have been developed in [106]. This approach is useful when turbine CAD files are available. Full three-dimensional simulations can reproduce turbocharger behaviour only at a very high computational cost [107] what means that these simulations are only performed at few operating points [18]. Therefore, for whole driving cycle simulations, 1D or 0D approaches must be used to keep low computational costs and an adequate precision.

2.4 Waste-Gate Discharge coefficient characterisation

As it has been studied in [108] several aspects of two stage turbochargers must be taken into account to well characterise the behaviour of the whole system. In that background, apart from taking into account the heat transfer effects that affect turbomachine performance it is also necessary to take into account the behaviour of the different valves. Two stage systems are generally composed of several valves to regulate the flow to control the boosting of the system. For instance, in [109] a two-stage system is described which is composed of three valves: by-pass valve between the turbines, a check valve between the compressors and a waste-gate valve for the low pressure turbine. In Figure 2.14 a schematic of this kind of systems is shown.

According to the equation 2.21 from [110] the mass flow through an orifice at sub-critical compressible flow depends on the gas properties, inlet conditions

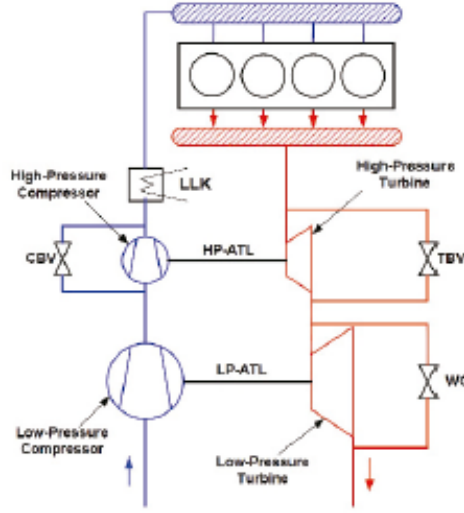


Figure 2.14: Schematic of a regulated two stage turbocharging system [109]

and pressure ratio between the inlet and the outlet of the orifice.

$$\dot{m}_{th} = \frac{p_{00}}{\sqrt{T_{00}}} \cdot A_{geom} \cdot \sqrt{\frac{\gamma}{R}} \left(\frac{1}{\pi_{t/s}} \right)^{\frac{1}{\gamma}} \sqrt{\frac{2}{\gamma-1} \left[1 - \left(\frac{1}{\pi_{t/s}} \right)^{\frac{\gamma-1}{\gamma}} \right]} \quad (2.21)$$

However, several effects of the flow crossing the orifice such as vena contracta take place [111]. In order to characterise this complex effects the simplest approach is to use a single parameter dependant on flow conditions to correct the mass flow of equation 2.21 as shown in equation 2.22. Using this approach the opening of the valve can also be considered in the discharge coefficient.

$$\dot{m}_{real} = C_D \cdot \dot{m}_{th} \quad (2.22)$$

The characterisation of the discharge coefficient can be useful in 1D modelling of the whole two-stage turbocharging system as actual mass flow thorough the different valves can be calculated with accuracy.

Several proposals have been made in the literature to characterise the behaviour of nozzles. In [112] a numerical CFD and experimental approaches have been used to calculate a discharge coefficients of a spray solid cone pressure nozzle with incompressible flow. In the case of incompressible flow equation 2.23 is used by the authors to compute the discharge coefficient. This equation

is based on Bernoulli principle and continuity equation that can be applied directly for incompressible flow.

$$C_D = \frac{Q}{A_0 \sqrt{\frac{2\Delta p'}{\rho}}} \quad (2.23)$$

The authors tested the nozzle at different operating conditions to observe the effects on the discharge coefficient. The influence of different flow conditions through the nozzle have a great impact on the discharge coefficient value.

In [113] it is shown experimentally that upstream flow disturbance and pressure drop have an important impact on discharge coefficient values of a standard orifice in incompressible flow. The effects of flow disturbance are shown in Figure 2.15 for a standard orifice in incompressible flow. In Figure 2.15 the discharge coefficient is plotted against the ratio between the distance to disturbance obstacle and pipe diameter for standard ('ST') and perforated orifices ('P'). It can be observed that the discharge coefficient is not constant and does not present any clear trend with porosity ratio (area of the orifice divided by the area of the pipe, defined by β). The same effects can appear in a compressible flow case. For that reason it is necessary for a proper estimation of the discharge coefficient of turbocharger valves to consider the effects in real operation.

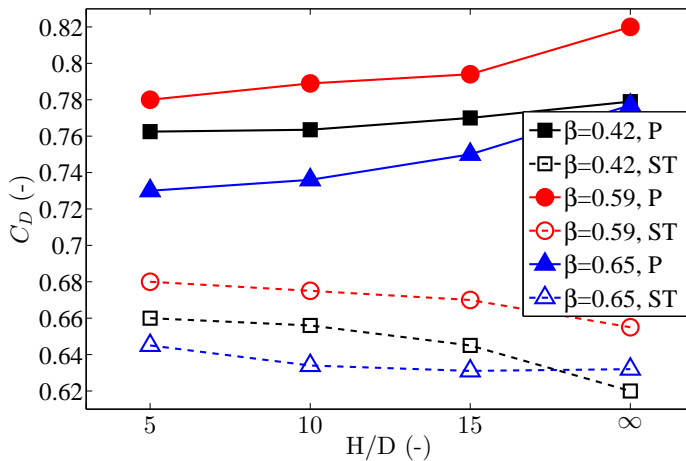


Figure 2.15: Effect of the obstacle disturbance on the discharge coefficient [113]

2.5 References

- [1] F. Payri, P. Olmeda, F. Arnau, A. Dombrovsky, and L. Smith. “External heat losses in small turbochargers: Model and experiments”. In: *Energy* 71 (2014), pp. 534–546. ISSN: 0360-5442. DOI: 10.1016/j.energy.2014.04.096 (cit. on pp. vii, 27, 60).
- [2] J. R. Serrano, P. Olmeda, F. Arnau, A. Dombrovsky, and L. Smith. “Analysis and Methodology to Characterize Heat Transfer Phenomena in Automotive Turbochargers”. In: *J. Eng. Gas Turbines Power* 137 (7) (2014). DOI: 10.1115/1.4028261 (cit. on pp. vii, 15, 55, 150, 160, 165).
- [18] M. Padzillah, S. Rajoo, and R. Martinez-Botas. “Influence of speed and frequency towards the automotive turbocharger turbine performance under pulsating flow conditions”. In: *Energy Conversion and Management* 80 (2014), pp. 416–428. DOI: 10.1016/j.enconman.2014.01.047 (cit. on pp. 5, 35).
- [19] R. Burke, C. Vagg, D. Chalet, and P. Chesse. “Heat transfer in turbocharger turbines under steady, pulsating and transient conditions”. In: *International Journal of Heat and Fluid Flow* 52 (2015), pp. 185–197. DOI: 10.1016/j.ijheatfluidflow.2015.01.004 (cit. on pp. 5, 31).
- [21] M. Barratta and E. Spessa. *Numerical Simulation Techniques for the Prediction of Fluid-Dynamics, Combustion and Performance in IC Engines Fuelled by CNG*. Computational Simulations and Applications, InTech, Dr. Zhu Jianping (Ed.), 2011. DOI: 10.5772/25081 (cit. on pp. 5, 15).
- [26] Miguel Ángel Reyes-Belmonte. “Contribution to the Experimental Characterization and 1-D Modelling of Turbochargers for IC Engines”. PhD thesis. Universitat Poliècnica de València, 2013 (cit. on pp. 6, 26, 51, 52, 60, 66, 89, 91, 94, 98, 114, 145, 151, 153, 190).
- [28] J. Serrano, P. Olmeda, A. Páez, and F. Vidal. “An experimental procedure to determine heat transfer properties of turbochargers”. In: *Measurement Science and Technology* 21.3 (2010). DOI: 10.1088/0957-0233/21/3/035109 (cit. on pp. 7, 27, 52, 54, 89).
- [29] J. R. Serrano, P. Olmeda, A. Tiseira, L. M. García-Cuevas, and A. Lefebvre. “Theoretical and experimental study of mechanical losses in automotive turbochargers”. In: *Energy* 55 (2013), pp. 888–898. DOI: 10.1016/j.energy.2013.04.042 (cit. on pp. 8, 27).
- [30] N. Watson and M. Janota. *Turbocharging the Internal Combustion Engine*. Macmillan Publishers, Ltd., 1982 (cit. on pp. 15, 18, 32, 113, 122, 123).

- [31] J. Bohbot, C. Chryssakis, and M. Miche. "Simulation of a 4-Cylinder Turbocharged Gasoline Direct Injection Engine Using a Direct Temporal Coupling Between a 1D Simulation Software and a 3D Combustion Code". In: *SAE Technical Paper 2006-01-3263* (2006) (cit. on p. 15).
- [32] O. Vitek, J. Macek, and M. Polásek. "New Approach to Turbocharger Optimization using 1-D Simulation Tools". In: *SAE Technical Paper 2006-01-0438* (2006) (cit. on p. 15).
- [33] M. Jung, R. G. Ford, K. Glover, N. Collings, U. Christen, and M. J. Watts. "Parameterization and Transient Validation of a Variable Geometry Turbocharger for Mean-Value Modeling at Low and Medium Speed-Load Points". In: *SAE Technical Paper 2002-01-2729* (2002) (cit. on p. 15).
- [34] P. Shah and C. Tan. "Effect of Blade Passage Surface Heat Extraction on Axial Compressor Performance". In: *Journal of Turbomachinery* 129 (2007) (cit. on p. 15).
- [35] F. Westin, J. Rosenqvist, and H.-E. Ångström. "Heat Losses from the Turbine of a Turbocharged SI-Engine - Measurements and Simulation". In: *SAE Technical Paper* (2004) (cit. on p. 16).
- [36] B. Sirakov and M. Casey. "Evaluation of Heat Transfer Effects on Turbocharger Performance". In: *ASME Journal of Turbomachinery* 135.2 (2012), p. 021011. DOI: 10.1115/1.4006608 (cit. on p. 16).
- [37] A. Romagnoli and R. Martinez-Botas. "Heat transfer analysis in a turbocharger turbine: An experimental and computational evaluation". In: *Applied Thermal Engineering* 38 (2012), pp. 58–77. DOI: 10.1016/j.applthermaleng.2011.12.022 (cit. on pp. 16, 17, 24).
- [38] H. Aghaali, H.-E. Ångström, and J. R. Serrano. "Evaluation of different heat transfer conditions on an automotive turbocharger". In: *International Journal of Engine Research* 16.2 (2015), pp. 137–151. DOI: 10.1177/1468087414524755 (cit. on pp. 16, 25).
- [39] M. V. Casey and T. M. Fesich. "The Efficiency of Turbocharger Compressors With Diabatic Flows". In: *Journal of Engineering for Gas Turbines and Power* 132 (7) (2012), p. 072302. DOI: 10.1115/1.4000300 (cit. on pp. 16, 17).
- [40] S. Shaaban and J. Seume. "Analysis of Turbocharger Non-Adiabatic Performance". In: *8th International Conference on Turbochargers and Turbocharging*. Woodhead Publishing, 2006. ISBN: 978-1-84569-174-5 (cit. on p. 18).
- [41] A. Diango, C. Perilhon, G. Descombes, and E. Danho. "Application of exergy balances for the optimization of non-adiabatic small turbomachines operation". In: *Energy* 36 (2011) (cit. on p. 18).

- [42] A. Diango, C. Perilhon, E. Danho, and G. Descombes. “Influence of Heat Transfer on Gas Turbine Performance”. In: *Advances in Gas Turbine Technology* (2011) (cit. on p. 18).
- [43] J. R. Serrano, P. Olmeda, F. Arnau, M. Reyes-Belmonte, and A. Lefebvre. “Importance of Heat Transfer Phenomena in Small Turbochargers for Passenger Car Applications”. In: *SAE Int. J. Engines* 6.2 (2013), pp. 716–728. DOI: 10.4271/2013-01-0576 (cit. on p. 19).
- [44] A. Sidorow, R. Isermann, F. Cianflone, and G. Landsmann. “Comparison of a turbocharger model based on isentropic efficiency maps with a parametric approach based on Euler’s turbo-machinery equation”. In: *18th IFAC World Congress*. 2011 (cit. on pp. 20, 21).
- [45] D. Lückmann, C. Schernus, T. Uhlmann, B. Höpke, and C. Nebbia. “Friction and Heat Transfer Effects on Turbocharger Modeling”. In: *GT 2012 Conference*. 2012 (cit. on p. 20).
- [46] D. Porzig, H. Raetz, H. Schwarze, and J. Seume. “Thermal analysis of small high-speed floating-ring journal bearings”. In: *11th International Conference on Turbochargers and Turbocharging*. Woodhead Publishing, 2014. ISBN: 978-0-08-100033-5 (cit. on p. 22).
- [47] D. Bohn, N. Moritz, and M. Wolff. “Conjugate Flow and Heat Transfer Investigation of a Turbo Charger: Part II — Experimental Results”. In: *Proceedings of ASME Turbo Expo*. Vol. 3. ASME, 2003, pp. 723–729. DOI: 10.1115/GT2003-38449 (cit. on pp. 22, 98, 139, 164).
- [48] B. Lüddecke, D. Filsinger, and M. Bargende. “On wide mapping of a mixed flow turbine with regard to compressor heat flows during turbocharger testing”. In: *10th International Conference on Turbochargers and Turbocharging*. Woodhead Publishing, 2012. ISBN: 978-0-85709-209-0 (cit. on pp. 22, 25).
- [49] S. Marelli, G. Marmorato, M. Capobianco, and A. Rinaldi. “Heat Transfer Effects on Performance Map of a Turbocharger Compressor for Automotive Application”. In: *SAE Technical Paper 2015-01-1287* (2015) (cit. on p. 22).
- [50] M. Schinnerl, J. Seume, J. Ehrhard, and M. Bogner. “Heat Transfer Correction Methods for Turbocharger Performance Measurements”. In: *Proceedings of ASME Turbo Expo*. 2016 (cit. on pp. 22–24).
- [51] M. Muqem, M. Ahmad, and A. Sherwani. “Turbocharging of Diesel Engine for Improving Performance and Exhaust Emissions A Review”. In: *IOSR Journal of Mechanical and Civil Engineering* (2015) (cit. on p. 23).

- [52] S. Shaaban and J. Seume. “Impact of Turbocharger Non-Adiabatic Operation on Engine Volumetric Efficiency and Turbo Lag”. In: *International Journal of Rotating Machinery* (2012) (cit. on p. 24).
- [53] M. Cormerais, J. F. Hetet, P. Chesse, and A. Maiboom. “Heat Transfer Analysis in a Turbocharger Compressor Modeling and Experiments”. In: *SAE Technical Paper* (2006) (cit. on p. 24).
- [54] A. Romagnoli and R. Martinez-Botas. “Heat Transfer in an Automotive Turbocharger Under Constant Load Points: an Experimental and Computational Investigation”. In: *The 4th International Symposium on Fluid Machinery and Fluid Engineering* November 24-27, 2008, Beijing, China (2008) (cit. on pp. 24, 30).
- [55] H. Aghaali and H.-E. Ångström. “Temperature Estimation of Turbocharger Working Fluids and Walls under Different Engine Loads and Heat Transfer Conditions”. In: *SAE Technical Paper 2013-24-0123* (2013). DOI: 710 .4271/2013-24-0123 (cit. on pp. 24, 25, 30).
- [56] D. Bohn, T. Heuer, and K. Kusterer. “Conjugate Flow and Heat Transfer Investigation of a Turbo Charger”. In: *J. Eng. Gas Turbines Power* 127 (2005) (cit. on p. 25).
- [57] D. Bohn, T. Heuer, and K. Kusterer. “Conjugate Flow and Heat Transfer Investigation of a Turbo Charger: Part I — Numerical Results”. In: *Proceedings of ASME Turbo Expo*. ASME, 2003. DOI: 10.1115/GT2003-38449 (cit. on p. 25).
- [58] R. D. Burke, C. Copeland, T. Duda, and M. A. Reyes-Belmonte. “Lumped Capacitance and 3D CFD Conjugate Heat Transfer Modelling of an Automotive Turbocharger”. In: *Proceedings of ASME Turbo Expo*. 2015 (cit. on p. 25).
- [59] H. Aghaali. “On-Engine Turbocharger Performance Considering Heat Transfer”. PhD thesis. Royal Institute of Technology, 2012 (cit. on p. 25).
- [60] H. Aghaali and H.-E. Ångström. “Improving Turbocharged Engine Simulation by Including Heat Transfer in the Turbocharger”. In: *SAE Technical Paper 2012-01-0703* (2012) (cit. on p. 25).
- [61] S. Shaaban, J. Seume, R. Berndt, H. Pucher, and H. Linnhoff. “Part-load Performance Prediction of Turbocharged Engines”. In: *8th International Conference on Turbochargers and Turbocharging*. Woodhead Publishing, 2006. ISBN: 978-1-84569-174-5 (cit. on p. 25).

- [62] M. Cormerais, J. F. Hetet, P. Chesse, and A. Malboom. “Heat transfers characterisations in a variable geometry turbocharger: experiments and correlations”. In: *Proceedings of Spring Technical Conference of the ASME Internal Combustion Engine Division* (2006), pp. 53 –64 (cit. on pp. 26, 70, 161).
- [63] M. Cormerais, P. Chesse, and J. F. Hetet. “Turbocharger heat transfer modeling under steady and transient conditions”. In: *International Journal of Thermodynamics* 12.4 (2010), pp. 193 –202 (cit. on pp. 26, 162).
- [64] J. Serrano, F. Arnau, R. Novella, and M. Reyes-Belmonte. “A Procedure to Achieve 1D Predictive Modeling of Turbochargers under Hot and Pulsating Flow Conditions at the Turbine Inlet”. In: *SAE Technical Paper 2014-01-1080* (2014) (cit. on p. 26).
- [65] F. Incropera, D. DeWitt, T. Bergman, and A. Lavine. *Fundamentals of Heat and Mass Transfer*. John Wiley & Sons, 2007 (cit. on pp. 26, 98, 101, 110).
- [66] J. R. Serrano, P. Olmeda, F. J. Arnau, M. A. Reyes-Belmonte, and H. Tartoussi. “A study on the internal convection in small turbochargers. Proposal of heat transfer convective coefficients”. In: *Applied Thermal Engineering* 89 (2015), pp. 587 –599. ISSN: 1359-4311 (cit. on pp. 26, 91).
- [67] S. Lavagnoli, G. Paniagua, C. D. Maesschalck, and T. Yasa. “Analysis of the Unsteady Overtip Casing Heat Transfer in a High Speed Turbine”. In: *Journal of Turbomachinery* (2013) (cit. on p. 26).
- [68] R. D. Burke, P. Olmeda, F. J. Arnau, and M. A. Reyes-Belmonte. “Modelling of turbocharger heat transfer under stationary and transient engine operating conditions”. In: *11th International Conference on Turbochargers and Turbocharging*. 2014 (cit. on p. 26).
- [69] P. Olmeda, V. Dolz, F. Arnau, and M. Reyes-Belmonte. “Determination of heat flows inside turbochargers by means of a one dimensional lumped model”. In: *Mathematical and Computer Modelling* 57.7 - 8 (2013), pp. 1847 –1852. ISSN: 0895-7177. DOI: 10.1016/j.mcm.2011.11.078 (cit. on pp. 26, 91).
- [70] P. Olmeda, A. Tiseira, V. Dolz, and L. García-Cuevas. “Uncertainties in power computations in a turbocharger test bench”. In: *Measurement* 59.0 (2015), pp. 363 –371. ISSN: 0263-2241. DOI: 10.1016/j.measurement.2014.09.055 (cit. on p. 27).

- [71] N. Baines, K. D. Wygant, and A. Dris. “The Analysis of Heat Transfer in Automotive Turbochargers”. In: *Journal of Engineering for Gas Turbines and Power* 132.4 (2010), p. 042301. DOI: 10.1115/1.3204586 (cit. on pp. 27, 138, 168).
- [72] S. Shaaban. “Experimental Investigation and Extended Simulation of Turbocharger non-adiabatic performance”. PhD thesis. Universität Hannover, 2004 (cit. on p. 27).
- [73] R. D. Burke. “Analysis and Modeling of the Transient Thermal Behavior of Automotive Turbochargers”. In: *J. Eng. Gas Turbines Power* 136 (2014) (cit. on p. 27).
- [74] H. Tadesse, C. Rakut, M. Diefenthal, M. Wirsum, and T. Heuer. “Experimental Investigation of Steady State and Transient Heat Transfer in a Radial Turbine Wheel of a Turbocharger”. In: *Proceedings of ASME Turbo Expo*. 2015 (cit. on pp. 27, 28).
- [75] I. A. Mohd, S. Rajoo, and A. N. Darus. “Heat Distribution Study on Turbocharger Turbine’s Volute”. In: *Jurnal Mekanikal* 35 (2012), pp. 63–81 (cit. on p. 28).
- [76] F. Hellstrom and L. Fuchs. “Heat transfer effects on the performance of a radial turbine working under pulsatile flow conditions”. In: *48th AIAA Aerospace Sciences Meeting* (2010) (cit. on p. 28).
- [77] F. Bet and G. Seider. “Thermal Management of a Turbocharger for Unsteady Operation”. In: *STAR European Conference Noordwijk, March 22- 23*. 2011 (cit. on p. 29).
- [78] M. Diefenthal, H. Tadesse, C. Rakut, M. Wirsum, and T. Heuer. “Experimental and Numerical Investigation of Temperature Fields in a Radial Turbine Wheel”. In: *Proceedings of ASME Turbo Expo*. 2014 (cit. on p. 29).
- [79] M. Diefenthal, C. Rakut, H. Tadesse, and M. Wirsum. “Temperature Distribution in a Radial Turbine Wheel During Transient Operation”. In: *MTZ worldwide* 76.9 (2015), pp. 50–55. ISSN: 2192-9114 (cit. on p. 29).
- [80] L. Gu, A. Zemp, and R. S. Abhari. “Numerical study of the heat transfer effect on a centrifugal compressor performance”. In: *Proc IMechE Part C: Journal Mechanical Engineering Science* 229.12 (2015), pp. 2207–2220 (cit. on p. 29).
- [81] T. Heuer, B. Engels, and P. Wollscheid. “Thermomechanical Analysis of a Turbocharger Based on Conjugate Heat Transfer”. In: *Proceedings of ASME Turbo Expo*. 2005 (cit. on pp. 29, 30).

- [82] T. Verstraete, Z. Alsalihi, and R. A. V. den Braembussche. “Numerical Study of the Heat Transfer in Micro Gas Turbines”. In: *Journal of Turbomachinery* 129 (2007) (cit. on p. 29).
- [83] A. Yamagata, S. Nagai, K. Nakano, and T. Kawakubo. “Prediction and measurement of Turbocharger compressor wheel temperature”. In: *8th International Conference on Turbochargers and Turbocharging*. Woodhead Publishing, 2006. ISBN: 978-1-84569-174-5 (cit. on p. 30).
- [84] P. Chesse, D. Chalet, and X. Tauzia. “Impact of the heat transfer on the performance calculations of automotive turbocharger compressor”. In: *Oil & Gas Science and Technology Rev. IFP Energies nouvelles* 66.5 (2011), pp. 791–800. DOI: 10.2516/ogst/2011129 (cit. on p. 30).
- [85] R. D. Burke, C. D. Copeland, and T. Duda. “Investigation into the assumptions for lumped capacitance modelling of turbocharger heat transfer”. In: *6th International conference on simulation and testing 2014-05-15 - 2014-05-16, Berlin*. 2014 (cit. on pp. 31, 32).
- [86] H Moustapha, M Zelesky, N Baines, and D Japikse. *Axial and radial turbines*. Concepts NREC, Vermont, 2003 (cit. on pp. 32, 113).
- [87] H Hiereth, K Drexl, and P Prenninger. *Charging the internal combustion engine*. Springer, 2007 (cit. on pp. 32, 113).
- [88] G. Martin, P. H. C. Caillol, and V. Talon. “Implementing turbomachinery physics into data map-based turbocharger models”. In: *SAE technical paper 2009-01-0310* (2009) (cit. on p. 32).
- [89] J. R. Serrano, A. O. Tiseira, L. M. García-Cuevas, L. B. Inhestern, and H. Tartoussi. “Radial Turbine Performance Measurement Under Extreme Off-Design Conditions”. In: *Submitted to Energy* () (cit. on pp. 33, 147, 192).
- [90] J. Galindo, J. R. Serrano, C. Guardiola, and C. Cervelló. “Surge limit definition in a specific test bench for the characterization of automotive turbochargers”. In: *Experimental Thermal and Fluid Science* 30.5 (2006), pp. 449–462. ISSN: 0894-1777. DOI: 10.1016/j.expthermflusci.2005.06.002 (cit. on p. 33).
- [91] A. Romagnoli and R. Martinez-Botas. “Performance prediction of a nozzleed and nozzleless mixed-flow turbine in steady conditions”. In: *International Journal of Mechanical Sciences* 53.8 (2011), pp. 557–574. ISSN: 0020-7403. DOI: 10.1016/j.ijmecsci.2011.05.003 (cit. on p. 33).
- [92] N. Baines. “A meanline prediction method for radial turbine efficiency”. In: *In: 6th International conference on turbocharging and air management systems. Proc. IMechE* C554-6 (1998), pp. 315–325 (cit. on p. 33).

- [93] R. Dambach and H. Hodson. “Tip leakage flow: a comparison between small axial and radial turbines”. In: *IMechE Sym S 767* (2000) (cit. on p. 33).
- [94] F. Payri, J. R. Serrano, P. Fajardo, M. A. Reyes-Belmonte, and R. Gozalbo-Belles. “A physically based methodology to extrapolate performance maps of radial turbines”. In: *Energy Conversion and Management* 55.0 (2012), pp. 149–163. ISSN: 0196-8904 (cit. on pp. 33, 113, 116, 118, 119, 121, 123).
- [95] L. Eriksson. “Modeling and control of turbocharged SI and DI engines”. In: *Oil Gas Sci Technology-Revue de l’IFP* 62(4) (2007), pp. 523–538 (cit. on p. 33).
- [96] M. Canova. “Development and validation of a control-oriented library for the simulation of automotive engines”. In: *Int J Engine Res* 5(3) (2004), pp. 219–228 (cit. on p. 33).
- [97] X. Fang and Q. Dai. “Modeling of turbine mass flow rate performances using the Taylor expansion”. In: *Applied Thermal Engineering* 30.13 (2010), pp. 1824–1831. ISSN: 1359-4311. DOI: 10.1016/j.applthermaleng.2010.04.016 (cit. on p. 33).
- [98] F. Bozza and V. D. Bellis. “Steady Modeling of a Turbocharger Turbine for Automotive Engines”. In: *J. Eng. Gas Turbines Power* 136 (2014) (cit. on p. 34).
- [99] G. Sieros, A. Stamatis, and K. Mathioudakis. “Jet Engine Component Maps for Performance Modeling and Diagnosis”. In: *Journal of Propulsion and Power* 13.5 (1997) (cit. on p. 34).
- [100] W. Zhuge, Y. Zhang, X. Zheng, M. Yang, and Y. He. “Zhuge W.-Development of an advanced turbocharger simulation method for cycle simulation of turbocharged internal combustion engines”. In: *Proc. IMechE Part D: J. Automobile Engineering* 223 (2009) (cit. on p. 34).
- [101] S. Zhu, K. Deng, and S. Liu. “Modeling and extrapolating mass flow characteristics of a radial turbocharger turbine”. In: *Energy* 87 (2015), pp. 628–637. ISSN: 0360-5442. DOI: 10.1016/j.energy.2015.05.032 (cit. on p. 34).
- [102] N. Baines. “Radial Turbines: An Integrated Design Approach”. In: *Proceedings of the 6th European Turbomachinery Conference, Lille, France, 2005* (cit. on p. 34).

- [103] M. Chiong, S. Rajoo, A. Romagnoli, A. Costall, and R. Martinez-Botas. “Integration of meanline and one-dimensional methods for prediction of pulsating performance of a turbocharger turbine”. In: *Energy Conversion and Management* 81 (2014), pp. 270–281. ISSN: 0196-8904. DOI: 10.1016/j.enconman.2014.01.043 (cit. on pp. 34, 35).
- [104] M. Chiong, S. Rajoo, A. Romagnoli, A. Costall, and R. Martinez-Botas. “Non-adiabatic pressure loss boundary condition for modelling turbocharger turbine pulsating flow”. In: *Energy Conversion and Management* 93 (2015), pp. 267–281. ISSN: 0196-8904. DOI: 10.1016/j.enconman.2014.12.058 (cit. on p. 34).
- [105] J. Macek, Z. Zak, and O. Vitek. “Physical Model of a Twin-scroll Turbine with Unsteady Flow”. In: *SAE Technical Paper 2015-01-1718* (2015). DOI: 10.4271/2015-01-1718 (cit. on p. 34).
- [106] M. Gugau and H. Roclawski. “On the Design and Matching of Turbocharger Single Scroll Turbines for Pass Car Gasoline Engines”. In: *J. Eng. Gas Turbines Power* 136.12 (2014). DOI: 10.1115/1.4027710 (cit. on p. 35).
- [107] D. Palfreyman and R. Martinez-Botas. “The pulsating flow field in a mixed flow turbocharger turbine: an experimental and computational study”. In: *Proceedings of the ASME Turbo Expo 2004* (2004), pp. 697–708 (cit. on p. 35).
- [108] C. Avola, C. Copeland, T. Duda, R. Burke, S. Akehurst, and C. Brace. “Review of Turbocharger Mapping and 1D Modelling Inaccuracies with Specific Focus on Two-Stag Systems”. In: *SAE Technical Paper 2015-24-2523* (2015) (cit. on p. 35).
- [109] O. Weber, R. Christmann, V. Gauckler, and R. Sauerstein. “R2S™ - modelling and consequences for the boost control”. In: *10th International Conference on Turbochargers and Turbocharging*. Woodhead Publishing, 2012 (cit. on pp. 35, 36).
- [110] J. B. Heywood. *Internal Combustion Engines Fundamentals*. McGraw-Hill, 1988 (cit. on p. 35).
- [111] J. F. Douglas, J. M. Gasiorek, and J. A. Swaffield. *Fluid Mechanics*. Pearson Education Limited., 2005 (cit. on p. 36).
- [112] M. Halder, S. Dash, and S. Som. “A numerical and experimental investigation on the coefficients of discharge and the spray cone angle of a solid cone swirl nozzle”. In: *Experimental Thermal and Fluid Science* 28.4 (2004), pp. 297–305. ISSN: 0894-1777 (cit. on p. 36).

- [113] S. Huang, T. Ma, D. Wang, and Z. Lin. “Study on discharge coefficient of perforated orifices as a new kind of flowmeter”. In: *Experimental Thermal and Fluid Science* 46 (2013), pp. 74 –83 (cit. on p. 37).

Experimental Analysis

Contents

3.1	Introduction	51
3.2	Themohydraulic test bench	52
3.3	Gas stand	55
	Uncertainty analysis	57
	Tests methodology	58
	Heat transfer characterization tests	59
	Friction losses characterization tests	61
	By-pass and waste-gate valves flow characterisation	62
	Extension of compressor heat transfer correlation	66
	Tests results analysis	70
3.4	Engine test bench	77
	Tests methodology (swept volume emulation)	79
	Engine characterization tests	80
	Tests results	82
3.5	References	84

Figures

3.1	Turbocharger geometry simplification	52
3.2	Thermohydraulic test bench layout	54
3.3	Gas stand layout	56
3.4	Gas stand layout	57
3.5	Detail of wall thermocouple installation	60
3.6	Wall thermocouples installed on a turbocharger	61

3.7	Two stage turbocharging system installed in the test bench.	63
3.8	Measured and interpolated mass flow on LPT map	65
3.9	Schematic of thermocouples installation and fluids distribution in the LPC	67
3.10	Location of the drills for thermocouples installation in LPC volute	68
3.11	Measured points for convection correlations characterization . . .	69
3.12	Comparison of pressure ratio measured at hot insulated conditions versus measurements at adiabatic conditions. Turbocharger without water cooling (T#2)	71
3.13	Comparison of compressor efficiency measured at hot insulated conditions versus efficiency measured at adiabatic conditions. Water-cooled turbocharger (T#1)	72
3.14	Comparison of compressor efficiency measured at hot insulated conditions versus efficiency measured at adiabatic conditions. Non water-cooled turbocharger (T#2)	73
3.15	Comparison of hot insulated measurements of turbine mass flow with adiabatic measurements (T#2)	74
3.16	Comparison of hot insulated measured TDE with adiabatic measurements (T#2)	75
3.17	Comparison of hot insulated measured ETE with adiabatic measurements (T#2)	76
3.18	Comparison of hot insulated measured ETE/TDE with adiabatic measurements (T#2)	76
3.19	Layout of the engine test cell	78
3.20	Flow coefficients of the intake and exhaust valves	81
3.21	RoHR during acceleration for T#1 (left) and T#2 (right)	82
3.22	In-cylinder conditions at EVO for T#1 (left) and T#2 (right)	82
3.23	Engine torque at steady conditions. Left: T#1, Right: T#2	83
3.24	Compressor outlet conditions. Left: T#1, Right: T#2	83
3.25	Turbine inlet conditions. Left: T#1, Right: T#2	84
3.26	Turbocharger speed. Left: T#1, Right: T#2	84

3.1 Introduction

In this thesis an important effort in measuring different turbocharger variables has been made. The experimental results of this chapter are crucial for the model validation that will be described in chapter 5. Measurements in gas stand and engine test bench have been performed in different configurations. In addition, thermohydraulic test bench tests have been performed for conductive heat transfer characterisation.

The gas stand has been traditionally used to measure turbine and compressor performance in hot or cold conditions. As it was discussed in the previous chapter, the performance is usually given in maps providing reduced or corrected mass flow and speed as well as total to total or total to static pressure ratio and efficiency. However, in order to refine the prediction of one-dimensional turbocharger and engine models, it is not sufficient with the information of the standard maps. In order to define proper testing methodologies it is necessary to take into account the following aspects:

- Distinguish the pure adiabatic behaviour from the non-adiabatic behaviour of compressor and turbine.
- Characterise the turbocharger mechanical losses.
- Characterise the flow in the waste-gate or by-pass valves of the turbocharger.
- Characterise the internal heat transfer between the different fluids and the turbocharger walls.
- Characterise the external heat transfer between the ambient and turbocharger walls.

The different experimental approaches described in this chapter contribute to a better characterisation and understanding of these aspects. Furthermore, the experimental information is used in the thesis in order to build more precise turbocharger models. An analysis of the pure experimental results will also be described in this chapter.

The database of available turbochargers from the previous work done by Reyes [26] has been extended with the analysis and measurement of two additional turbochargers and a two stage turbocharging system. The first two of these four additional turbochargers have been tested in an engine test bench, in the thermohydraulic test bench and in the gas stand. The two turbochargers of the two stage system have been only tested in the gas stand at certain points corresponding to full load engine operation. In Table 3.1 the main characteristics of the turbochargers that have been analysed in this thesis are presented. In

addition, the tests benches in which each turbocharger has been tested are presented. The acronyms used in Table 3.1 correspond to the geometric definitions of Figure 3.1. The turbochargers measured in this thesis correspond to the turbochargers T#1 to T#4 (both included) from Table 3.1 and the remaining turbochargers correspond to the previous work done by Reyes [26]. Therefore, in this thesis the turbocharger database has been extended with measurements of four additional turbochargers and the information of the new database has been used for the development of the models and for analysis.

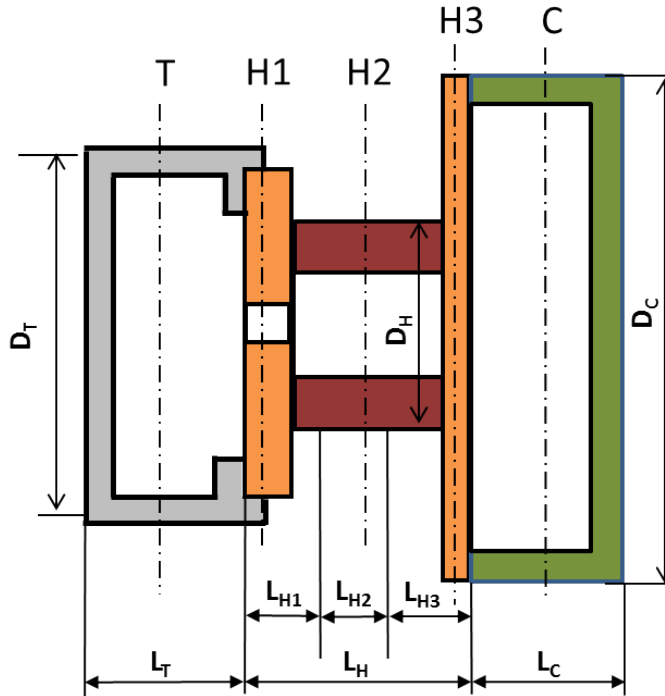


Figure 3.1: Turbocharger geometry simplification

3.2 Themohydraulic test bench

In the thermohydraulic test rig an incompressible fluid is passed through the turbocharger in order to determine metal conductance and an initial estimation of thermal capacitances [28]. An incompressible fluid is chosen to avoid fluid expansion, so measured temperature variations are only due to heat transfer. The selected incompressible fluid was thermal oil due to its thermal properties and the simplicity to measure mass flow and detect possible leakages.

Table 3.1: Turbochargers characteristics (a sketch of geometrical acronyms is shown in Figure 3.1)

Turbocharger	T#1	T#2	T#3	T#4	T#5	T#6	T#7
Engine displacement (l)	2.0	1.6	2.0	2.0	1.6	2.0	1.2
Engine type	diesel	diesel	diesel	diesel	petrol	diesel	petrol
Comp. wheel diam. (mm)	49	46	65	30	40	48.5	40
Turb. wheel diam. (mm)	39	37.5	53	36	38	40	37.5
VGT	Yes	Yes	No	Yes	No	Yes	No
Water cooled?	Yes	No	Yes	No	No	Yes	Yes
DT (mm)	110	122	105	115	106	110	80
LT (mm)	75	70	40	42	40	70	30
DC (mm)	115	123	139	97	62	125	104
LC (mm)	35	32	44	36	34	30	27
DH (mm)	60	70	59	36	51	60	57
LH (mm)	30	31	41	31	37	30	35
Gas Stand?	Yes	Yes	Yes	Yes	No	Yes	Yes
Engine bench?	Yes	Yes	No	No	No	No	No
Thermohydraulic bench?	Yes	Yes	No	No	Yes	Yes	Yes

A schematic view of the test rig is shown in Figure 3.2. As it is observed the turbocharger unit was placed in the centre of the installation and it was connected to two different oil circuits. There was a high temperature circuit and a low temperature circuit. On one hand, the heat source in the high temperature circuit was provided by three electrical resistances (12.5 kW of nominal power each of them) to a heat transmitter fluid (thermal oil). On the other hand, the heat drain system consisted of a low temperature oil circuit with an external heat exchanger, at which cold oil delivered its heat energy to a glycol-based coolant solution. Oil temperature and mass flow in both circuits can be varied in a wide range of operative conditions by using PID controllers and manual valves.

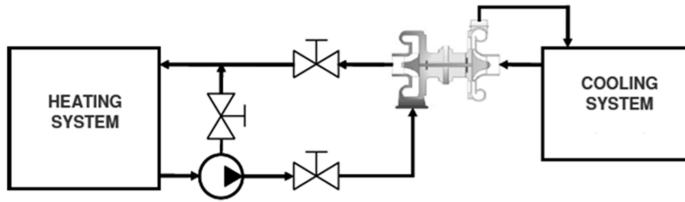


Figure 3.2: Thermohydraulic test bench layout

As it has been mentioned, metal nodes are connected by means of a conductive conductance $K_{i,j}$. The heat flow between two contiguous nodes can be calculated using Fourier's Law given in equation 3.1.

$$\dot{Q}_{i,j}^{cond.} = K_{i,j} \cdot (T_i - T_j) \quad (3.1)$$

It has been assumed that these conductances are constant for any operative condition; i.e. conductivity is constant with temperature.

The metal nodes temperatures have been measured at different positions along the turbocharger by means of K-type thermocouples fixed to the metal external surface. Three thermocouples were installed on each of the five planes of the lumped model at several azimuthal locations in order to check the assumption of negligible radial heat transfer.

Fluids temperature measurement was accomplished using RTDs due to their higher precision. Oil flow was measured by using two Coriolis flow meters (one for the high temperature oil circuit and the other for the low temperature oil circuit).

Two types of tests were performed at this rig: steady and transient. In both tests the turbocharger shaft is blocked and the absence of leakages and communication between circuits is granted. The initial quantification of the storage of energy by metal nodes and the calculation of conductive conductances is based on a correct combination of both types of tests [28].

3.3 Gas stand

The tests needed to characterise turbocharger performance and heat transfer have been performed in a gas stand. Several configurations for gas stands can be used. The main features are the possibility of generating hot or cold flow in the turbine, an independent lubrication system and sensors to measure turbocharger speed, pressure, temperature and mass flow of the different fluids at the inlet and outlet sections. It is also crucial to have the possibility of changing the outlet conditions of the compressor through a backpressure valve. In Figure 3.3 the layout of the first gas stand used in this thesis is shown. More details about this test bench can be found in [114] and [2]. The main features of this test cell are the following:

- A screw compressor with a maximum mass flow capacity of 0.2 kgs^{-1} , at a maximum discharging pressure of 3.5 bar (gauge), which provides the mass flow to the turbine.
- The mass flow is heated by five parallel tube-type electrical heaters. This system can reach up to 720 K at the maximum mass flow rate. This hot flow is collected in a plenum and conducted to the turbine inlet.
- After passing through the turbine, the air is cooled by means of a heat exchanger in order to allow the mass flow measurement by hot plate flow meter. All mass flow sensors in the facility have been previously calibrated.
- The compressor takes air from the atmosphere. The air passes first through a filter and then the flow rate is measured in a hot plate flow meter. Downstream of the compressor, there is a vortex type flow meter (with double check purpose) and an electronically driven backpressure valve to control compressor outlet pressure.
- An independent lubrication system is used to control oil flow rate, pressure and temperature. The oil mass flow rate is measured using a Coriolis flow meter. Lubrication inlet and outlet temperatures are measured by means of low uncertainty platinum resistance temperature detectors.
- An independent cooling system is used for water cooled turbochargers. The coolant mass flow rate is measured by means of a magnetic flow meter. Coolant inlet and outlet temperatures are measured by means of low uncertainty platinum resistance temperature detectors.
- Temperature and pressure sensors are installed on the inlet and the outlet pipes of the compressor and the turbine according to SAE J1723 [115] and SAE J1826 [116] standards.

3. EXPERIMENTAL ANALYSIS

- Compressor and turbine inlet and outlet pipes have been insulated using fibreglass in order to make the heat losses to the ambient negligible and ensure a more precise measurement of the temperatures at each stage.
- A rotary valve can be used to generate pulsating flow of given amplitude and frequency in turbine and/or compressor inlet.

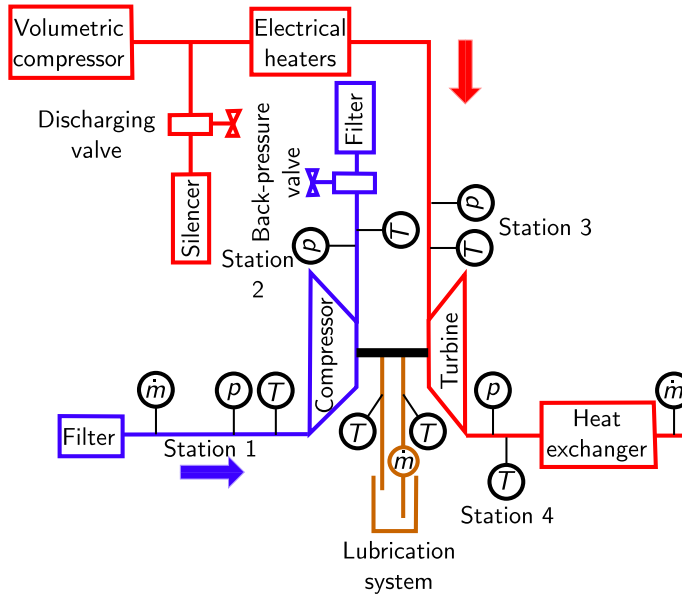


Figure 3.3: Gas stand layout

Table 3.2 shows the main characteristics of the employed sensors, indicating measurement range and uncertainty.

Table 3.2: Accuracies of measurement sensors

Variable	Sensor type	Accuracy
Gas pressure	Piezoresistive	± 2500 Pa
Gas and metal temperature	K-type thermocouple	± 2.2 K
Gas mass flow	V-cone	± 0.5 %
Oil pressure	Piezoresistive	± 2500 Pa
Oil temperature	RTD	± 0.15 K
Oil mass flow	Coriolis	± 0.1 %

Another gas stand with higher power output has been also used. The layout of the second gas stand is shown in Figure 3.4. It has similar capabilities making

possible the achievement of higher turbine inlet temperature and pressure so bigger turbochargers can be tested. Up to 5 bar pressures and 870 K temperatures at turbine inlet can be achieved in this facility. The following elements have been added in this gas stand in comparison with the first one in order to improve the quality of the measurement process:

- A heat exchanger to use the thermal energy of the hot gases of turbine outlet. In this way the gas arriving to the thermal resistances is hotter.
- A heat exchanger downstream the screw compressor is installed in order to cool the turbine inlet air below the operating temperature of the screw compressor. This element is useful for adiabatic testing.
- An intercooler is installed in the compressor circuit in order to control the compressor inlet temperature.

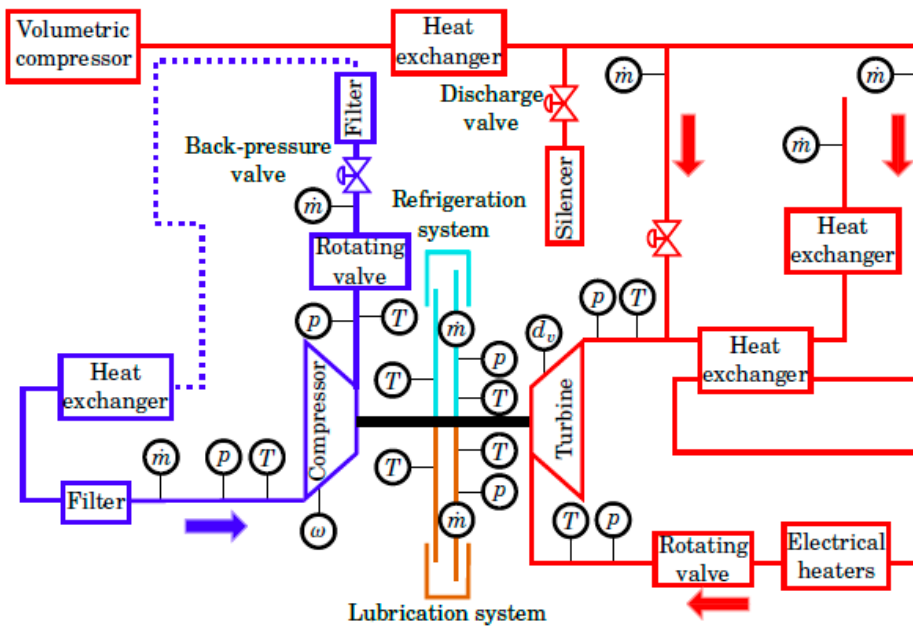


Figure 3.4: Gas stand layout

Uncertainty analysis

The uncertainty of a measurement is a parameter that characterises the dispersion of the values that could reasonably be attributed to the action of measuring.

As it has been proposed in [117] the uncertainty estimation can be evaluated by using a statistical analysis of series of observations and by other means, such as manufacturers data. In the case of the measurements of the current work both types of evaluations have been performed. On one hand, the standard deviation due to the repetitiveness of the measurement, u_a , is calculated using equation 3.2, where n is the number of measurements, \bar{x} is the arithmetical mean of these measurements and x_i the measurement. On the other hand, the standard deviation due to the inaccuracy of each sensor can be computed using manufacturer data of the probability distribution of the error or assuming uniform rectangular distribution of probability if only the limits of inaccuracy are given [117]. This last way has been used in this thesis and the standard deviation from the sensor manufacturer data, u_b , is calculated using equation 3.3. Uniform rectangular distribution of probability has been used, where a_- and a_+ are the lower and the upper limits of the sensor inaccuracy. Depending on the available information one of the ways of calculating the uncertainty has been used.

$$u_a = \sqrt{\frac{\sum_{i=1}^n (x_i - \bar{x})^2}{n - 1}} \quad (3.2)$$

$$u_b = \sqrt{\frac{(a_+ - a_-)^2}{12}} \quad (3.3)$$

Finally, the standard deviation that represents combined uncertainty, u_c is calculated using equation 3.4, where u represents one of the types of uncertainty calculations from equations 3.2 or 3.3. The combined uncertainty is used for variables that are calculated from several measured variables. It is necessary to compute the different derivatives, $\partial f / \partial x_i$, of the combined variable with respect to the different measured variables as shown in equation 3.4.

$$u_c = \sqrt{\sum_{i=1}^k \left(\frac{\partial f}{\partial x_i} \right)^2 \cdot u^2(x_i)} \quad (3.4)$$

Tests methodology

As it has been stated in the introduction, the proposed procedure must separate heat transfer from friction losses and from adiabatic efficiency of the turbomachine. To achieve that decomposition several types of tests must be carried out in the gas stand.

When the conductive conductances of the model are known and thermocouples are installed on turbocharger walls, convective heat flows can be calculated

for each measured point of the gas stand. This can be done performing an energy balance on the desired nodes when external heat fluxes are negligible (the turbocharger is thermally insulated). In that way it can be said that the turbocharger is a heat flux sensor.

For example, to calculate the heat flow in the turbine in hot insulated tests an energy balance on node 'T' (which represents the turbine casing) can be performed. Equation 3.5 is used for this calculation. If the conductive conductance between the turbine casing and the backplate ($K_{T/H1}$) is known (from thermohydraulic test bench) and node temperatures have been measured during the hot insulated tests, then the heat flow can be calculated. This heat flow can be used to correct the efficiency of the turbine according to Figure 2.3b, where point 30a can be calculated after subtracting heat from point 30.

$$\dot{Q}_{GAS/T} = K_{T/H1} \cdot (T_T - T_{H1}) \quad (3.5)$$

Similar calculations can be performed for air heat flow in the compressor and for the heat flow between oil and housing, performing the appropriate energy balances based on the nodes in which the heat transfer model is divided.

Heat transfer characterization tests

In order to characterize the different heat fluxes in the turbocharger during the measurements, the experimental approach must include at least the following tests:

- Hot tests where the turbocharger is insulated from the ambient (hot insulated tests).
- Hot tests without insulation on the turbocharger (hot exposed tests).
- Thermal transient tests.

The performance maps of the turbocharger are measured three times. First they are measured in hot insulated conditions and a second time in hot exposed conditions. In addition to these tests a third map measured in adiabatic conditions has been performed in order to make comparisons. In that way comparisons between the three different maps can be performed for the same turbocharger.

All the tests have been performed in steady flow conditions since it has been decided to avoid the more complex pulsating tests that are unnecessary to make comparisons between the different maps regarding heat transfer effects. The operative conditions of the test bench are chosen in order to obtain turbocharger performance maps at the highest turbine inlet temperature. In hot insulated tests external heat transfer is avoided (both convection and radiation)

by insulating the turbocharger from the ambient using glass wool. From these tests, the internal convective heat transfer between the working fluids and the turbocharger can be calculated as it was shown by Equation 3.5. In hot exposed tests the turbocharger is exposed to ambient. These tests are performed in order to estimate the external natural and forced convection and radiation heat transfer as proposed in [1] and will be explained in the following chapter.

In thermal transient tests the turbocharger is firstly thermally stabilized at a desired point without heating the air; i.e. the electrical heaters of the gas stand (see Figure 3.3) are switched off. Then the heaters are switched on and the additional energy accelerates the turbocharger increasing the rotational speed. After thermal stabilization is reached, which can take several hours, the heaters are switched off, the turbo decelerates and the initial stable point is obtained again. All the turbo variables are recorded during the process. These tests can be used to characterize thermal inertia of the different nodes of the heat transfer model.

As it was stated previously, thermocouples in turbocharger walls must be installed in order to have the possibility of measuring heat fluxes and wall temperatures on the turbocharger during the tests. For thermocouples installation it is important to have redundant measurements. As it has been stated in [26] the turbocharger heat distribution can be assumed as homogeneous in the radial plane. Therefore, different thermocouples at the same axial position and different radial positions must be used for each plane. The main reason for the redundancy is the delicate installation of these thermocouples.

These thermocouples are installed making small drills in the surface and introducing the thermocouple, covering it after that to fix it in place. Figure 3.5 shows how that installation is made, where the thermocouple and the external covering can be observed.

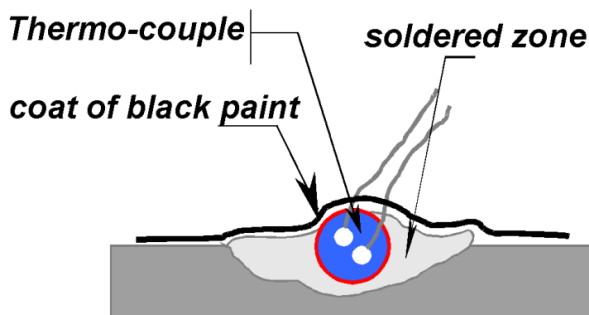


Figure 3.5: Detail of wall thermocouple installation

The final appearance of an instrumented turbocharger with wall thermocouples is shown in Figure 3.6. It can be observed that different axial sections

have been chosen in which three thermocouples for each section have been installed. In the processing of the experimental data the average value of the three radial thermocouples is taken for each node since it has been checked that the differences between them are small and that implies 1D behaviour.

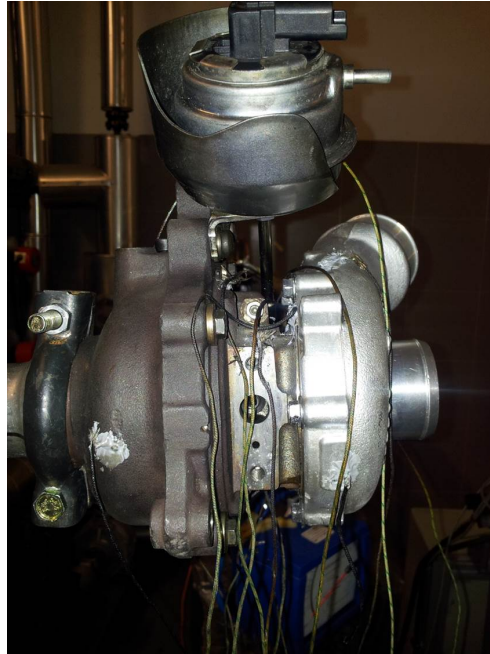


Figure 3.6: Wall thermocouples installed on a turbocharger

Friction losses characterization tests

For friction losses measurement and characterization adiabatic tests have been used. The procedure is based on the imposition of the compressor outlet temperature at the turbine inlet and oil inlet, minimizing in that way the heat flow across the turbocharger.

This procedure of testing the turbocharger is based on providing the lowest possible temperature gradients between its elements, thus minimizing the heat transfer between them. In that way the effects of heat transfer are avoided and purely adiabatic efficiencies can be computed. In addition, as the heat transfer to the oil is very small, the enthalpy of the oil represents only friction losses. Table 3.3 shows the mean differences between the turbine inlet and compressor outlet temperatures and the oil inlet temperature for a given turbocharger for a typical adiabatic test. The measurements performed go from 30 krpm to 190 krpm in steps of 20 krpm in compressor corrected speed for the tested

turbocharger between surge and choke. As it can be observed in Table 3.3, at minimum compression ratios (i.e. 30 krpm and 50 krpm), the adiabaticity is difficult to achieve as the temperatures are close to ambient conditions [118]. More details about the adiabatic measuring procedure can be found in the thesis of García-Cuevas [27]. The adiabatic measurement procedure achieves an experimental separation of mechanical losses from heat transfer.

Apart from measuring friction losses using adiabatic tests, getting the adiabatic efficiency of the turbomachinery is also possible with the data of these tests. It is important to state that adiabatic tests are not regular cold tests because specific conditions must be given (absence of heat flows along the turbocharger) to properly measure the adiabatic efficiency. The installation of wall thermocouples is recommended to compensate residual heat fluxes of difficult control in conventional gas stands.

Table 3.3: Temperature differences in adiabatic tests

n [rpm]	Toil,in [K]	T2-Toil,in [K]	T3-Toil,in [K]
30 000	297.0	-3.1	4.9
50 000	298.8	-0.2	0.8
70 000	3103	-1.7	4.3
90 000	321.2	0.6	1.0
110 000	343.7	-9.0	0.7
130 000	357.8	-1.7	1.5
150 000	379.0	3.1	2.0
170 000	400.2	3.6	1.4

By-pass and waste-gate valves flow characterisation

A two stage turbocharging system has been studied experimentally in the second gas stand that has been described above. In order to adapt this kind of systems to the different engine operating points turbocharger manufacturers make use of regulating valves. On one hand, a relatively large turbocharger is needed to provide appropriate nominal operating point of the engine. On the other hand to obtain higher torque at lower speeds a smaller turbine is needed since in that case the transient response is faster. The two stage system that has been studied in this section makes use of a by pass valve between the turbine stages in order to achieve both goals.

In Figure 3.7 the scheme of the turbocharging system as well as the installation of the system in the gas stand is shown. It can be observed that the system is composed of three control valves and a VGT actuator for the high pressure turbine. The by-pass valve is used to direct the flow directly to the low pressure turbine avoiding the high pressure turbine. The low pressure turbine

is regulated by a waste-gate valve. On the compressor side there is a check valve, i.e. a on/off valve that bypasses high pressure compressor when its outlet pressure is lower than the outlet pressure of the low pressure compressor. Since this last valve works by pressure a control unit in the gas stand is unnecessary.

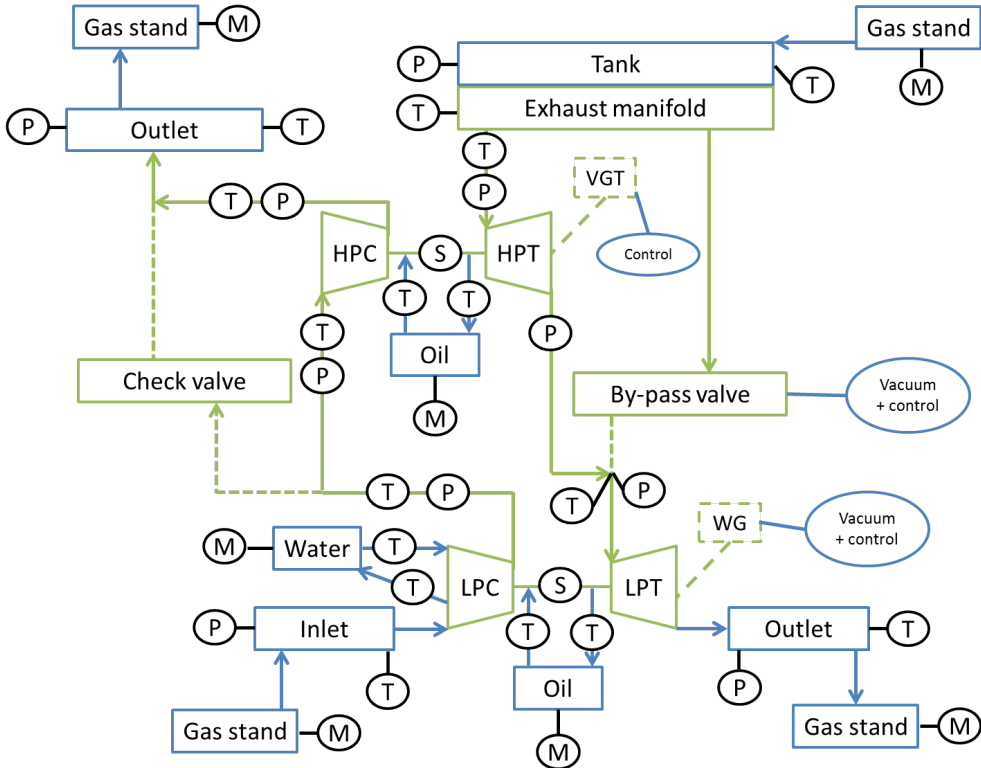


Figure 3.7: Two stage turbocharging system installed in the test bench.

In Figure 3.7 the measured variables and their position are also shown. The distribution of the sensors makes possible a comprehensive analysis of the valves since pressure and temperature variables are measured at the inlet and outlet of each stage. The test campaign of Table 3.4 has been designed to characterise the valves behaviour at full loads. has been performed. These points are based on the conditions of full load engine points. In the valve characterisation campaign five measurements with different turbine expansion ratios (from 1.5 to 4.5) have been performed (65 points). An additional test campaign has been performed to better characterise the waste-gate and the by-pass valves outside of the full load points range. These new points also allow to check if the trends of the previous measurements are followed by the new ones. The additional points are summarised in Table 3.5. Four different expansion ratios have been measured

for each proposed point.

The objective of these test campaigns is the characterisation of the discharge coefficient of the three valves. The geometrical area (A_{geom}) for each valve was obtained from the turbocharger CAD file for a maximum opening of each valve. The values are given in Table 3.6. Pressures at the inlet and outlet of each valve were obtained from the measurements. Inlet temperature was also obtained from the adequate sensor for each valve. Fluid properties are considered constant for a given temperature.

Table 3.4: Test campaign for valves characterisation at full load points

Point (-)	Waste gate valve (%)	By-pass valve (%)	Check valve (-)	Expansion Ratio (-)
1	92.6	0	Opened	1.5; 2.25; 3; 3.75; 4.5
2	93.5	35	Opened	1.5; 2.25; 3; 3.75; 4.5
3	94.1	73.6	Opened	1.5; 2.25; 3; 3.75; 4.5
3.1	94.1	75	Opened	1.5; 2.25; 3; 3.75; 4.5
3.2	94.1	80	Opened	1.5; 2.25; 3; 3.75; 4.5
3.3	94.1	90	Opened/ Closed	1.5; 2.25; 3; 3.75; 4.5
4	94.9	95	Closed	1.5; 2.25; 3; 3.75; 4.5
7	95.1	98	Closed	1.5; 2.25; 3; 3.75; 4.5
8	95.3	97.7	Closed	1.5; 2.25; 3; 3.75; 4.5
10	96.5	98.8	Closed	1.5; 2.25; 3; 3.75; 4.5
11	96.4	98.8	Closed	1.5; 2.25; 3; 3.75; 4.5
12	97.7	99	Closed	1.5; 2.25; 3; 3.75; 4.5
13	98.6	99.3	Closed	1.5; 2.25; 3; 3.75; 4.5

The actual mass flow through waste-gate and by-pass valves is calculated as the difference between the measured mass flow through both turbines and

Table 3.5: Test campaign for valves characterisation outside of full load points

Point (-)	Check valve (-)	Waste gate valve (%)	By-pass valve (%)	Expansion Ratio (-)
A.1		80	20	1.5; 2.25; 3; 4
A.2		80	55	1.5; 2.25; 3; 4
A.3	Opened in almost all points	80	85	1.5; 2.25; 3; 4
B.1		94	20	1.5; 2.25; 3; 4
B.2		94	55	1.5; 2.25; 3; 4
B.3		94	85	1.5; 2.25; 3; 4

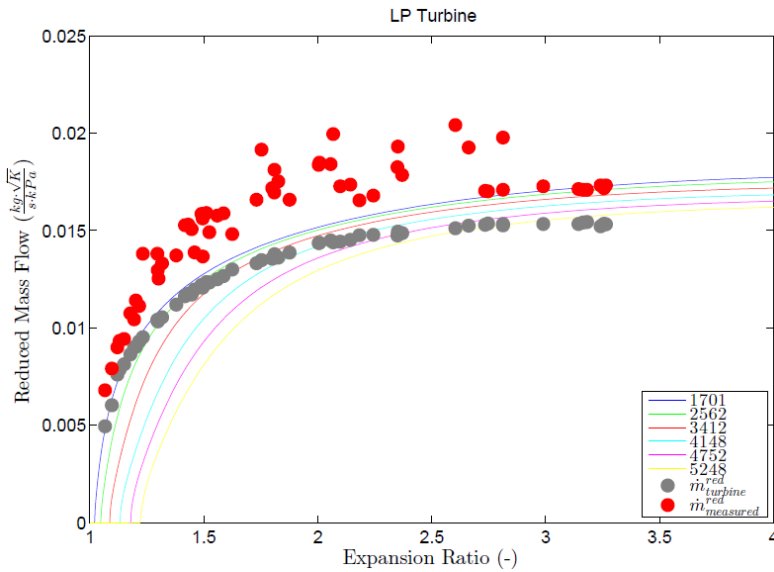


Figure 3.8: Measured and interpolated mass flow on LPT map

turbine mass flow calculated from the reduced mass flow as shown in Equation 3.6. This is possible due to the availability of manufacturers maps of both the HPT and the LPT.

$$\dot{m}_{real} = \dot{m}_{measured} - \dot{m}_{turbine} \quad (3.6)$$

The reduced mass flow is obtained from the corresponding turbine maps (HPT for by-pass valve and LPT for waste-gate) interpolating with the expansion ratio and the reduced speed. In Figure 3.8 an example is shown for the LPT where red points correspond to the measured total reduced mass flow and the grey points represented the interpolated values on the map. The difference between both is the mass flow through the waste-gate valve.

Table 3.6: Geometrical area of the fully open valves (in mm²)

Check valve	Waste gate valve	By-pass valve
1547.3	907.9	157.2

Extension of compressor heat transfer correlation

The LPC of two stage turbocharging system has water cooling around the compressor volute. This layout is used in the present section to design an experimental campaign in which water enthalpy is used to measure the heat flow in the compressor volute. In that way the correlation for the convection in the compressor volute between the air and the wall can be extended. Moreover, an accurate correlation for the heat transfer between the compressor and the water can be obtained for future use in 1D models of two stage turbochargers.

In order to make a comprehensive and extended correlation it is necessary to consider all the possibilities of heat transfer between the compressor case (C) and the air (A). Water cooling is used to change the heat flux vector sense since in normal turbocharger operation C/AIR heat flow can be positive (when the heat flows from the wall to the air) or negative (when the wall is heated by the air) [26]. Therefore, two different conditions have been measured:

- The water temperature is higher than the compressor case temperature so there is a net heat flux from the water to the compressor case.
- The water temperature is lower than the compressor case temperature so there is a net heat flux from the compressor case to the water.

The distribution of the different fluids is shown in Figure 3.9. It can be observed that the outer part of the water case will be insulated using fiberglass layers so it can be assumed that the heat transfer from the water to the outside is negligible. In this case, the heat transfer from the water to the compressor case is the variation of the enthalpy of the water times water flow as shown in Equation 3.7. The measurements have been made using the adiabatic tests methodology described previously. In those conditions the heat transfer from the compressor to the central housing is negligible. Besides, the measurements will

be taken after the temperature of the compressor case is stabilized (steady along the whole C wall). Taking into account all these considerations, the heat transfer from the water to the compressor equals the heat transfer from the compressor to the air (Equation 3.8). Taking into account all the previous considerations the heat transfer from C to the air (A) can be calculated as shown in Equation 3.9. To reduce the relative measurement error, the variation of the water temperature between the outlet and the inlet will be kept as high as possible. To achieve the highest temperature difference the water mass flow will be kept at minimum level.

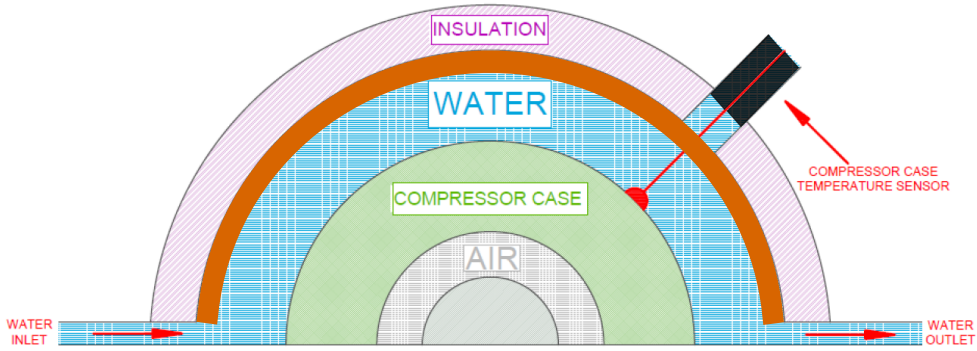


Figure 3.9: Schematic of thermocouples installation and fluids distribution in the LPC

$$\dot{Q}_{W/C} = \Delta h_W \cdot \dot{m}_W \quad (3.7)$$

$$\dot{Q}_{W/C} = \dot{Q}_{C/A} \quad (3.8)$$

$$\dot{Q}_{W/C} = \dot{m}_W \Delta h_W = \dot{m}_W c_W (T_{outW} - T_{inW}) \quad (3.9)$$

Once the heat transfer from C to A is known, the heat transfer coefficient $h_{C/A}$ can be calculated using the Newton's law of Cooling given in Equation 3.10. To use the equation it is necessary to measure the compressor case temperature. For that purpose small drills have been made in the compressor volute to install thermocouples as it can be observed in the schematic of Figure 3.9. Three radial locations have been chosen for themocouples installation in order to check if one-dimensional heat transfer assumption is correct. The locations of the drills are shown in Figure 3.10.

$$\dot{Q}_{C/A} = h_{C/A} A (T_A - T_C) \quad (3.10)$$



Figure 3.10: Location of the drills for thermocouples installation in LPC volute

Solving the heat transfer coefficient in Equation 3.10, the Nusselt number can be calculated as shown in Equation 3.11. After that the Nusselt number can be fitted to a standard expression of the form of Equation 2.14. The same approach is followed to find a correlation for the water. However, mass flow and temperature conditions must have considerable variation to operate in a sufficiently wide range so a different testing campaign for water characterisation is needed.

$$Nu = \frac{h_{C/A} \cdot L}{k_A} \quad (3.11)$$

To achieve the wide range conditions a test campaign has been designed. Some facts must be considered in the testing campaign to assure accurate results:

- The Oil Inlet Temperature (OIT), the Compressor Outlet Temperature (COT) and the Turbine Inlet Temperature (TIT) must be kept as nearly equal as possible in order to minimize the heat transfer through the whole turbocharger. This means that all of them have to be kept below 130°C (to avoid oil cocking). This procedure is similar to the adiabatic measurement procedure employed for friction losses characterisation. With this procedure the heat flow between the compressor and central housing is negligible.

- In order to model the heat flux from the air, the Water Inlet Temperature (WIT) will be kept at 30°C. At this temperature it can be assured that there will be a net heat flux from the air to the water at relatively low pressure ratios.
- In order to model the heat flux to the air the Water Inlet Temperature (WIT) will be kept at 95°C. At this temperature it can be assured that there will be a net heat flux from the water to the air at relatively low and medium pressure ratios.

In order to vary the pressure ratio of the compressor, six points for each measured iso-speed line are considered giving a total of 66 measured points for compressor heat flow estimation. In Figure 3.11 the measured points of this campaigns are shown on the low pressure compressor map.

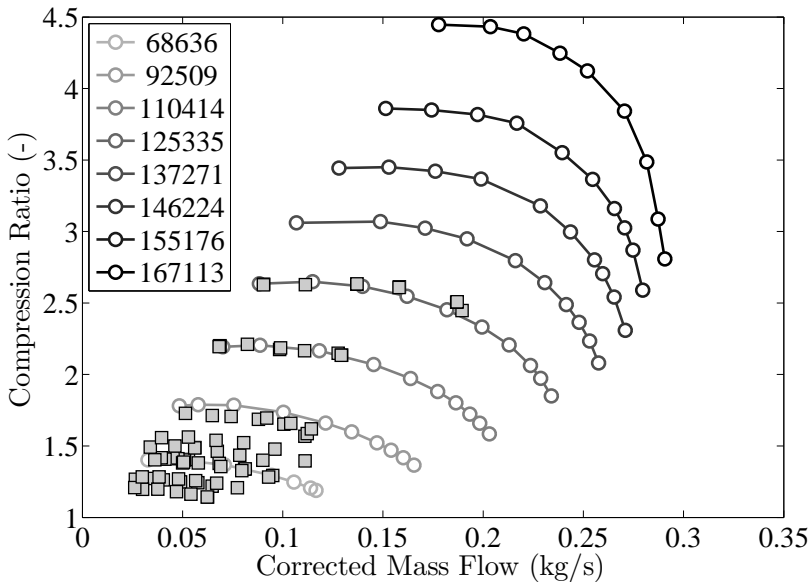


Figure 3.11: Measured points for convection correlations characterization

For water correlation a fixed iso-speed is used with 7 different temperatures for four different water mass flows as it is shown in Table 3.7, with a total of 28 points measured for this last purpose.

Table 3.7: Water correlation test campaign

Turbo Speed (rpm)	Water Mass Flow (kg/h)	Water Inlet Temperature (degC)
70000	100	30
		40
	175	50
		60
		70
	250	80
		90
325		

Tests results analysis

In this section, the discussion of the obtained experimental results for two turbochargers: one water cooled (T#1) and another without water cooling (T#2), is performed. Both turbochargers were tested in hot gas conditions (about 600 K at turbine inlet) and in adiabatic conditions; but in both cases they were externally insulated. The results are discussed for compressor and turbine efficiency, mass flow and pressure ratio.

In Figure 3.12, where the numbers in the legend indicate VGT position percentage (0% – completely closed), a comparison in compressor pressure ratio is presented plotted against corrected mass flow. It can be observed that the differences between the two maps (hot insulated and adiabatic) are insignificant. The reason of this behaviour is that heat transfer phenomena do not affect the aerodynamic behaviour of the compressor [62]. Repetitiveness of the experiment is also shown in Figure 3.12 since the effect of the different VGT positions have no effect on the map.

Nevertheless, when it comes to compressor efficiency the differences can be very significant as shown in Figure 3.13. In the very low speed region these differences rise up to 30 basic points of efficiency what clearly shows that in that region compressor is highly diabatic. The absence of heat transfer along the turbocharger arriving to the compressor allows lower compressor outlet temperatures for quasi-adiabatic tests, what increases the calculated compressor efficiency values defined in equation 2.7. While for hot tests, and mainly at low compression ratios, the compressor receives heat from the rest of the turbocharger increasing outlet temperature what increases the compressor total enthalpy drop. Such decrement does not mean that the compressor is working aerodynamically different that in adiabatic tests, but that additional heat is increasing compressor outlet temperature what affects to the definition of efficiency in equation 2.7.

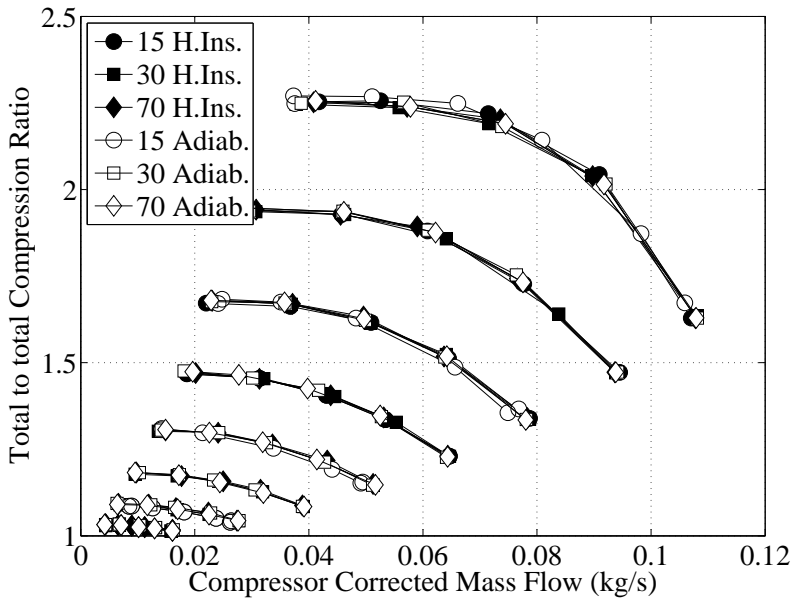


Figure 3.12: Comparison of pressure ratio measured at hot insulated conditions versus measurements at adiabatic conditions. Turbocharger without water cooling (T#2)

This fact evidences that both heat and aerodynamic phenomena must be decoupled for a correct analysis and that maps measured in hot conditions do not capture correctly the efficiency of the machine at low speeds. These facts justify the importance of internal convection heat transfer determination. However, at high speeds the heat transfer effect on compressor outlet temperature is negligible in comparison to mechanical power of the compressor what explains that the differences in efficiency in Figure 3.13 are insignificant from 130 krpm to 170 krpm.

For a not water-cooled turbocharger (T#2) the results are globally similar to that shown in Figure 3.14. In spite of this, in this case the differences between hot and adiabatic tests are appreciable even at 130 krpm and much higher for 90 krpm and 110 krpm. This effect is due to the absence of the important thermal barrier that water cooling generates between turbine and compressor. In the case of 30 krpm and 50 krpm the differences are similar in Figure 3.13 and Figure 3.14, showing that water cooling is not so efficient when residence time is high, as occurs at these low speeds. Moreover, in this case the water temperature is higher than the air temperature what means that there is no thermal barrier.

3. EXPERIMENTAL ANALYSIS

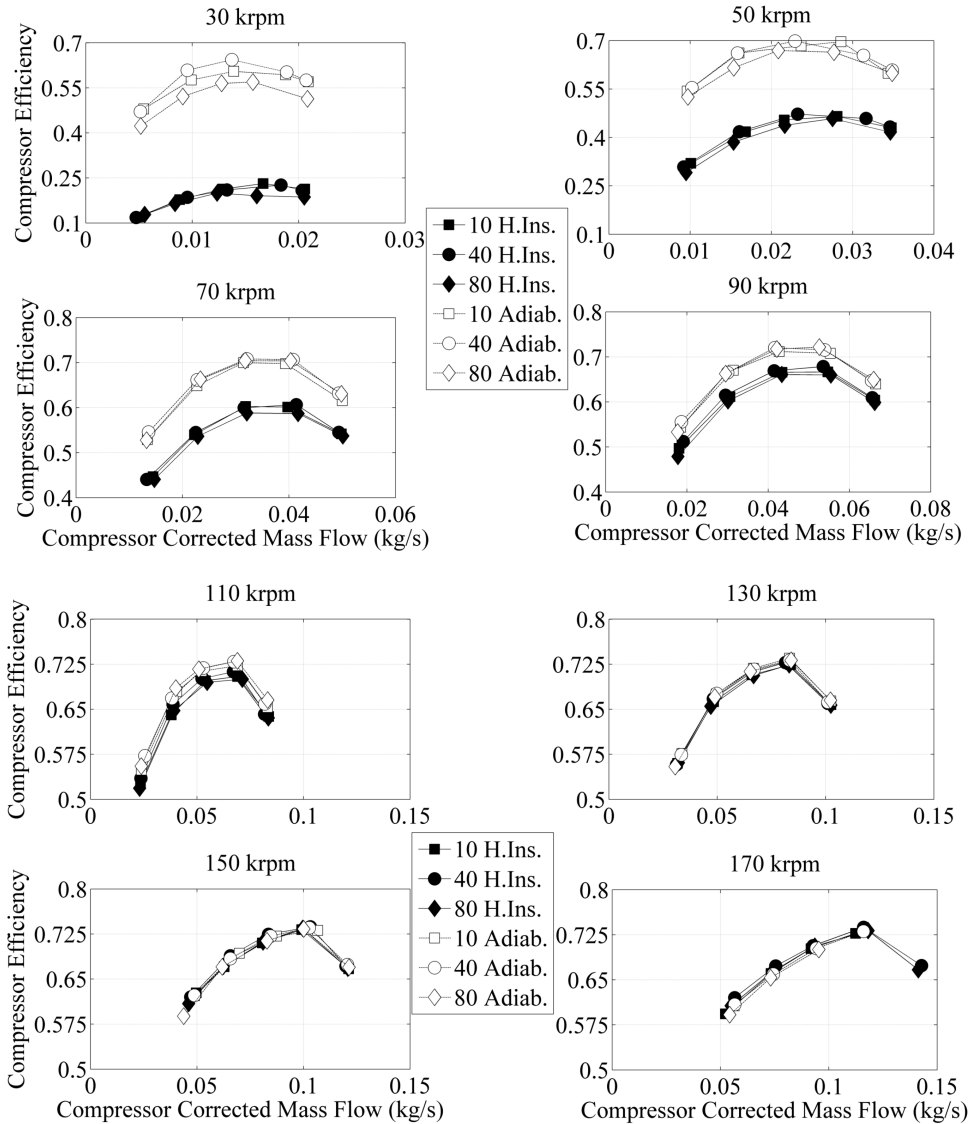


Figure 3.13: Comparison of compressor efficiency measured at hot insulated conditions versus efficiency measured at adiabatic conditions. Water-cooled turbocharger (T#1)

In Figure 3.15 reduced mass flow is plotted against turbine pressure ratio for four different reduced speeds of T#2. It can be observed that there are no significant deviations between the adiabatic and the hot externally insulated tests. The only difference is the amount of energy that is provided in each test.

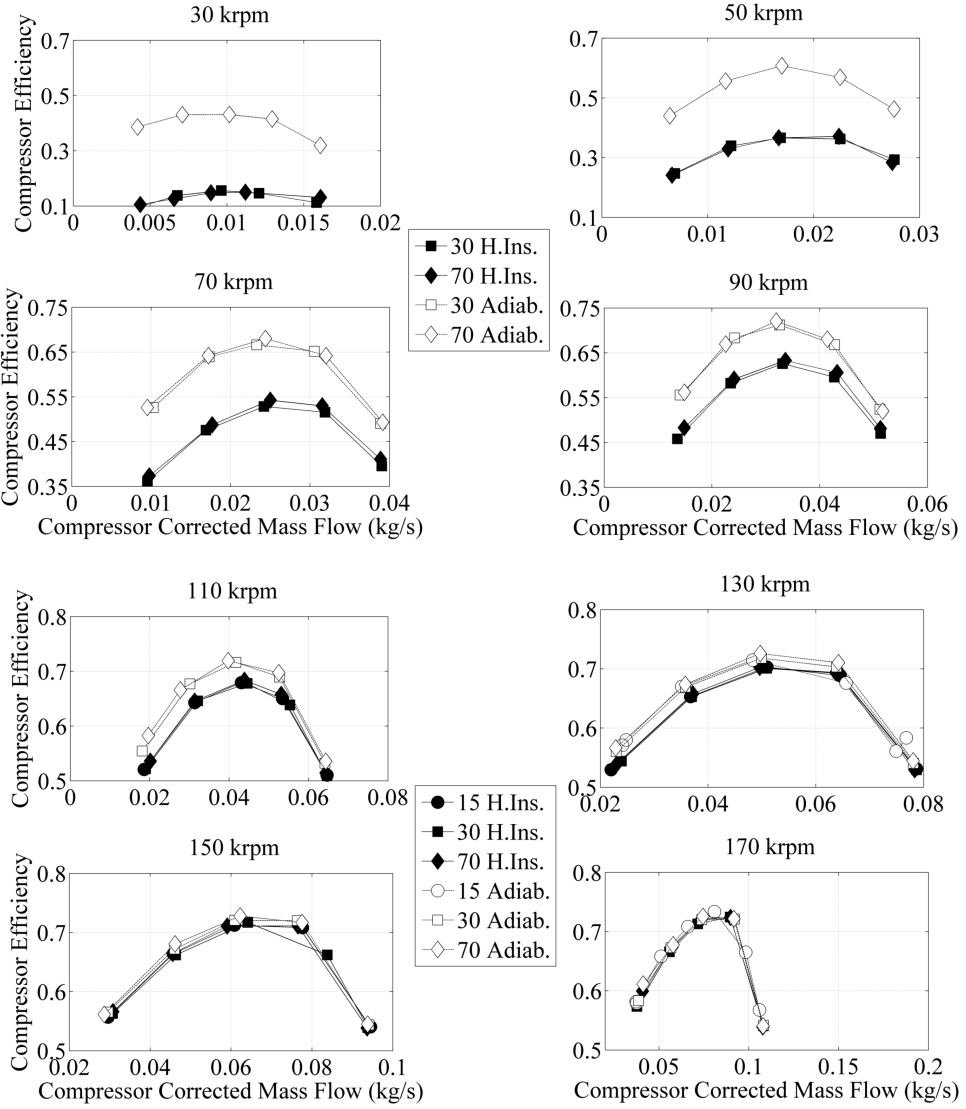


Figure 3.14: Comparison of compressor efficiency measured at hot insulated conditions versus efficiency measured at adiabatic conditions. Non water-cooled turbocharger (T#2)

In the hot insulated tests the turbine inlet temperature is higher, so for the same reduced speed it is possible to measure higher expansion ratios. It must be taken into account that in hot insulated tests the turbine inlet temperature (TIT) was about 600 K while for adiabatic tests was about 300 K.

3. EXPERIMENTAL ANALYSIS

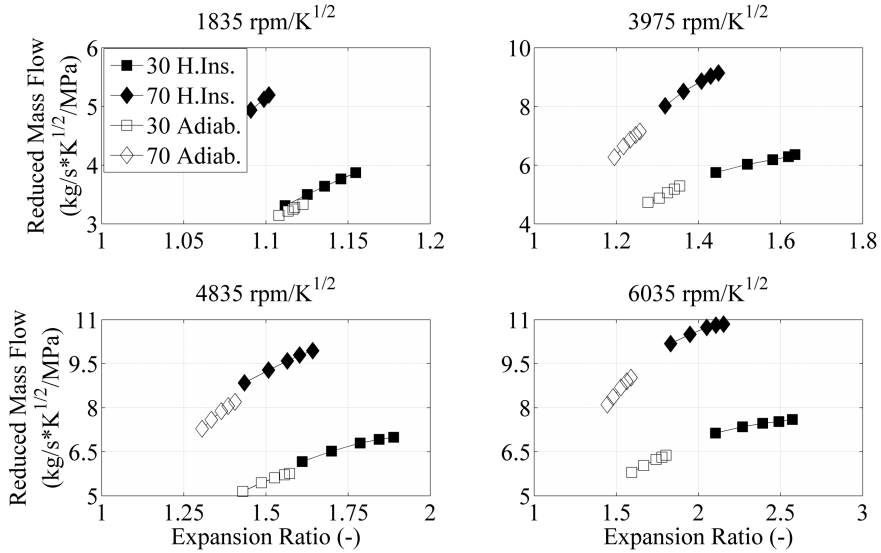


Figure 3.15: Comparison of hot insulated measurements of turbine mass flow with adiabatic measurements (T#2)

Assuming that the heat transfer processes occur before the expansion process, the effective turbine inlet temperature will be lower than the measured one as shown in Figure 2.3b. After the expansion process from point 30a the resulting turbine outlet temperature (point 4a), which coincides with the measured one, can be lower than the temperature at 4s. This produces values of turbine diabatic efficiency (TDE), defined in equation 2.8, much higher than unity as can be observed in Figure 3.16. This effect occurs at the low expansion ratio area due to the relatively higher importance of turbine heat fluxes in comparison to isentropic enthalpy drops. Figure 3.16 shows that TDE will be higher than unity for pressure ratio below 1.25.

For that reason, among others, turbocharger manufacturers usually give the effective turbine efficiency (ETE), defined in equation 2.9, and generally provide data above 90 krpm of turbocharger speed (while in this analysis measurements above 30 krpm are presented).

In Figure 3.17 the ETE definition of turbine efficiency is plotted. As compressor power is in the numerator which can never be superior to turbine mechanical power (power that moves the whole turbocharger) it seems reasonable that ETE value will never be superior to unity. However, if heat transfer takes place the compressor enthalpy drop is the sum of pure mechanical power plus compressor heat flow. This fact enables the possibility of ETE values higher than unity, when the compressor heat fluxes are high enough compared to total compressor

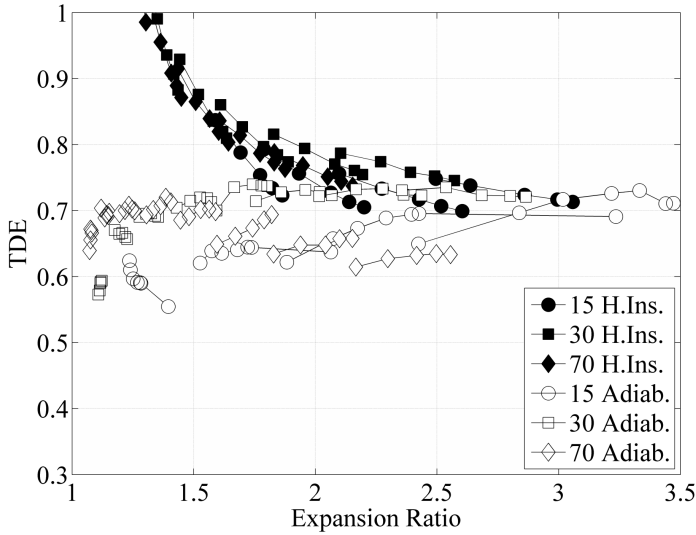


Figure 3.16: Comparison of hot insulated measured TDE with adiabatic measurements (T#2)

enthalpy drop. This behaviour occurs at very low turbocharger speeds when the pure mechanical power is low. In Figure 3.17 the ETE values higher than unity only take place at turbine pressure ratio below 1.1, in contrast with the TDE results.

Figure 3.16 and Figure 3.17 shows that in adiabatic tests the values of both efficiencies are always below hot insulated tests at low pressure ratio and only equals to hot tests at high pressure ratios (high turbo speeds) when heat fluxes are relatively less important. It proves that the heat fluxes present during hot conditions are responsible of the behaviour described above.

The TDE considers only turbine behaviour, so no mechanical losses are included. For that reason in absence of heat fluxes (adiabatic map) the value of the TDE depends only on turbine aerodynamic design. When the TDE is applied to hot measurements the value depends on turbine aerodynamic design and heat flow along the turbocharger. Conversely, the ETE depends on both the turbine and the compressor involving mechanical losses. For that reason, in absence of heat flows the value of the ETE is a function of turbine design and mechanical losses and will be always lower than the TDE. In the case of hot measurements the ETE is also a function of heat flows. In Figure 3.16 it can be observed that in the case of adiabatic measurements the TDE values are between 0.55 and 0.75 typical in turbomachinery theory while in Figure 3.17 at low expansion ratios the ETE values fall to 0.2. The reason is that mechanical

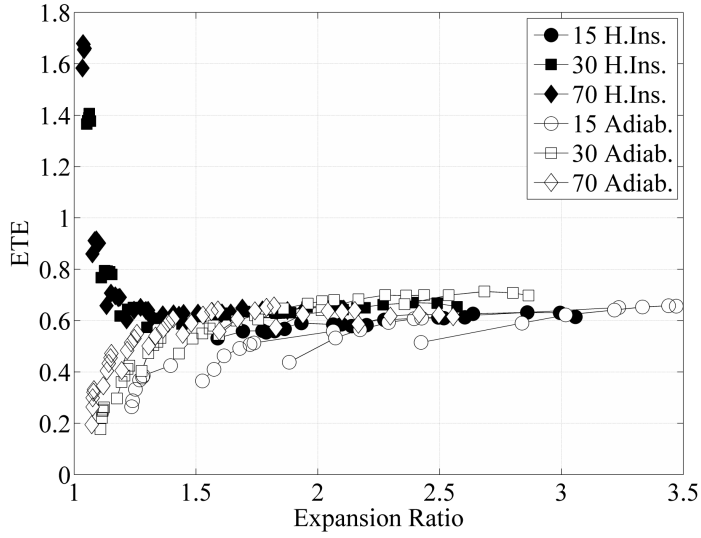


Figure 3.17: Comparison of hot insulated measured ETE with adiabatic measurements (T#2)

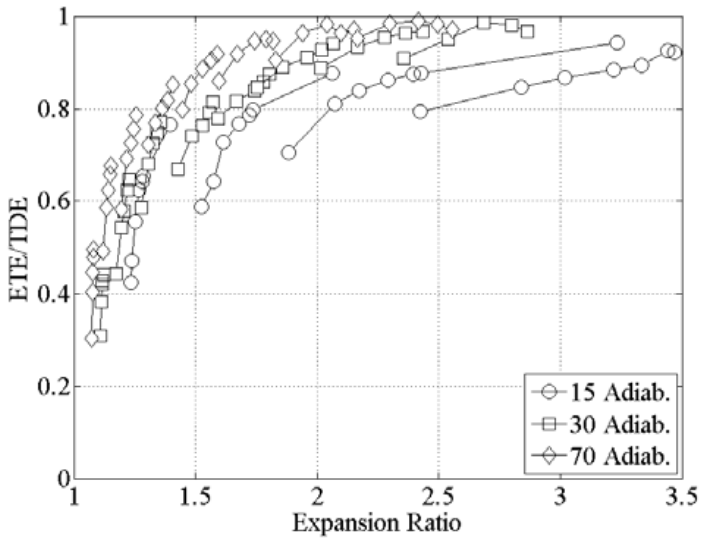


Figure 3.18: Comparison of hot insulated measured ETE/TDE with adiabatic measurements (T#2)

efficiency at low speeds is very small so the product of mechanical efficiency and the TDE is very low as well.

Mechanical efficiency can be roughly calculated as a ratio between the ETE and the TDE from adiabatic tests as it is shown in Figure 3.18. Showing that it can be as low as 0.3 for low turbocharger speeds. Part of this low value is explained by the low oil temperatures required to perform adiabatic tests at such low turbo speeds [118].

In conclusion, heat flows inside the turbocharger are very significant at low engine loads for the compressor and turbine efficiency determination. Only using adiabatic measurement techniques the heat flows are negligible and the resulting efficiencies are closer to theoretical adiabatic behaviour. ETE definition allows approaching hot tests ETE to adiabatic definition at high turbo speeds (pressure ration over 1.5 in Figure 3.17) but can provide values higher than unity for low energy conditions.

3.4 Engine test bench

The test rig used to validate the proposed model in a real application, i.e. mounted on an engine, is a standard engine test rig, designed for the study of internal combustion engines up to 200 kW of power. The facility is assembled to control and evaluate the engine performance in steady and transient states. The most important devices of the engine test bench are described as follows and a scheme of the facility and its instrumentation is shown in Figure 3.19:

- AC- Dynamometer, variable frequency and high response.
- High frequency analogical data acquisition system.
- Last generation test room control device and data acquisition system.
- Continuous smoke measurement device.
- Control strategies design hardware.
- Airflow measurement system (Hot-wire anemometer).
- Transient fuel-flow measurement balance.
- Piezoelectric and piezoresistive cooled pressure transducer.
- Exhaust gas analyser.
- Thermocouples and Thermoresistances

3. EXPERIMENTAL ANALYSIS

The engine is installed in a bench fixed by means of metallic beams joined by screws or weldings. The structure is designed in a way that prevents the longitudinal movement of the engine and makes easier the alignment with the dynamometer.

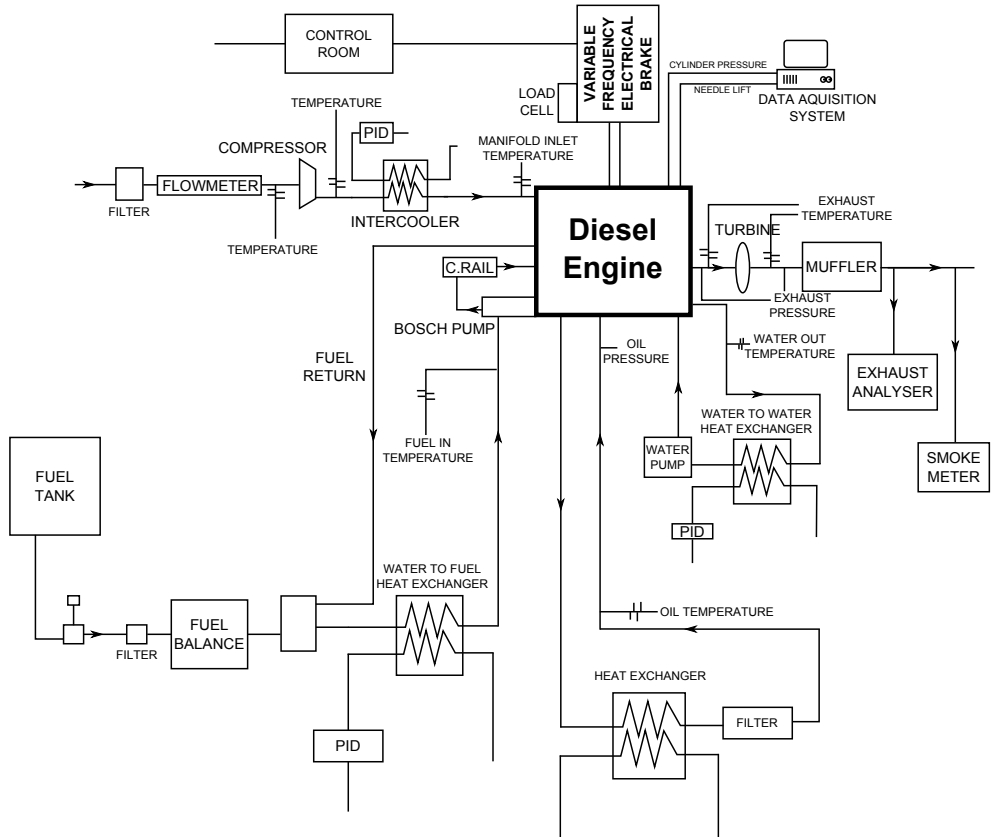


Figure 3.19: Layout of the engine test cell

The load rate and the engine speed are controlled by this asynchronous dynamometer (APA) and an automatic acceleration system called Throttle which are both introduced into a control and data acquisition system called PUMA. The dynamometer offers the necessary resistant torque for the engine in order to test different rates of charge and dissipates the heat generated by the engine by means of a water cooling systems. The thermal state of the different fluids (cooling water, admission air, fuel and oil) is controlled by means of heat exchangers, in which the mass flow of the coolant is adjusted by an electric valve controlled by a PID controller.

In an engine test bench the measurement conditions are more restrictive, although the test conditions are similar to the real operation of the turbocharger.

A turbocharged Diesel engine with a variable geometry turbine and an exhaust gas re-circulation valve is mounted on the facility. The main technical characteristics of this engine are presented on Table 3.8.

Table 3.8: Main characteristics of the employed engine

Parameter	Value
Engine displacement [cm^3]	1997
Bore [mm]	85
Stroke [mm]	88
Number of cylinders	4 in line
Valves	4 valves per cylinder
Compression ratio	16

The facility is controlled automatically by the control system (PUMA V5) which allows the acquisition of a set of variables that characterize the behavior of the different systems of the engine. The sensors acquired by this system are of medium frequency (100 Hz). In order to acquire instantaneous (high frequency) measurements an oscillographic recorder Yokogawa DL716 digital scope (from now on YOKO) is used.

Finally, engine calculator (ECU) variables are measured by specific control software INCA V5. Some of the measured parameters, like turbocharger pressures, are acquired by two type of sensors which are recorded by an acquisition system depending on their frequency (high or low). The torque of the engine is measured by means of a load cell coupled to the dynamometer. The engine speed and the crankshaft rotation angle are measured using of a Kistler 2613B optical angular encoder.

The fuel flow rate is measured using a gravimetric balance (AVL-733S), allowing the measurement of both instantaneous and average fuel consumption. In the same way, as in the gas stand several instantaneous piezoresistive KISTLER pressure sensors are installed in order to measure pressure fluctuations. When no pressure fluctuations must be measured average pressure sensors are used (called FEM-P in PUMA acquisition system). For temperature measurements either Pt100 thermoresistances or type K thermocouples are used.

Tests methodology (swept volume emulation)

A 2.0 litres turbocharged diesel engine has been instrumented in the test bench. Its main technical characteristics were presented in Table 3.8. In order to tests the same one stage turbochargers that have been tested in the gas stand (T#1 and T#2 from Table 3.1) it was necessary to make some adaptations for T#2 since it is designed for a smaller engine. For that reason for T#2 tests, downspeeding

has been applied in order to avoid turbocharger overspeed. This means that the engine speeds were adapted to emulate a 1.6 litre engine volumetric flow rate for the smaller turbocharger (T#2). For T#1 no adaptations were necessary since it is the turbocharger of the instrumented engine. In this way full load engine points at different speeds have been measured for both turbochargers.

In equation 3.12 the expression of engine power is shown as a function of air to fuel ratio, engine effective efficiency, air mass flow and fuel power. In downspeeding procedure the power of the engine is reduced by the ratio 2/1.6, so the air mass flow according to equation 3.12 will be reduced in the same ratio, as the rest of the parameters are fixed for a given engine. In that way the mass flow through T#2 in the tests will be equal to the mass flow that it would have in a 1.6 litres engine.

$$P = \eta \left(\frac{1}{AFR} \right) \dot{m}_a Q_f \quad (3.12)$$

Engine characterization tests

Previously to the full load tests a set of different tests on the engine have been performed to characterise the valves flow coefficients and the combustion process in order to build an accurate 1D engine model. Valves flow coefficients are important for calibrating the gas exchange process in the cylinder and to predict intake mass flow correctly using the model. The characterisation of the combustion process is necessary for a good estimation of the in-cylinder conditions at the exhaust valve opening which affects the available energy at the turbine inlet. This characterisation has been performed using instantaneous in-cylinder pressure signal from full load tests as will be described below.

Valves flow coefficients were obtained using a cold flow gas stand [119]. The cylinder head was disassembled from the engine and set up in a gas stand where the flow coefficients of all the valves have been measured for direct and reverse flow. The measurements were performed modifying the valve lift. These tests provided curves for all valves that correlated flow coefficients with valve lift as shown in Figure 3.20.

Combustion process was characterised using an in-house combustion diagnosis tool (CALMEC) [120] and [121], which is based on the measured instantaneous in-cylinder pressure and the characterization of some uncertainties [122]. From this measurement and other parameters that define the engine working point, CALMEC is able to determine the heat release law by using the first principle of thermodynamics. The main objective of this task is to provide enough information to predict the in-cylinder conditions at the exhaust valve opening and then the fluid thermal state at turbine inlet. The combustion process of the engine has been characterized for both steady and transient behaviour.

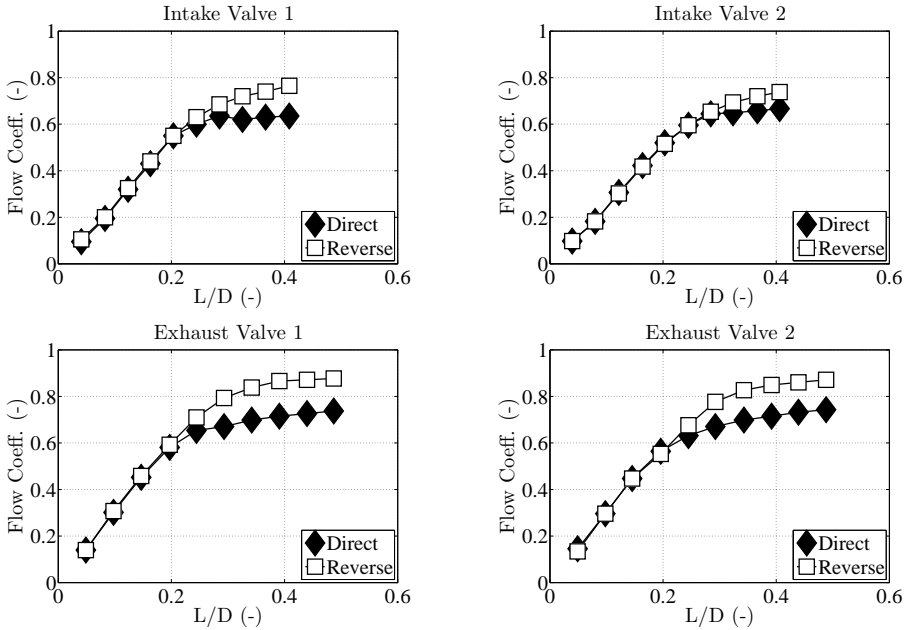


Figure 3.20: Flow coefficients of the intake and exhaust valves

Special interest shows the combustion characterization in transient engine conditions. In order to characterize the combustion in transient conditions the signals must be processed.

- Firstly the signals have to be synchronized due to the fact that there are signals sampled at constant frequency and others at constant crank angle.
- Moreover the fuel signal must be calibrated.
- The air mass flow must be corrected due to:
 - Time delay as a consequence of wave displacement.
 - Gas accumulation in the intake system.
- The EGR has to be estimated. Instantaneous EGR measurement are not available, and then it has to be estimated using the engine volumetric efficiency as shown in equation 3.13.

$$\dot{m}_{EGR} = \left[V_T \frac{n}{2} \rho_{inlet} \right] \eta_V - \dot{m}_{air} \quad (3.13)$$

Once the signals are prepared, the combustion process during the transient tests was analysed cycle to cycle. Figure 3.21 shows the Ratio of Heat Release

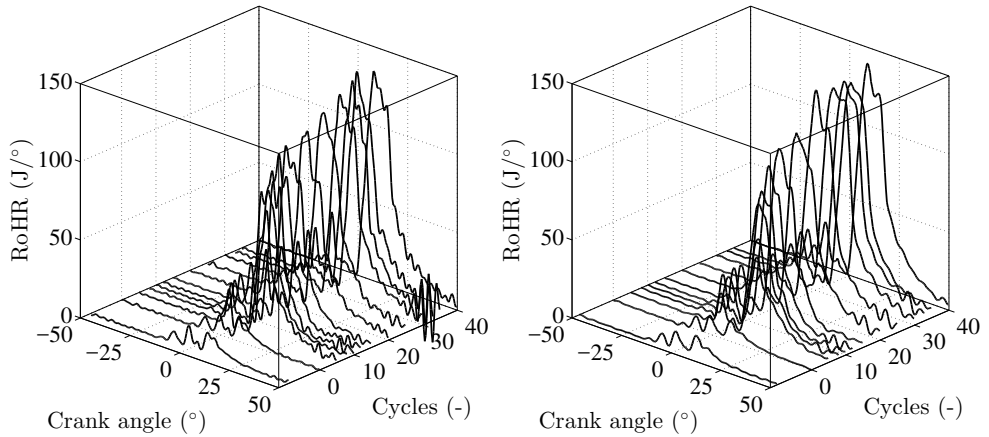


Figure 3.21: RoHR during acceleration for T#1 (left) and T#2 (right)

(RoHR) for different cycles of two transient tests using T#1 (left) at 1500 rpm engine speed and using T#2 (right) at 1600 rpm engine speed.

As it has been commented before, the main objective of this analysis is to provide to the model the capability to predict in-cylinder conditions at exhaust opening. Figure 3.22 provides the evolution of in-cylinder pressure and temperature at that moment of the cycle.

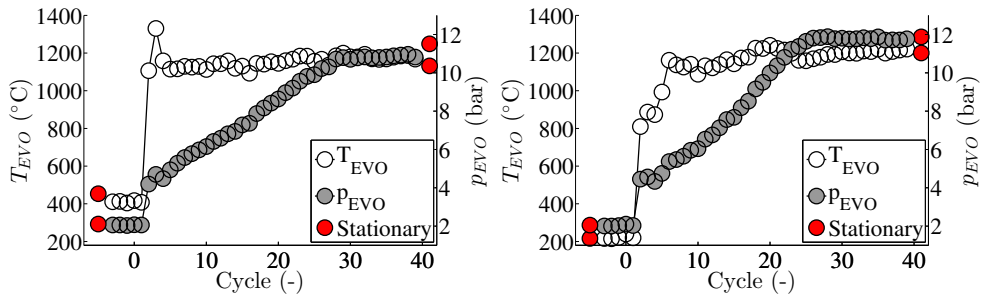


Figure 3.22: In-cylinder conditions at EVO for T#1 (left) and T#2 (right)

Tests results

Steady tests have been performed covering all the engine speed range (from 1000 rpm to 4000 rpm) for both turbochargers taking into account the downspeeding of T#2. Partial load tests have also been performed. In Figure 3.23 the torque of full and partial loads for both turbochargers is plotted against the engine speed. For T#2 in this and the following figures the emulated engine speed is represented. In Figure 3.24 compressor outlet conditions are plotted. The outlet temperature of the compressor will be predicted by the model that will

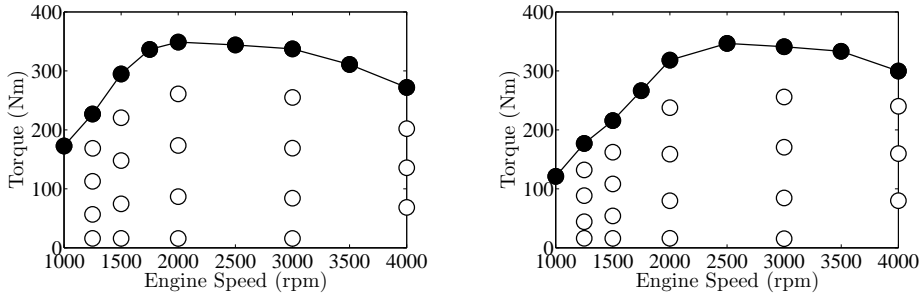


Figure 3.23: Engine torque at steady conditions. Left: T#1, Right: T#2

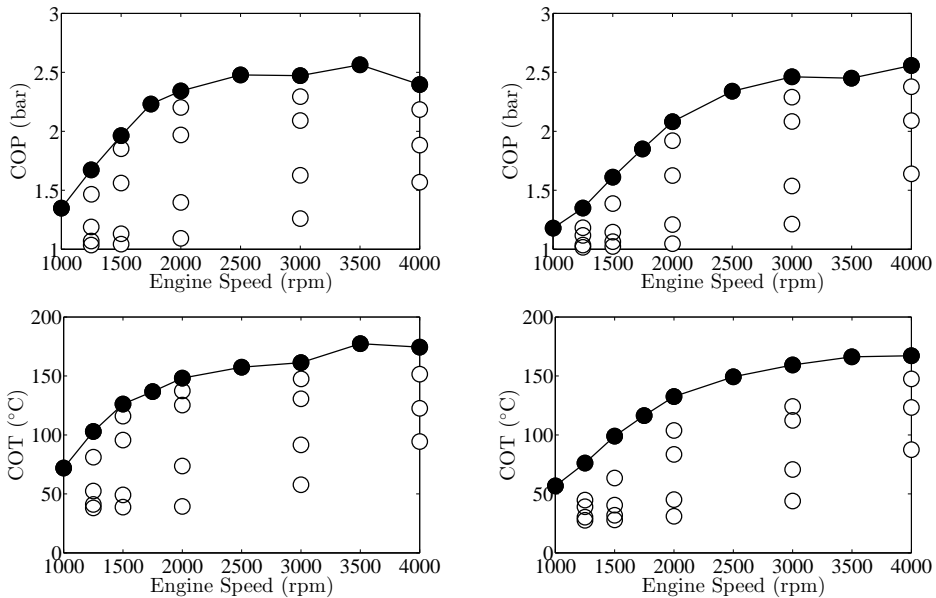


Figure 3.24: Compressor outlet conditions. Left: T#1, Right: T#2

be developed in the next chapter and compared with the temperature of this figure. The maximum outlet pressure of T#2 is corresponds to the maps of this turbocharger.

Figure 3.25 shows the inlet turbine conditions. Turbine inlet temperature is necessary for the modelling of the engine with 1D tools. Finally in Figure 3.26 turbocharger speed is shown. It can be observed that T#2 is not overspeeded, what justifies the engine downspeeding method.

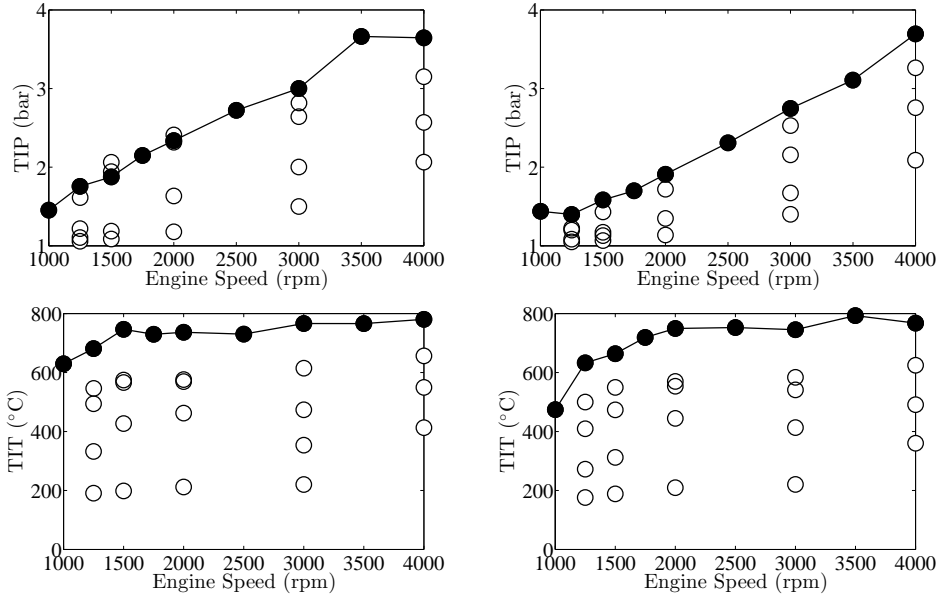


Figure 3.25: Turbine inlet conditions. Left: T#1, Right: T#2

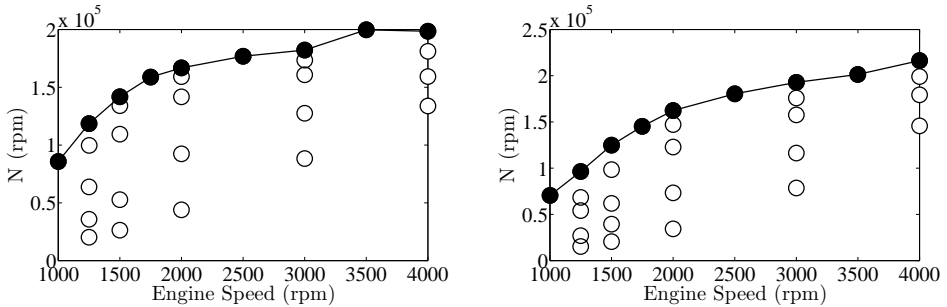


Figure 3.26: Turbocharger speed. Left: T#1, Right: T#2

3.5 References

- [1] F. Payri, P. Olmeda, F. Arnau, A. Dombrovsky, and L. Smith. “External heat losses in small turbochargers: Model and experiments”. In: *Energy* 71 (2014), pp. 534–546. ISSN: 0360-5442. DOI: 10.1016/j.energy.2014.04.096 (cit. on pp. vii, 27, 60).
- [2] J. R. Serrano, P. Olmeda, F. Arnau, A. Dombrovsky, and L. Smith. “Analysis and Methodology to Characterize Heat Transfer Phenomena in Automotive Turbochargers”. In: *J. Eng. Gas Turbines Power* 137 (7) (2014). DOI: 10.1115/1.4028261 (cit. on pp. vii, 15, 55, 150, 160, 165).

- [26] Miguel Ángel Reyes-Belmonte. “Contribution to the Experimental Characterization and 1-D Modelling of Turbochargers for IC Engines”. PhD thesis. Universitat Poliècnica de València, 2013 (cit. on pp. 6, 26, 51, 52, 60, 66, 89, 91, 94, 98, 114, 145, 151, 153, 190).
- [27] Luis Miguel García-Cuevas González. “Experiments and Modelling of Automotive Turbochargers under Unsteady Conditions”. PhD thesis. Universitat Poliècnica de València, 2014 (cit. on pp. 6, 62, 113, 114, 118).
- [28] J. Serrano, P. Olmeda, A. Páez, and F. Vidal. “An experimental procedure to determine heat transfer properties of turbochargers”. In: *Measurement Science and Technology* 21.3 (2010). DOI: 10.1088/0957-0233/21/3/035109 (cit. on pp. 7, 27, 52, 54, 89).
- [62] M. Cormerais, J. F. Hetet, P. Chesse, and A. Malboom. “Heat transfers characterisations in a variable geometry turbocharger: experiments and correlations”. In: *Proceedings of Spring Technical Conference of the ASME Internal Combustion Engine Division* (2006), pp. 53–64 (cit. on pp. 26, 70, 161).
- [114] J. Serrano, P. Olmeda, A. Tiseira, L. García-Cuevas, and A. Lefebvre. “Importance of Mechanical Losses Modeling in the Performance Prediction of Radial Turbochargers under Pulsating Flow Conditions”. In: *SAE Int. J. Engines* 6.2 (2013), pp. 729–738. DOI: 10.4271/2013-01-0577 (cit. on p. 55).
- [115] Society of Automotive Engineers. “Supercharger Testing Standard”. In: *SAE SAE J1723* (1995) (cit. on p. 55).
- [116] Society of Automotive Engineers Inc. “Turbocharger Gas Stand Test Code”. In: *SAE SAE J1826* (1995) (cit. on p. 55).
- [117] Joint Committee for Guides in Metrology. *Evaluation of measurement data – Guide to the expression of uncertainty in measurement*. Ed. by JCGM. JCGM, 2008 (cit. on p. 58).
- [118] F. Payri, J. R. Serrano, P. Olmeda, A. Páez, and F. Vidal. “Experimental Methodology to Characterize Mechanical Losses in Small Turbochargers”. In: *Proceedings of ASME Turbo Expo*. 2010 (cit. on pp. 62, 77).
- [119] F. Payri, A. J. Torregrosa, A. Broatch, and J. Brunel. “Pressure loss characterisation of perforated ducts”. In: *SAE Technical Paper 980282* (1998). DOI: 10.4271/980282 (cit. on p. 80).
- [120] F. Payri, P. Olmeda, J. Martín, and A. García. “A complete 0D thermodynamic predictive model for direct injection diesel engines”. In: *Applied Energy* 88.12 (2011), pp. 4632–4641. ISSN: 0306-2619. DOI: 10.1016/j.apenergy.2011.06.005 (cit. on p. 80).

- [121] F. Payri, S. Molina, J. Martín, and O. Armas. “Influence of measurement errors and estimated parameters on combustion diagnosis”. In: *Applied Thermal Engineering* 26.2 - 3 (2006), pp. 226 –236. DOI: 10.1016/j.applthermaleng.2005.05.006 (cit. on p. 80).
- [122] J. Benajes, P. Olmeda, J. Martín, and R. Carreno. “A new methodology for uncertainties characterization in combustion diagnosis and thermodynamic modelling”. In: *Applied Thermal Engineering* 71.1 (2014), pp. 389 –399. ISSN: 1359-4311. DOI: 10.1016/j.applthermaleng.2014.07.010 (cit. on p. 80).

Theoretical development of turbocharger model

Contents

4.1	Introduction	89
4.2	Heat flow models	89
	Convective heat transfer modelling	90
	Water to compressor volute correlation	93
	Extension of C/AIR correlation	94
	External heat transfer modelling	98
	External radiation	98
	Calculation of view factors for each surface	100
	External Convection	106
	Conductive heat transfer modelling	107
	Capacitances determination	107
	Conductive conductances determination	109
4.3	Gas flow models	113
	Extended model for VGT performance maps extrapolation	113
	Sub-model for Mass flow parameter prediction	113
	Total to static efficiency model	121
	Discharge coefficient modelling in valves	126
	By-pass valve	126
	Waste-gate valve	127
4.4	References	131

Figures

4.1	Lumped heat transfer model	90
4.2	GAS/T fitting	92
4.3	H ₂ /O fitting	92
4.4	H ₂ /W fitting	93
4.5	$Nu_{C/W}$ modelling results	95
4.6	$Q_{C/W}$ modelling results	95
4.7	Schematic of sensors location on the compressor	96
4.8	Thermal network of the cooled compressor	97
4.9	$Q_{C/AIR}$ modelling results	97
4.10	Simplification of turbocharger geometry	99
4.11	Capacitance fitting for each turbocharger	110
4.12	Nodes equivalent width	111
4.13	Conductive conductances fitting for each turbocharger	112
4.14	(a) Reduction of a radial turbine to an equivalent nozzle and stations distribution. (b) Measured ratio of pressure drop in the rotor to total pressure drop in the turbine ('d') in the VGT map [27] of T#6	114
4.15	(a) Geometrical relations of a VGT stator vanes (b) Linear relations between stator vanes angle and VGT opening	115
4.16	Reduced mass flow coefficients dependence with VGT position (a, c and e) and final fitted coefficients (b, d and f)	120
4.17	Difference between fitted and geometrical z_3^{geom} coefficient (a) and modelled 'z' versus fitted 'z' (b)	123
4.18	Procedure for mass flow parameter and efficiency extrapolation	125
4.19	Real mass flow against theoretical mass flow for by-pass valve	127
4.20	Average C_D versus average by-pass valve polynomial fitting	128
4.21	Modelled by-pass valve mass flow against theoretical mass flow	128
4.22	Averaged waste-gate valve C_D against by-pass valve position	129
4.23	Modelled discharge coefficient of the waste-gate valve	130
4.24	Modelled waste-gate valve mass flow against theoretical mass flow	130

4.1 Introduction

The information of the experimental tests described in the previous chapter along with the available data from the turbochargers of previous works (see Table 3.1) will be used to develop the following models:

- Heat flow models
 - Internal convection heat transfer in compressor and turbine.
 - External heat transfer in turbochargers.
 - General conductive heat transfer modelling.
- Gas flow models
 - Extended VGT performance maps extrapolation.
 - Discharge coefficients modelling.

The model developed by Reyes [26] has been modified with the inclusion of the turbochargers T#1 and T#2, improving the internal convection correlations. Moreover, the model has been extended with the inclusion of external heat transfer, VGT position extrapolation, general conductive heat transfer procedure and discharge coefficient model.

4.2 Heat flow models

In order to have the possibility of calculating heat flows when testing the turbocharger on gas stand a lumped model is proposed as shown in Figure 4.1. This model has been developed by Reyes [26]. The turbocharger has been divided in five nodes corresponding to turbine casing (T), turbine backplate (H1), central housing (H2), compressor backplate (H3) and compressor casing (C). The heat transfer by conduction between the metal nodes is characterised by conductive conductances. The conductive conductances can be obtained from CAD files of the turbocharger using a FEM approach or from alternative methodologies as the one proposed by [28].

The general correlations of the heat transfer properties in order to use the lumped model must provide all the capacitances and conductances of Figure 4.1. The work can be split in conductive and convective conductances, in addition to a general procedure for accounting external heat transfer (convection and radiation) and mechanical losses model constants determination. In Table 3.1 the main data of the turbochargers that will be used for correlation development is presented.

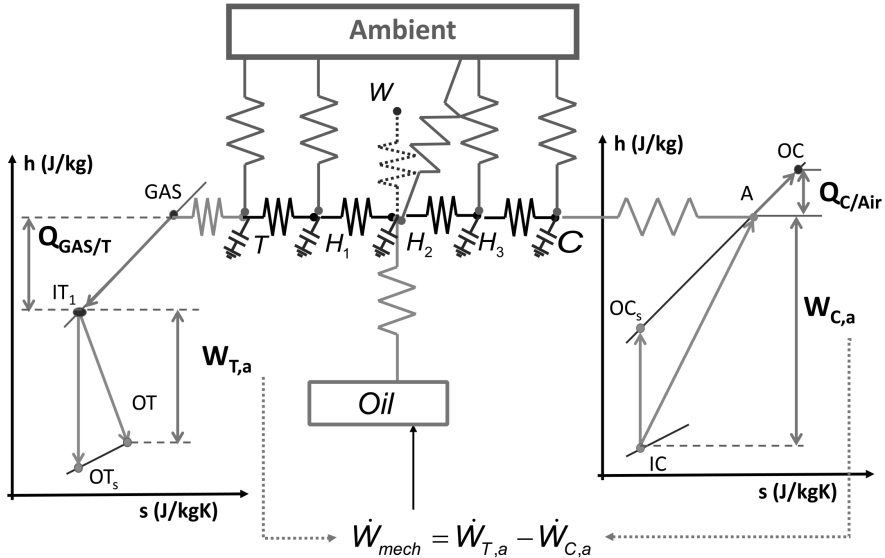


Figure 4.1: Lumped heat transfer model

Turbochargers T#2, T#5, T#6, T#7 have been used for the development of the correlations while T#1 have been used to check the ability of the correlations to predict heat transfer parameters in the next chapter. The selected turbochargers have different external geometry, different rotor geometry and are used in engines of different displacement. Moreover, three of the turbochargers are water cooled while the remaining two are not. This variety of turbochargers will allow getting more accurate correlations, i.e. better prepared to fit turbochargers of different characteristics.

Convective heat transfer modelling

For convective conductances a correlation must be given in terms of dimensionless numbers to give the value of the conductance (or heat flow) for any operative condition of the turbocharger. The correlation must be general and unique for any turbochargers giving satisfactory results for all of them. Four correlations must be obtained (one for each convective conductance of the model shown in Figure 4.1):

- GAS/T: corresponds to the heat flux from the hot gases entering the turbine (fluid node GAS) to turbine casing (metal node T).
- C/A: corresponds to the heat flux from compressor casing (metal node C) to the air leaving the compressor (fluid node A) or vice versa.

- H2/OIL: corresponds to the heat flux from central housing (metal node H2) to the lube oil (fluid node OIL).
- H2/W: corresponds to the heat flux from central housing (node H2) to coolant fluid (node W) for water cooled turbochargers.

Using the experimental metal thermal properties of each turbocharger (i.e. the conductive conductances empirically obtained), the internal heat flow through convective branches of the model can be obtained from experiments at hot insulated conditions in the gas stand [3]. Indeed, the experimental convective heat flows were calculated performing a heat balance in every node of the nodal model shown in Figure 4.1.

To obtain general relationships the seven turbochargers must be tested in different operative conditions. Then Nusselt number correlations for the convective branches can be obtained in the form of equation 2.14 using additional factors when needed [26]. These factors can take into account dynamic viscosity of the corresponding fluids or the dependence of VGT position, if turbocharger stator is not fixed. The values of the coefficients (a, b and c) from equation 2.14 must be fitted using the experimental data of heat fluxes. These coefficients cannot correspond to typical values available in the general literature for internal convection in ducts due to the complex internal geometry of the turbocharger.

For the definition of dimensionless numbers several additional external geometrical parameters must be used. These are turbine inlet port diameter, compressor outlet port diameter, and oil and coolant inlet port diameters. Combinations of these parameters with the lengths and diameters of Table 3.1 give the proper effective geometry for the dimensionless numbers as explained in detail in [69].

The correlation for GAS/T heat transfer has been improved compared to the work of Reyes [26]. A new factor has been included to improve the correlation depending on the size of the turbocharger. The expression used in this thesis is shown in equation 4.1. The last term depends on the size of the turbine making the correlation more flexible for different turbocharger applications. Furthermore, the maximum efficiency of the VGT position has been included to take into account the effect of the different VGT positions on the heat flow as suggested in [66]. Figure 4.2 shows the agreement of the developed correlation for the heat coming from the hot gases to turbine case.

$$Nu_{GAS/T} = a \cdot Re^b \cdot Pr^{1/3} \cdot \left(\frac{\mu}{\mu_w} \right)^{0.14} \cdot \left(\frac{\eta_{maxVGT} D_{eff}}{L_{eff}} \right)^c \quad (4.1)$$

The same procedure holds for the determination of the correlations for convective heat transfers in central housing, represented by Q(H2/Oil) (heat to the oil) and Q(H2/W) (to the coolant). The form of the correlations for these

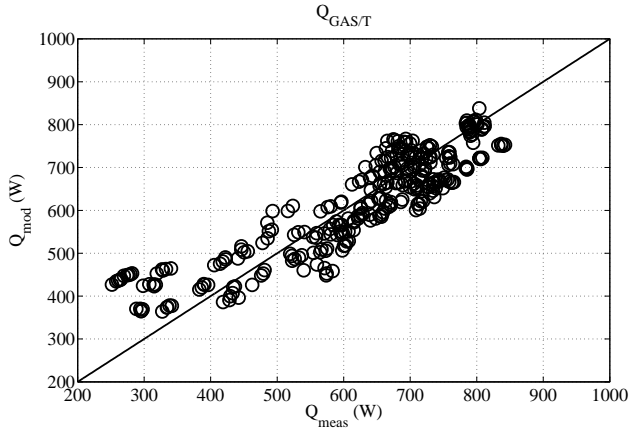


Figure 4.2: GAS/T fitting

cases are provided in equation 4.2 and 4.3. In Figure 4.3 and Figure 4.4 the agreement of the fitting is shown for these heat transfer branches. The branch corresponding to C/AIR will be explained in the next section since the correlation has been developed following a different testing procedure.

$$Nu_{H2/OIL} = a \cdot Re^{0.8} \cdot Pr^{0.3} \cdot \left(\frac{\mu}{\mu_p} \right)^{0.14} \quad (4.2)$$

$$Nu_{H2/W} = a \cdot Re^{0.8} \cdot Pr^{0.4} \quad (4.3)$$

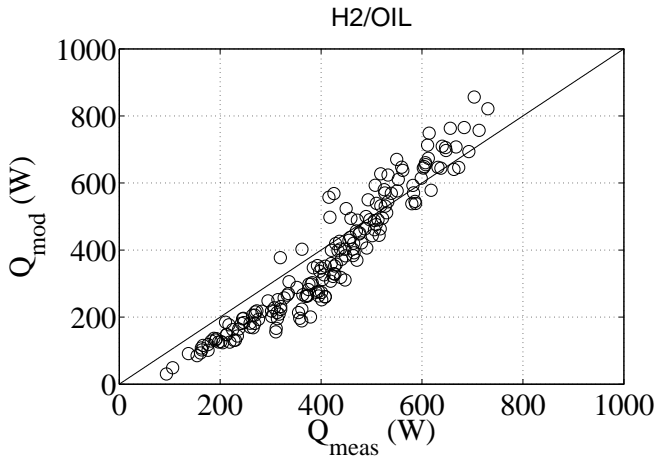


Figure 4.3: H2/O fitting

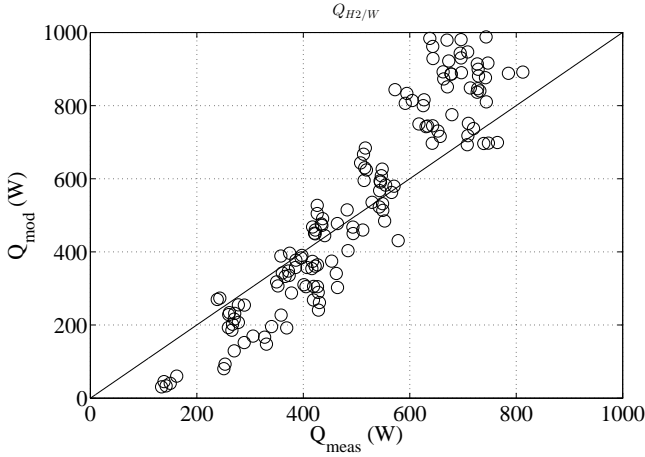


Figure 4.4: H2/W fitting

Water to compressor volute correlation

Taking into account the test campaign described in the previous chapter (Table 3.7) a convective correlation to model the heat transfer between compressor volute and coolant has been developed.

In the first place, it is necessary to define the temperature at which coolant thermal properties are evaluated. The average temperature between the inlet and the outlet is used as it is shown in equation 4.4.

$$T_W = \frac{T_{inW} + T_{outW}}{2} \quad (4.4)$$

The heat flow transfer through the coolant duct can be calculated using equation 4.5. This heat flow can be calculated directly from the measurements as the variables of right hand side of equation 4.5 are measured values.

$$\dot{Q}_{C/W} = \dot{m}_W c_W (T_{outW} - T_{inW}) \quad (4.5)$$

Since the main heat transfer mode is the convection the heat flow, $\dot{Q}_{C/W}$, can also be expressed in terms of Newton's Law of cooling as it is shown in equation 4.6. The heat transfer coefficient $h_{C/W}$ between the coolant and compressor wall can be calculated from that equation. The area of coolant duct A_W has been extracted from the CAD file of the turbocharger.

$$\dot{Q}_{C/W} = h_{C/W} A_W (T_C - T_W) \quad (4.6)$$

Once the heat transfer coefficient is calculated from the measured data solving equation 4.6 the Nusselt number can be calculated using equation

4.7. In this equation d_W is the hydraulic diameter of coolant duct. Hydraulic diameter is used since the duct section is not circular. The definition of the hydraulic diameter of the coolant duct is given in equation 4.8. In this equation A_W^{trans} is the mean transversal section of the coolant duct and l_W is its perimeter.

$$Nu_W = \frac{h_{C/W} \cdot d_W}{\kappa_W} \quad (4.7)$$

$$d_W = \frac{4A_W^{trans}}{l_W} \quad (4.8)$$

Other dimensionless numbers used to build the correlation are described in equation 4.9 and equation 4.10.

$$Pr_W = \frac{c_{pW} \cdot \mu_W}{\kappa_W} \quad (4.9)$$

$$Re_W = \frac{\dot{m}_W \cdot d_W}{\mu_W \cdot A_W^{trans}} \quad (4.10)$$

In the same way as it has been done in the convective correlations described in this chapter the ducts cannot be considered as smooth so Dittus-Boelter correlation cannot be used in its original shape. Therefore the obtained Nusselt numbers will be correlated to the expression of equation 4.11.

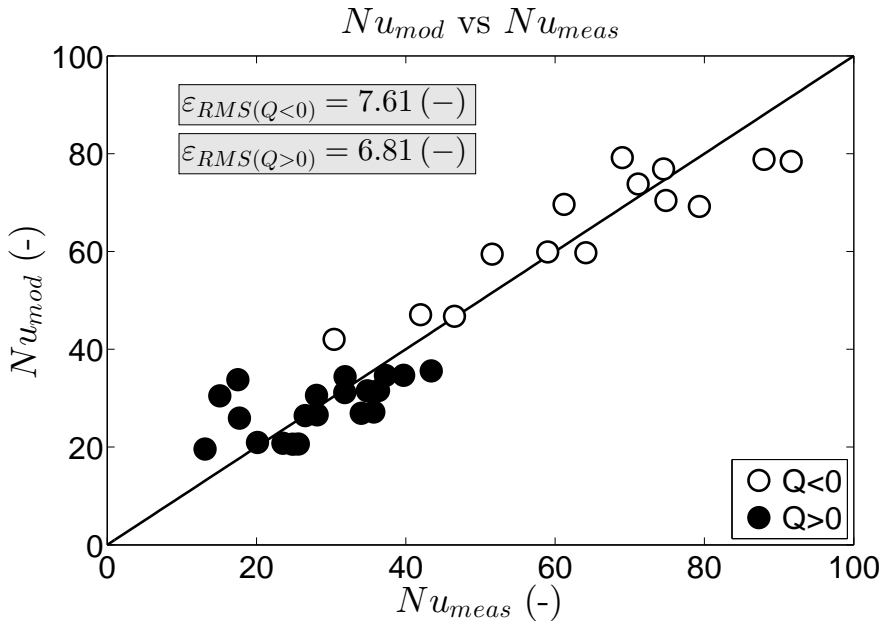
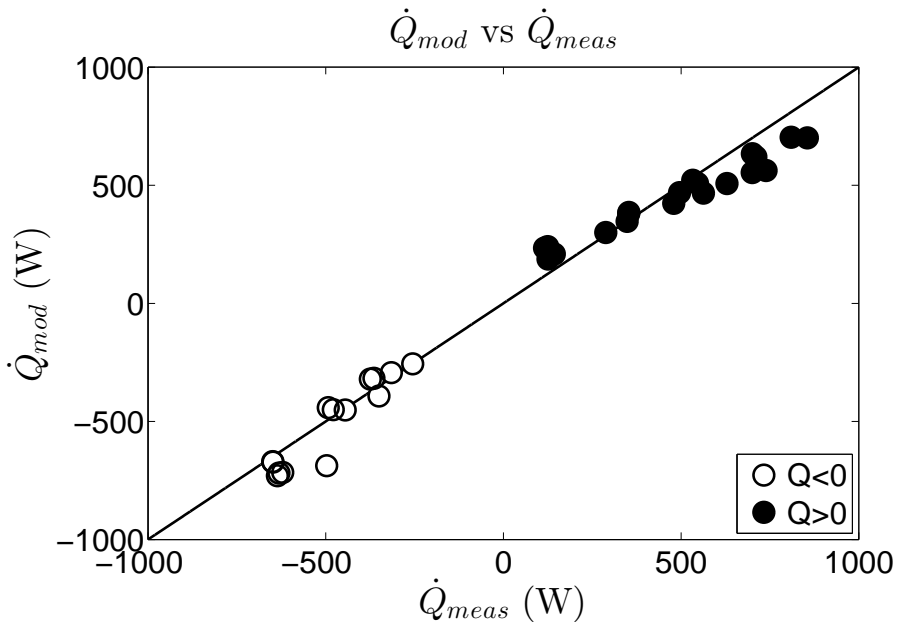
$$Nu_W = a Re_W^\alpha \cdot Pr_W^\beta \quad (4.11)$$

The values of a and α are fitted using experimental data while β can take two values depending of the sign of the heat flow. When the water is cooling the wall $\beta = 0.4$ while when the wall is cooler than the water $\beta = 0.3$. Using a non linear fitting procedure the fitting coefficients have been obtained. Nusselt number prediction is accurate as it can be observed in Figure 4.5. It can be observed that the relative error for both signs of heat flow is similar and low.

Modelling the heat flow in the coolant duct, Figure 4.6 can be obtained. Again the results are accurate for both signs of the heat flow. These results confirm that the fitted coefficients offer sufficiently accurate results for modelling the heat transfer between the coolant and compressor volute.

Extension of C/AIR correlation

Taking into account the test campaign described in the previous chapter a convective correlation for the heat transfer between compressor air and compressor will be developed in this section. The water cooling of compressor volute is used to measure higher heat flows than in the work performed by Reyes [26].

Figure 4.5: $Nu_{C/W}$ modelling resultsFigure 4.6: $Q_{C/W}$ modelling results

In the first place the interaction between the different walls and fluids is presented in Figure 4.7. The water cooling is designed to cool the air of the internal wall (T_{Vol}) of the compressor (where the air is compressed). However, the external wall ($T_{Vol_{ExtW}}$) of the compressor is not affected by water cooling what is confirmed by the measurements since the external wall has a higher temperature.

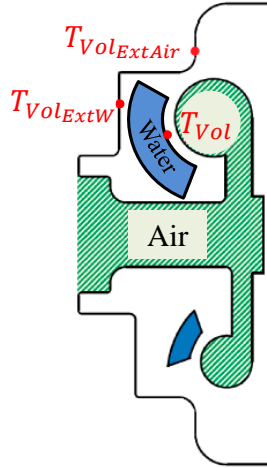


Figure 4.7: Schematic of sensors location on the compressor

Due to the reasons explained above and the testing condition from the previous chapter the thermal network of Figure 4.8 is established. It can be observed that the compressor walls have been divided in two parts. The cold compressor wall (C_C) is cooled by water while the hot compressor wall (C_H) is not affected by water cooling.

The heat flow between the compressor walls and the air is expressed by equation 4.12. In this equation it has been assumed that the heat transfer coefficient with both the hot and the cold compressor wall and the air are equal ($h_{C_C/A} = h_{C_H/A}$).

$$\dot{Q}_{C/A} = \dot{Q}_{C_C/A} + \dot{Q}_{C_H/A} = h_{C/A} [A_{C_C} (T_{C_C} - T_A) + A_{C_H} (T_{C_H} - T_A)] \quad (4.12)$$

Taking into account the thermal network of Figure 4.8 it is deduced that the enthalpy of the water (\dot{h}_W) must be equal to the heat transfer between compressor walls and air ($\dot{Q}_{C/A}$). Moreover, taking the total area of the volute (A_T) and defining the parameter $\alpha = A_{C_H}/A_T$ it is possible to rewrite equation

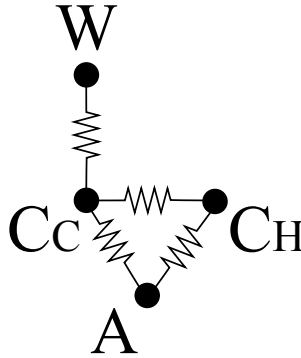
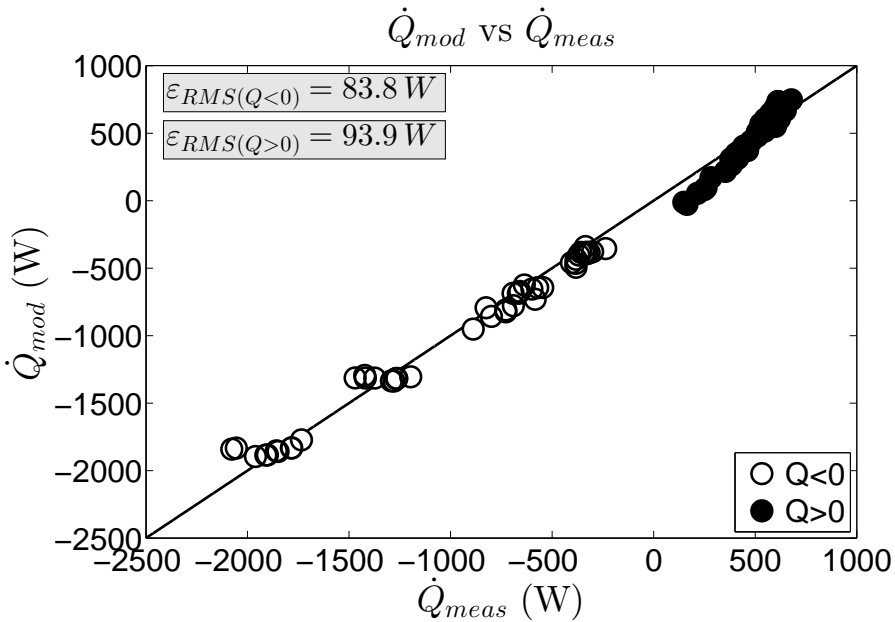


Figure 4.8: Thermal network of the cooled compressor

4.12 into equation 4.13.

$$\dot{h}_W = h_{C/A} A_T [(1 - \alpha)(T_{C_C} - T_A) + \alpha(T_{C_H} - T_A)] \quad (4.13)$$

Figure 4.9: $Q_{C/AIR}$ modelling results

Using the Nusselt number to model heat transfer coefficient (equation 3.11) it is possible to combine the expression given by equation 4.11 with equation 4.13 obtaining equation 4.14. Furthermore, in equation 4.14 the exponent 0.8

has been used for Reynolds number as it has been done in the work of Reyes [26]. The exponent of Prandtl number has also been fixed depending on the sign of the heat flow. For positive $Q_{C/A}$ 0.3 is used while $c = 0.4$ is used for negative heat flow. Therefore, only α and a constants were fitted in equation 4.14.

$$\dot{h}_W = \left(\frac{\alpha R e^{0.8} Pr^c k}{L} \right) A_T [(1 - \alpha)(T_{C_C} - T_A) + \alpha(T_{C_H} - T_A)] \quad (4.14)$$

Equation 4.14 can be directly fitted using the experimental values of water enthalpy drop flow. Figure 4.9 is obtained after the fitting procedure. It can be observed that the results are accurate for both signs of the heat flow. Therefore, the fitted coefficient provide a correlation with enough accuracy for heat flow modelling.

External heat transfer modelling

As it has been stated in the introduction of this chapter an external heat transfer model has been developed in this thesis. This model represents a new feature that is not found in the literature that covers the different approaches of heat transfer modelling in turbochargers. for the external heat transfer, two different mechanisms are considered: radiation and convection. The proposed models for each one are explained in the following sections

External radiation

The heat radiation between two gray surfaces (as the turbocharger can be considered [47]) can be calculated as [65], using Equation 4.15

$$\dot{Q}_r = \frac{\sigma \cdot (T_1^4 - T_2^4)}{\frac{1 - \varepsilon_1}{A_1 \cdot \varepsilon_1} + \frac{1}{A_1 \cdot F_{1-2}} + \frac{1 - \varepsilon_2}{A_2 \cdot \varepsilon_2}} \quad (4.15)$$

where: \dot{Q}_r is the net heat flux due to radiation, T is the absolute temperature of each of the surfaces, $\sigma = 5.67 \cdot 10^{-8} \text{ W} \cdot \text{m}^{-2} \cdot \text{K}^{-4}$ is the Steffan-Boltzman constant, ε is the emissivity of the surface, A is the Area and F is the view factor (ratio of radiation leaving the surface and reaching another surface).

The exact calculation of the view factors is possible to be performed in some simple geometries (in other case, they are estimated by different mathematical algorithms such as Monte Carlo method).

In the case of a turbocharger 1D modeling programs (as GT-POWER™, ..) using mathematical methods is computationally unfeasible (even simplifying the complex geometry). For this reason, the turbocharger has been geometrically simplified as three cylinders (turbine, Housing and compressor) as shown in Figure 4.10 (where the external dimensions needs to be known)

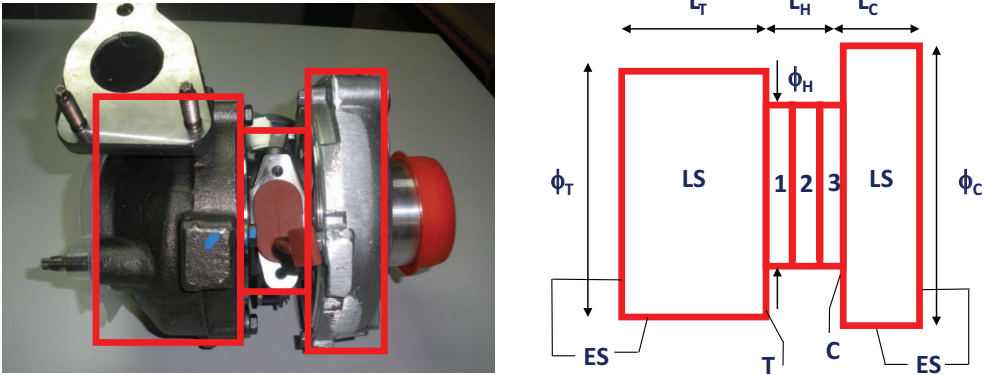


Figure 4.10: Simplification of turbocharger geometry

Three different surfaces are considered in both compressor and turbine:

1. Interior surface. Disc that can interchange radiative heat transfer with the center housing.
2. Exterior surface: Disc in the opposite side of central housing, it would only exchange heat to the environment (ambient, engine, ...).
3. Lateral surface of the cylinder, it would exchange heat with the outside of the turbocharger (ambient, engine, ...).

The central housing is divided in three surfaces or nodes as it has been explained in the previous chapter. Therefore it is necessary to have three radiant exchange surfaces. As a first approach it was decided that this division would be the provided in equation 4.16, where α represents the quotient of a given housing surface with the total housing area.

$$\alpha_{H1} = \alpha_{H2} = \alpha_{H3} = \frac{1}{3} \quad (4.16)$$

According to this division, the mathematical model is composed of 10 surfaces: three for the compressor, three for the turbine, three for central housing and one for ambient. This fact means that 90 view factors must be calculated although only for few of them a direct calculation is needed due to the following facts:

- Nodes pertaining to the same cylinder (compressor, turbine or housing) cannot radiate to each other, removing 18 view factors due to this fact.

- The external surfaces of compressor and turbine can only radiate to ambient being impossible the radiation to any other surface, removing 22 view factors.
- The lateral surfaces of compressor and turbine cannot radiate to the three housing surfaces, removing 12 view factors.
- Since only the view factors of the different nodes to ambient are needed for the model, the reciprocal values can be removed, eliminating another 9 view factors.
- The lateral surfaces of compressor and turbine cannot radiate to each other, removing 2 view factors.
- Since in both turbochargers compressor and turbine diameters are not identical, the biggest inner surface will radiate to the smallest lateral surface, but not vice versa, eliminating 2 view factors.

After all these considerations the surfaces that can exchange heat by radiation are the following:

- Turbine (inner surface) with H1, H2, H3, C (inner surface) and environment, where 9 view factors must be considered.
- Compressor (inner surface) with H1, H2, H3, T (lateral surface) and environment, where 9 view factors must be considered.
- H1, H2, H3, C (external surface), T (external surface), C (lateral surface), T (lateral surface) with environment, where 7 view factors must be considered.

Summarising, from the 90 possible connections between the considered surfaces there are 65 connections in which radiative heat transfer is impossible or irrelevant for the model and 25 connections that must be calculated. This fact forces the evaluation of 25 view factors, that has been performed using the expressions and properties described below.

Calculation of view factors for each surface

In the literature, the analytic expressions of the view factors provided in Table 4.1 can be found for the following cases (shown in Table 4.2):

- Between two concentric discs separated by a concentric cylinder [123].
- Between a ring and the lateral surface of a cylinder [124].

- Between a disc and a lateral surface of separated coaxial cylinder [125].

The different view factors of the simplified geometry (Figure 4.10) can be calculated using the analytic expressions of Table 4.1 and the properties of the view factors [65]: reciprocity (equation 4.17), summation (equation 4.18) and subdivision (equation 4.19),

$$F_{1 \rightarrow 2} A_1 = F_{2 \rightarrow 1} A_2 \quad (4.17)$$

$$\sum_j F_{i \rightarrow j} = 1 \quad (4.18)$$

$$F_{j \rightarrow i} = \frac{\sum_{k=1}^n A_k F_{k \rightarrow i}}{\sum_{k=1}^n A_k} \quad (4.19)$$

So the 25 necessary view factors of the turbocharger can be calculated using the following methodology:

View Factors of turbine inner surface:

1. F_{T-C} : The view factor between turbine and compressor can be calculated:

- a) If turbine diameter, ϕ_T , is smaller than compressor external diameter, ϕ_C , using directly the analytic expression of view factor between two concentric discs separated by a concentric cylinder, using the equations of Table 4.1
- b) Otherwise, the same expression can be used to calculate the view factor between compressor and turbine, F_{C-T} , and then applying the reciprocity property of view factors (Equation 4.17), one can lead to:

$$F_{T-C} = \frac{F_{C-T} \cdot A_C}{A_T} = F_{C-T} \frac{\phi_C^2 - \phi_H^2}{\phi_T^2 - \phi_H^2} \quad (4.20)$$

2. F_{T-H1} : The view factor between turbine and H1 nodes can be calculated in two steps methodology:

- a) Using the analytic expression of view factor between a ring and a cylinder lateral surface (ie: obtaining F_{H1-T}) from Table 4.1
- b) applying the reciprocity property (Equation 4.17):

$$F_{T-H1} = \frac{F_{H1-T} \cdot A_{H1}}{A_T} = F_{H1-T} \frac{4 \cdot \alpha_{H1} \cdot L_H \cdot \phi_H}{\phi_T^2 - \phi_H^2} \quad (4.21)$$

3. F_{T-H2} : in this case the methodology is:

- a) Applying the subdivision property (Equation 4.19) by defining a surface composed by H1 and H2 external surfaces:

$$F_{T-H2} = F_{T-H1+H2} - F_{T-H1} \quad (4.22)$$

- b) Now, the view factor $F_{T-H1+H2}$ can be calculated as F_{T-H1} with different geometrical length, i.e.:

$$\begin{aligned} F_{T-H1+H2} &= \\ &= F_{H1+H2-T} \frac{A_{H1+H2}}{A_T} = \\ &= F_{H1+H2-T} \frac{4 \cdot (\alpha_{H1} + \alpha_{H2}) \cdot L_H \cdot \phi_H}{\phi_T^2 - \phi_H^2} \end{aligned} \quad (4.23)$$

where $F_{H1+H2-T}$ is calculated as the view factor between a ring and a cylinder lateral surface (Table 4.1)

4. F_{T-H3} , the methodology is similar to the one explained for F_{T-H2} :

- a) Apply the subdivision property by defining a surface composed by H1, H2 and H3 external surfaces, so:

$$F_{T-H3} = F_{T-H1+H2+H3} - F_{T-H1+H2} \quad (4.24)$$

being:

- $F_{T-H1+H2+H3} = F_{H1+H2+H3-T} \frac{A_{H1+H2+H3}}{A_T}$
- $F_{H1+H2+H3-T}$ is calculated as the view factor between a ring and a cylinder lateral surface (Table 4.1)
- the ratio between the areas is: $\frac{A_{H1+H2+H3}}{A_T} = \frac{4 \cdot L_H \cdot \phi_H}{\phi_T^2 - \phi_H^2}$

5. Finally, the view factor between turbine and the ambient is calculated using the summation property (Equation 4.18) as:

$$F_{T-amb} = 1 - (F_{T-H1} + F_{T-H2} + F_{T-H3} + F_{T-C}) \quad (4.25)$$

The reciprocal view factors can be evaluated using Equation 4.17, with the exception of the ambient view factor, so the 9 view factors corresponding to turbine inner surface are computed with these considerations.

View Factors in Compressor side:

1. $F_{C-T(LS)}$: in the case the compressor external diameter, ϕ_C is greater than the turbine external diameter, ϕ_T , this view factor is calculated using the expression of the third case of Table 4.1

2. F_{C-H3} . The view factor between compressor and H3 nodes can be calculated in two steps:

- a) Using the analytic expression of view factor between a ring and a cylinder lateral surface (i.e: obtaining F_{H3-C}) (from the expressions of Table 4.1)
- b) Applying the reciprocity property (Equation 4.17):

$$F_{C-H3} = \frac{F_{H3-C} \cdot A_{H3}}{A_C} = F_{H3-C} \frac{4 \cdot \alpha_{H3} \cdot L_H \cdot \phi_H}{\phi_C^2 - \phi_H^2} \quad (4.26)$$

3. F_{C-H2} : in this case the methodology is:

- a) Applying the subdivision property (Equation 4.19) by defining a surface composed by H2 and H3 external surfaces:

$$F_{C-H2} = F_{C-H2+H3} - F_{C-H3} \quad (4.27)$$

- b) Now, the view factor $F_{C-H2+H3}$ can be calculated as F_{C-H3} with different geometrical length, i.e.:

$$\begin{aligned} F_{C-H2+H3} &= \\ &= F_{H2+H3-C} \frac{A_{H2+H3}}{A_C} = \\ &= F_{H2+H3-C} \frac{4 \cdot (\alpha_{H2} + \alpha_{H3}) \cdot L_H \cdot \phi_H}{\phi_C^2 - \phi_H^2} \end{aligned} \quad (4.28)$$

where $F_{H2+H3-C}$ is calculated as the view factor between a ring and a cylinder lateral surface (Table 4.1)

4. F_{C-H1} , the methodology is similar to the one explained for F_{T-H3} (see point 4 in the turbine view factors section)

- a) Apply the subdivision property by defining a surface composed by H1, H2 and H3 external surfaces, so:

$$F_{C-H1} = F_{C-H1+H2+H3} - F_{C-H2+H3} \quad (4.29)$$

being:

- $F_{C-H1+H2+H3} = F_{H1+H2+H3-C} \frac{A_{H1+H2+H3}}{A_C}$
- $F_{H1+H2+H3-C}$ is calculated as the view factor between a ring and a cylinder lateral surface (Table 4.1)
- the ratio between the areas is: $\frac{A_{H1+H2+H3}}{A_C} = \frac{4 \cdot L_H \cdot \phi_H}{\phi_C^2 - \phi_H^2}$

5. Finally, the view factor between compressor and the ambient is calculated using the summation property (Equation 4.18) as:

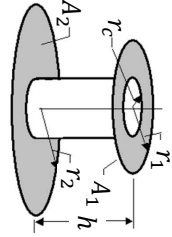
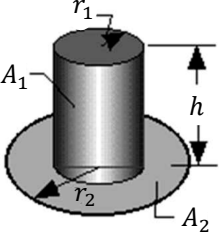
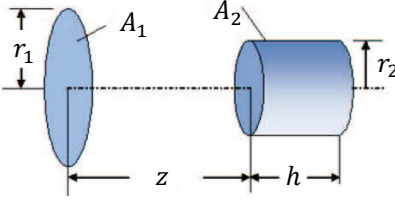
$$F_{C-amb} = 1 - (F_{C-H1} + F_{C-H2} + F_{C-H3} + F_{C-T}) \quad (4.30)$$

Table 4.1: View factor equations

Case	View factor equation	Parameters
1	$\frac{1}{\pi \cdot A} \left[\frac{A}{2} \cos^{-1} \frac{R_c}{R_2} + \frac{B}{2} \cos^{-1} \frac{R_c}{R_1} \right. \\ + 2R_c \left(\tan^{-1} Y - \tan^{-1} A^{1/2} - \tan^{-1} B^{1/2} \right) \\ - \left[(1 + C^2)(1 + D^2) \right]^{1/2} \\ \cdot \tan^{-1} \left[\frac{(1+C^2)(Y^2-D^2)}{(1+D^2)(C^2-Y^2)} \right]^{1/2} \\ + \left\{ \left[1 + (R_1 + R_c)^2 \right] \left[1 + (R_1 - R_c)^2 \right] \right\}^{1/2} \\ \cdot \tan^{-1} \left\{ \frac{\left[1 + (R_1 + R_c)^2 \right] (R_1 - R_c)}{\left[1 + (R_1 - R_c)^2 \right] (R_1 + R_c)} \right\}^{1/2} \\ + \left\{ \left[1 + (R_2 + R_c)^2 \right] \left[1 + (R_2 - R_c)^2 \right] \right\}^{1/2} \\ \cdot \tan^{-1} \left\{ \frac{\left[1 + (R_2 + R_c)^2 \right] (R_2 - R_c)}{\left[1 + (R_2 - R_c)^2 \right] (R_2 + R_c)} \right\}^{1/2} \left. \right]$	$R_1 = \frac{r_1}{h} \\ R_2 = \frac{r_2}{h} \\ R_c = \frac{r_c}{h} \\ A = R_1^2 - R_c^2 \\ B = R_2^2 - R_c^2 \\ C = R_2 + R_1 \\ D = R_2 - R_1 \\ Y = A^{1/2} + B^{1/2}$
2	$\frac{B}{8RH} + \frac{1}{2\pi} \left\{ \cos^{-1} \left(\frac{A}{B} \right) \right. \\ - \frac{1}{2H} \left[\frac{(A+2)^2}{R^2} - 4 \right]^{1/2} \cos^{-1} \left(\frac{AR}{B} \right) \\ \left. - \frac{A}{2RH} \sin^{-1} R \right\}$	$R = \frac{r_1}{r_2} \\ H = \frac{h}{r_2} \\ A = H^2 + R^2 - 1 \\ B = H^2 - R^2 + 1$
3	$\left(\frac{R_2 H}{\pi R_1^2} \right) \left\{ \cos^{-1} \left[\frac{(1+H)^2 - R_1^2 + R_2^2}{(1+H)^2 + R_1^2 - R_2^2} \right] \right. \\ - \cos^{-1} \left[\frac{1 - R_1^2 + R_2^2}{1 + R_1^2 - R_2^2} \right] \left. \right\} \\ - \left(\frac{H}{\pi R_1^2} \right) \left\{ \frac{\left[(1+H)^2 + R_1^2 + R_2^2 \right]^2 - 4R_1^2 R_2^2}{2(1+H)} \right\}^{1/2} \\ \cdot \cos^{-1} \left\{ \left(\frac{R_2}{R_1} \right) \left[\frac{(1+H)^2 - R_1^2 + R_2^2}{1 + R_1^2 - R_2^2} \right] \right\} \\ + \left(\frac{H}{\pi R_1^2} \right) \left\{ \frac{\left[(1^2 + R_1^2 + R_2^2)^2 - 4R_1^2 R_2^2 \right]^{1/2}}{2} \right. \\ \cdot \cos^{-1} \left[\left(\frac{R_2}{R_1} \right) \left(\frac{1 - R_1^2 + R_2^2}{1 + R_1^2 - R_2^2} \right) \right] \left. \right\} \\ + \left(\frac{H^2}{2\pi R_1^2} \right) \left\{ \cos^{-1} \left(\frac{R_2}{R_1} \right) \right. \\ \left. - \left(\frac{R_1^2 - R_2^2}{1+H} \right) \left[\frac{\pi}{2} + \sin^{-1} \left(\frac{R_2}{R_1} \right) \right] \right\}$	$R_1 = r_1/z \\ R_2 = r_2/z \\ H = h/z \\ R_1 > R_2$

The reciprocal view factors can be evaluated using Equation 4.17, with the exception of the ambient view factor, so the 9 view factors corresponding to compressor inner surface are computed with these considerations.

Table 4.2: View factor equations

Case	Description	Figure
1	Two concentric discs separated by a concentric cylinder	
2	Ring and cylinder lateral surface	
3	Disc and separated coaxial cylinder lateral surface	

View Factors in ambient:

For radiation to ambient Equation 4.15 is simplified to:

$$\dot{Q}_r = \frac{\varepsilon_1 \cdot F_{1 \rightarrow 2}}{\varepsilon_1 \cdot (1 - F_{1 \rightarrow 2}) + F_{1 \rightarrow 2}} A_1 \cdot \sigma \cdot (T_1^4 - T_{amb}^4) \quad (4.31)$$

The different view factors can be calculated as follows:

1. The view factor between housing nodes and the ambient are calculated using the summation property (Equation 4.18) as:

$$F_{H1-amb} = 1 - (F_{H1-C} + F_{H1-T}) \quad (4.32)$$

$$F_{H2-amb} = 1 - (F_{H2-C} + F_{H2-T}) \quad (4.33)$$

$$F_{H3-amb} = 1 - (F_{H3-C} + F_{H3-T}) \quad (4.34)$$

2. The view factor between external surfaces of turbine and compressor and ambient is equal to unity since these surfaces only exchange heat by

radiation with the ambient. The same conclusion holds for the lateral surface that do not exchange radiative heat with the opposite inner surface.

3. The view factor between the lateral surface that radiates to the opposite inner surface and the ambient can be calculated using the summation property as follows:

$$F_{LS-amb} = 1 - F_{LS-C} \quad (4.35)$$

With these considerations the 7 view factors to the ambient can be calculated.

Radiation shield

In the case that one of the surfaces had a radiation shield (typical in turbine side, when the turbocharger is mounted on an engine) a procedure has been developed in order to avoid the inclusion of additional nodes. The methodology consists on changing the view factor between the shielded surface and the others, which has been possible assuming that the external surface of the shielded surface is the same as the non-shielded. Comparing the heat fluxes between two gray surfaces with (Equation 4.36) and without shield (Equation 4.15) and after some calculations one can led to equation 4.37:

$$\dot{Q}_r = \frac{\sigma \cdot (T_1^4 - T_2^4)}{\frac{1-\varepsilon_1}{A_1 \cdot \varepsilon_1} + \frac{2}{A_1 \cdot F_{1-2}} + 2 \cdot \frac{1-\varepsilon_s}{A_1 \cdot \varepsilon_s} + \frac{1-\varepsilon_2}{A_2 \cdot \varepsilon_2}} \quad (4.36)$$

$$F_{1s-2} = \frac{F_{1-2}}{2} \left(\frac{\varepsilon_s}{F_{1-2} + \varepsilon_s (1 - F_{1-2})} \right) \quad (4.37)$$

External Convection

In the case of external convection, three cases are considered: free, forced and mixed convection, depending on the external conditions:

Free convection

The geometric simplification is the same that in external radiation (see Figure 4.10). The calculation of the convective conductances between the ambient air and each of the five metal nodes is calculated as:

$$K_{CN} = h_{CN} \cdot A_{node} \quad (4.38)$$

The coefficient of heat transfer by free convection, h_{CN} , is calculated from the correlation of Churchill and Chu [126]:

$$\overline{Nu}_{D,CN} = \left\{ 0.825 + \frac{0.387 \cdot Ra_D^{1/6}}{[1 + (0.559/Pr)^{9/16}]^{8/27}} \right\}^2 \quad (4.39)$$

where: $Ra_D = Gr \cdot Pr$ is the Rayleigh number, $Gr = \frac{g \cdot \beta \cdot (T_w - T_{amb}) \cdot \phi^3}{\nu^2}$ is the Grashof number; $\beta = \frac{1}{(T_w + T_{amb})/2}$ and ν is the kinematic viscosity.

All the properties in Equation 4.39 are calculated at mean temperature between wall, T_w , and fluid, T_{amb}

Forced convection

In the case of forced convection, the used correlation [127] correspond to the perpendicular flow through a horizontal cylinder:

$$\overline{Nu_{D,CF}} = 0.3 + \frac{0.62 \cdot Re_D^{1/2} \cdot Pr^{1/3}}{[1 + (0.4/Pr)^{2/3}]^{1/4}} \left[1 + \left(\frac{Re_D}{282000} \right)^{5/8} \right]^{4/5} \quad (4.40)$$

All the properties in Equation 4.40 are calculated at mean temperature between wall, T_w , and fluid, T_{amb} and it is valid for $Re_D \cdot Pr \geq 0.2$

Mixed Convection

In the case that there is no predominant kind of convection (forced or free) a mixed of both is used. Therefore Equation 4.41 is used:

$$0.1 \leq \frac{Gr_D}{Re_D^2} \leq 10 \rightarrow \overline{Nu_D}^3 = \overline{Nu_{D,CN}}^3 + \overline{Nu_{D,CF}}^3 \quad (4.41)$$

After the calculation of the different Nusselt numbers the heat transfer coefficient corresponding to external convection can be calculated using Nusselt number definition given in Equation 3.11. Knowing the heat transfer coefficient it is possible to compute the convective conductance.

Conductive heat transfer modelling

Capacitances determination

In order to calculate steady and transient heat transfer of the turbocharger conductive conductances and capacitances must be determined. Both parameters are assumed to be constant for any operative condition of the turbocharger. In order to provide general correlation of these parameters several steps must be performed.

The division of the turbocharger must correspond to the node definition of the lumped model. In Figure 3.1 a scheme of the turbocharger is given where the lengths and diameters of each component and plane are shown.

The capacitance of each node, in first approximation, can be calculated as the product of the mass of the node and the specific heat capacity of the material of the node given in Table 4.3, as shown in equation 4.42. It must be noted that if detailed data of turbocharger materials is available the information of Table

4.3 should not be used. When the information of the materials is not available Table 4.3 represents a good estimation of material properties.

$$C_i = m_i \cdot c_i = \rho_i \cdot V_i \cdot c_i \quad (4.42)$$

Table 4.3: Turbocharger material data

Part	Material	c ($Jkg^{-1}K^{-1}$)	ρ (kgm^{-3})	k ($Wm^{-1}K^{-1}$)
Turbine	SIMO cast iron	460	7100	36
Housing	FT200 cast iron	525	7059	48.4
Compressor	Aluminium	860	2670	205

However, the division of the housing in three nodes does not allow the usage of the above expression directly. The capacitance of housing casing must be distributed between the three nodes. Furthermore, the division of the turbocharger in nodes is rather artificial so small contribution of the turbine node capacitance to the capacitance of the adjacent housing node (H1) can exist, as well as in the case of the compressor to the H3 node. Assuming linear contribution in each case the capacitance determination can be done using equation 4.43, where four fitting constants (α, β, γ and ϵ) must be calculated. The constraints for the constants which avoid contributions higher than unity or lower than zero are given in equation 4.44. In the case of central housing to avoid zero contribution $\beta + \gamma$ must be inferior to unity. The same sum must be superior to zero to avoid node H2 to take the contribution of the whole physical housing of the turbocharger, which must be necessarily distributed between the three housing nodes.

$$\begin{aligned}
 C_T &= \alpha \cdot m_T \cdot c_T \\
 C_{H1} &= (1 - \alpha) \cdot m_T \cdot c_T + \beta \cdot m_H \cdot c_H \\
 C_{H2} &= (1 - \beta - \gamma) \cdot m_H \cdot c_H \\
 C_{H3} &= (1 - \epsilon) \cdot m_C \cdot c_C + \gamma \cdot m_H \cdot c_H \\
 C_C &= \epsilon \cdot m_C \cdot c_C
 \end{aligned} \quad (4.43)$$

$$\begin{aligned}
 0 &\leq \alpha, \beta, \gamma, \epsilon \leq 1 \\
 0 &\leq \beta + \gamma \leq 1
 \end{aligned} \quad (4.44)$$

The mass of each part of the turbocharger can be accounted using a simplified geometry. A cone frustum is assumed for the housing and flat cylinders for

the compressor and turbine. Equations 4.45 and 4.46 give the mass using these simplified geometries, the density of the materials (Table 4.3) and fitting constants (θ_i) to correct the geometry simplification. Those constants take into account that the geometry is not a solid cone or a solid cylinder because of the fluid passages inside the turbocharger. For that reason a unity value for these parameters will correspond to a perfect solid body, and due to the presence of holes inside turbocharger parts, the values of θ_i must be between zero and one.

$$m_H = \theta_H \cdot \rho_H \cdot \frac{\pi}{12} \cdot L_H \cdot (D_T^2 + D_C^2 + D_T D_C) \quad (4.45)$$

$$m_{T/C} = \theta_{T/C} \cdot \rho_{T/C} \cdot \left(\frac{\pi \cdot D_{T/C}^2}{4} \cdot L_{T/C} \right) \quad (4.46)$$

Summarizing seven constants; three for the geometry (θ_T, θ_H and θ_C) and four for the capacitance distribution (α, β, γ and ϵ) must be fitted using the capacitance data of the four turbochargers (20 capacitances) from the thermohydraulic test bench. Using a non-linear optimization tool to minimize the root mean square difference between the measured and the modelled capacitances the value of the seven constants can be determined. Considering the uncertainties of such a long and intensive testing procedure and the inherent simplifications of equations 4.45 and 4.46; the agreement between modelled and measured data is acceptable as it can be observed in Figure 4.11. As it has been stated previously Turbocharger #5 is used for validation purposes and its data has not been used in the minimization procedure. However, the modelled capacitances of this turbocharger show good accordance with measured values. This fact supports the proposed capacitance determination procedure based on the first four turbochargers.

In Table 4.4 the values of these fitting constants are shown. In the case of turbine and compressor capacitances the coefficients θ_T and θ_C are close to 0.6 what means that 60% of a solid cylinder mass is used for compressor and turbine nodes. For bearing housing nodes the values of β, γ and $1 - \beta - \gamma$ are close to one third so the whole bearing housing division is close to an equitable case. While θ_H is close to 0,5 (about 50% of a solid cone frustum mass should be used for bearing housing).

Conductive conductances determination

For the simplified case, based on the assumptions of the developed model, the equation for conductive conductance corresponds to a one dimensional case of

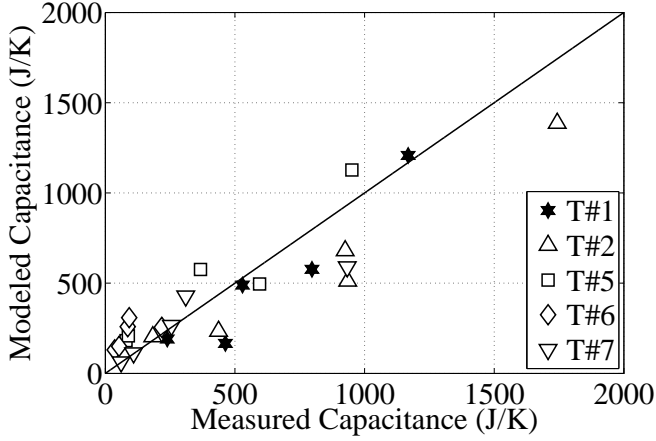


Figure 4.11: Capacitance fitting for each turbocharger

Table 4.4: Capacitance fitting constants values

Constant	Value
α	0.78
β	0.40
γ	0.32
ϵ	1
θ_T	0.60
θ_H	0.51
θ_C	0.59

conduction between two adjacent planes [65], i.e. as shown in equation 4.47. This equation is based on two conductances connected in series.

$$K_{ij} = (k_i \cdot k_j) / (e_i \cdot k_j + e_j \cdot k_i) \cdot A_{ij} \quad (4.47)$$

In order to be able to calculate the conductive conductance, it is necessary to know the conductivity of the materials (k_i), the distance between the planes (equivalent width, e_i , as shown in Figure 4.12) and the contact areas (A_{ij}).

Conventionally, turbine and central housing are made of cast iron while the compressor is made of aluminium. In Table 4.3 some data of conductivity of the turbocharger materials (k_i) is given, where a distinction in the cast iron of turbine and housing is made.

The width of each plane can be measured externally for compressor and turbine but not for the housing. The reason is that compressor and turbine

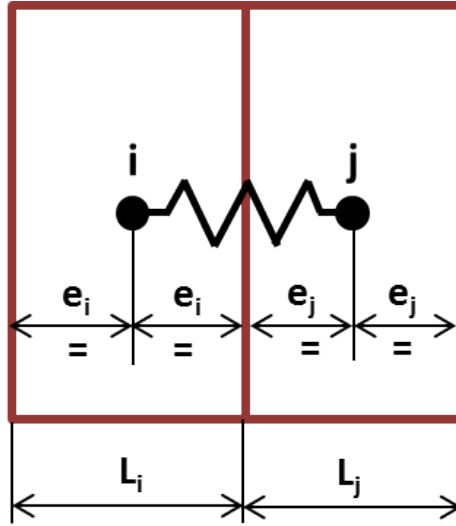


Figure 4.12: Nodes equivalent width

casing correspond to a node in the model but the bearing housing case is divided in three parts. Therefore the external length of the housing (available value in Table 3.1) must be distributed among its three nodes (H1, H2 and H3) as sketched in Figure 3.1. Furthermore, the values of contact area cannot be calculated directly from the simple external geometry values of Table 3.1. The passages for the flow of the different fluids inside the turbocharger do not allow the simplification of contact areas to circumferential areas. Therefore, a closer analysis of these parameters is performed, as follows.

For a given turbocharger the bearing housing length must be divided accordingly to the node divisions of the model. The final width for equation 4.47 will be half of the plane length, as shown in Figure 4.12, because the lumped model node is located in the centre of each plane.

The fitting constants for distributing the capacitances of the housing nodes can be used to make a correct division of the housing length for conductances determination. So, the length of housing is divided using the previous coefficients from equation 4.43 as shown in equation 4.48.

$$\begin{aligned}
 L_{H1} &= \beta \cdot L_H \\
 L_{H2} &= (1 - \beta - \gamma) \cdot L_H \\
 L_{H3} &= \gamma \cdot L_H
 \end{aligned}
 \tag{4.48}$$

Finally, an assumption for contact area must be done to use equation 4.47. The contact area between the planes is assumed to be circumferential ($A_{eff}^{ij} =$

$\pi/4 \cdot (D_{eff}^{ij})^2$) due to the assumption of cylinders and cone frustum for turbo parts. However, as turbocharger real geometry is not solid an effective diameter (D_{eff}) of the circumference must be determined. This diameter must be between the values of the corresponding turbocharger external geometry (turbine, bearing housing or compressor). This is shown in equation 4.49, where two fitting constants have been used to account for the contribution of the diameter of adjacent planes.

$$D_{eff}^{ij} = \delta_i \cdot D_i + \xi_j \cdot D_j \quad (4.49)$$

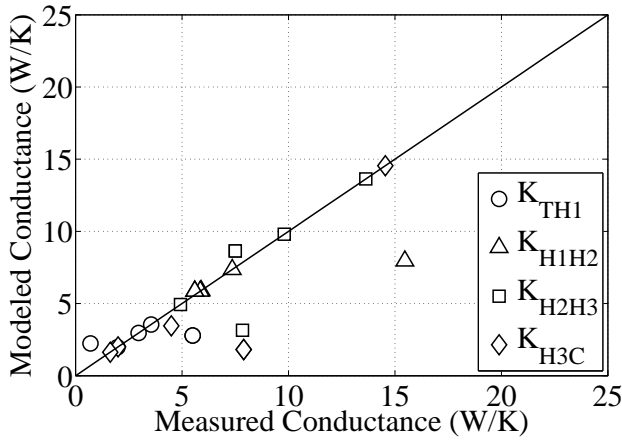


Figure 4.13: Conductive conductances fitting for each turbocharger

The diameters of turbine, compressor and bearing housing correspond to direct geometric measures of a turbocharger given in Table 3.1. For the conductances $K_{T/H1}$ and $K_{H1/H2}$ turbine and housing diameters are involved, while for $K_{H2/H3}$ and $K_{H3/C}$ compressor and housing diameters must be used. Summarizing, two constants (δ_i and ξ_j) must be fitted for each conductive conductance. However, the effective contact areas of water cooled turbochargers should be different from those of non-water cooled turbochargers (due to the additional water passages inside the housing). Moreover, the design of non-water cooled turbochargers should be less solid because proper temperatures at compressor casing must be assured without water at the bearing housing. For that reasons different fitting must be done for water cooled (δ_i^c and ξ_j^c) and non-water cooled (δ_i^{nc} ξ_j^{nc}) turbochargers.

Using an optimization tool to minimize the root mean square difference between measured and modelled conductances and distinguishing between water and non-water turbochargers the constants can be determined. In Figure

4.13 the results of the fitting are shown giving acceptable accuracy, validating the approach.

4.3 Gas flow models

In this section a VGT extrapolation model will be developed and a discharge coefficient model in two stage turbocharger valves. The validation of the models will be done in the next chapter based on the experimental data of the previous chapter.

The gas flow modelling of the compressor has been left outside of the contents of this thesis. The compressor gas flow model that has been used in the thesis is presented in previous works of Torregrosa [128]. Moreover, the recent model proposed by Galindo [129] has been used for compressor map extrapolation.

Extended model for VGT performance maps extrapolation

As it is showed in [30], during engine transient and partial load design conditions for the ICE the turbocharger turbine works at off-design conditions. In these off-design conditions the turbine works at high blade to jet speed ratios (σ) or low pressure ratios and low power outputs as shown in [86] due to turbocharger wheel inertia and pulsating flow in the exhaust of the ICE. Traditional measurements of turbine maps in gas stands are unable to capture this behaviour [87]. Only a narrow range turbine map is provided by manufacturers as a standard practice. For this reason it is necessary to develop a model capable of extrapolating turbine mass flow parameter and efficiency.

Sub-model for Mass flow parameter prediction

Model development and main hypotheses

The extrapolation procedure is based on modelling the turbine as a single equivalent nozzle. In that way, an equation of the throat area of that equivalent nozzle must be deduced and it must depend only on easy measurable geometry of the turbine and on the information available in a standard map. In Figure 4.14a this procedure is sketched, where it is shown that the equivalent nozzle covers from station 0 to 4 of the radial turbine. Continuity equation can be applied to stator, rotor and equivalent nozzle, as shown in equation (4.50). The velocity of the equivalent nozzle in that equation can be obtained comparing the enthalpy drop of the stages (stator and rotor) with the enthalpy drop of the equivalent nozzle [94]. Figure 4.14b shows the ratio of pressure drop in the rotor to total pressure drop in the VGT, measured for T#6 in [27] plotted on a reduced mass flow map. From this comparison equation (4.52) can be obtained, where the velocities v_2' and w_4 have been introduced as function of mass flow using

equation (4.50). For the derivation of the equation (4.52) it has been assumed that $p_3 = p_{2'}$ and that the flow is incompressible ($\rho_3 = \rho_{2'}$) due to the small size of the vaneless space. Solving for the mass flow and substituting in equation (4.51) it is possible to find the expression for the equivalent nozzle area shown in equation (4.53). Equation (4.51) has been obtained comparing the enthalpy drop of the equivalent nozzle with the enthalpy drops of the stator and the rotor [26]. After this steps it is necessary to transform equation (4.53) into an equation where only the variables available in turbine maps appear, as well as some global geometrical definitions.

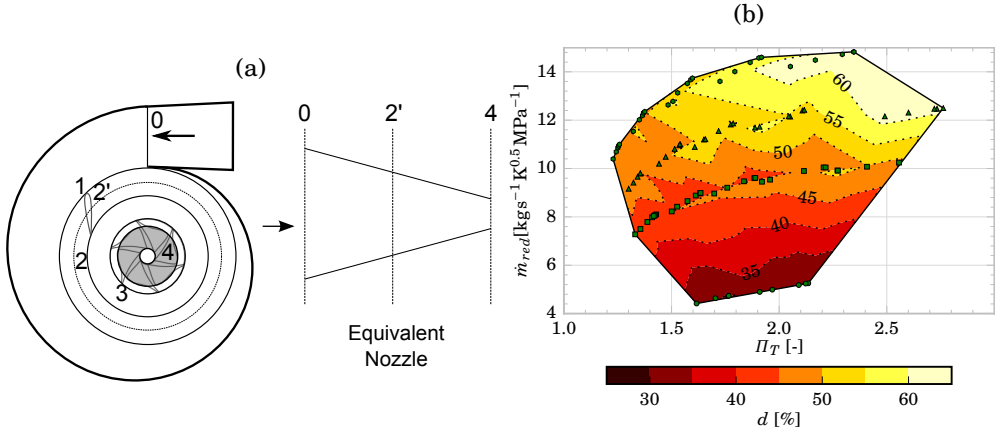


Figure 4.14: (a) Reduction of a radial turbine to an equivalent nozzle and stations distribution. (b) Measured ratio of pressure drop in the rotor to total pressure drop in the turbine ('d') in the VGT map [27] of T#6

$$\dot{m}_T = A_{2'} \rho_{2'} v_{2'} = A_4 \rho_4 w_4 = A_{Neq} \rho_4 v_{Neq} \quad (4.50)$$

$$v_{Neq}^2 = v_{2'}^2 + u_3^2 - u_4^2 + w_4^2 - w_3^2 \quad (4.51)$$

$$v_{Neq}^2 = \left(\frac{\dot{m}_T}{A_{2'} \rho_{2'}} \right)^2 + u_3^2 - u_4^2 + \left(\frac{\dot{m}_T}{A_4 \rho_4} \right)^2 - w_3^2 \quad (4.52)$$

$$A_{Neq} = A_4 \sqrt{\frac{1 + \left(\frac{u_4}{v_{Neq}} \right)^2 - \left(\frac{u_3}{v_{Neq}} \right)^2 + \left(\frac{w_3}{v_{Neq}} \right)^2}{\left(\frac{A_4}{A_{2'}} \right)^2 \left(\frac{\rho_4}{\rho_{2'}} \right)^2 + 1}} \quad (4.53)$$

The model must have the capability to compute the geometrical throat section of the stator vanes ($A_{2'}^{geom}$) based on VGT position and geometry of the

turbine. Equation (4.54) shows how the throat length of the stator ($l_{th2'}$) can be obtained, making use of Figure 4.15a and of equation (4.55).

$$l_{th2'} = 2r_2 \cdot \sin(\delta/2) \cdot \cos(\varphi_2^{metal}) \quad (4.54)$$

$$r_2 = \sqrt{(r_{2a} - L_{TE} \cdot \cos(\varphi_2^{metal}))^2 + (\sin(\varphi_2^{metal}) \cdot L_{TE})^2} \quad (4.55)$$

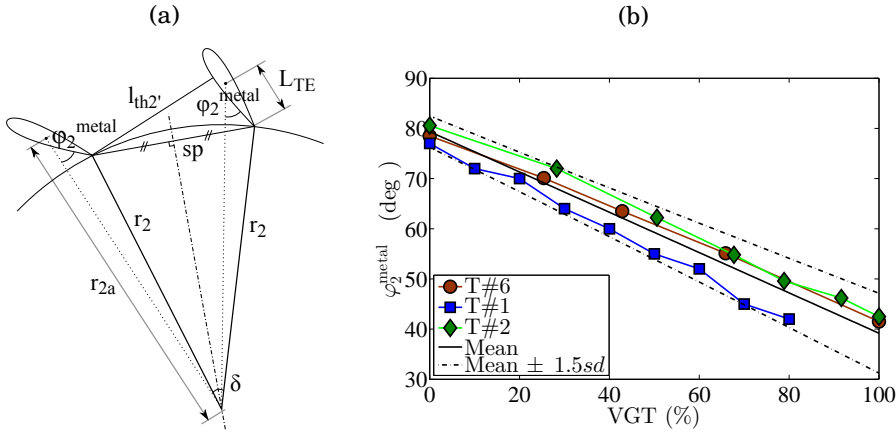


Figure 4.15: (a) Geometrical relations of a VGT stator vanes (b) Linear relations between stator vanes angle and VGT opening

In order to get the necessary φ_2^{metal} value for equation (4.54) the VGTs corresponding to turbochargers T#1, T#2 and T#6 from Table 3.1 have been characterised. If detailed vanes geometry was available, a more accurate geometrical characterisation would be possible, as the one described in [130]. Figure 4.15b shows empirically obtained relations between stator blades average angle (φ_2^{metal}) and VGT position for the three tested turbines (T#1, T#2 and T#6). In the case that this information was not possible to be obtained, the average values of slope and y-intercept of the mean line shown in Figure 4.15b can be used. The angle of the stator vanes can then be calculated using equation (4.56), obtained from Figure 4.15b for any VGT position percentage.

$$\varphi_2^{metal} \text{ (deg)} = -0.004 \cdot VGT + 79.36 \quad (4.56)$$

It must be taken into account that the relations shown in Figure 4.15b come from cold conditions and variations at hot operational conditions, due to metal thermal expansion and loading in the blades mechanism, must be expected. These thermal expansions introduce further uncertainty in calculating

geometrical throat length ($l_{th2'}$). Finally $A_{2'}^{geom}$ can be calculated as shown in equation (4.57)

$$A_{2'}^{geom} = l_{th2'} \cdot t_2 \cdot n_2 \quad (4.57)$$

Continuing with the simplifications of equation (4.53) and knowing the diameters of turbine rotor it is possible to group the terms of u_3 and u_4 . After that, using the blade to jet speed ratio definition it is possible to introduce the isentropic velocity c_{ss} to replace the equivalent nozzle velocity (v_{Neq}). An additional approximation can be made in this point following the dimensional analysis of equation (4.58).

$$\frac{v_{Neq}^2}{c_{ss}^2} = \eta_{ts} + \frac{v_4^2}{c_{ss}^2} = O[10^{-1}] + O[10^{-4}] \Rightarrow \frac{v_{Neq}^2}{c_{ss}^2} \approx \eta_{ts} \quad (4.58)$$

With this approximation it is now possible to introduce the blade to jet speed ratio, defined in equation (4.59), in the equivalent nozzle area expression. At this point the equivalent nozzle area can be approximated by equation (4.60), where the term $(w_3/c_{ss})^2$ is lumped in 'b' fitting coefficient.

$$\sigma = \frac{2 \cdot \pi \cdot n \cdot r_3}{\sqrt{2 \cdot \bar{c}_p \cdot T_{0t} \cdot \left[1 - \left(\frac{p_4}{p_{0t}} \right)^{\frac{\gamma-1}{\gamma}} \right]}} \quad (4.59)$$

$$A_{Neq} = A_4 \sqrt{\frac{1 + \frac{\sigma^2}{\eta_{ts}} \left[\left(\frac{D_4}{D_3} \right)^2 - 1 \right] + \frac{b}{\eta_{ts}}}{\left(\frac{A_4}{A_{2'}} \right)^2 \left(\frac{\rho_4}{\rho_{2'}} \right)^2 + 1}} \quad (4.60)$$

There is an inherent problem with equation (4.60). At certain conditions; mainly at high reduced speeds and low pressure ratios; the term inside of the square root may become negative, specially at very low values of η_{ts} . To avoid possible instabilities during extrapolations a constant average value of efficiency is assumed ($\eta_{ts} = \bar{\eta}_{ts} = 0.8$), relying on 'b' coefficient to provide sufficient numerical flexibility to the model.

Finally, it is necessary to find an expression for the density ratio shown in equation (4.60). The hypotheses taken in [94] are not consistent enough for non-measured VGT positions extrapolation. So, these hypotheses have been revised and changed here with the objective of finding an expression for the density ratio by using the equation of ideal gases and expressing the density ratio as a product of pressure ratio (p_4/p_3) and temperature ratio (T_3/T_4). The temperature ratio can be estimated using adiabatic efficiency of the rotor. However, rotor adiabatic efficiency is not available in turbine maps so an additional assumption is made in this point and for this single purpose: i.e. the efficiency of the rotor is

equal to turbine total to static efficiency. This strong hypothesis is made for the single purpose of getting a temperature ratio and it implies the following thermodynamic assumptions:

- The polytropic index is equal in the rotor and in the stator.
- Absolute kinetic term at turbine inlet and relative kinetic term at rotor inlet are neglected.
- Turbine inlet velocity is equal to the outlet velocity ($v_1 = v_4$).

Taking into account the previous assumption it is possible to express the area of the equivalent nozzle using equation (4.61).

$$A_{Neq} = \frac{a \cdot A_4^{geom} \cdot \sqrt{1 + \frac{\sigma^2 \cdot \left[\left(\frac{D_4}{D_3} \right)^2 - 1 \right] + b}{\bar{\eta}_{ts}}}}{\sqrt{1 + \left(c \cdot \frac{A_4^{geom}}{A_{2'}^{geom}} \right)^2 \cdot \frac{\left(\frac{1}{\Pi_{2',4}} \right)^2}{\left(1 - \eta_{ts} \cdot \left(1 - \left(\frac{1}{\Pi_{2',4}} \right)^{\frac{\gamma-1}{\gamma}} \right) \right)^2}}}} \quad (4.61)$$

In this equation a new constant ('d') has been introduced (equation (4.62)) through the term $\Pi_{2',4}$ (equation (4.63)). $\Pi_{2',4}$ represents pressure ratio in the VGT rotor and 'd' term has been shown in Figure 4.14b on the VGT map of T#6. This means another last assumption: the stator pressure drop to total pressure drop ratio is constant for a VGT position. It is easy to obtain equation (4.63) from that assumption introducing the 'd' fitting coefficient.

$$d = \frac{p_{2'} - p_4}{p_{0t} - p_4} \quad (4.62)$$

$$\Pi_{2',4} = 1 + d \left[\Pi_{0,4}^{ts} - 1 \right] \quad (4.63)$$

Analysis of the coefficients

Summarizing, both coefficients 'b' and 'd' of equation (4.61) have physical meaning, as they come from theoretical considerations, even with simplifying hypotheses. The validity of introduced hypotheses for mass flow parameter extrapolation in radial VGTs will be further checked in the next chapter describing experimental validation of the model. Therefore their values must have a coherent order of magnitude. The analysis of all the coefficients of equation (4.61) is detailed below:

- Coefficient 'a': it represents the discharge coefficient of the rotor (equation (4.64)). As the rotor outlet geometrical area (A_4^{geom}) is independent of

VGT position 'a' can be considered constant for a given turbocharger. The order of magnitude of this coefficient must be between 0 and 1 based on the definition of discharge coefficient.

$$A_4 = A_4^{geom} \cdot a \quad (4.64)$$

- Coefficient 'b': it comes from velocity triangles [94]. It is a difficult parameter to be calculated experimentally but its order of magnitude can be estimated as shown in equation (4.65). It can also be expected that more open VGT positions must give higher 'b' values than closer VGT positions; due to the higher radial velocities at rotor inlet, for the same pressure ratio and peripheral speed values.

$$\begin{aligned} b &= \left(\frac{v_0}{c_{ss}} \right)^2 + \left(\frac{w_3}{c_{ss}} \right)^2 = \frac{A_{Neq}}{A_0} \cdot \left(\frac{1}{\Pi_T} \right)^{(1/\gamma)} + O[10^{-1}] = \\ &= O[10^{-1}] + O[10^{-1}] \rightarrow O[10^{-1}] \leq b \leq O[10^0] \end{aligned} \quad (4.65)$$

- Coefficient 'c': it represents the quotient between rotor discharge coefficient (coefficient 'a') and the stator discharge coefficient (C_{Ds} as shown in equation (4.66)), which in case of VGT should be dependant on stator vanes position (equation (4.54)). For more open VGT positions A_2^{geom} is high so 'c' is expected to be low. In addition 'c' must fulfil always inequation (4.67) since in spite of the effect of throat variation in the stator, effective section, introduced through the discharge coefficient (C_{Ds}), must be always below 1.

$$A_{2'} = A_2^{geom} \cdot C_{Ds} \quad (4.66)$$

$$C_{Ds} = \frac{a}{c} \leq 1 \quad (4.67)$$

- Coefficient 'd' (equation (4.62)): from experimental measurements of pressure in the space between stator and rotor in a VGT, it is possible to estimate the order of magnitude of the coefficient 'd' [27] and to confirm that the assumption of constant value for a given VGT position is coherent for small radial VGTs. Figure 4.14b shows that the coefficient increases with VGT opening with a variation in the range of [0.35, 0.6].

Once the equivalent nozzle area (equation (4.61)) is known, the reduced mass flow can be calculated using the expression of flow through an orifice with isentropic expansion, equation (4.68).

$$\dot{m}_{red} = A_{Neq} \sqrt{\frac{\gamma}{R}} \left(\frac{1}{\Pi_{0,4}^{(ts)}} \right)^{\frac{1}{\gamma}} \sqrt{\frac{2}{\gamma-1} \left[1 - \left(\frac{1}{\Pi_{0,4}^{(ts)}} \right)^{\frac{\gamma-1}{\gamma}} \right]} \quad (4.68)$$

As it has been already explained, the extrapolation model discussed above is evolved from a previous model described in [94]. That model had the problem of being unable to extrapolate to non-measured VGT positions. Their hypotheses have been revised and improved here. Nevertheless, in order to get the new extrapolation capabilities the following procedure is also needed.

The main approach to develop the possibility of extrapolation to VGT positions is based on the analysis of the physical meaning of the fitting coefficients of the model. These coefficients are constant for a given VGT position, i.e. they are independent of turbine speed and of pressure ratio.

Table 4.5: Coefficient 'a' values

	Average	T#6	T#1	T#2
$a \pm sd$	0.40 ± 0.07	0.41	0.47	0.33

Using the turbochargers T#1, T#2 and T#6 from Table 3.1, it is possible to provide a first approach for the behaviour of the fitting coefficients that give good precision in terms of reduced mass flow prediction compared to experiments. So fitting the coefficients of equation (4.61) for several VGTs it is possible to survey their behaviour with VGT position. The fitting is performed using the available data of the map in which the reduced mass flow is known. Previously described physical trends have been imposed in the fitting procedure, for instance the 'b' coefficient of more open VGT position is imposed to be higher or equal than for the closer position. Significance test have been performed to check the necessity of the different coefficient proving each of them to be statistically significant with a p-value lower than 0.05.

In Figure 4.16 the obtained results for the fitting coefficients that vary with VGT position ('b', 'c' and 'd') are shown for the turbochargers T#1, T#2 and T#6. This results were used to detect the trends in the coefficients. For the coefficient 'b' an increasing trend is obtained, according to the expected behaviour. Figure 4.16a shows that the values of this coefficient are close to a linear behaviour of positive slope. For 'c' coefficient the trend with VGT position must be decreasing;

this has been confirmed in Figure 4.16c, obtained from the fitting of several VGTs and several positions after imposing such a negative trend. Again 'c' trend is close to linear behaviour but now with a negative slope. Coefficient 'd' behaviour is in accordance with experimental results from Figure 4.14b and shows similar positive trend than constant 'b', as it is shown in Figure 4.16e. In that way, coefficients dependence on VGT position has been obtained.

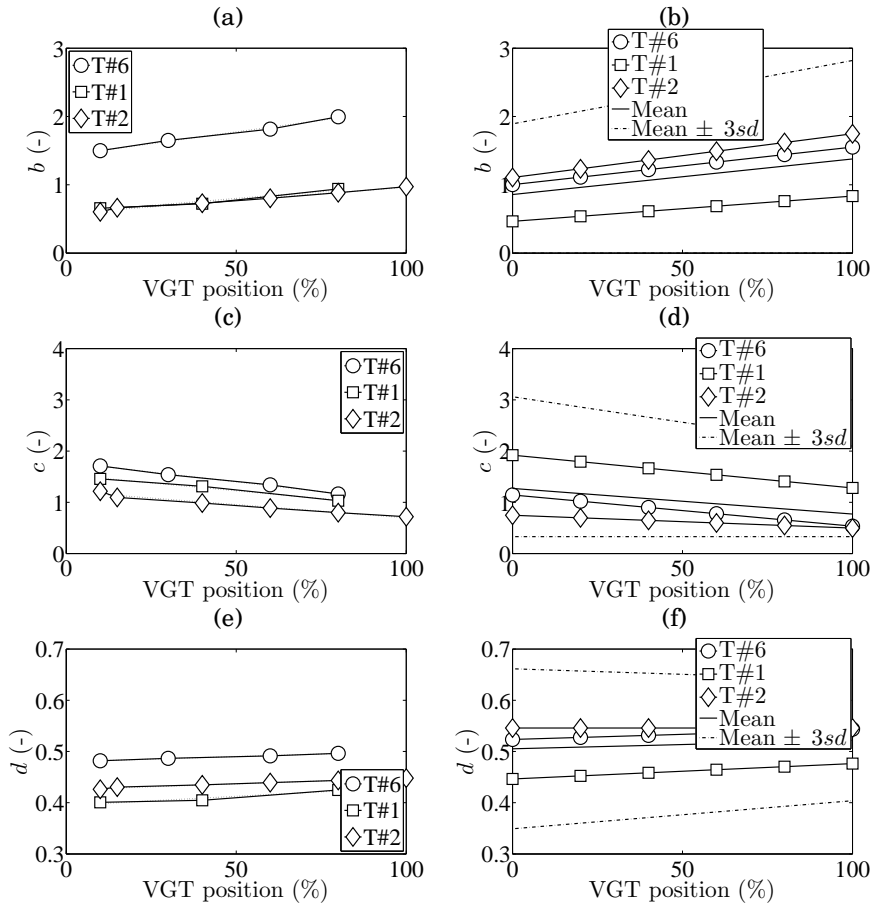


Figure 4.16: Reduced mass flow coefficients dependence with VGT position (a, c and e) and final fitted coefficients (b, d and f)

Using the previous information it is possible to provide an imposed trend for the global map fitting. Only one fitting will be now needed for each turbocharger in which 'a' will be constant and a linear trend with VGT position for the other three coefficients will be imposed. In that way, seven coefficients must be fitted using a non-linear fitting procedure for each VGT. The values of the discharge

coefficient of the rotor ('a'), for the three turbochargers, are summarised in Table 4.5. It can be observed that for T#2 rotor discharge coefficient ('a') is lower than for T#6 and T#1, probably due to lower wheel diameter. As initial values for the fitting, average values from the dependence study have been used and the upper and lower bounds are 3 times standard deviation. Furthermore it is necessary to add the condition of equation (4.67) to make 'c' coefficient to be fully physical, as the discharge coefficient of the stator cannot be higher than unity. In that way the results of Figure 4.16b, Figure 4.16d and Figure 4.16f have been obtained for the three coefficients and the three VGTs. The linear fitting of the 'b', 'c' and 'd' constants is shown for the three VGTs as well as the average value and the boundaries for the fitting of new turbochargers. Lower boundary of 'b' coefficient is zero instead of using standard deviation in order to avoid negative values, which are not physically possible. Lower boundary of 'c' is calculated to avoid stator discharge coefficient values higher than one (equation (4.67)).

In that way, for extrapolating a new turbine reduced mass flow map using this approach a first fitting of seven coefficients must be done using the data from the map. After that fitting the reduced mass flow for any VGT position and pressure ratio or reduced speed can be calculated.

Total to static efficiency model

Model development and main hypotheses

In order to improve efficiency fitting model it is necessary to extrapolate both in rotational speeds and in VGT position. As the model constants developed in [94] are dependant on both variables new revision and analysis must be performed. The procedure to develop the model is based on the analysis of the available data of the turbines used to refine the models.

As described in [94] the efficiency extrapolation is based on using the Euler equation of turbomachinery and assuming constant meridional component velocities. In that way in equation (4.69), which represents the definition of total to static adiabatic efficiency, it is possible to express the numerator in terms of velocities using Euler equation and turbine enthalpy drop as shown equation (4.70). The tangential velocities in that equation can be expressed in terms of meridional velocity using equation (4.71) and equation (4.72). Using them now in equation (4.69) and taking into account the isentropic evolution in the denominator it is possible to obtain equation (4.73).

$$\eta_{ts} = \frac{T_{0t} - T_{4t}}{T_{0t} - T_{4ts}} \quad (4.69)$$

$$\dot{W} = \dot{m} c_p (T_{0t} - T_{4t}) = \dot{m} (u_3 v_{\theta 3} - u_4 v_{\theta 4}) \quad (4.70)$$

$$v_{\theta 3} = v_0 \tan \alpha_3 \quad (4.71)$$

$$v_{\theta 4} = u_3 \left(\frac{r_4}{r_3} \right) - v_0 \tan \beta_4 \quad (4.72)$$

$$\eta_{ts} = \frac{u_3 v_0 \tan \alpha_3 - \left[u_3 \left(\frac{r_4}{r_3} \right) - v_0 \tan \beta_4 \right] u_3 \left(\frac{r_4}{r_3} \right)}{c_p T_{0t} \left(1 - \left(\frac{1}{\Pi_{0,4}^{(ts)}} \right)^{\frac{\gamma-1}{\gamma}} \right)} \quad (4.73)$$

From these assumptions it is possible to obtain equation (4.74) for constant tip speed maps using the definition of σ . It is worth noting the dependence of equation (4.74) on A_{Neq} term that must be calculated using equation (4.61). In equation (4.74) the tangent of rotor inlet angle (α_3) is a numerically unstable term since due to the behaviour of the tangent function. However, a transformation can be used to convert rotor inlet angle into stator outlet angle as shown in equation (4.75), using mass flow and angular momentum conservation equations [30]. Coefficient z_3^{geom} is a geometrical coefficient that can be obtained theoretically from Figure 4.15a, as shown in equation (4.76), where $l_{th2'}$ can be obtained from equation (4.54) and φ_2^{metal} for equation (4.56) respectively and 'c' coefficient is defined in equation (4.67). In that way the dependence with VGT position has been also introduced here. The coefficient 'c' has been fitted previously along with the rest of the reduced mass flow coefficient using the available data of the map.

$$\begin{aligned} \eta_{ts} &= \quad (4.74) \\ &= -2 \left(\frac{r_4}{r_3} \right)^2 \sigma^2 + 2 \frac{A_{Neq}}{A_0^{geom}} \left(\tan \alpha_3 + \frac{r_4}{r_3} \tan \beta_4 \right) \left[\frac{1}{\Pi_{0,4}^{(ts)}} \right]^{\frac{1}{\gamma}} \sigma \end{aligned}$$

$$\tan \alpha_3 = z_3^{geom} \sin \varphi_2^{metal} \quad (4.75)$$

$$z_3^{geom} = c \cdot \frac{r_2 \cdot 2\pi \cdot t_3}{t_2 \cdot l_{th2'} \cdot n_b} \cdot \frac{A_0^{geom}}{A_3^{geom}} \quad (4.76)$$

From all the previous steps, equation (4.77) can be written for the extrapolation, where some terms have been lumped into K_i coefficients for simplification (equations (4.78), (4.79) and (4.80)). In equation (4.77), K_2^* coefficient, shown in equation (4.80), plays an important role as a fitting constant ('z') has been added multiplying the sine function. The rest of the parts of efficiency equation (4.77) are related to physical values from turbine geometry or from the map as

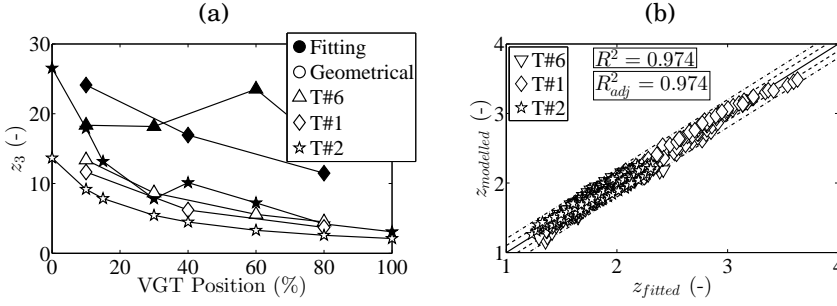


Figure 4.17: Difference between fitted and geometrical z_3^{geom} coefficient (a) and modelled 'z' versus fitted 'z' (b)

it has been already described in [94]. φ_2^{metal} and β_4^{metal} assumes that there are negligible deviation angles in expansion stages, what is usually accepted at high pressure ratios [30].

$$\eta_{ts} = -K_1\sigma^2 + K_2^* \left(1 - \frac{K_3}{\sigma^2}\right)^{\frac{1}{\gamma-1}} \cdot \sigma \quad (4.77)$$

$$K_1 = 2 \left(\frac{r_4}{r_3}\right)^2 \quad (4.78)$$

$$K_3 = \frac{u_3^2}{2c_p} \quad (4.79)$$

$$\begin{aligned} K_2^* &= \quad (4.80) \\ &= 2 \frac{A_{Neq}}{A_0^{geom}} \left(z \cdot z_3^{geom} \sin(\varphi_2^{metal}) + \sqrt{\frac{K_1}{2}} \tan(\beta_4^{metal}) \right) \end{aligned}$$

The reason for using a fitting coefficient 'z' lies in the various simplifications made to obtain equation (4.77) that make impossible a good fitting of the efficiency, specially if off-design conditions must be covered. For example, assuming radial velocity equal to the axial one, assuming incompressible flow between stator and rotor stages and negligible flow deviation in stator and rotor blades. Indeed, comparing the z_3^{geom} coefficient using equation (4.76) and fitting it to match experimentally obtained adiabatic efficiency gives different results as shown in Figure 4.17a.

Model calibration procedure

There is a fitting 'z' coefficient for each point of turbine map. If this coefficient is calculated and plotted against blade to speed ratio and reduced speed,

different planar surfaces appear one for each VGT position. From these surfaces the most simple approach is to use linear decreasing trend for blade to speed ratio, being the slope and the y-intercept values linearly dependant on reduced speed. As the normal vector of the surfaces is similar the VGT dependence can be added directly in the independent term of the surface equation. This is done considering that the 'z' coefficient tends to increase until the maximum efficiency VGT position is reached and decrease later on. Therefore a parabolic trend with VGT position is proposed since maximum efficiency is reached around 60% of VGT opening. All these considerations lead to equation (4.81) for the 'z' coefficient where n_{red} is in ($rpm/K^{1/2}$) and VGT is in (%). In this equation, six constants must be fitted for a given turbocharger using the data of the whole map (all available positions). In Figure 4.17b the level of correlation between fitted 'z' values and modelled 'z' values using equation (4.81) is shown. It can be observed that modelled values correlate with the fitted ones as proved by the R^2 and R_{adj}^2 values. Significance test have been performed to check the necessity of the different coefficient proving each of them to be statistically significant with a p-value lower than 0.05. The standard deviation of the six coefficients are shown in the third column of Table 4.6. It is advised to use three times the standard deviation for new calibrations boundaries. For initial values the average values of the coefficients of Table 4.6 can be used.

$$z = -(a' \cdot n_{red} + b') \cdot \sigma + (c' \cdot n_{red} + d' \cdot VGT^2 + e' \cdot VGT + f') \quad (4.81)$$

Table 4.6: Efficiency coefficients average and standard deviation

Coefficient	Average	<i>sd</i>
a'	$1.47 \cdot 10^{-4}$	$3.58 \cdot 10^{-4}$
b'	3.33	$3.34 \cdot 10^{-1}$
c'	$3.59 \cdot 10^{-4}$	$3.21 \cdot 10^{-4}$
d'	$-7.67 \cdot 10^{-5}$	$9.05 \cdot 10^{-5}$
e'	$2.73 \cdot 10^{-2}$	$9.45 \cdot 10^{-3}$
f'	1.68	$2.38 \cdot 10^{-1}$

In Figure 4.18 a flowchart of the procedure used to extrapolate mass flow and efficiency is presented. Following the flowchart, the extrapolation procedure starts with the input of the available map data. Using this information the equivalent nozzle area can be solved from equation (4.68) and used in a non-linear fitting procedure in order to calibrate the coefficients 'a', 'b', 'c' and 'd'. For that purpose the boundaries of the different coefficients for the fitting procedure

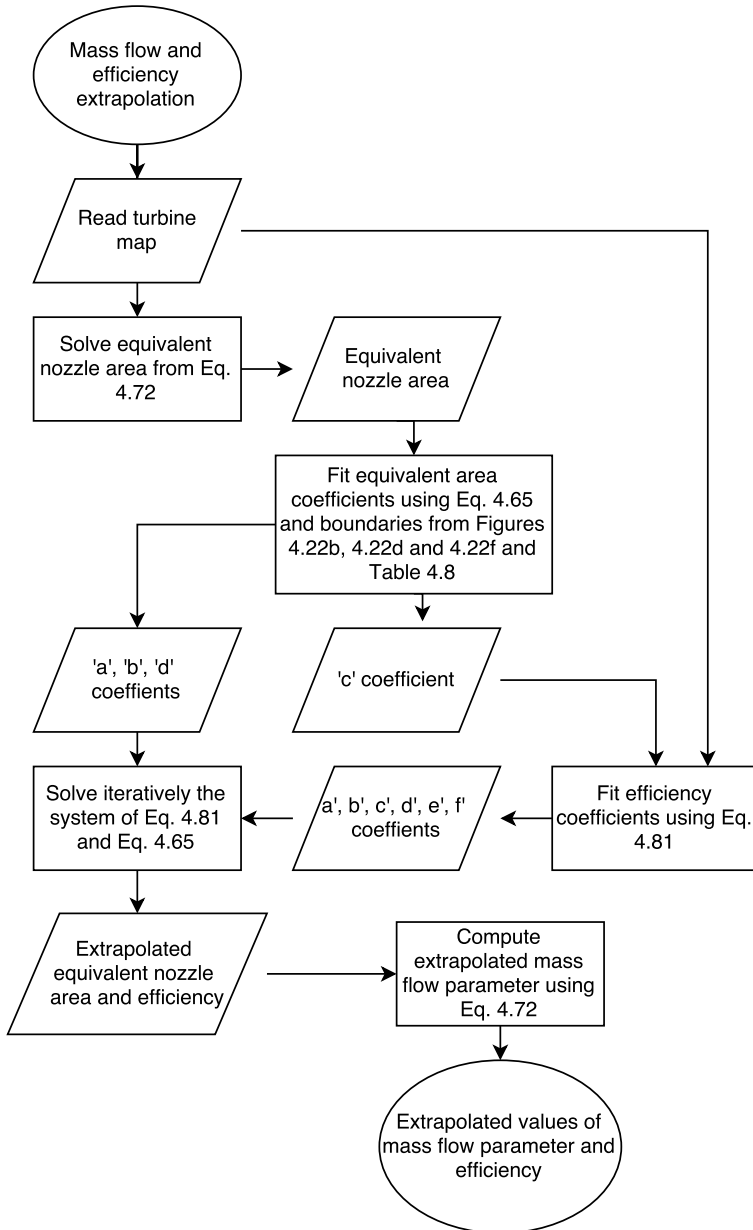


Figure 4.18: Procedure for mass flow parameter and efficiency extrapolation

are taken from Table 4.5 and Figures 4.16b, 4.16d, 4.16f. Using the fitted 'c' value and the information from the map the efficiency fitting coefficients are calibrated. After this step all the necessary coefficients are calibrated so

the system of equations composed of equation (4.61) and equation (4.77) can be solved with an iterative procedure to obtain the extrapolated values of equivalent nozzle area and efficiency. Finally, the extrapolated mass flow parameter is obtained from equation (4.68) substituting the extrapolated equivalent nozzle area.

Discharge coefficient modelling in valves

In this section the analysis of discharge coefficient modelling of the two stage turbocharging system described in the previous chapter is studied. The by-pass valve between the two turbines, the waste gate valve of the HPT will be analysed.

Using the experimental data from the previous chapter a model will be fitted in order to predict the mass flow through the valves. This model can be used in 1D simulations in order to improve the predictions of overall engine performance. In order to characterise the discharge coefficient the theoretical mass flow through each valve is calculated for each measured point using Equation 4.82.

$$\dot{m}_{theoretical} = \frac{p_{00}}{\sqrt{T_{00}}} A_{geom} \sqrt{\frac{\gamma}{R}} \left(\frac{1}{\pi_{t/s}} \right)^{\frac{1}{\gamma}} \sqrt{\frac{2}{\gamma-1} \left(1 - \left(\frac{1}{\pi_{t/s}} \right)^{\frac{\gamma-1}{\gamma}} \right)} \quad (4.82)$$

By-pass valve

From the analysis of the measurements described in the previous chapter Figure 4.19 can be plotted. In this figure the real mass flow (measured) is represented against the theoretical mass flow given by equation 4.82 for different closure positions of the valve. By-pass valve positions have been averaged with maximum standard deviation of 1%. It can be observed that a single discharge coefficient for each position can be fitted since there is a linear behaviour in most of the points, what is in correspondence with equation 2.22.

Calculating the slope of each line (that represent the discharge coefficient of each position) in Figure 4.19 it is possible to obtain a trend that can be fitted to a third order polynomial as shown in Figure 4.20. The polynomial expression form is provided in equation 4.83. It is important to state here that this expression is only used for values of the valve closure above 30% since for lower closures the flow in the valve is choked and therefore the discharge coefficient is constant. This fact is confirmed by the behaviour of the points between 0% and 60% closures in Figure 4.20.

$$C_D^{BPV} = a \left(1 - \frac{\%BPV}{100} \right)^3 - b \left(1 - \frac{\%BPV}{100} \right)^2 + c \left(1 - \frac{\%BPV}{100} \right) \quad (4.83)$$

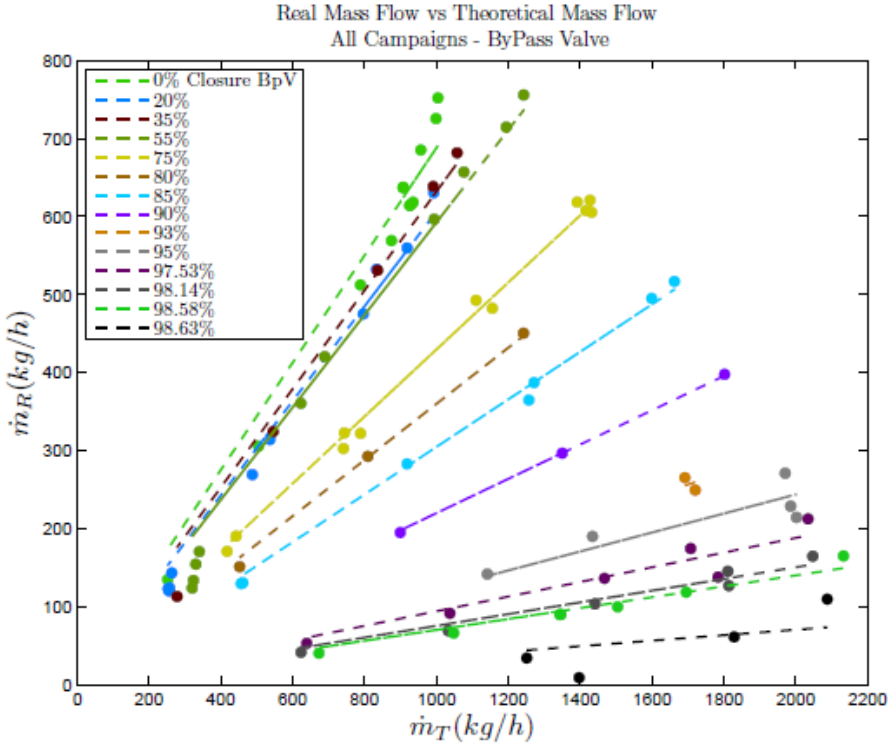


Figure 4.19: Real mass flow against theoretical mass flow for by-pass valve

It must be observed that averaged discharge coefficient was obtained for averaged positions. In order to improve the precision of the fitting the third polynomial expression coefficients were fitted using all the measured points individually. Equation 4.84 to calculate the real mass flow from the theoretical one was obtained, taking into account the definition of 2.22. In Figure 4.21 the modelled mass flow through by-pass valve is compared to the measured one. A root mean square error of 29.704 kg/h in the mass flow prediction is observed what represents sufficiently accurate model for 1D modelling.

$$\dot{m}_{mod}^{BPV} = \left(a' \left(1 - \frac{\%BPV}{100} \right)^3 - b' \left(1 - \frac{\%BPV}{100} \right)^2 + c' \left(1 - \frac{\%BPV}{100} \right) \right) \dot{m}_{th}^{BPV} \quad (4.84)$$

Waste-gate valve

To model the discharge coefficient of the waste-gate valve of the LPT the same approached used in the by-pass valve have been used. The averaged discharge

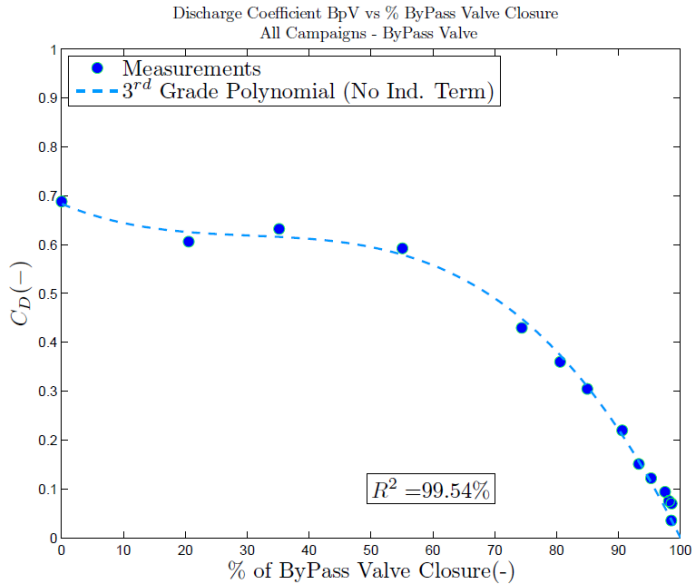


Figure 4.20: Average C_D versus average by-pass valve polynomial fitting

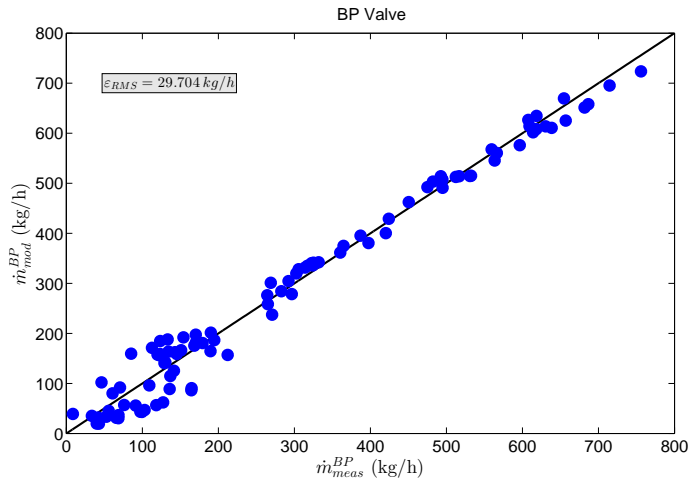


Figure 4.21: Modelled by-pass valve mass flow against theoretical mass flow

coefficient does not present any clear trend against the averaged valve closing. However, a strong dependency on the by-pass valve position is presented as it can be observed in Figure 4.22. That dependency appears because of the place that each valve occupy in the turbocharger. A more open by-pass valve

directs the flow towards turbine inlet while a more closed position directs the flow towards the waste-gate orifice. In that way, the position of the by-pass valve affects the flow that enters in the LPT and therefore impacts the flow that passes through the waste-gate valve.

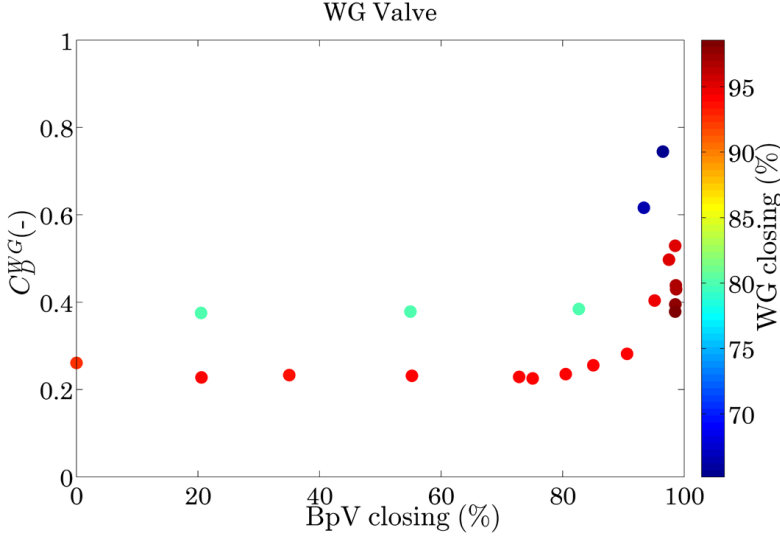


Figure 4.22: Averaged waste-gate valve C_D against by-pass valve position

In Figure 4.22 it can be observed that the dependence of the C_D is exponential with the by-pass valve. In order to obtain an expression that can be used for predictions it is also necessary to take into account that at fully closed waste-gate the discharge coefficient must be zero. For that reason a logarithmic expression is used multiplied by the exponential function. Finally a constant dependant on the waste-gate position must be used to predict the C_D at lower percentages of by-pass valve closing (Figure 4.22). This constant is different for each waste-gate position and it is modelled using a logarithmic expression in order to simplify the final equation to fit. In equation 4.85 all these effects have been combined. It can be observed that the valves positions have been divided by one hundred in order to obtain fitting coefficients with orders of magnitude around unity.

$$\dot{m}_{mod}^{WGV} = \left(a \left(\ln \left(2 - \frac{\%WG V}{100} \right) \right)^b + c \cdot \exp \left(d \cdot \frac{\%BPV}{100} \right) \left(\ln \left(2 - \frac{\%WG V}{100} \right) \right)^e \right) \dot{m}_{th}^{WGV} \quad (4.85)$$

As it can be observed in Figure 4.23 the equation is consistent since the

discharge coefficient is inferior to unity for the whole range of both valves closing and at fully closed WGV the discharge coefficient is zero.

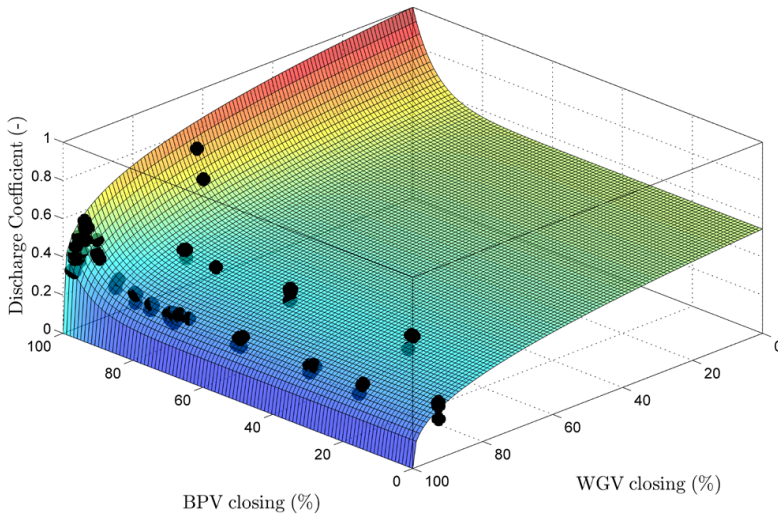


Figure 4.23: Modelled discharge coefficient of the waste-gate valve

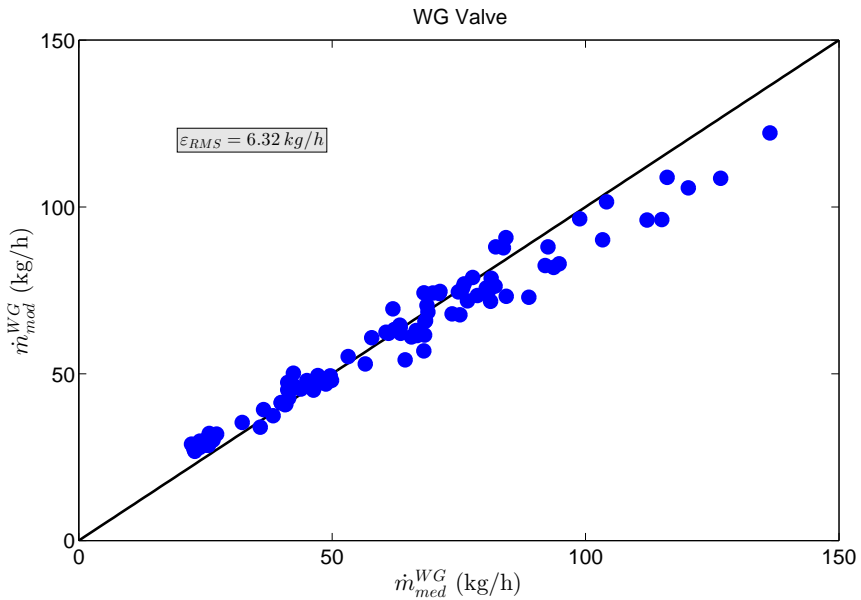


Figure 4.24: Modelled waste-gate valve mass flow against theoretical mass flow

In the same way as it has been done in the by-pass valve in order to improve the model a global fitting without averaging was done using the full expression of equation 4.85. In Figure 4.24 the modelled mass flow through waste gate valve is compared to the measured one. A root mean square error of 6.32kg/h in the mass flow prediction is observed what represents sufficiently accurate model for 1D modelling.

4.4 References

- [3] J. R. Serrano, P. Olmeda, F. J. Arnau, A. Dombrovsky, and L. Smith. “Methodology to Characterize Heat Transfer Phenomena in Small Automotive Turbochargers: Experiments and Modelling Based Analysis”. In: *Proceedings of ASME Turbo Expo 2014*. 2014 (cit. on pp. vii, 91).
- [26] Miguel Ángel Reyes-Belmonte. “Contribution to the Experimental Characterization and 1-D Modelling of Turbochargers for IC Engines”. PhD thesis. Universitat Poliècnica de València, 2013 (cit. on pp. 6, 26, 51, 52, 60, 66, 89, 91, 94, 98, 114, 145, 151, 153, 190).
- [27] Luis Miguel García-Cuevas González. “Experiments and Modelling of Automotive Turbochargers under Unsteady Conditions”. PhD thesis. Universitat Poliècnica de València, 2014 (cit. on pp. 6, 62, 113, 114, 118).
- [28] J. Serrano, P. Olmeda, A. Páez, and F. Vidal. “An experimental procedure to determine heat transfer properties of turbochargers”. In: *Measurement Science and Technology* 21.3 (2010). DOI: 10.1088/0957-0233/21/3/035109 (cit. on pp. 7, 27, 52, 54, 89).
- [30] N. Watson and M. Janota. *Turbocharging the Internal Combustion Engine*. Macmillan Publishers, Ltd., 1982 (cit. on pp. 15, 18, 32, 113, 122, 123).
- [47] D. Bohn, N. Moritz, and M. Wolff. “Conjugate Flow and Heat Transfer Investigation of a Turbo Charger: Part II — Experimental Results”. In: *Proceedings of ASME Turbo Expo*. Vol. 3. ASME, 2003, pp. 723–729. DOI: 10.1115/GT2003-38449 (cit. on pp. 22, 98, 139, 164).
- [65] F. Incropera, D. DeWitt, T. Bergman, and A. Lavine. *Fundamentals of Heat and Mass Transfer*. John Wiley & Sons, 2007 (cit. on pp. 26, 98, 101, 110).
- [66] J. R. Serrano, P. Olmeda, F. J. Arnau, M. A. Reyes-Belmonte, and H. Tartoussi. “A study on the internal convection in small turbochargers. Proposal of heat transfer convective coefficients”. In: *Applied Thermal Engineering* 89 (2015), pp. 587–599. ISSN: 1359-4311 (cit. on pp. 26, 91).

- [69] P. Olmeda, V. Dolz, F. Arnau, and M. Reyes-Belmonte. “Determination of heat flows inside turbochargers by means of a one dimensional lumped model”. In: *Mathematical and Computer Modelling* 57.7 - 8 (2013), pp. 1847–1852. ISSN: 0895-7177. DOI: 10.1016/j.mcm.2011.11.078 (cit. on pp. 26, 91).
- [86] H Moustapha, M Zelesky, N Baines, and D Japikse. *Axial and radial turbines*. Concepts NREC, Vermont, 2003 (cit. on pp. 32, 113).
- [87] H Hiereth, K Drexl, and P Prenninger. *Charging the internal combustion engine*. Springer, 2007 (cit. on pp. 32, 113).
- [94] F. Payri, J. R. Serrano, P. Fajardo, M. A. Reyes-Belmonte, and R. Gozalbo-Belles. “A physically based methodology to extrapolate performance maps of radial turbines”. In: *Energy Conversion and Management* 55.0 (2012), pp. 149–163. ISSN: 0196-8904 (cit. on pp. 33, 113, 116, 118, 119, 121, 123).
- [123] D. Bornside and R. Brown. “View factor between differing-diameter, coaxial disks blocked by a coaxial cylinder”. In: *J. Thermophys. Heat Transfer* 4.3 (1990), pp. 414–416 (cit. on p. 100).
- [124] E. Sparrow, G. Miller, and V. Jonsson. “Radiative effectiveness of annular-finned space radiators, including mutual irradiation between radiator elements”. In: *J. Aerospace Sci.* 29.11 (1962), pp. 1291–1299 (cit. on p. 100).
- [125] K. Shukla and D. Ghosh. “Radiation configuration factors for concentric cylinder bodies”. In: *Indian J. Technology* 23 (1985), pp. 244–246 (cit. on p. 101).
- [126] S. W. Churchill and H. H. Chu. “Correlating equations for laminar and turbulent free convection from a horizontal cylinder”. In: *International Journal of Heat and Mass Transfer* 18.9 (1975), pp. 1049–1053. ISSN: 0017-9310. DOI: 10.1016/0017-9310(75)90222-7. URL: <http://www.sciencedirect.com/science/article/pii/0017931075902227> (cit. on p. 106).
- [127] S. W. Churchill and M. Bernstein. “A Correlating Equation for Forced Convection From Gases and Liquids to a Circular Cylinder in Crossflow”. In: *Journal of Heat Transfer* 99.2 (1977), pp. 300–306. DOI: 10.1115/1.3450685 (cit. on p. 107).
- [128] A. Torregrosa, F. Arnau, P. Piqueras, M. Reyes-Belmonte, M. Knutsson, and J. Lennblad. “Acoustic One-Dimensional Compressor Model for Integration in a Gas-Dynamic Code”. In: *SAE Technical Paper*. SAE International, Apr. 2012. DOI: 10.4271/2012-01-0834 (cit. on p. 113).

- [129] J. Galindo, A. Tiseira, R. Navarro, D. Tarí, H. Tartoussi, and S. Guilain. “Compressor Efficiency Extrapolation for 0D-1D Engine Simulations”. In: *SAE Technical Paper*. SAE International, Apr. 2016. DOI: 10.4271/2016-01-0554 (cit. on p. 113).
- [130] F. S. Ahmed, S. Laghrouche, A. Mehmood, and M. E. Bagdouri. “Estimation of exhaust gas aerodynamic force on the variable geometry turbocharger actuator: 1D flow model approach”. In: *Energy Conversion and Management* 84 (2014), pp. 436 –447. ISSN: 0196-8904. DOI: 10.1016/j.enconman.2014.03.080 (cit. on p. 115).

Models Validation

Contents

5.1	Introduction	138
5.2	Experimental analysis and validation	138
	External heat transfer model set-up	138
	External heat transfer estimation from experimental data	138
	Adjustment external heat transfer model	139
	External heat transfer prediction under engine conditions	141
	Model application	142
	VGT maps extrapolation model adjustment to a real turbine map	145
5.3	Model validation in gas stand conditions	150
	Turbocharger model integration in a 1D modelling software . . .	150
	Reduced model: gas stand	151
	Generalised heat transfer model validation	153
	Ability to extrapolate to other turbochargers	154
5.4	Model validation in engine conditions	156
	Engine 1D model	156
	Steady simulations: Full and partial loads	158
	Full loads	159
	Partial loads	171
	Transient simulations: Tip in and tip out	179
5.5	References	186

Figures

5.1	Comparison between measured external heat transfers and model prediction	139
5.2	Difference, in dimensionless form, between measured external heat transfer and model results	140
5.3	Comparison between external heat transfers: adjusted external model and unbalance method	141
5.4	Comparison between external heat transfers: adjusted external model and unbalance method in engine	141
5.5	Importance of modelled external heat fluxes compared to turbine enthalpy drop	142
5.6	Analysis of modelled external heat transfer in turbine side	143
5.7	Analysis of modeled external heat transfer in compressor side . .	144
5.8	Fitted equivalent area and reduced mass flow for T#1 (a) and for T#2 (b) and measured versus modelled A_{Neq} (c)	146
5.9	Root mean square error of efficiency fitting for the different turbochargers	147
5.10	Efficiency extrapolation in blade to jet speed ratio for different VGT positions of T#6, T#1 and T#2 (dots correspond to experimental data and solid lines to model results)	148
5.11	Reduced mass flow rate extrapolation results where extreme rotational speeds were fully extrapolated (dots correspond to experimental data and solid lines to model results)	149
5.12	Efficiency extrapolation results for T#6 checking model capabilities at high blade to jet speed ratio (dots correspond to experimental data and solid lines to model results)	150
5.13	Modelling procedure	151
5.14	GT-POWER™ model of turbocharger test bench	152
5.15	Turbine (a) and compressor (b) outlet temperatures for T#2	153
5.16	Turbine (a) and compressor (b) outlet temperatures for T#1	154
5.17	Turbine (a) and compressor (b) outlet temperatures for T#1 using re-elaborated correlations	155
5.18	Transient evolution compressor and turbine outlet temperatures for T#1	155
5.19	Engine Model in GT-POWER™	157
5.20	In-cylinder pressure and temperature for T#1 at 2500 rpm and full load (2.0 litres engine)	157
5.21	In-cylinder pressure and temperature at EVO for T#1 (2.0 litres engine)	158
5.22	Engine variables T#1. Actual 2.0 litres engine	159
5.23	Engine variables T#2. Emulated 1.6 litres engine	159
5.24	T#1 Compressor pressure ratio and temperature increment	160

5.25	T#2 Compressor pressure ratio and temperature increment	160
5.26	T#1 Turbine pressure ratio and temperature drop	162
5.27	T#2 Turbine pressure ratio and temperature drop	162
5.28	T#1 and T#2 turbocharger speed	164
5.29	T#1 and T#2 compressor efficiency	165
5.30	T#1 and T#2 turbine efficiency	166
5.31	T#1 and T#2 turbocharger efficiency	167
5.32	T#1 and T#2 heat power balance	168
5.33	T#1 and T#2 mechanical power balance	169
5.34	Modelled against measured torque for T#1 and T#2	172
5.35	Modelled against measured air mass flow for T#1 and T#2	173
5.36	Compressor pressure ratio and temperature increment for T#1	175
5.37	Compressor pressure ratio and temperature increment for T#2	176
5.38	Turbine pressure ratio and temperature drop for T#1	177
5.39	Turbine pressure ratio and temperature drop for T#2	178
5.40	Turbocharger speed for T#1 and T#2	179
5.41	Nodes temperatures for T#1	180
5.42	Nodes temperatures for T#2	180
5.43	Correlation between engine VGT position signal and real VGT displacement	181
5.44	Torque during tip in and tip out tests for T#1 at 1500 rpm	183
5.45	Torque during tip in and tip out tests for T#2 at 1000 rpm	183
5.46	Air mass during tip in and tip out tests for T#1 at 2000 rpm	184
5.47	Air mass during tip in and tip out tests for T#2 at 1600 rpm	184
5.48	Compressor outlet temperature during tip in and tip out tests for T#1 at 1500 rpm	185
5.49	Compressor outlet temperature during tip in and tip out tests for T#2 at 1600 rpm	185
5.50	Turbine outlet temperature during tip in and tip out tests for T#1 at 1250 rpm	186
5.51	Turbine outlet temperature during tip in and tip out tests for T#2 at 2400 rpm	186

5.1 Introduction

In this chapter the models described in the previous chapter are validated against experimental results. The validation is mainly done using a gas stand and engine 1D models. However, the external heat transfer model and the VGT extrapolation procedure are analysed in the first place using additional experimental data.

5.2 Experimental analysis and validation

In this section the turbine maps extrapolation model and the external heat transfer model are analysed and compared with the experimental information from gas stand tests.

External heat transfer model set-up

In order to validate the turbocharger external heat transfer model described in the previous chapter, exposed measurements in the gas stand test rig, explained in the second chapter were performed and used. However, engine test bench tests are also useful for validation. Turbochargers number 1 and 2 have been used, since engine test bench measurements at high temperature are available for these turbochargers (see Table 3.1).

External heat transfer estimation from experimental data

In exposed tests, turbocharger can exchange energy with environment. In order to obtain external heat transfer an energy balance has been performed [71], i.e. the measured energy unbalance is assumed to be equal to external heat transfer. The advantage of this approach is the simplicity (equation 5.1) but its main disadvantage is that only global behaviour can be determined (that is, the contribution of the different nodes to external losses can not be determined directly neither the possible interactions among them). Nevertheless, the most important contribution to external heat transfer to the environment will be the turbine, due to its higher temperature (radiative contribution) and big contact area.

$$\begin{aligned}
 \dot{Q}_{ext} &\approx \dot{Q}_{unb} = \sum_i \dot{m}_i \cdot \Delta h_i = \\
 &= \dot{m}_{gas} \cdot \Delta h_{gas} + \dot{m}_{air} \cdot \Delta h_{air} + \dot{m}_{oil} \cdot \Delta h_{oil} + \dot{m}_{cool} \cdot \Delta h_{cool} = \\
 &= \dot{m}_T \cdot \overline{c_{p,T}} \cdot (T_{IT} - T_{OT}) + \dot{m}_C \cdot \overline{c_{p,C}} \cdot (T_{IC} - T_{OC}) + \\
 &\quad \dot{m}_{oil} \cdot \overline{c_{p,oil}} \cdot (T_{IO} - T_{OO}) + \dot{m}_{cool} \cdot \overline{c_{p,cool}} \cdot (T_{IC} - T_{OC})
 \end{aligned} \tag{5.1}$$

Adjustment external heat transfer model

Figure 5.1 shows the comparison between unbalance results and the estimation by the external heat transfer model (see previous chapter) where the emissivity values are shown in Table 5.1 and air velocity in the benches has been imposed to 1 ms^{-1} after some measurements performed. The values of Table 5.1 have been proven to be consistent for different turbochargers, so they have been used for both T#1 and T#2.

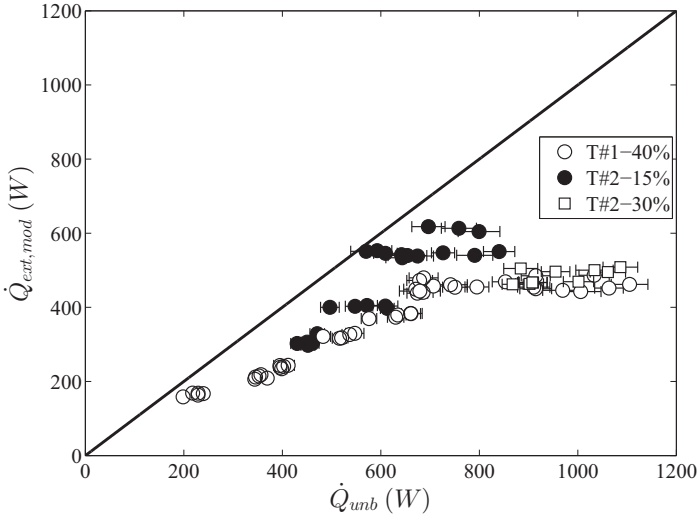


Figure 5.1: Comparison between measured external heat transfers and model prediction

Table 5.1: Emissivity values for turbocharger zones

Parameter	Zone			Source
	T	H	C	
ϵ	0.93	0.93	0.64	[47] and thermographic measurements

As Figure 5.1 shows, there is some deviation between modelled and experimental data (it must be pointed out that the model means a high geometric simplification and no adjustment constant has been used), resulting that the proposed external heat transfer model underestimates the experimental values. However, this deviation is small compared with turbine enthalpy drop as can be shown in Figure 5.2 where the dimensionless difference between measured external heat transfer and the one obtained directly with external heat transfer model are presented. As Figure 5.2 shows, the main differences come at low

turbine enthalpy drops, being in this case below than 10 % while it is lower than a 3 % at high turbine powers, i.e. $N_T > 3kW$.

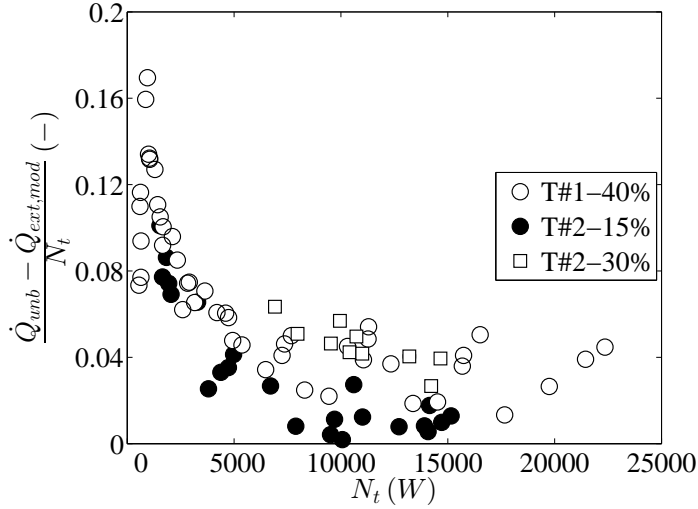


Figure 5.2: Difference, in dimensionless form, between measured external heat transfer and model results

The difference between experimental and model results has the same trend for all the measured range (the model underpredicts experimental values). This fact means that the deviation cannot be originated by measurement errors and may be corrected using a constant parameter in the model. The real geometry of the turbine is complex and therefore the estimated external surface is possibly higher than the estimated one using the cylinder approximation. To take into account this effect a multiplying coefficient on the external diameter of the turbine is proposed. This coefficient, shown in equation 5.2, will be adjusted using experimental data.

$$\phi_T = \psi_T \cdot D_t \quad (5.2)$$

Results of the adjustment are shown in Figure 5.3 where, for both turbochargers, $\psi_T = 1.25$, which means an increment of effective surface respect to the proposed cylinder used for turbine simplification. It is justified watching at Figure 4.10, where turbine flanges were not included inside the proposed simplification of turbine geometry.

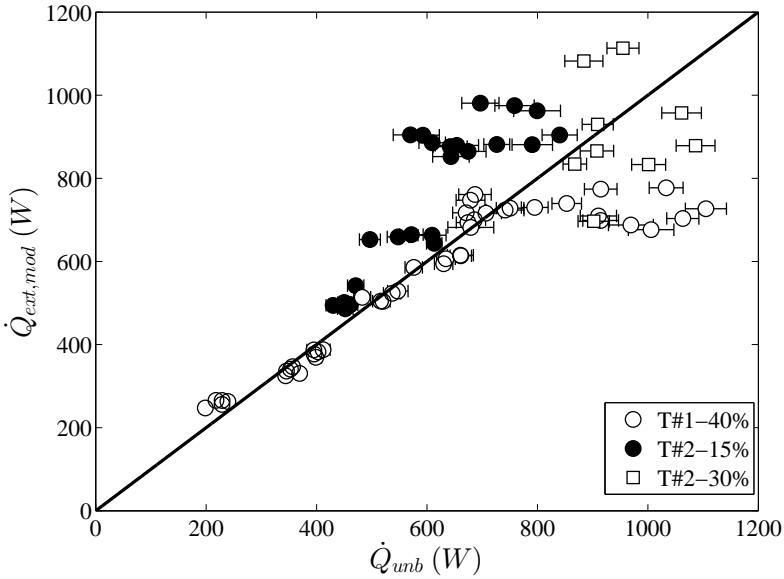


Figure 5.3: Comparison between external heat transfers: adjusted external model and unbalance method

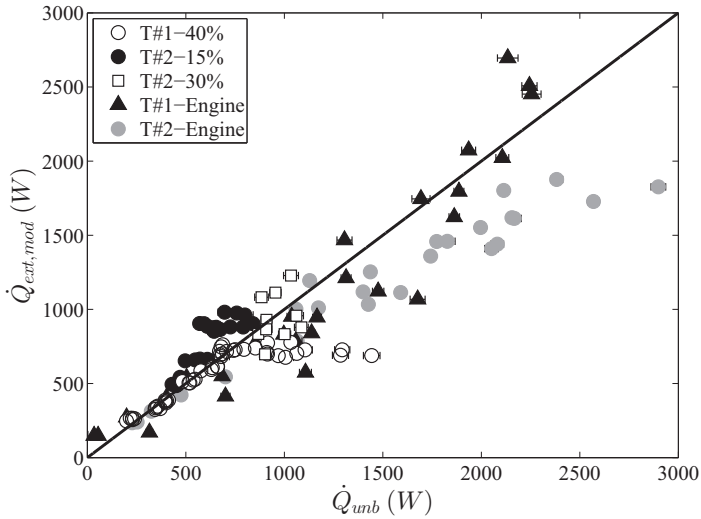


Figure 5.4: Comparison between external heat transfers: adjusted external model and unbalance method in engine

External heat transfer prediction under engine conditions

In order to validate the model, both turbochargers were installed on an engine: the external heat transfer has been obtained as explained in the experimental

chapter. Figure 5.4 shows the same data of Figure 5.3 but including the data from engine test measurements, where a good agreement is observed.

Maximum turbine inlet temperature was about 450°C in gas stand tests used for model elaboration, but around 900°C in engine tests used for proposed model validation.

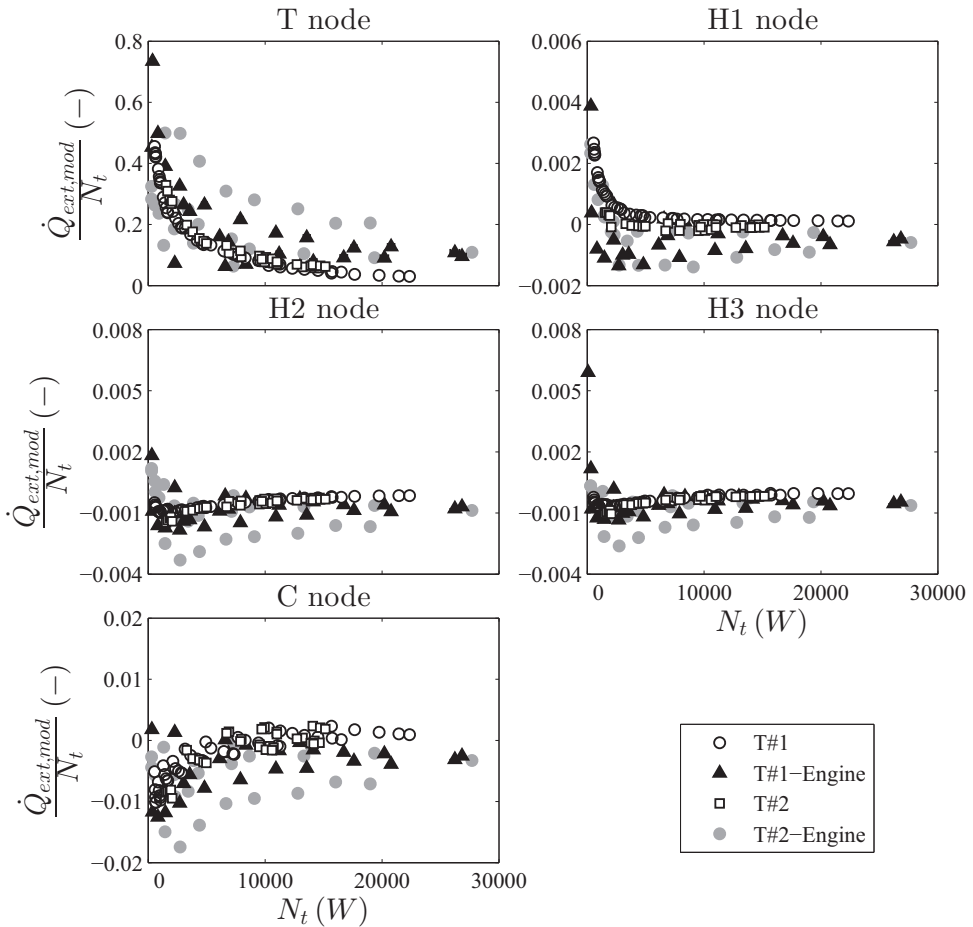


Figure 5.5: Importance of modelled external heat fluxes compared to turbine enthalpy drop

Model application

Once the external heat transfer model has been validated, it has been used in order to estimate the different heat flows among turbochargers nodes. Figure 5.5

shows the external heat (absorbed or lost) by each of the five nodes compared to the total enthalpy drop in the turbine, the following conclusions can be extracted:

- The main important external heat losses comes from turbine node (they can reach up to a half of the turbine enthalpy drop. This fact can be explained by two main reasons: on one hand the high temperature of the turbine external surface and, on the other, the high exposed area.
- In compressor side, in most of the cases, heat is absorbed by the compressor case (negative values), indicating that compressor case is receiving a higher heat quantity from turbine side by radiation than the heat lost to the ambient (both convective and radiative).
- External heat fluxes at housing nodes is almost negligible compared to the turbine enthalpy drop. They are about two order of magnitude lower than heat losses from turbine node.

Due to the previous results a deeper study on heat transfer in turbine and compressor side has been performed.

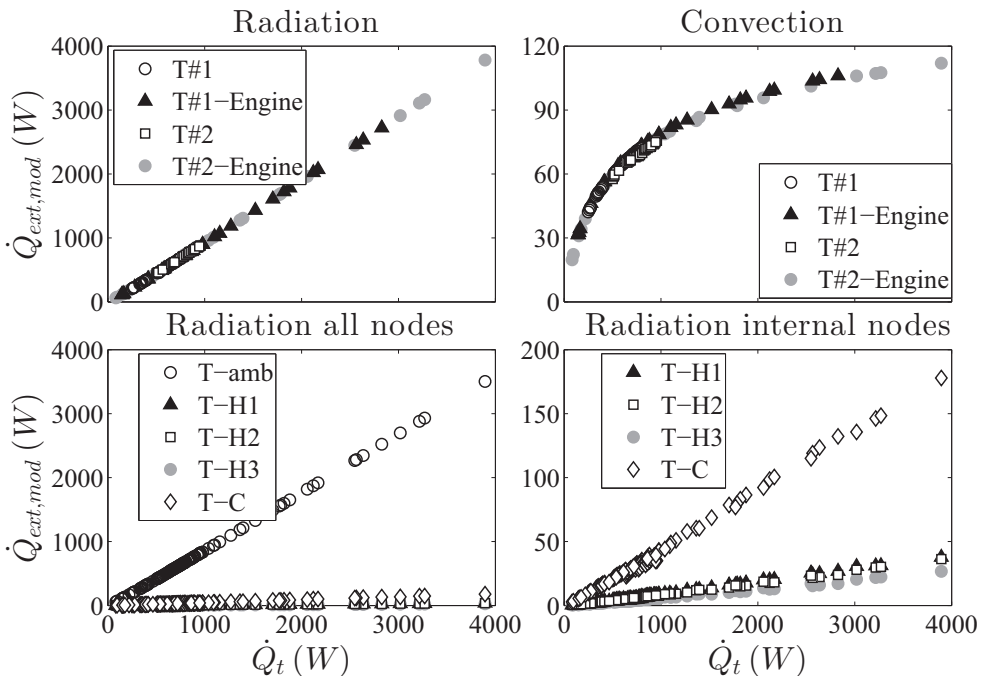


Figure 5.6: Analysis of modelled external heat transfer in turbine side

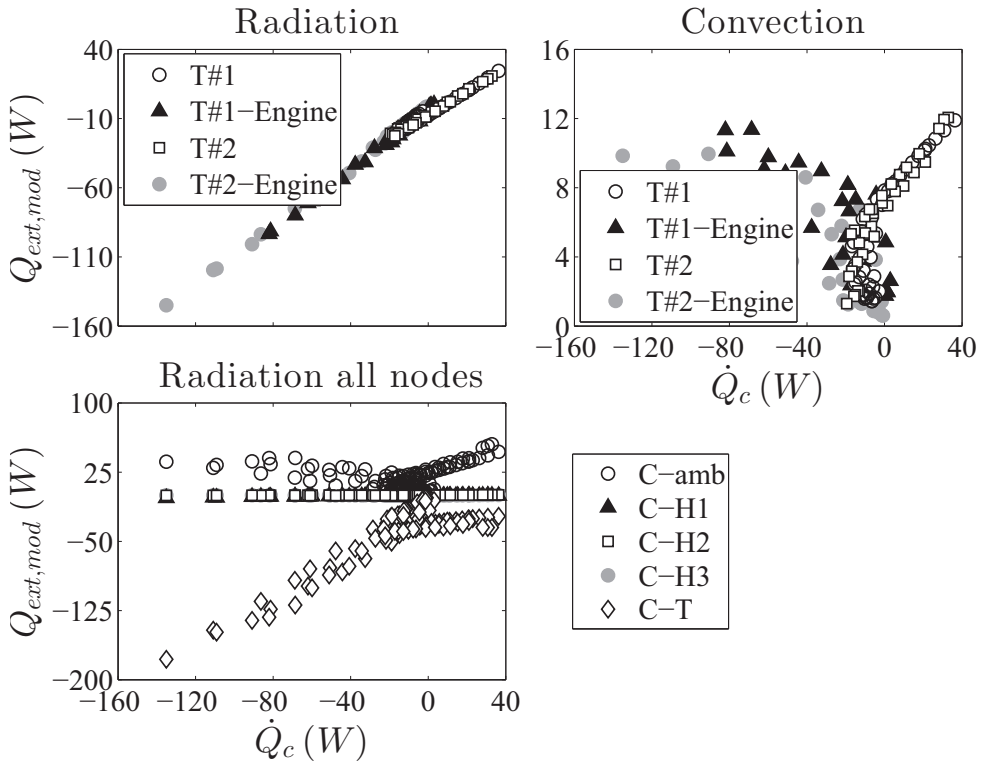


Figure 5.7: Analysis of modeled external heat transfer in compressor side

Turbine side

Figure 5.6 shows the external heat flows obtained in the turbine side for both turbochargers, where it is observed that the radiation heat flux is almost equal to the total heat lost by the turbine (left top of Figure 5.6), while convective heat losses (right top of Figure 5.6) are negligible in comparison.

The different radiation losses in turbine are shown in the left bottom of Figure 5.6 where the most important contribution is due to ambient losses, but right bottom of Figure 5.6 shows a zoom of left bottom of Figure 5.6 where it is shown that the radiation to compressor is quite more important than radiation to the other nodes.

Compressor side

In compressor side, external heat fluxes can be reversed, i.e. compressor can absorb some heat from the environment (mostly from the turbine case). Top left of Figure 5.7 shows that, as in the case of the turbine, the whole external heat to/from compressor is almost equal to the radiative part, while top right of Figure 5.7 indicates that convective heat losses have no clear relationship with total external heat of compressor. Finally, bottom of Figure 5.7 indicates

that the most important radiative heat flux comes from turbine side, but due to the smaller quantities the other fluxes cannot be neglected.

VGT maps extrapolation model adjustment to a real turbine map

The values of the fitted coefficients of the extrapolation model of the previous chapter correspond to the mass flow parameter fittings shown in Figure 5.8. In Figure 5.8 the dots correspond to measured reduced mass flow and the lines to interpolated and extrapolated values for the different VGT positions of T#1 and T#2. Figure 5.8 shows that the errors in modelling reduced mass flow are small enough to consider valid the procedure developed in the previous chapter. Figure 5.8 also shows the calculated values of A_{Neq} that range between 1/3 and 1/10 of A_0^{geom} (refers to station 0 in Figure 4.14a), depending on VGT position, mass flow and turbo speed. It is important to point out that in case of T#2, Figure 5.8b, the values of the most open VGT position (80%) have not been used for model fitting but extrapolated. Therefore these results have been fully generated by the model.

After fitting both the reduced mass flow coefficients and the efficiency coefficients using the data of the map, the model can be used for extrapolations. As the efficiency appears in the equivalent nozzle area (equation (4.61)) and the equivalent nozzle area appears in the efficiency expression (equation (4.77)) both equations must be solved at the same time. It can be done using an iterative procedure as defined in [26]. In Figure 5.9 the modelled efficiency is plotted against the measured one for the whole map of each turbocharger and the root mean square error is shown. In Figure 5.9 the solid line indicates perfect fit, the dashed line indicates 2.5 efficiency points deviation and the dash and dotted line indicates 5 efficiency points deviation. In Figure 5.10 the model is extrapolating in blade to jet speed ratio using all the available experimental data to fit the coefficients of the model. Exception is made for the 80% VGT position in T#2 that has been fully extrapolated (Figure 5.10f) while the rest of the cases were interpolated between measured points. Good agreement between experimental data (dots) and extrapolated results (lines) can be observed as deduced from Figure 5.9.

Figure 5.10f shows that for $4874 rpm/K^{1/2}$ the measured efficiency is equal to the corresponding to $5814 rpm/K^{1/2}$ what makes no sense. The model extrapolation is showing a more coherent behaviour and probably correcting measurements errors.

Figure 5.11 shows the model results against the experimental data for T#6 corresponding to the extrapolation results for reduced mass flow rate. Figure 5.11 shows the experimental data as points and the model results as solid lines. In Figure 5.11, the model is fitted using only five points per speed line, the ones

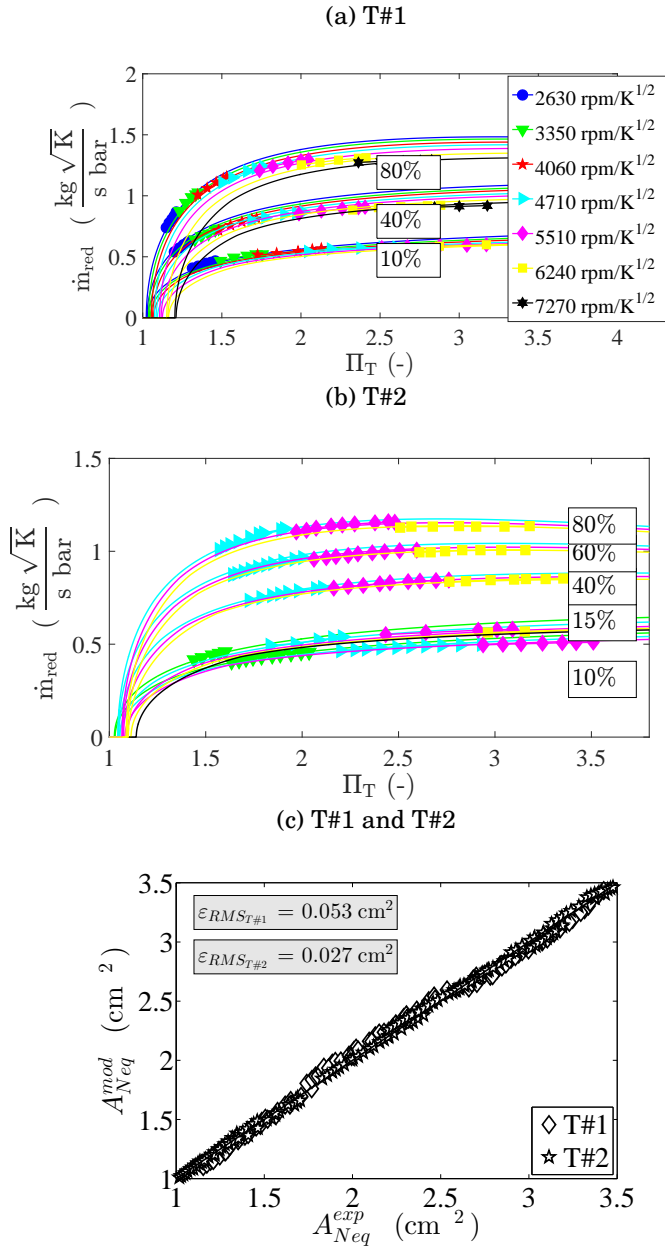


Figure 5.8: Fitted equivalent area and reduced mass flow for T#1 (a) and for T#2 (b) and measured versus modelled A_{Neq} (c)

of maximum pressure ratio (minimum σ) corresponding to the full points in Figure 5.11. Indeed, neither the maximum nor the minimum rotational speeds for each VGT have been used during the fitting process, so Figures 5.11a and

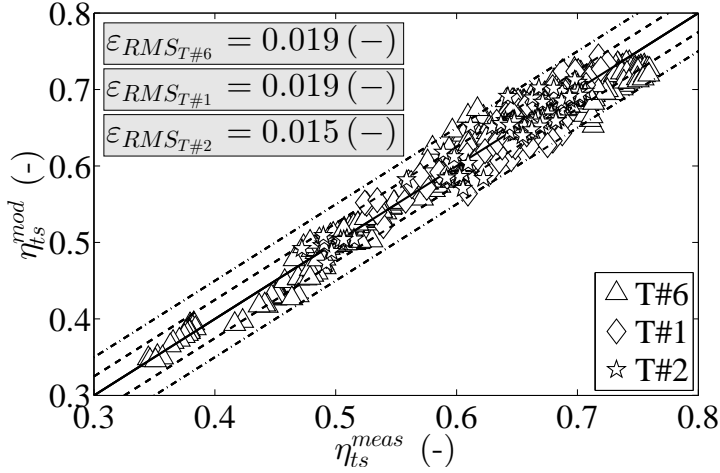


Figure 5.9: Root mean square error of efficiency fitting for the different turbochargers

5.11f show only extrapolated results. In this way the model has to extrapolate in both σ and turbine reduced speed. Therefore, $1706 \text{ rpm}/K^{1/2}$ and $6679 \text{ rpm}/K^{1/2}$ have been fully extrapolated.

The model shows very good agreement with the experimental data when extrapolating at both lower and higher reduced speeds. At extremely low expansion ratios (high σ), the error starts to grow: it occurs at points where the adiabatic efficiency of the turbine is lower than zero and it consumes power instead of producing it, so very off-design flow patterns should take place in the turbine at those conditions [89]. Biggest errors appear at VGT 80% and VGT 10% at reduced speed of $4874 \text{ rpm}/\sqrt{K}$ (figure 5.11d)

Figure 5.12 shows the model extrapolation results for efficiency against blade to jet speed ratio. Filled points correspond to the data used for model fitting and empty points correspond to data used for blind checking. The mean square error of the whole extrapolation in this case is $\epsilon_{RMS} = 0.02(-)$. Only the experimental data corresponding to central reduced speeds and low σ were used for model fitting (bold points in Figure 5.12). In Figure 5.12d VGT 80 % position was fully extrapolated by the model (all experimental points are empty). In this case the model is able to reproduce with good precision an entire VGT position, up to very high σ . The differences between the model and the experimental data are maximum at the reduced speed of $4874 \text{ rpm}/\sqrt{K}$ and a VGT position of 60 %. This might be explained by the experimental error, caused by the very low enthalpy drops measured in the turbine at high σ [89]. They are affected by the residual heat transfer effects since at high σ uncertainty is introduced, even when measuring in almost adiabatic conditions and when compensating

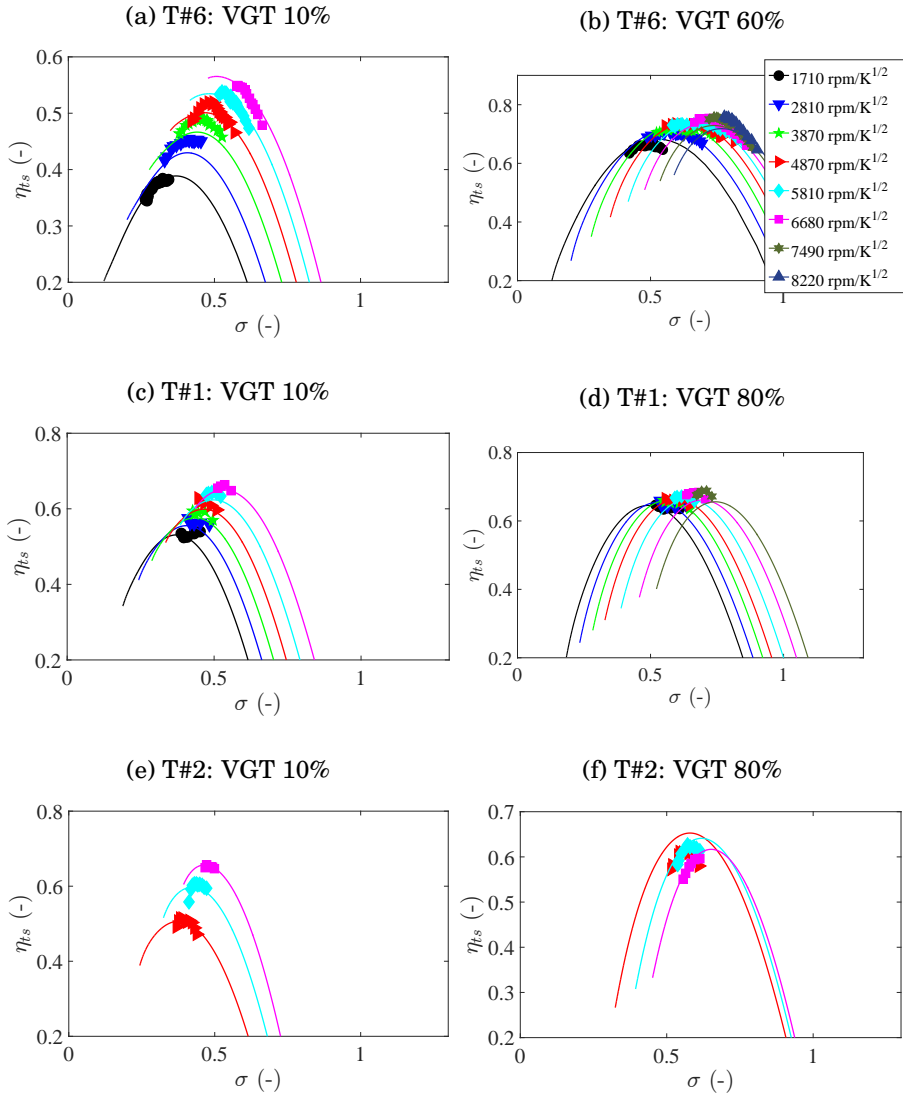


Figure 5.10: Efficiency extrapolation in blade to jet speed ratio for different VGT positions of T#6, T#1 and T#2 (dots correspond to experimental data and solid lines to model results)

these effects. In general turbine adiabatic efficiency experimentally obtained is affected by the relatively high combined uncertainty of the turbine enthalpy drop, residual heat transfer and isentropic power at very low speeds. At other speeds, the worst results have an error of 5% to 7% points of efficiency. However, the general quality of the prediction is high and, the model is able to produce

good extrapolations very far from the points to which it was fitted.

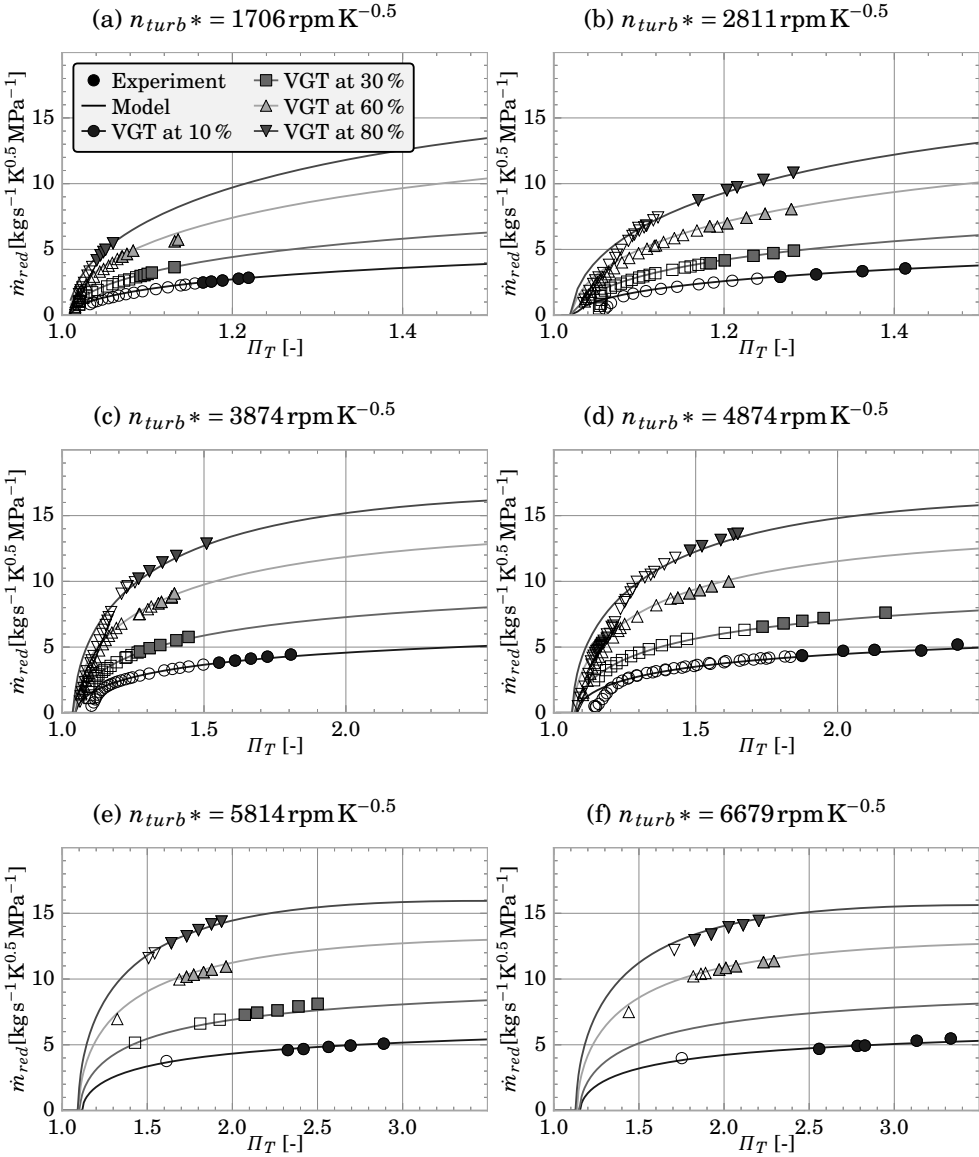


Figure 5.11: Reduced mass flow rate extrapolation results where extreme rotational speeds were fully extrapolated (dots correspond to experimental data and solid lines to model results)

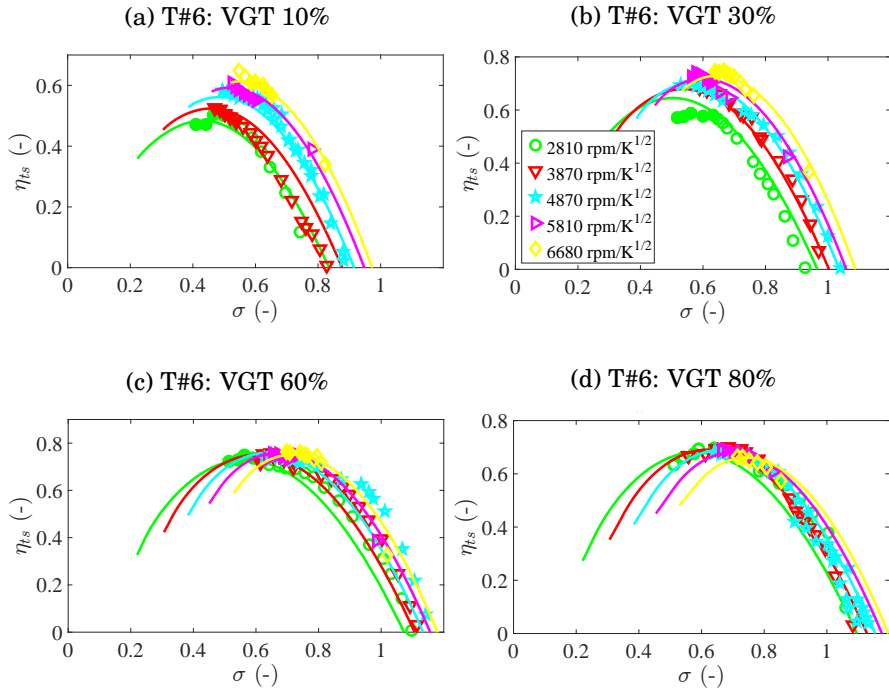


Figure 5.12: Efficiency extrapolation results for T#6 checking model capabilities at high blade to jet speed ratio (dots correspond to experimental data and solid lines to model results)

5.3 Model validation in gas stand conditions

In this section the simplified model of the gas stand is developed to validate the different models. The results using the externally programmed library containing the models described in the thesis are compared with standard 1D simulations in which look up map method is used.

Turbocharger model integration in a 1D modelling software

The main objective of the model is the easiness to be used coupled with a general purpose models like GT-POWER™. All the provided data from the models described in the thesis make possible the correct computation of the model parameters in order to use it coupled with a 1D modelling software, in a similar way to the work done in [2] in which only gas stand data have been analysed. The procedure is outlined in Figure 5.13, which shows that the heat transfer and mechanical losses (proposed turbocharger) model is built on the basis of thermal properties and heat transfer correlations for convection. Those correlations have

been obtained from test campaigns on both thermohydraulic test bench and gas stand and from turbocharger simple geometrical data (detailed geometry is not needed). The model for a given turbocharger is programmed in an external library for further use. It is important to take into account that the turbocharger model coupled with the engine model uses adiabatic compressor and turbine performance maps previously extrapolated by the presented procedure. These maps can be obtained from direct adiabatic measurements or from supplier (or hot) maps using the heat transfer model in the inverse form, i.e. removing the heat from the measured hot map [26]. For that inverse use additional information about map measurement conditions (temperatures, mass flows, etc.) is needed. Using the described arrangement, simulations in GT-POWER™ can be performed taking into account the turbocharger heat transfer and mechanical losses model and using on engine test data for boundary conditions definition.

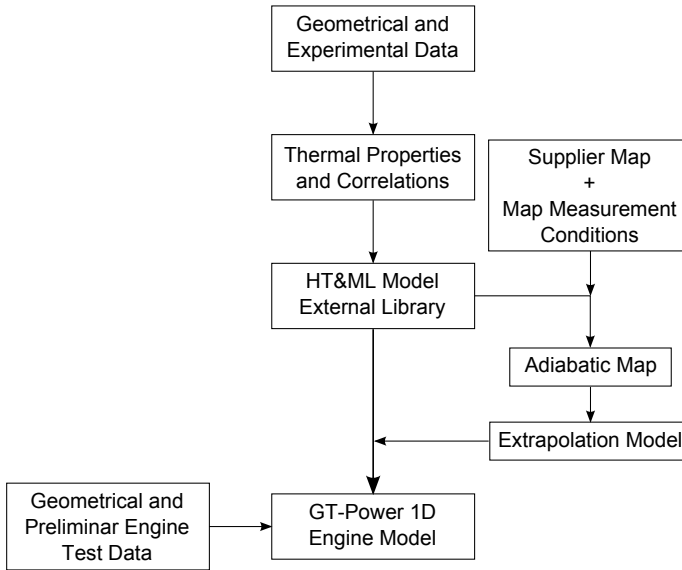


Figure 5.13: Modelling procedure

Reduced model: gas stand

In order to check the model prediction ability for different turbocharger variables, hot exposed tests (without thermal insulation) measured with steady flow at gas stand have been modelled. This kind of verification has the advantage compared to a whole engine model of eliminating spurious effects due to the complex engine model and pulsating flow characteristics. The model of turbocharger test bench used in GT-POWER™ is sketched in Figure 5.14.

The geometry values of a given turbocharger must be used in order to correctly simulate the behaviour of the model. In order to perform a simulation using the model the following variables are imposed:

- Compressor and turbine inlet temperature.
- Compressor and turbine inlet pressure.
- Turbine outlet pressure.
- Back-pressure valve position in the compressor line.
- VGT position.
- Oil inlet temperature and mass flow.
- Water inlet temperature and mass flow (if exists)
- Ambient temperature.

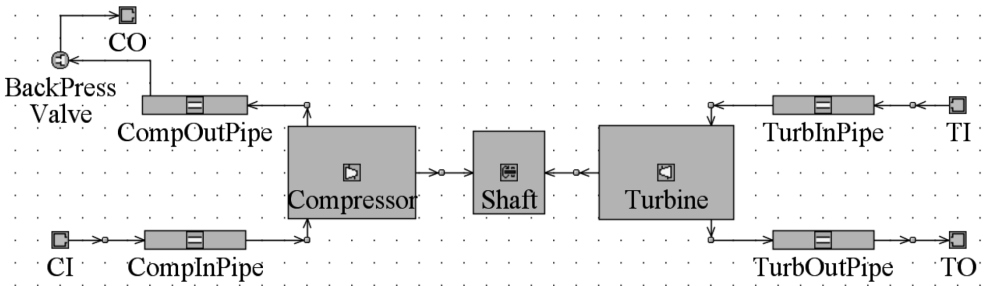


Figure 5.14: GT-POWER™ model of turbocharger test bench

Using these inputs it is possible to calculate turbine and compressor outlet temperatures, compressor outlet pressure, turbine and compressor mass flow and turbocharger speed.

In order to check the thermal model predictability two sets of simulations have been used. In the first, the externally programmed library is not used, so the predictions made by the gas stand model correspond to a look up maps technique. In the second set, the turbocharger model developed on the basis of the previous sections is used coupled with GT-POWER™ code, so all the correlations and thermal properties come into play.

In the first set up the turbocharger maps used in the simulation were obtained from hot exposed measurements while in the second case an adiabatic (cold map) is used because the heat transfer model actuates adding the heat

transfer to the map. In the first case, heat transfer and aerodynamic phenomena are mixed in the map and in the second case the aerodynamic phenomena are separated from heat transfer. Adiabatic map is constructed on the basis of the heat transfer correlations applied to the same hot exposed map of the look up method using the same heat transfer model but subtracting the heat from the map, as explained by Reyes in [26].

Generalised heat transfer model validation

In Figure 5.15 a comparison of the prediction of compressor and turbine outlet temperatures is shown for three different simulations for T#2 (Table 3.1).

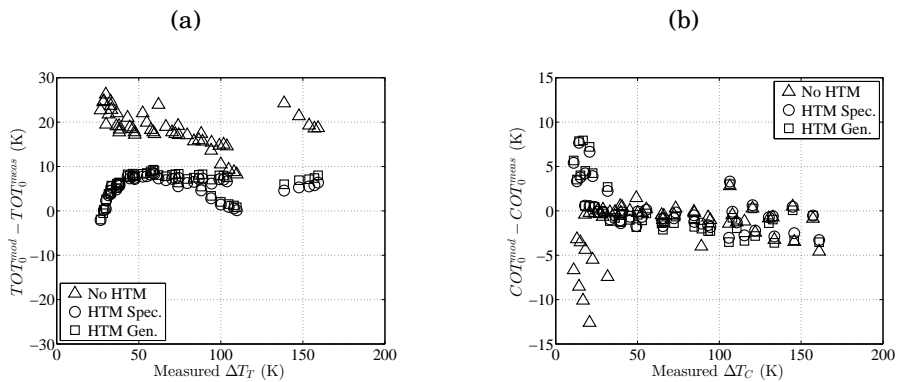


Figure 5.15: Turbine (a) and compressor (b) outlet temperatures for T#2

First, when no heat transfer model (no HTM) is used two main results can be observed. On one side, at low pressure ratios (i.e. low total temperature delta) the difference between measured and modelled temperatures is high due to the higher impact of heat transfer phenomena. On the other side, when pressure ratio (or total temperature delta) increases the error in temperature prediction tends to decrease for compressor outlet temperature (Figure 5.15b) but not for turbine outlet temperature (Figure 5.15a). In the second simulations set, empirical correlations specifically obtained for T#2 are used (HTM Spec.) what means specific values for the different conductive conductances and convective correlations of T#2 obtained in thermohydraulic bench and gas stand. This type of correlations were used in Reyes [26]. The results are similar for the compressor with a little improvement at low pressure ratios and with more stable behaviour. In the case of turbine outlet temperature the prediction of the heat model is up to 20 K better than using the original simulations without any model. These improvements can be crucial when engine aftertreatment, two stage turbocharging or exhaust energy recovering devices have to be modelled.

Finally, it can be observed that using the HTM based on the general correlations developed in this work gives very similar results to the specific ones. Only $1K$ or $2K$ differences can be observed in turbine outlet temperature between those two configurations.

Those results state the validity of the approach for the improvement of the estimation of turbine and compressor outlet temperature. Furthermore, the results prove that the general correlation provide a model with accurate outlet temperature predictions without the need of experimental characterisation of the turbocharger in different test benches.

Ability to extrapolate to other turbochargers

The extrapolation ability to other turbochargers that have not been used in the correlation determination is here checked. To prove that the described procedure is able to improve the prediction of outlet temperatures of non-tested turbochargers, T#1, which has not been used for general correlation, is simulated and compared to experimental data.

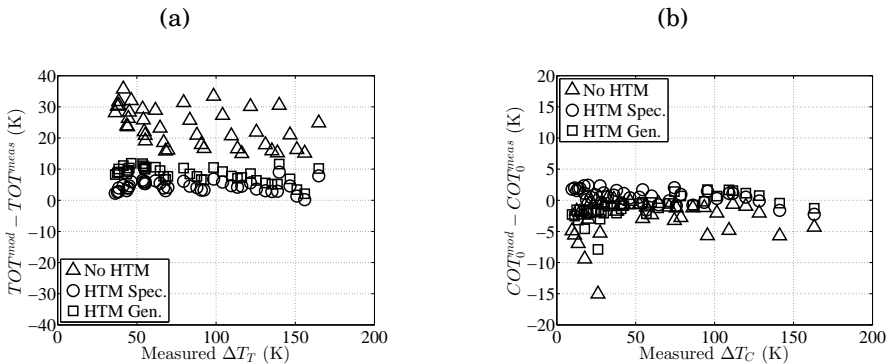


Figure 5.16: Turbine (a) and compressor (b) outlet temperatures for T#1

The results of compressor and turbine outlet temperatures for T#1 are shown in Figure 5.16 with the three different configurations of the simulation as in Figure 5.15. The results with respect to not using any HTM give a $15K$ improvement in turbine outlet temperature. For compressor outlet temperature in the case of this turbocharger the general correlations are always within $\pm 5K$ difference respect to measured values while in some cases without HTM this difference is much higher. Finally it can be observed that even using a turbocharger that has not be used in general correlations development the difference between specific correlations and general ones is small.

These results show that the methodology can easily be used for other turbochargers different form the ones used to obtain the generalized correlations. If the data of T#1 are introduced to re-elaborate general correlations the results

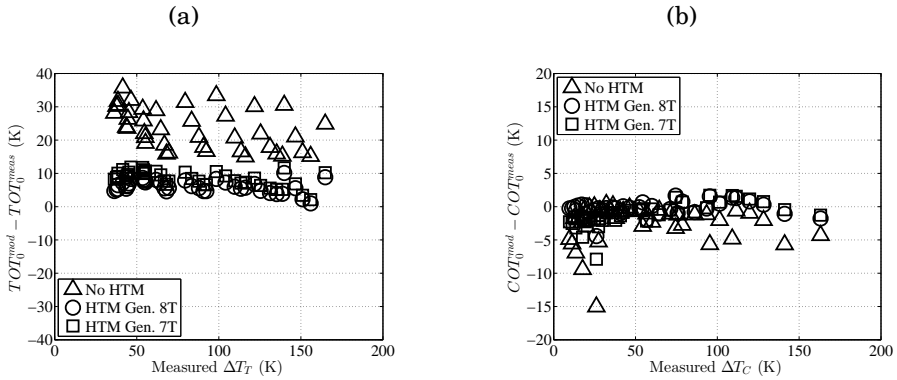


Figure 5.17: Turbine (a) and compressor (b) outlet temperatures for T#1 using re-elaborated correlations

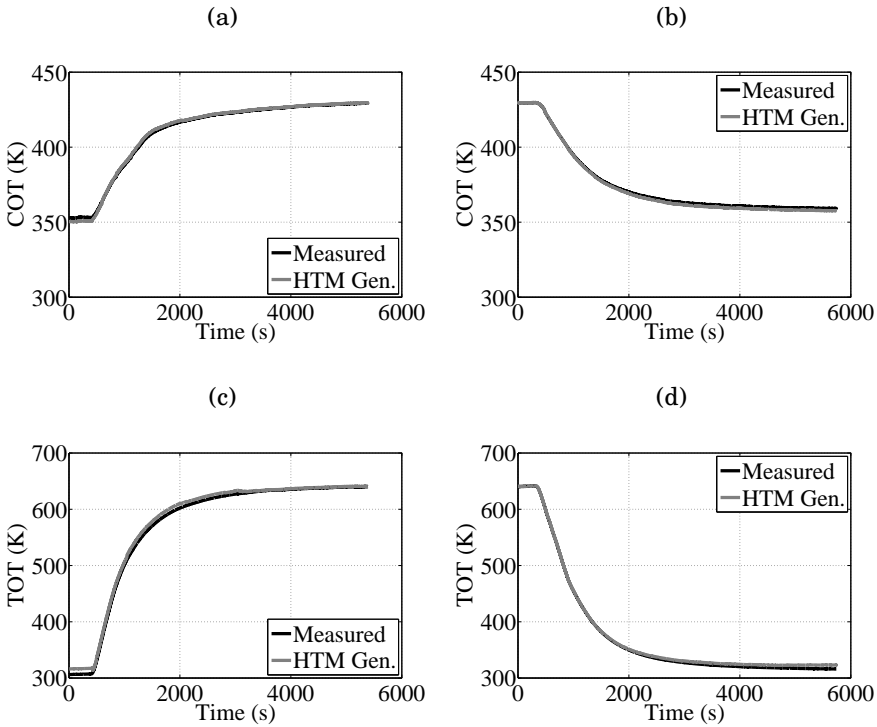


Figure 5.18: Transient evolution compressor and turbine outlet temperatures for T#1

may be little better for T#1. In Figure 5.17 the results using T#1 data are shown compared to four previous turbochargers correlation. Only a slight improvement is observed for both outlet temperatures. This fact proves that additional data

may improve the correlations accuracy but the learning curve is approaching the asymptotical region concerning the ability for outlet temperature predictions.

Thermal transient tests in gas stand can be simulated and compared to experimental values in order to check the validity of the procedure for transient operation of the turbocharger. Those tests impose a temperature rise (from minimum to maximum value of the gas stand capability) in the gas at the turbine inlet and record the evolution of turbocharger parameters until stabilization. In Figure 5.18 the evolution of compressor and turbine outlet temperatures can be observed for the temperature rise and temperature drop tests for T#1. These evolutions are compared to simulations using HTM with the properties calculated from the general correlations. It can be observed that the differences between measured and modelled temperatures are small in both cases. Such results confirm that capacitances determination using general correlations is adequate for predicting turbocharger outlet temperatures in transient operation.

5.4 Model validation in engine conditions

The whole engine modelling work has been divided in three parts. In the first part the turbocharger model developed in this thesis has been integrated in a commercial code for engine simulations (GT-POWER™). Then, an engine model has been developed and validated in GT-POWER™ environment. Finally, simulations with and without the proposed turbocharger model have been performed in order to analyse the benefits and drawbacks of this model in engine simulations. In the configuration without the proposed model, original GT-POWER™ model has been used. This model does not include a turbocharger heat transfer and mechanical losses model and the maps are extrapolated using a purely mathematical approach and not a physically based model as it was done in this thesis.

Engine 1D model

A general scheme of the engine model in GT-POWER™ is shown in Figure 5.19. The proposed turbocharger model has been introduced in the engine model acting on the compressor, turbine and shaft variables in order to take into account the heat transfer and mechanical losses phenomena in the turbocharger during the simulation.

In order to assure correct turbine inlet conditions the in-cylinder instantaneous variables values provided by the model have been analysed. As it had been described in the previous chapter, heat release laws obtained by an in-house combustion diagnosis tool (CALMEC) have been imposed in the cylinder, so GT-POWER™ inbuilt heat release models have not been used. Moreover, in-cylinder heat transfer coefficients have been fitted in order to meet in-cylinder measured

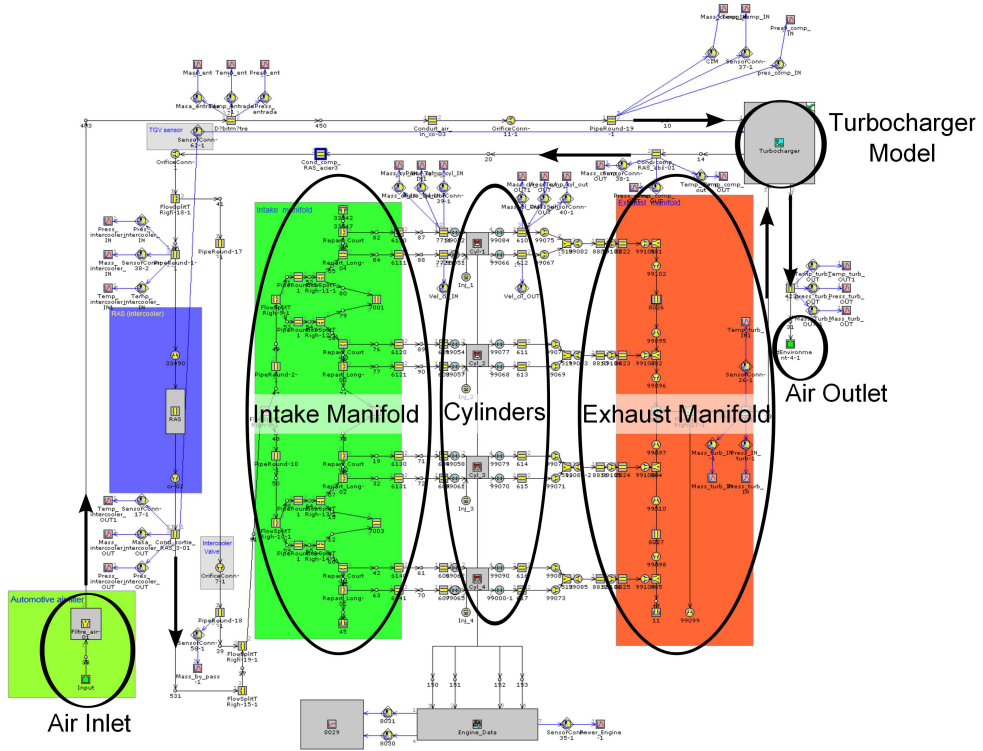


Figure 5.19: Engine Model in GT-POWER™

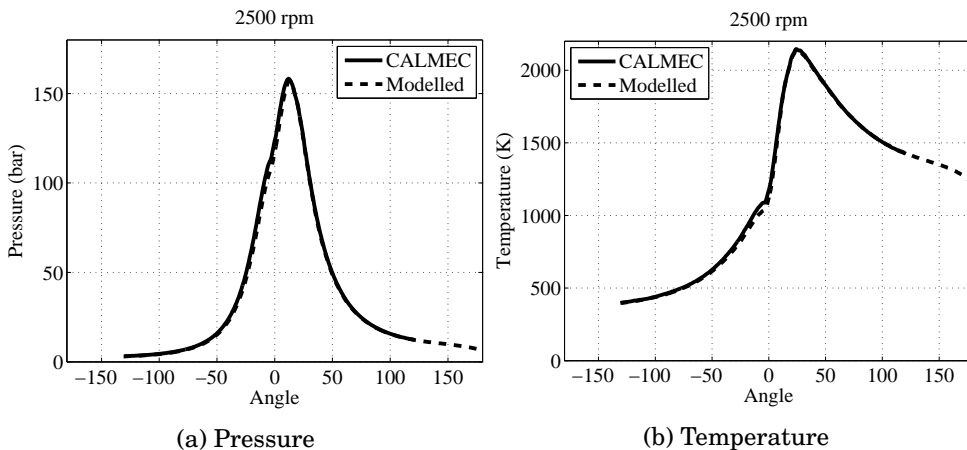


Figure 5.20: In-cylinder pressure and temperature for T#1 at 2500 rpm and full load (2.0 litres engine)

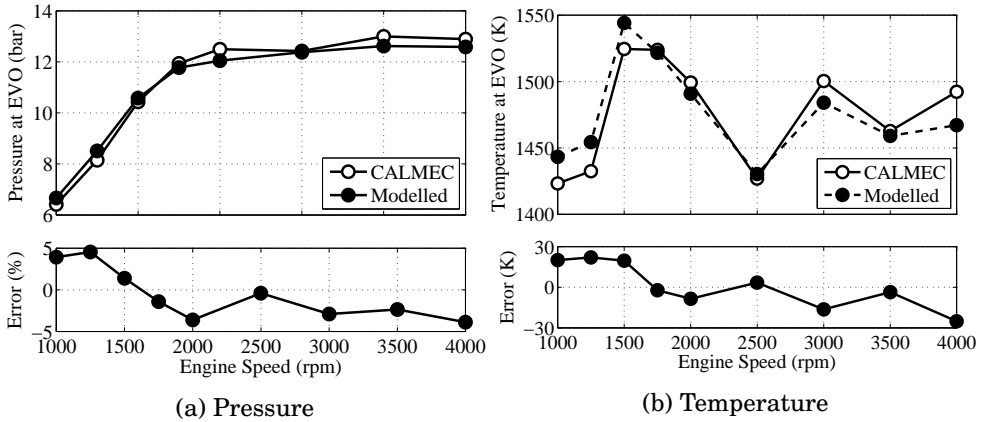


Figure 5.21: In-cylinder pressure and temperature at EVO for T#1 (2.0 litres engine)

values. In Figure 5.20 instantaneous in-cylinder pressure and temperature are shown comparing the modelled values with instantaneous experimental values for a given engine speed. The differences are small, a fact that validates in-cylinder heat transfer coefficients adjustment. It can be observed, in Figure 5.21, that in-cylinder pressure at exhaust valve opening is also very similar for all the modelled engine speeds, being the errors within $\pm 5\%$. The same holds for temperature, where errors are in the range of $\pm 20\text{ K}$, using the same set of in-cylinder heat transfer coefficients for all calculated engine speeds. Identical results from in-cylinder variables have been obtained using the turbocharger model or not (for that reason only one curve for modelled values is shown in Figures 5.20 and 5.21), meaning that in-cylinder conditions are not affected by the proposed turbocharger model in the modelled cases, what indicates that any difference in cylinder outlet variables (primary the turbine inlet temperature), cannot be caused by the use of the new turbocharger model.

Steady simulations: Full and partial loads

All the previous engine characterisation is used in both the original 1D model and the model that includes heat transfer and mechanical losses. However, in the proposed turbocharger model the turbocharger heat transfer and mechanical losses sub-models are included in the same way as it has been done for the gas stand simulations of the previous section. The boost pressure value provided by the engine model has been controlled using a PID to impose the experimental value.

Full loads

Figure 5.22 and Figure 5.23 compare the results of the models with the experimental data in torque and air mass flow. Good agreement has been achieved using both configurations (with and without the proposed turbocharger model) compared to experimental data. As it can be observed, from the point of view of these two parameters, related with the engine behaviour, the differences between both configurations are insignificant. At steady conditions the heat transfer model has a small effect on these variables since thermal inertia effects does not exist. Furthermore the boost pressure has been imposed, what implies good prediction of the torque.

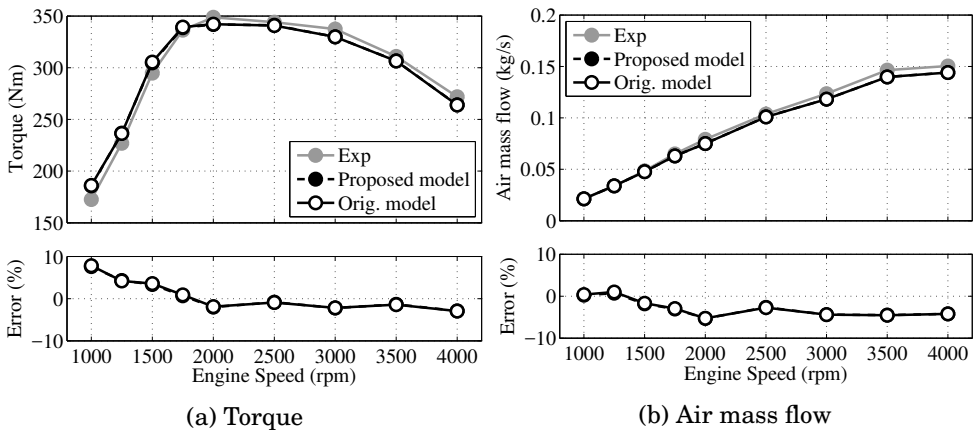


Figure 5.22: Engine variables T#1. Actual 2.0 litres engine

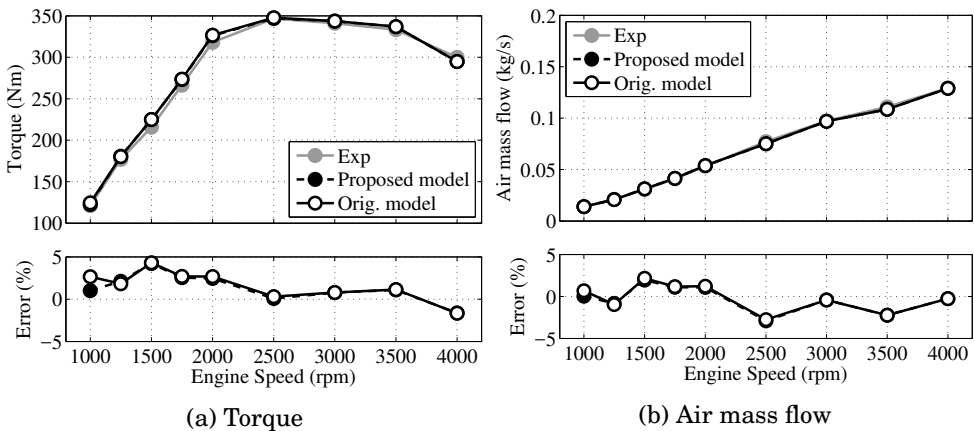


Figure 5.23: Engine variables T#2. Emulated 1.6 litres engine

Figure 5.24 and Figure 5.25 show compressor parameters for both turbochargers. From the point of view of pressure ratio the proposed turbocharger model offers similar results to those calculated without using it. Both models present a good agreement between modelled pressure ratio and experimental data due to the fact that a PID controller is used to impose experimental boost pressure. It must be reminded that original model uses the compressor map measured in hot conditions while in case of proposed turbocharger model the compressor map used is the adiabatic one, i.e. it does not include the effect of the heat transfer that will have to be provided by the proposed turbocharger

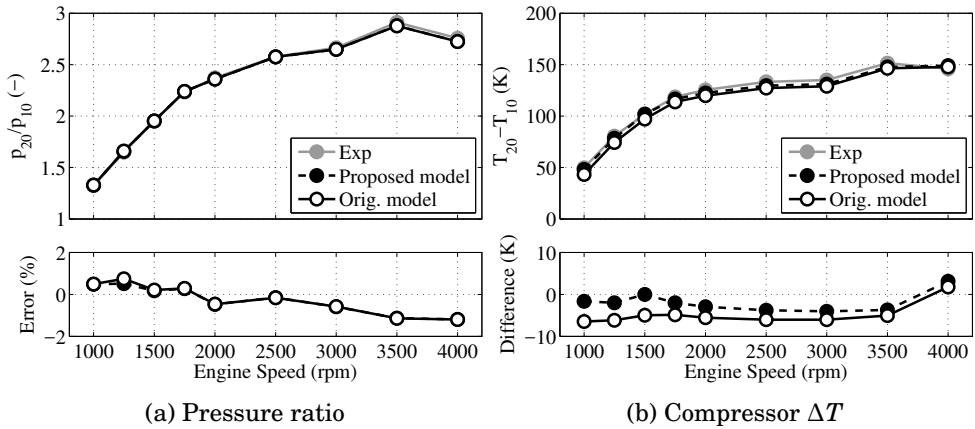


Figure 5.24: T#1 Compressor pressure ratio and temperature increment

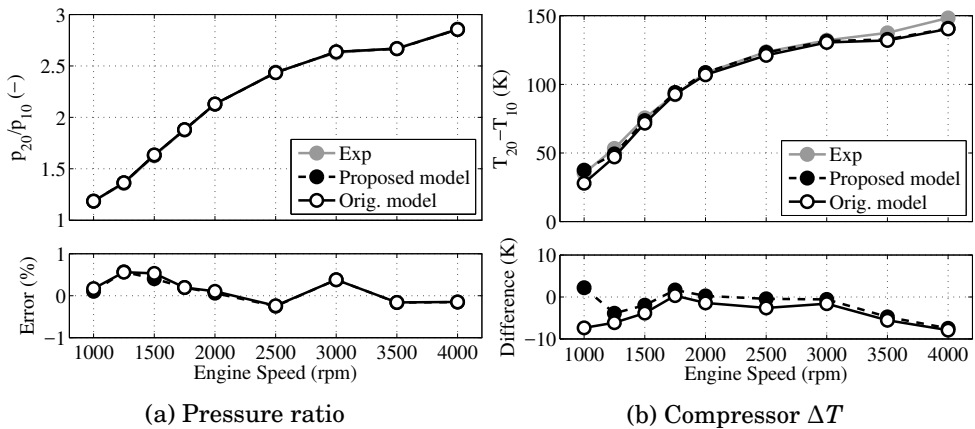


Figure 5.25: T#2 Compressor pressure ratio and temperature increment

model. Pressure ratio against mass flow maps are identical with and without proposed turbocharger model [2] and the effect of heat transfer is reflected in

the compressor efficiency [62] i.e. in the air temperature increment across the compressor. Compressor outlet temperature is related with the compression ratio (both cases have the same value) and the efficiency, so this parameter is affected by heat transfer and must be used properly. In the case of the original model the heat transfer effects are included in the map efficiency which is only valid when simulation conditions are similar to the conditions during map measurement. In the case of the new approach (using a proposed turbocharger model), the employed efficiencies are adiabatic, so point '20a' in Figure 2.3a can be obtained. Furthermore, heat transfer in the compressor is computed using proposed turbocharger model taking into account simulation conditions so adding that heat flow makes possible the calculation of the final COT (point '20' in Figure 2.3a).

As it has been discussed in chapter 2 the definition of efficiencies for the compressor in adiabatic and diabatic maps are presented in Equations 2.10 and 2.11, where the temperature definitions are shown in Figure 2.3a.

The hot map includes the effect of the heat transfer and mechanical losses in the turbocharger for the map measurement conditions. For this reason, the prediction of a model using hot maps, in principle, will be accurate if the conditions of turbine inlet temperature and oil inlet temperature are similar between the modelled and the experimental ones when the maps were measured. Since T_{20} can be derived from the diabatic compressor efficiency ($\eta_{c,diab.}$) by using Equation 2.11.

The simulations of this section for the original model use a hot map, where the map measurement temperatures were similar to those measured at full load engine conditions. If the map conditions were different, the measured diabatic efficiency would be also different. Then compressor outlet temperature prediction would be worse than the results shown in Figures 5.24b and 5.25b.

On the contrary, proposed turbocharger model uses adiabatic map, i.e. considering that the air is only heated due to the compression process and the internal irreversibilities. The heat transfer model estimates the heat to or from the compressor ($\dot{Q}_{C/Air}$) for each operating condition and this heat is added/removed at the compressor outlet as can be observed in Figures 4.1 and 2.3a. So, the same T_{20} is obtained in both cases: using a hot map measured with identical temperature conditions than in engine measurements and using the evolution given by $\eta_{c,diab.}$ and using a two step evolution given by the efficiency $\eta_{c,adiab.}$ of an adiabatic map and the additional heat power ($\dot{Q}_{C/Air}$) of the proposed turbocharger model. For this reason, the differences observed between the results obtained using the proposed turbocharger model and those obtained with the original model are small. However, when the conditions of the map are not similar, proposed turbocharger model would still give the correct value while the original model may underpredict or overpredict COT.

In spite of this, proposed turbocharger model shows better results, specially

at the low speed range (below 2000 rpm) as in Figure 5.24b and 5.25b. It is due to the fact that generally the heat transfer in the compressor is very small in comparison to the compressor power except for very low turbocharger speed, as it has been studied in [63]. Despite of these small differences, up to 10 K improvement is observed using proposed turbocharger model which is more relevant for the higher power water cooled turbocharger (T#1).

Figure 5.26 and Figure 5.27 compare modelled pressure ratio and temperature drop at the turbine versus experimental data for both turbochargers. Once again, significant differences have not been detected between both configurations from the point of view of pressure ratio. Only in the case of the lowest engine speed (1000 rpm) and T#2 (Figure 5.27), some improvements are obtained.

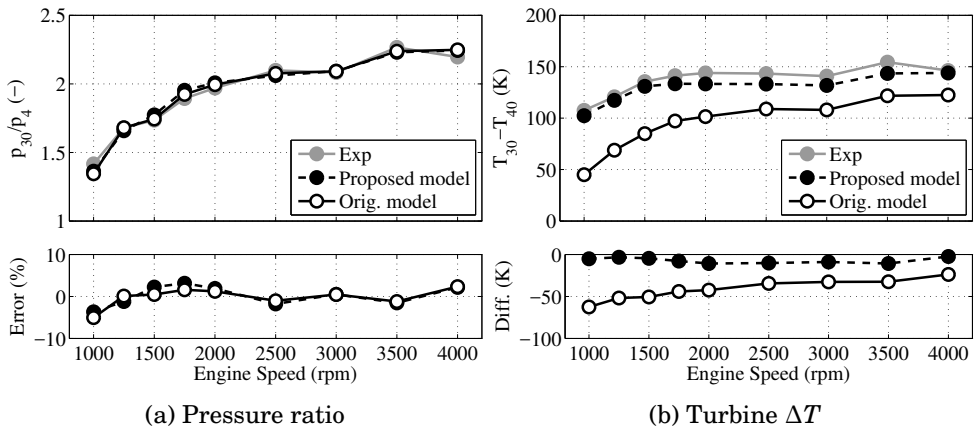


Figure 5.26: T#1 Turbine pressure ratio and temperature drop

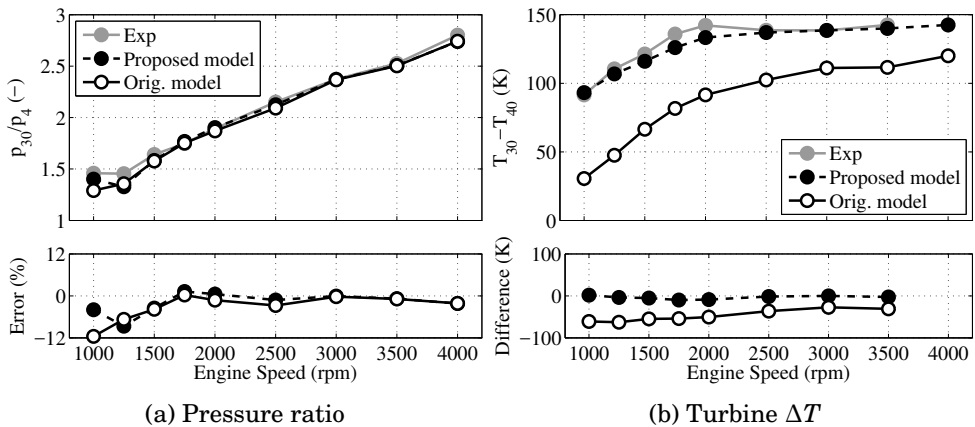


Figure 5.27: T#2 Turbine pressure ratio and temperature drop

The most significant differences between both models appear in temperatures. Supplier turbine map, used by the original model includes the effect of the heat transfer and the mechanical losses as has been shown in Equation 2.9. Furthermore, in the case of using ETE the isentropic power does not correspond to the pure adiabatic efficiency definition as it can be observed in Figure 2.3b. On the contrary, proposed turbocharger model calculates the heat transfer and mechanical losses for every simulated engine conditions, for that reason it uses an adiabatic map where the efficiency, expressed in Equation 5.3, represents only the internal irreversibilities in the turbine flow. The heat ($\dot{Q}_{GAS/T}$) is extracted from the gas before it is expanded in the turbine stator (see Figure 4.1 and Figure 2.3b). Additionally, the turbocharger mechanical losses are removed directly in the shaft.

$$\eta_{t,adiab.} = \frac{T_{30a} - T_{4a}}{T_{30a} - T_{4as}} = \frac{\dot{W}_t}{\dot{W}_{tsa}} \quad (5.3)$$

In both simulation sets, the predicted turbine inlet temperature shows similar values due to the fact that this parameter is almost independent of the model used as it has been explained in the previous chapter. The most important difference is observed in turbine outlet temperature. Figure 5.26b and Figure 5.27b show that without proposed turbocharger model turbine temperature differences arrive up to $-70K$ at low end torque conditions and original model never get differences below $-20K$. These errors contrast with the accurate results obtained with the proposed turbocharger model where maximum errors are around $5K$. Using the hot map, the gas undergoes an enthalpy drop related with the isentropic turbine enthalpy drop and the ETE mapped efficiency. This process is represented in Figure 2.3b between points '30' and '4' where $W'_t = W'_c + W_{mech}$. Using the proposed turbocharger model, the heat losses ($Q_{GAS/T}$) have been also considered, consequently, the enthalpy drop undergone by the gas is higher and much more realistic, following the points '30', '30a' and '4a' in Figure 2.3b, where the evolution between '30a' and '4a' is given by the efficiency of an adiabatic map. As it can be observed the proposed turbocharger model is able to predict correctly the temperature in the turbine outlet. This result is very important in order to model the different after-treatment elements placed in the exhaust line or any exhaust energy recovery device, like second stage turbochargers and bottoming ORC.

Figure 5.28 shows a comparison of turbocharger speed for both turbochargers. Good agreement has been obtained for both configurations due to the fact that boost pressure and mass flow through the compressor are controlled. Differences in this parameter can appear due to errors in the compressor map used or in the volumetric efficiency estimated by the engine model. The differences between both models are negligible, fact that will be recalled in the discussion of results section.

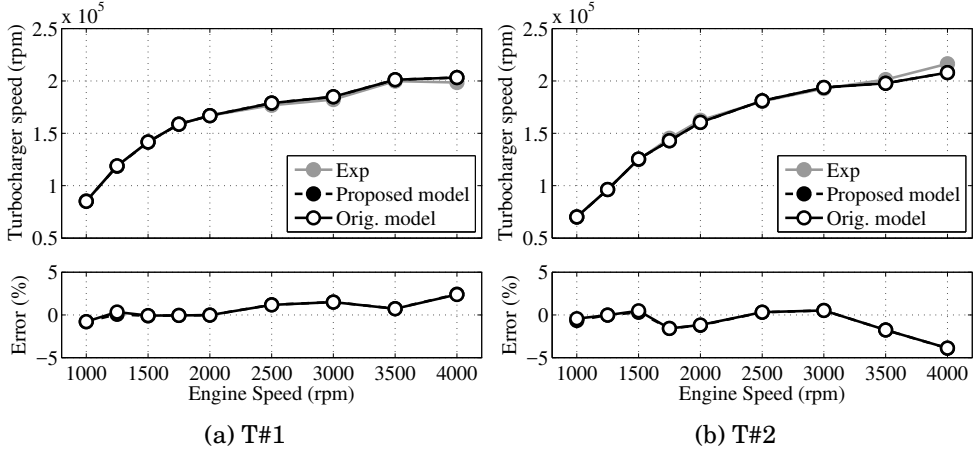


Figure 5.28: T#1 and T#2 turbocharger speed

Additional features of the proposed turbocharger model

The developed model provides additional analysis capabilities which allows a deeper understanding of the different energetic transformations in the turbocharger. For example, Figure 5.29 compares the compressor efficiency for the full load test using different definitions. On one hand, adiabatic efficiency (Equation 2.10) can be provided by the proposed turbocharger model and it compares mechanical compressor power versus isentropic compressor power. On the other hand, the diabatic efficiency can be obtained from the temperature drops in the compressor and it includes the effect of the heat transfer. It must be taken into account that the powers are instantaneous variables obtained as a result of a non-linear calculation and the temperatures are weighted with instantaneous mass flow as shown in Equation 5.4. When the model is used, the adiabatic efficiency is interpolated in the adiabatic map and the diabatic efficiency is obtained from the modelled temperatures.

$$\eta_{c,diab.}^{model} = \frac{\sum \dot{W}_{cs}^i}{\sum \dot{W}_c^i} = \frac{\sum \dot{m}_c^i \cdot \Delta T_s^i}{\sum \dot{m}_c^i \cdot \Delta T^i} \quad (5.4)$$

Using T#1, which is water cooled, both compressor efficiencies are very similar from 2000 rpm in advance due to the small heat transfer in the compressor compared with mechanical power, proving that water-cooling makes a thermal barrier from turbine to compressor as it was also pointed in [47]. At low engine speed, as the relative heat transfer effect increases, the compressor diabatic efficiency decreases. In the case of T#2, for all engine speeds the compressor receives heat power coming from the turbine. This phenomenon is much more important at low engine speed. In these conditions, the compressor outlet tem-

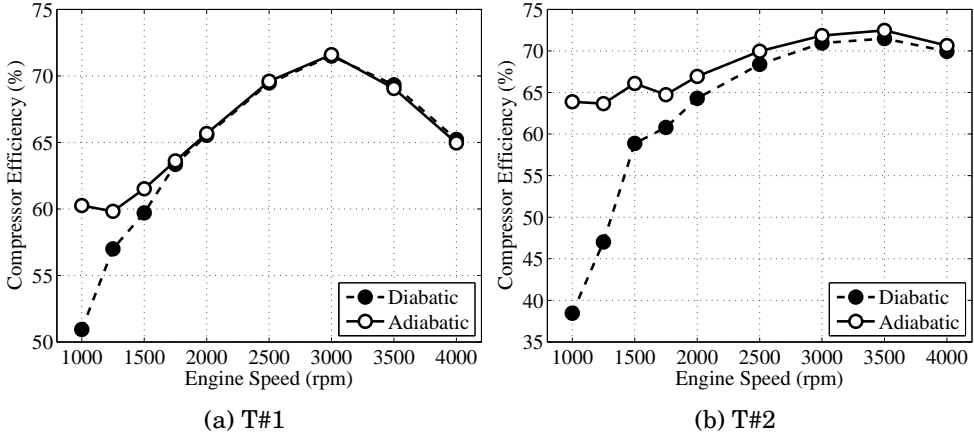


Figure 5.29: T#1 and T#2 compressor efficiency

perature increases due to heat transfer and, as a consequence, the diabatic efficiency decreases.

Similar analysis can be performed for the turbine. In this case four different definitions for the turbine efficiency can be used. The first efficiency definition is the most used in turbine maps provided by suppliers and it compares total compressor power with the turbine isentropic power. This definition, called ETE (Effective Turbine Efficiency), includes the effects of the heat transfer in turbine and compressor and the mechanical losses in the shaft, as it has been stated previously (Equation 2.9). It is important to note that ETE definition uses W_{ts} instead of W_{tsa} , since W_{tsa} is unknown without a HT model, as shown in Figure 2.3b. The second definition for turbine efficiency compares mechanical power of the turbine versus isentropic power and is called adiabatic efficiency (Equation 5.3). If the mechanical efficiency is included in the definition, the result is given in Equation 5.5. Finally, the last definition can be obtained from the temperatures at turbine inlet and outlet. It is called diabatic efficiency which is shown in Equation 5.6 weighted with instantaneous mass flow. This definition is not commonly used since, in some cases, it can provide values higher than one or even lower than zero [2]. It includes the effect of heat transfer in the turbine that can be very important. When this effect is important T_{4a} can become lower than T_{4s} giving values higher than one. For that reason when heat losses are important compared to turbine power the diabatic efficiency does not represent the actual aerodynamic efficiency of the turbine.

$$\eta_{t,adiab.}^{model} \cdot \eta_{mech}^{model} = \frac{\dot{W}_t}{\dot{W}_{tsa}} \frac{\dot{W}_c}{\dot{W}_t} = \frac{\dot{W}_c}{\dot{W}_{tsa}} = \frac{\sum \dot{m}_t^i \cdot c_{p,c}^i \cdot (T_{20a} - T_{10})^i}{\sum \dot{m}_c^i \cdot c_{p,t}^i \cdot (T_{30a} - T_{4as})^i} \quad (5.5)$$

$$\eta_{t,diab.}^{model} = \frac{\sum \dot{m}_t^i \cdot (T_{30} - T_{4a})^i}{\sum \dot{m}_t^i \cdot (T_{30} - T_{4s})^i} = \frac{\dot{W}_t + \dot{Q}_{GAS/T}}{\dot{W}_{ts}} \quad (5.6)$$

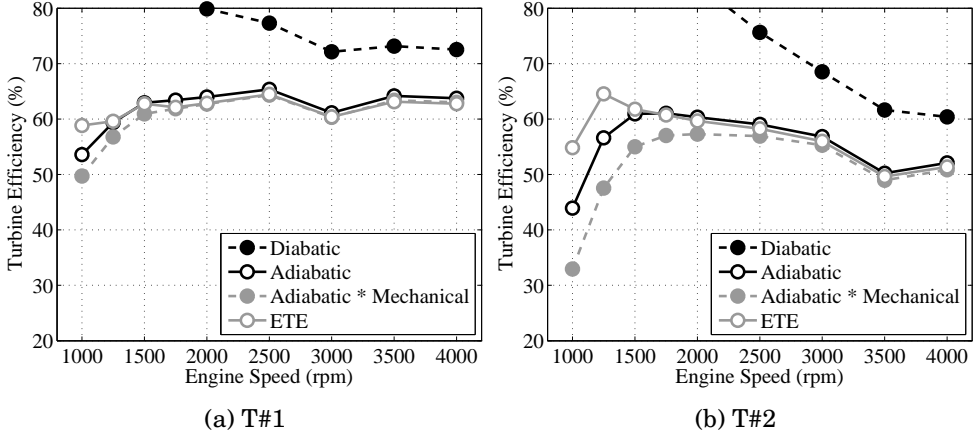


Figure 5.30: T#1 and T#2 turbine efficiency

Figure 5.30 compares the four turbine efficiencies for the full load engine tests, where obtained values for diabatic efficiency higher than 80% have been removed. It shows that diabatic efficiency is very high (in some cases higher than one), the reason is the lower turbine outlet temperature caused by the heat transfer in the turbine. This effect is more noticeable at lower speeds because turbine heat losses are higher, in relative terms, compared to turbine power. The difference between adiabatic (Equation 5.3) and adiabatic times mechanical (Equation 5.5) represents the turbocharger friction losses, and hence the adiabatic efficiency is always higher. In general, the effect of the friction losses in the turbocharger is more important at low engine speed (i.e. low turbocharger speeds). Comparing ETE (Equation 2.9) with the product of adiabatic and mechanical efficiencies (Equation 5.5), the differences are caused by the inclusion of the heat in the compressor ($\dot{Q}_{C/Air}$) and the different turbine isentropic power used in both definitions (\dot{W}_{tsa} or \dot{W}_{ts}). As can be observed the differences between these two definitions are more important when the turbocharger is not water-cooled (T#2), what increases the transfer of heat power from bearing housing to the compressor. In the case of T#1, due to water cooling, only at 1000 rpm appears a big difference between the three definitions.

Finally, an important parameter to analyse is turbocharger efficiency because of its influence on engine performance. If proposed turbocharger model is used, the turbocharger efficiency is calculated according to Equation 5.7, while for simulations without proposed turbocharger model, this efficiency is given by Equation 5.8. In the first case, an adiabatic map is used to compute turbocharger

efficiency, whereas, in the second case, a hot map is used for the purpose. For both of these parameters, the calculations of the values from the models are obtained averaging the pulsating power.

$$\eta_{TG,adiab.}^{model} = \eta_{t,adiab.}^{model} \cdot \eta_{c,adiab.}^{model} \cdot \eta_{mech}^{model} = \frac{\dot{W}_t}{\dot{W}_{tsa}} \frac{\dot{W}_{cs}}{\dot{W}_c} \frac{\dot{W}_c}{\dot{W}_t} = \frac{\dot{W}_{cs}}{\dot{W}_{tsa}} \quad (5.7)$$

$$\eta_{TG,map}^{model} = ETE \cdot \eta_{c,diab.}^{model} = \frac{\dot{W}_c + \dot{Q}_{C/Air}}{\dot{W}_{ts}} \frac{\dot{W}_{cs}}{\dot{W}_c + \dot{Q}_{C/Air}} = \frac{\dot{W}_{cs}}{\dot{W}_{ts}} \quad (5.8)$$

It is worth noting that the simplification given in Equation 5.8 is possible only if compressor heat $\dot{Q}_{C/Air}$ is equal in ETE and compressor diabatic efficiency. This fact occurs only when turbine and compressor maps are measured at the same time without disassembling the turbocharger. With this assumption, the difference between both turbocharger efficiency definitions is just the turbine isentropic power (\dot{W}_{tsa} or \dot{W}_{ts}). As it can be deduced from Figure 2.3b, at high pressure ratios the relative difference between both isentropic powers will be small. Pressure ratio increases when engine speed (and also turbocharger speed increases), so at high speeds both turbine isentropic enthalpy drops will be similar. Figure 5.31a shows clearly this situation at high engine speeds and full load. That is when the difference between the values given by Equation 5.7 and Equation 5.8 will be small. Consequently, this effect of turbocharger heat transfer (\dot{W}_{tsa} vs \dot{W}_{ts}) on turbocharger efficiency (defined in Equations 5.7 and 5.8) is low at high engine speeds.

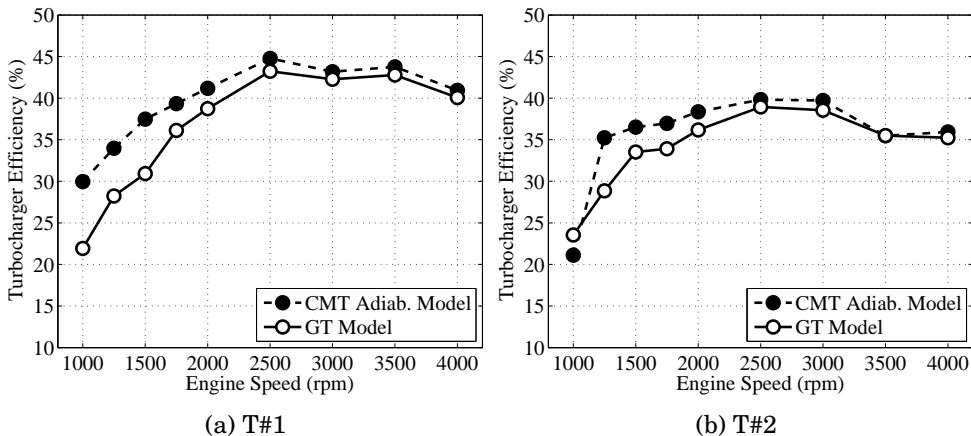


Figure 5.31: T#1 and T#2 turbocharger efficiency

In addition to this analysis, the proposed turbocharger model also makes possible the evaluation of an energy balance between the different parts of the turbocharger distinguishing between heat flows and mechanical power. When

the turbocharger is working on the engine, heat and mechanical energy is transferred between the different elements. Using the information provided by the model, energy balances in the turbocharger can be computed from the point of view of heat power exchanged.

Figure 5.32 represents this heat balance for all full load working points. For the compressor the sign of heat flow depends on the operating conditions. For T#2 (Figure 5.32b) the comparison is easier since, in this case, only the turbine losses heat. This behaviour occurs only when the compressor absorbs the heat coming from the turbine for all operating points. For the oil it is a predictable behaviour as it works as a heat sink in the absence of water cooling.

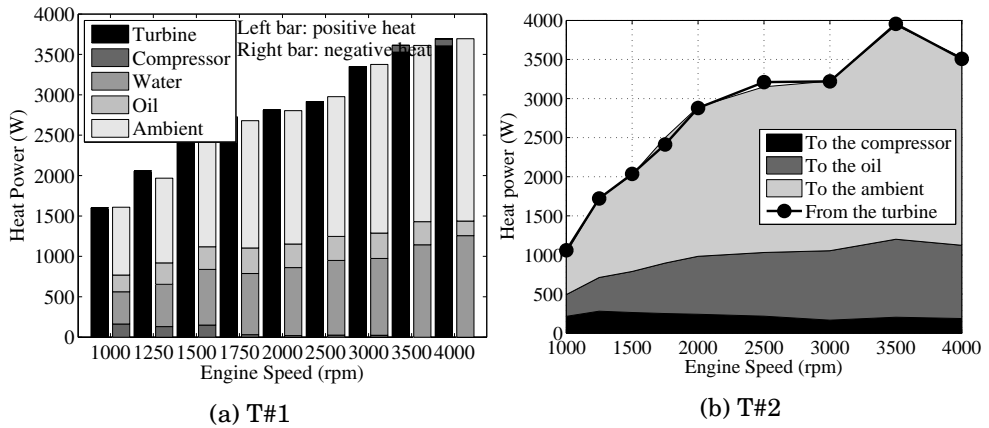


Figure 5.32: T#1 and T#2 heat power balance

For full load operating points, the maximum temperature of the turbocharger always corresponds to the turbine. Therefore, the heat will always flow from the turbine to the rest of the turbocharger. The water and the oil act like coolants (heat sinks) due to their low temperature. In the case of the compressor it can act as both a heat sink or a heat source depending of the operating point and the easiness of heat flow through central housing.

At high pressure ratios, the compressor can lose heat that will be absorbed by the oil, ambient or the water (as shown in Figure 5.32a for T#1 when the engine is running at 3500 rpm and 4000 rpm). Figure 5.32b also shows how the heat is distributed in T#2. More than 50% of the heat losses in the turbine go to the ambient and this percentage increases at higher engine speeds. This result extracted from the proposed turbocharger model is in concordance with different studies of other authors such as [71]. The compressor receives similar heat power for all engine speeds in absolute value only slightly higher at low engine speeds. Nevertheless, this heat in relative terms and at high engine speed is negligible in comparison to compressor power. In Figure 5.32a for T#1,

each engine test is represented by two different bars. The left bar is the sum of all heats flowing to the metal parts of the turbocharger and right bar is the sum of all heats flowing from the metal parts. In this case, turbine casing always losses heat power that is always received it by the ambient, the water and the oil. However, the heat flow in the compressor can change its direction (from/to central housing) depending on the operating conditions, as has been stated previously. In this case the ambient is again the node that receives a higher rate of heat and the oil receive low heat quantity due to the water-cooling. However, the compressor air at the engine speeds of 3500 rpm and 4000 rpm losses heat (positive sign) since it works with high pressure ratios, while at lower engine speeds (i.e. lower pressure ratios) the compressor air receives heat (negative sign).

Using the proposed turbocharger model a turbocharger mechanical power balance can be also performed. Figure 5.33 represents this balance where a logarithmic y-axis has been used to remark the different orders of magnitude among turbine and compressor mechanical powers and turbocharger friction losses power. As can be observed in Figure 5.33, despite the fact that the mechanical losses are higher at high engine speed tests, the effect of these losses is much more important at low engine speed points because compressor and turbine power decrease faster than mechanical losses at low engine speeds.

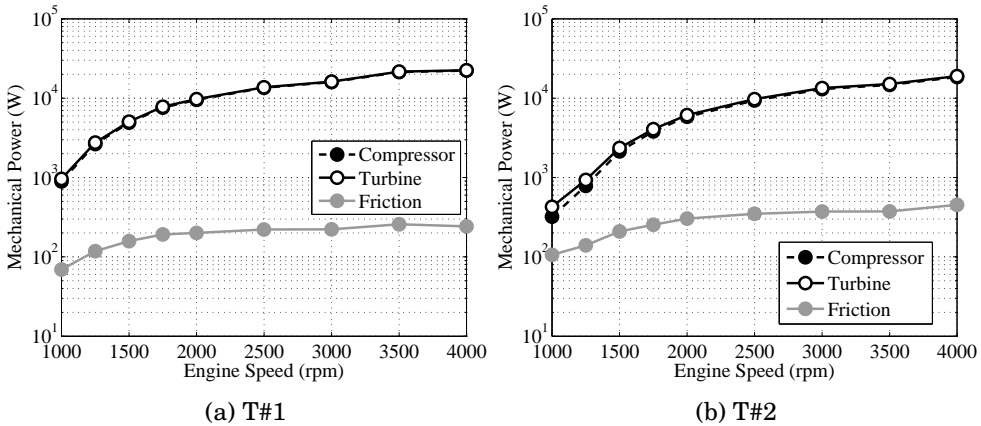


Figure 5.33: T#1 and T#2 mechanical power balance

The comparison between the results of both kind of simulations and the experimental data shows that COT and TOT prediction is the main substantial improvement using a heat transfer and mechanical losses model for the turbocharger. This improvement is crucial in inter-cooling [131], combustion process [132] where there is no intercooler, aftertreatment [133], exhaust energy recovery [134], exhaust heat transfer modelling [135] and two stage turbocharg-

ing [136] modelling. Even the simulation of full load conditions can be improved using proposed turbocharger model. However, the improvements of the model result only in the prediction of COT and TOT and do not affect the engine performance variables if the turbocharger map, used in the original configuration, is chosen properly. This map must have been measured in similar conditions to those desired to be modelled, so turbocharger manufacturer maps that hold this condition are suitable to be used in order to predict well all the variables associated to the engine excepting TOT. Cold maps can also be used but always coupled with a proposed turbocharger model. In that case the prediction of all variables, including TOT is precise. The turbo speed is not affected by the different models as it has been shown in this work and it has been demonstrated by the development shown in Equations 5.9, 5.10 and 5.11 showing turbocharger speed increment, where K primarily depends on turbocharger shaft inertia and time step. Previously in Equation 5.9 ETE definition is derived; where the compressor mechanical power has been replaced by the product of mechanical efficiency and turbine mechanical power. Since the only difference between \dot{W}_{ts} and \dot{W}_{tsa} is the turbine inlet temperature, it is possible to introduce turbine adiabatic efficiency in the equation as has been done in Equation 5.9.

$$ETE = \frac{\eta_{mech} \cdot \dot{W}_t + \dot{Q}_{C/Air}}{\dot{W}_{ts}} = \left(\eta_{mech} \cdot \eta_{t,adiab.} + \frac{\dot{Q}_{C/Air}}{\dot{W}_{tsa}} \right) \frac{T_{30a}}{T_{30}} \quad (5.9)$$

In Equation 5.10, the turbo speed increment expression has been derived using the proposed turbocharger model approach. The resulting equation is function of compressor and turbine adiabatic efficiencies, turbocharger friction losses efficiency and isentropic power of compressor and turbine.

$$\begin{aligned} \Delta N &= K (\dot{W}_t - \dot{W}_{mech} - \dot{W}_c) = \\ &= K (\eta_{mech} \cdot \dot{W}_t - \dot{W}_c) = \\ &= K \left(\eta_{mech} \cdot \eta_{t,adiab.} \cdot \dot{W}_{tsa} - \frac{\dot{W}_{cs}}{\eta_{c,adiab.}} \right) \end{aligned} \quad (5.10)$$

In Equation 5.11, the turbo speed increment expression has been derived using the original model approach, i.e using map efficiencies definitions (ETE and $\eta_{c,diab.}$). Introducing Equations 2.11 and 5.9 it gives the same expression as in Equation 5.10. It is important to underline that this equivalence between both models is only valid when the compressor heat measured in the turbine map ($\dot{Q}_{C/Air}^t$) is equal to the heat measured in the compressor map ($\dot{Q}_{C/Air}^c$). This conditions occurs when the turbine and compressor maps have been measured at the same time. If the map of the compressor or the turbine is measured independently using an external motor or a brake the $\dot{Q}_{C/Air}$ will be different in each case.

$$\begin{aligned}
 \Delta N &= K (\dot{W}'_t - \dot{W}'_c) = \\
 &= K \left(ETE \cdot \dot{W}_{ts} - \frac{\dot{W}_{cs}}{\eta_{c,diab.}} \right) = \\
 &= K \left(ETE \cdot \frac{T_{30}}{T_{30a}} \cdot \dot{W}_{tsa} - \frac{\dot{W}_{cs}}{\eta_{c,diab.}} \right) = \\
 &= K \left(\eta_{mech} \cdot \eta_{t,adiab.} \cdot \dot{W}_{tsa} + \dot{Q}_{C/Air}^t - \frac{\dot{W}_{cs}}{\eta_{c,diab.}} \right) = \\
 &= K (\eta_{mech} \cdot \eta_{t,adiab.} \cdot \dot{W}_{tsa} + \dot{Q}_{C/Air}^t - (\dot{W}_c + \dot{Q}_{C/Air}^c)) = \\
 &= K \left(\eta_{mech} \cdot \eta_{t,adiab.} \cdot \dot{W}_{tsa} - \frac{\dot{W}_{cs}}{\eta_{c,adiab.}} \right) \tag{5.11}
 \end{aligned}$$

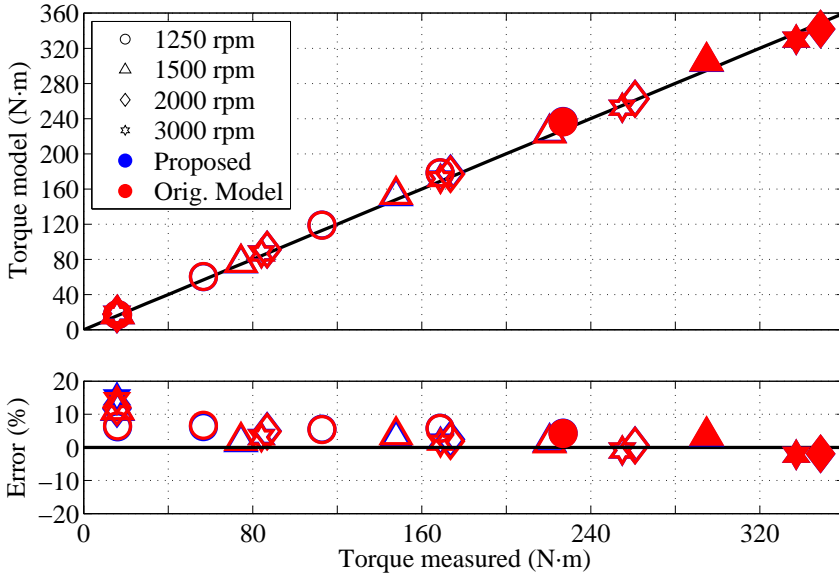
So, it can be concluded that the usage of ETE definition for turbine efficiency without proposed turbocharger model is suitable if compressor and turbine outlet temperature prediction is not important for simulations purposes and turbine maps were measured at same time to cancel $\dot{Q}_{C/Air}^t$ terms. As a drawback, the prediction of turbine outlet temperature is not satisfactory. Concluding, if a proposed turbocharger model with an adiabatic map is used every variable prediction is satisfactory, while special care must be taken with turbine efficiency definition if simulations are performed without using the proposed turbocharger model.

Partial loads

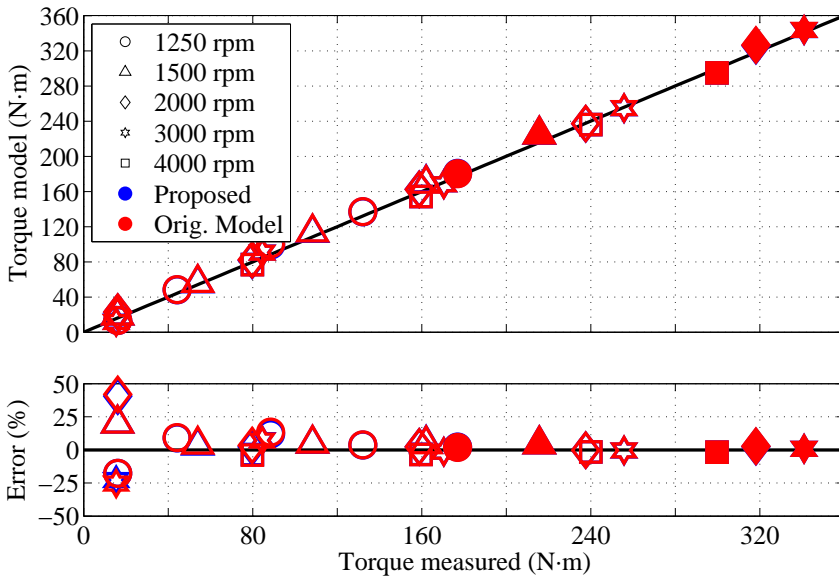
The proposed turbocharger model has been also tested under engine partial load conditions. A new representation has been used to show these results which depend on two different parameters, speed and load. For that reason, the figures of this section present the experimental data on the 'X' axis versus the modelled results on the 'Y' axis. Accurate modelled results will appear plotted on the diagonal. The different symbols used represent the engine speed and if the symbol is filled it represents a full load test.

Figure 5.34 compares the modelled torque versus measured data. A good agreement can be observed. Moreover, no significant differences can be found between both models (proposed turbocharger model in blue and original look up maps model in red). Only for the 1 bar of BMEP tests the models do not offer a good agreement in percentage due to the small torque of this point that causes important errors with very small variations in torque.

Good agreement is also reached in predicted air mass flow (Figure 5.35). Errors lower than 2.5% is observed in most of the engine test modelled. Again, the differences observed between both models in this parameter are insignificant.



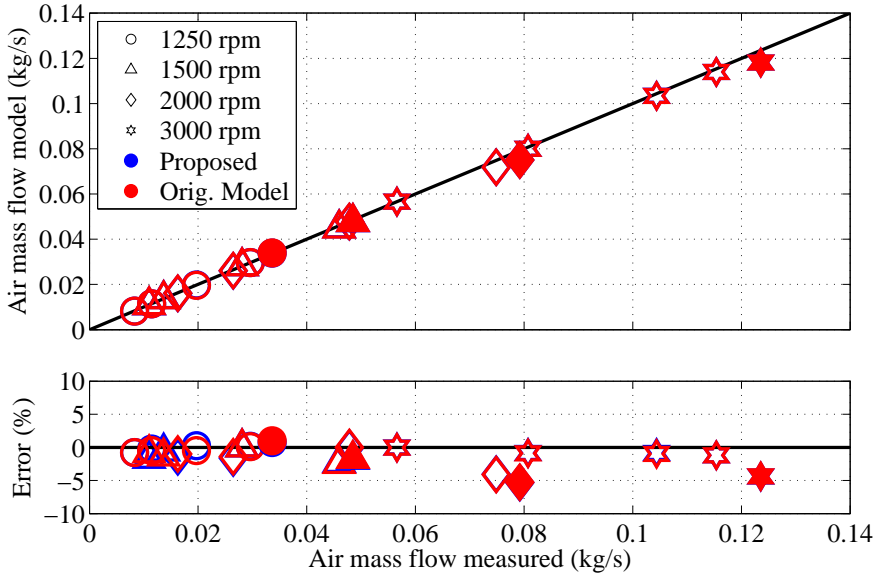
(a) T#1



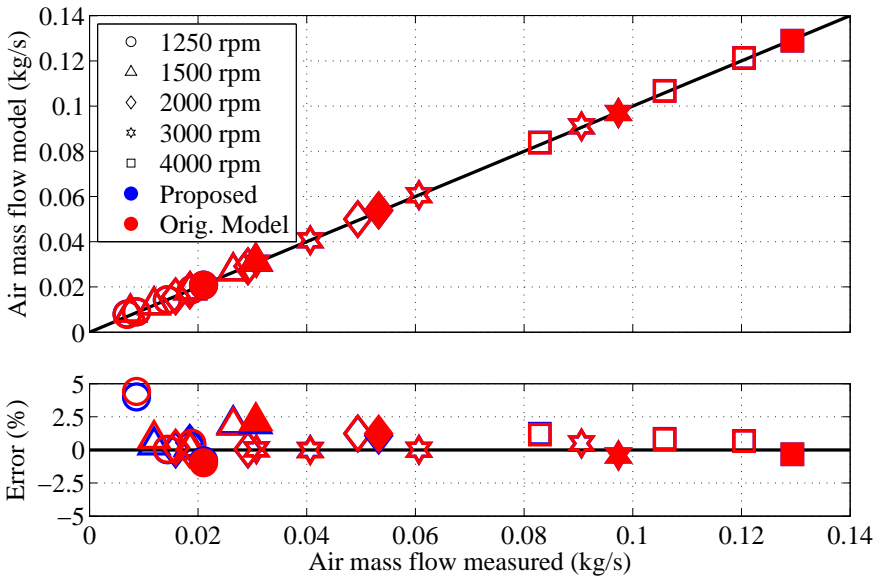
(b) T#2

Figure 5.34: Modelled against measured torque for T#1 and T#2

Figure 5.36 and Figure 5.37 represent different parameter of the compressor for the T#1 and the T#2. Compressor pressure ratio and temperature increment



(a) T#1



(b) T#2

Figure 5.35: Modelled against measured air mass flow for T#1 and T#2

are represented. As it has been commented previously, a good prediction of these parameters depends on the accuracy of the compressor map used. At high

load tests (high outlet pressure and temperature) both models presents a good agreement with the experimental data and the differences between both models are not significant. The main discrepancies appear at low load tests. Observing the results of T#1, proposed turbocharger model presents better results, mainly for temperatures. With the same compression ratio the temperature drop in the compressor is better predicted by the proposed model.

For T#2 both models show opposite errors as much in compression ratio as in temperature drop. While the proposed model calculates a higher temperature drop with a lower pressure ratio, the original model does the opposite. The reason of this behaviour can be the fact that different compressor extrapolation models are used in the proposed model and in the original one.

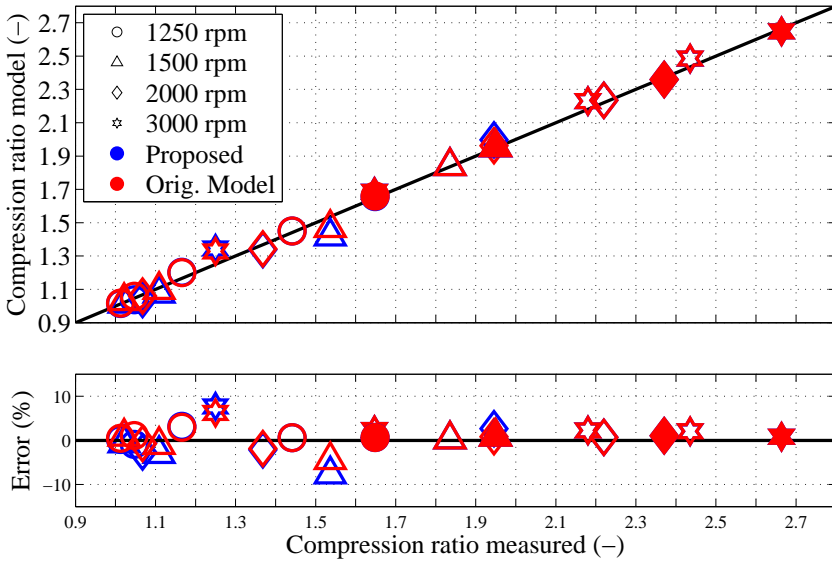
The comparison of the different parameters that describe the behaviour of the turbine in the partial load test is shown in Figure 5.38 and Figure 5.39 for T#1 and T#2 respectively. Once again, in order to reproduce correctly the behaviour of the turbine it is very important to impose the correct turbine inlet temperature which depends highly on the heat transfer and combustion processes in the cylinder.

As it was explained in the previous chapter the cylinder parameters have been fitted in order to obtain a value of turbine inlet pressure as accurate as possible. From the point of view of expansion ratio, both models show good agreement with the experimental data with errors limited to 5% in most of cases.

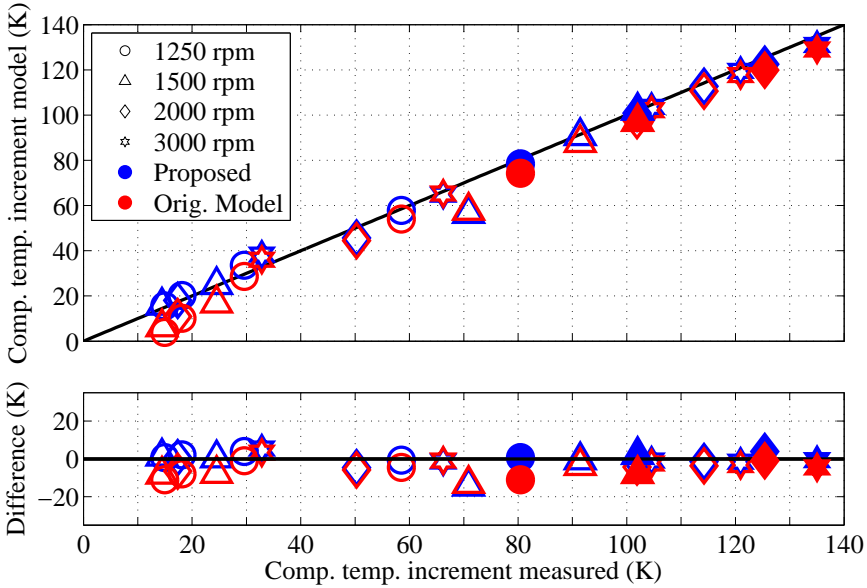
As it was observed in the results at full load, turbine outlet temperature is the parameter where the differences between both models are more important. As it is shown in Figure 5.38b and Figure 5.39b, the proposed model is able to predict turbine outlet pressure while original model always overestimates it. This difference between both models is clearer if the effect of the turbine inlet temperature errors is removed as it has been done by comparing temperature drop in the turbine. It can be observed that the proposed model is able to predict that difference of temperatures but the original model calculates a lower temperature drop. The reason for this difference is while the temperature drop calculated by the original model is related with the mechanical power, the proposed turbocharger model also include the reduction in temperature due to the heat losses from the exhaust gas to the turbocharger walls.

Figure 5.40 compares the turbocharger speed calculated by the models and the experimental data. The figure shows good agreement at high speed but discrepancies between both models at low turbocharger speed. Here, it is important to remark that the compressor maps used only provide information for turbocharger speed higher than 70 krpm for T#1 and higher that 90 krpm for the T#2. Below those values, the model needs to extrapolate the map.

The proposed model is also able to predict the temperature at the different nodes of the turbocharger. Figure 5.41 and Figure 5.42 show the comparison



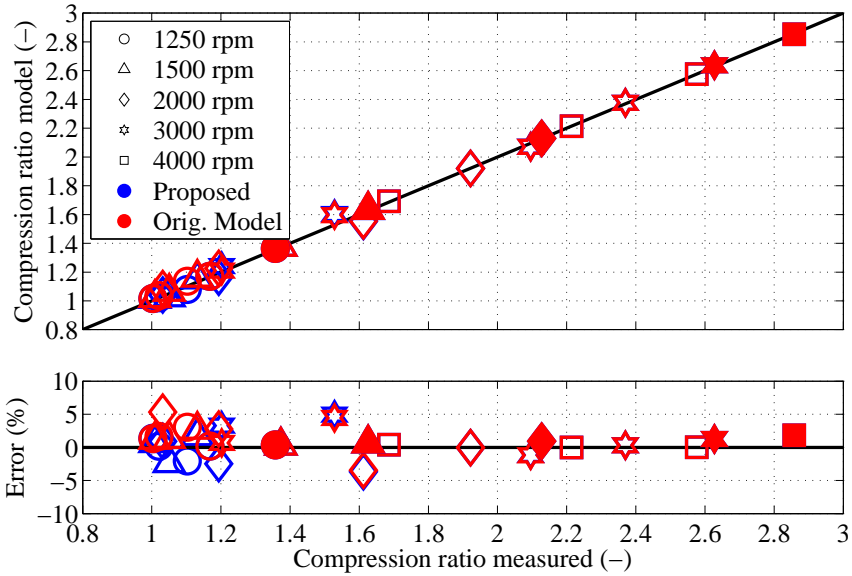
(a) Pressure ratio



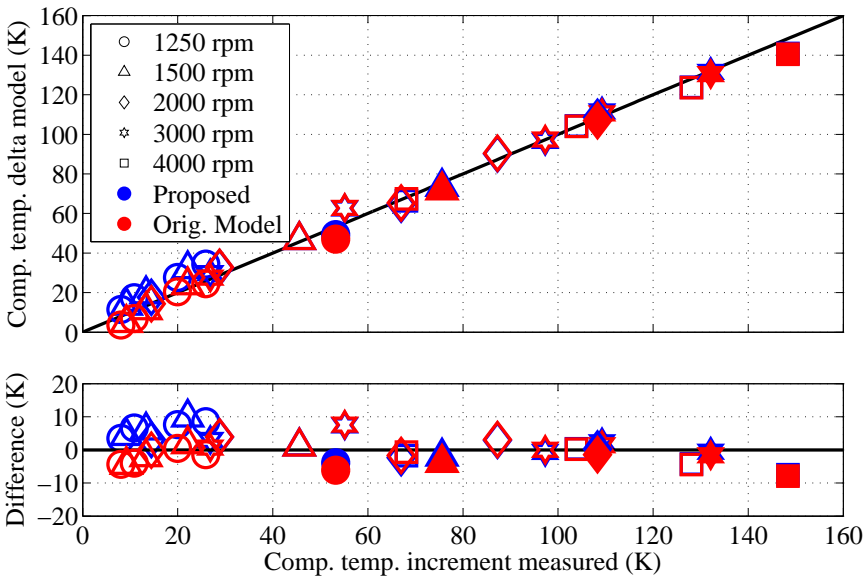
(b) Temperature increment

Figure 5.36: Compressor pressure ratio and temperature increment for T#1

between the experimental data and the modelled results for T#1 and T#2 respectively. The results are grouped by engine speed and each engine load test is



(a) Pressure ratio

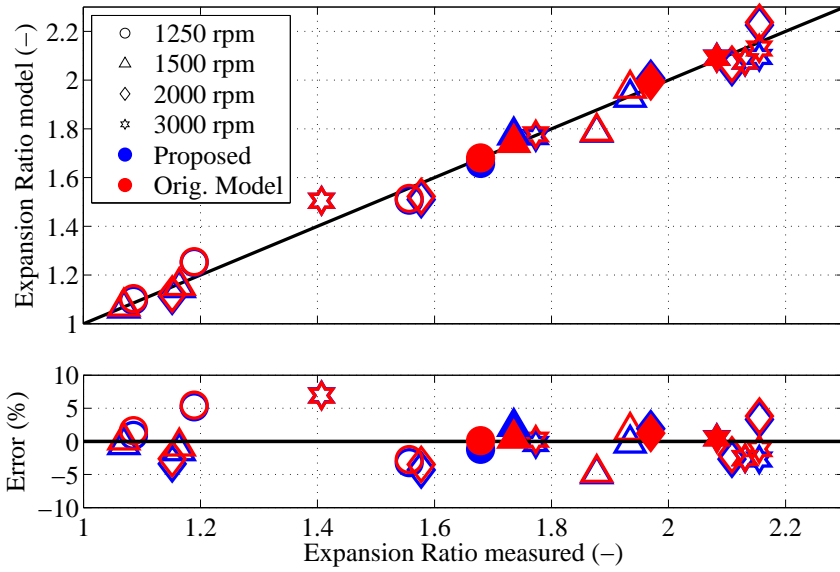


(b) Temperature increment

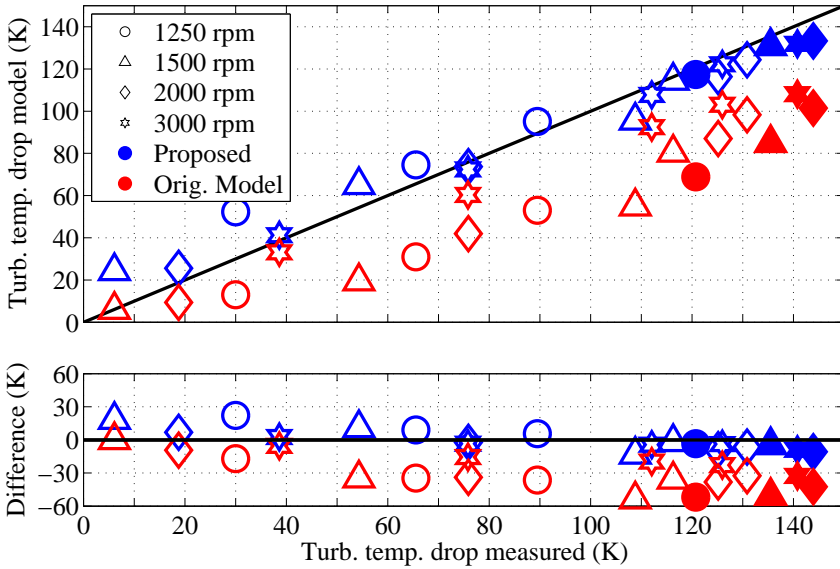
Figure 5.37: Compressor pressure ratio and temperature increment for T#2

represented by a different symbol.

It can be observed that at lower loads nodes temperatures are also lower.



(a) Pressure ratio



(b) Temperature drop

Figure 5.38: Turbine pressure ratio and temperature drop for T#1

Moreover, the main differences versus the load appear near the turbine. Other observed phenomenon is how with the T#1 (water cooled) the temperature

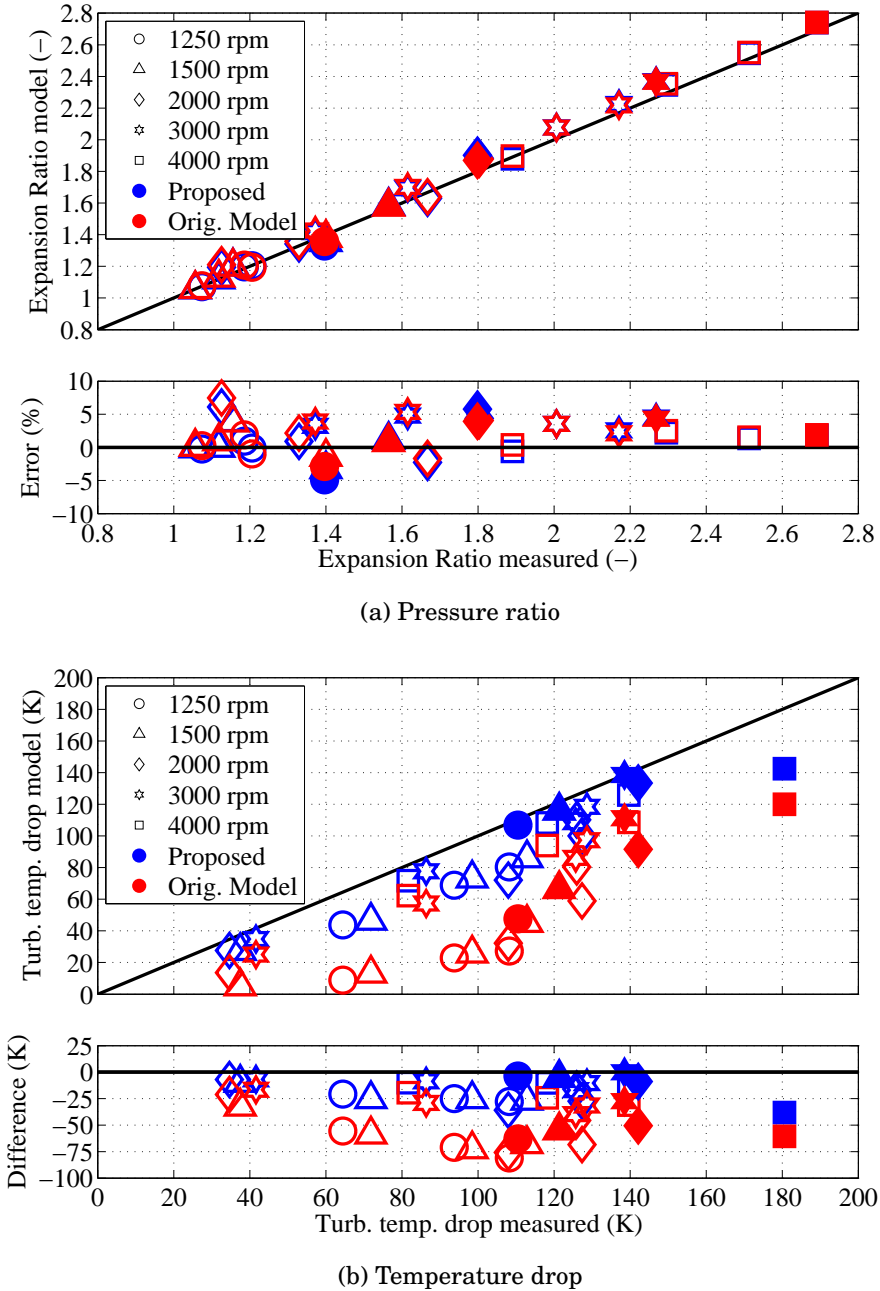
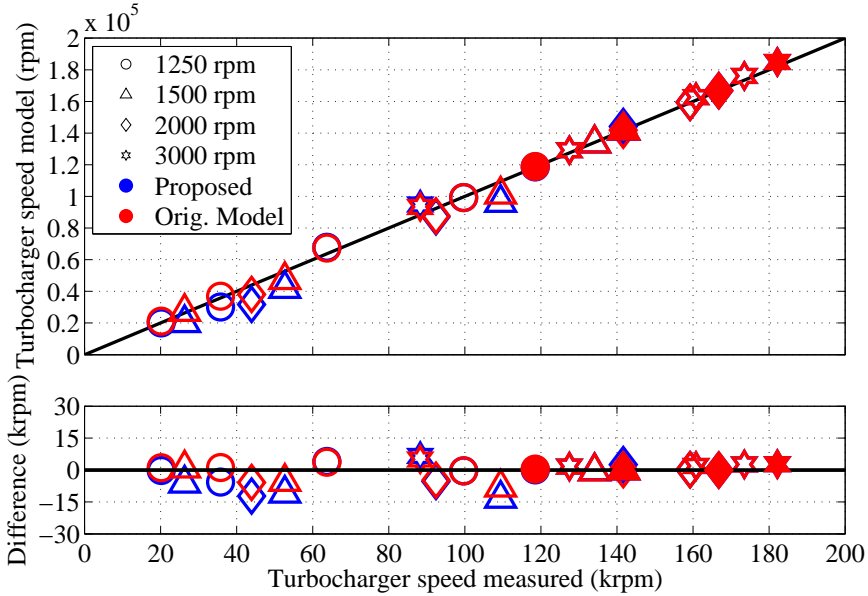
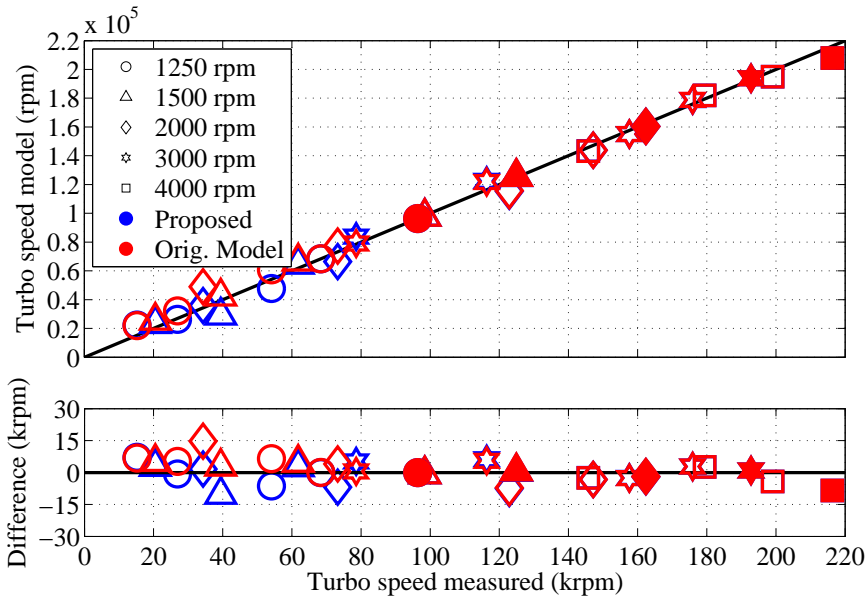


Figure 5.39: Turbine pressure ratio and temperature drop for T#2

variations near the compressor are lower than for the T#1. It can be observed as all these phenomena are predicted by the model.



(a) T#1



(b) T#2

Figure 5.40: Turbocharger speed for T#1 and T#2

Transient simulations: Tip in and tip out

The capabilities of the model have been analysed in transient conditions simulating tip in and tip out tests. The results obtained in these calculations have a

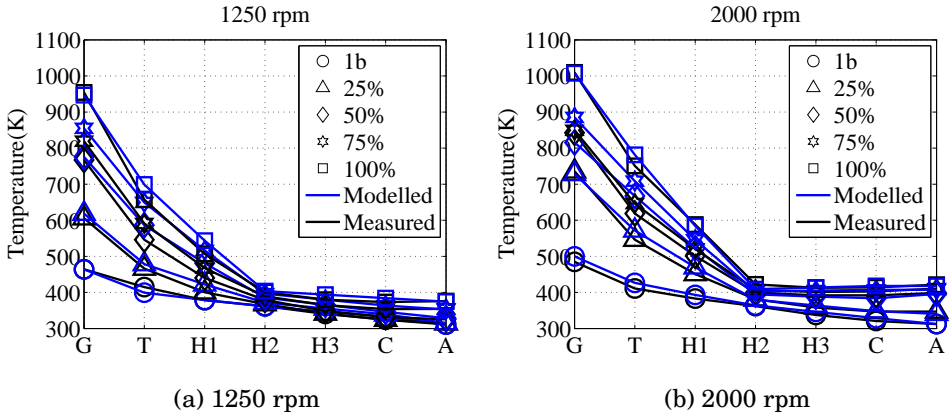


Figure 5.41: Nodes temperatures for T#1

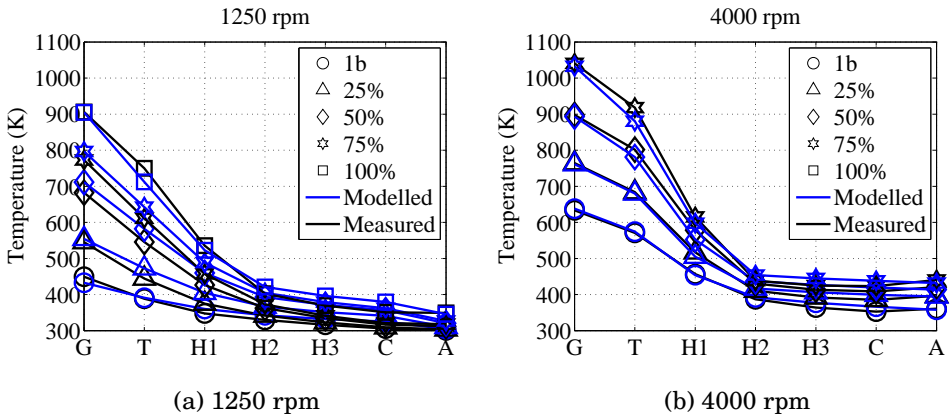


Figure 5.42: Nodes temperatures for T#2

lot of uncertainties that have been minimized by imposing some parameters or performing some previous analysis. The following information is not available for the engine model:

- Control strategy used by the engine to decide the injected fuel.
- Control strategy used by the engine to move the turbine stator blades.
- Relation between the control signal used to move the VGT and the real VGT position.
- Control strategy used by the engine to open the EGR valve and fix the admitted air mass flow.

- Wall temperatures of the engine and the manifolds and how they change during the test.
- Heat transfer coefficient in the cylinder. Along with wall temperatures, they are the most important parameter for determining the heat losses in the engine. Imposed the correct fuel, it allows an accurate prediction of the torque.
- Turbocharger wheel inertia.

To solve all these difficulties several actions have been carried out. The evolution of the fuel versus time has been imposed. The experimental information used has been provided by the engine control unit (ECU) but it has been corrected by the unbalance parameter calculated by the combustion diagnostic model (CALMEC) which gives an idea about the ratio between burned and injected fuel. This parameter changes during the transient test and in the worst cycles it can take the value of 70%.

The signal of the ECU for the VGT has been also used to fix the VGT displacement versus time during the different transient test. Anyway this value has had to be corrected to correlate the control signal with the real VGT displacement. To perform this correction the full load test results have been used. Figure 5.43 compares the real VGT position and the engine control unit signal and the correlation used to correct the VGT displacement for the load transients using T#2.

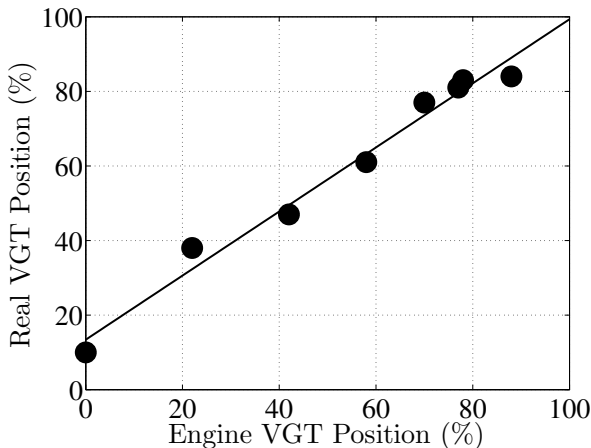


Figure 5.43: Correlation between engine VGT position signal and real VGT displacement

A similar correction was performed for T#1. To model the EGR valve a discharge coefficient has been used in the recirculation circuit. The value of that

discharge coefficient has been imposed proportional to the EGR control signal provided by the ECU. This signal has been multiplied by a constant in order to fit correctly the air mass flow during the period when the EGR valve is open.

The values of the wall temperatures calculated by CALMEC at the beginning of the load transient have been imposed in the cylinder, the piston and the cylinder head. This is not a critical problem due to the small variation of the temperatures during the twelve seconds that have been calculated. Using these temperatures, the heat transfer coefficient in the cylinder has been fitted to obtain the same heat transfer as the one predicted by CALMEC.

Finally, an important parameter to fit correctly the engine tip in and tip out load transients is the inertia of the turbocharger. The values provided by the manufacturer have been used for both turbochargers.

Due to the difficulties and the strategies described above the modelled tests cannot be compared with the experimental information. The high uncertainties of the engine model make this comparison not useful. Moreover, special thermocouples with very low thermal inertia had to be used to make proper temperature comparisons. For these reasons, the results of both models (proposed turbocharger model and original map based model) are compared between them. The purpose of this comparison is the analysis of the effect of the proposed model on transient calculations since this model includes heat transfer, an important phenomenon in this kind of tests. Tip in and tip out load transient have been modelled for 1250 rpm, 1500 rpm, 2000 rpm and 3000 rpm. A period of 10 seconds after the moment in which the pedal changes has been chosen to represent the results. Moreover, two seconds before that moment are used to stabilize the model. Since the conclusions of the modelling are similar for the different engine speeds only part of the results will be presented in the following discussion.

The first parameter compared is the torque (Figure 5.44 and Figure 5.45). In order to obtain accurate results for the torque, the most important parameter is the fuel. As it has been commented before the same fuel is imposed for both model from the ECU signal corrected by the results of CALMEC. The second factor that affects the prediction of the torque is the heat transfer. Heat transfer has been also fitted for both models comparing with CALMEC results. Finally, the last parameter that has influence in the torque provided by the model are the pumping losses, that reflect the efficiency of the scavenging process.

For the tip in load transient tests, the wall temperatures of the turbocharger are low at the beginning. When the pedal is pushed, the exhaust gas temperature suddenly increases due to a higher fuel mass burned and a high fuel to air ratio. This hot gas passes through the turbocharger whose walls are still cool causing high heat losses. These heat losses are much higher than in steady state conditions and the supplier turbine maps do not include them. That energy is used to warm up the turbocharger metal parts, reducing the efficiency of

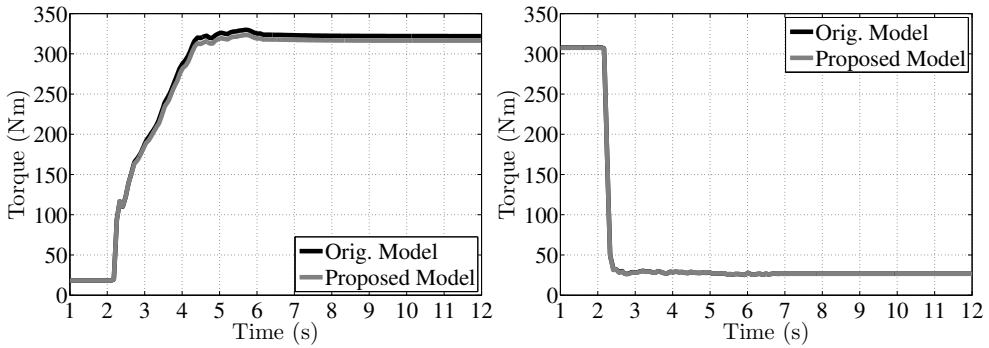


Figure 5.44: Torque during tip in and tip out tests for T#1 at 1500 rpm

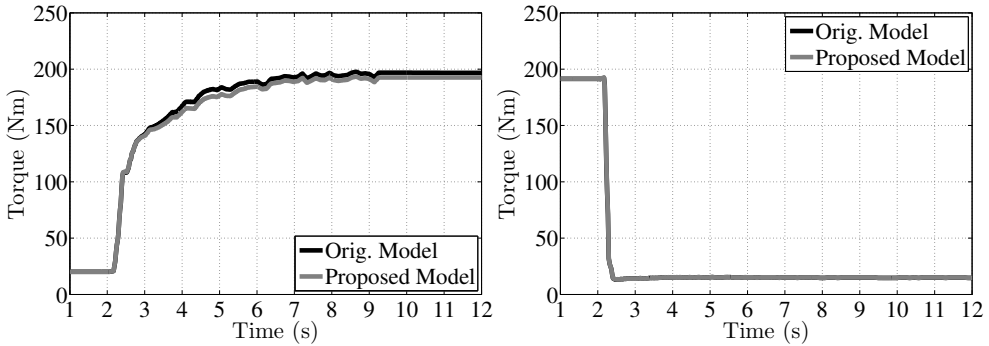


Figure 5.45: Torque during tip in and tip out tests for T#2 at 1000 rpm

the turbocharging system and increasing the pumping losses. For that reason, during tip in load transient, mainly at low engine speed, the proposed model predicts slightly lower torque compared to the map based model. At high speed the influence on the torque of this effect is lower and both models predict similar torque.

For tip out load transient tests, the opposite phenomenon happens. When the fuel is cut off, the wall temperatures of the turbocharger are high. Then, during a small period of time after, the turbine has more energy available due to the fact that the exhaust gas does not lose heat power or even can receive heat from the hotter walls. However, due to the low fuel flow after the cut off, the torque is not significantly affected in these transient tests.

Figure 5.46 and Figure 5.47 represent the evolution for the admitted air mass flow during tip in and tip out load transient tests. This parameter shows more differences between the map based model and the model presented in this thesis. For the tip in load transient test, supplier map does not consider the

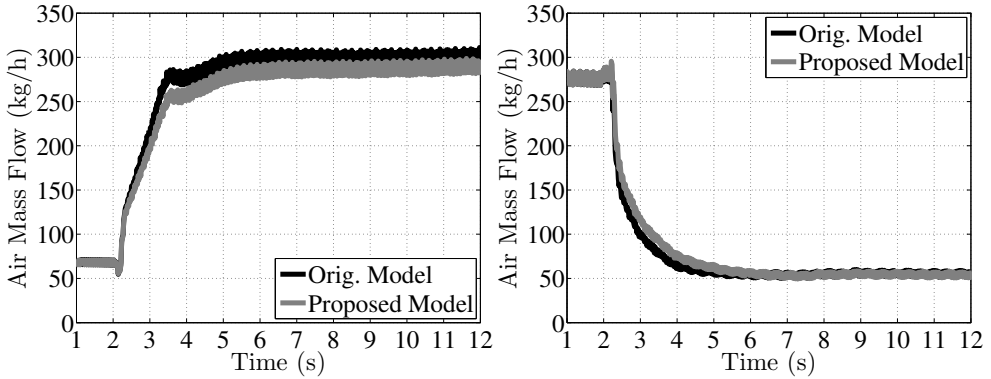


Figure 5.46: Air mass during tip in and tip out tests for T#1 at 2000 rpm

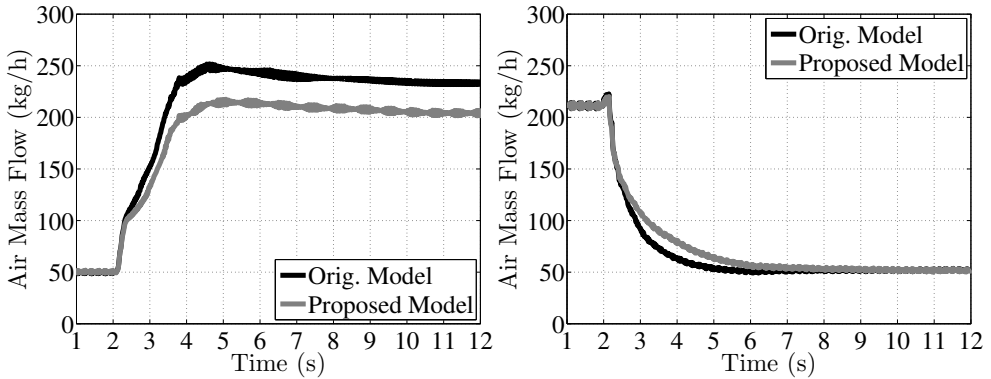


Figure 5.47: Air mass during tip in and tip out tests for T#2 at 1600 rpm

high heat losses that exhaust gases undergo at the beginning of the acceleration. This additional energy makes the turbocharger to have a higher increment of the speed and as a consequence the air mass flow admitted is higher. During tip out tests, higher wall temperatures that warm up the gases allow higher energy disposal and higher mass flow during a period of time after the cut off.

Compressor outlet pressure is affected by the same phenomenon that the air mass flow. This value depends on the energy available in the turbine. Therefore, if heat losses are not considered, the evolution during tip in load tests is faster. Regarding compressor outlet temperature the differences between the models are higher as it can be observed in Figure 5.48 and Figure 5.49. The proposed model must predict a more realistic evolution. During tip in load test the increment of the air temperature is lower due to the warm up of the compressor case. The opposite effect happens during tip out load tests. The thermal energy

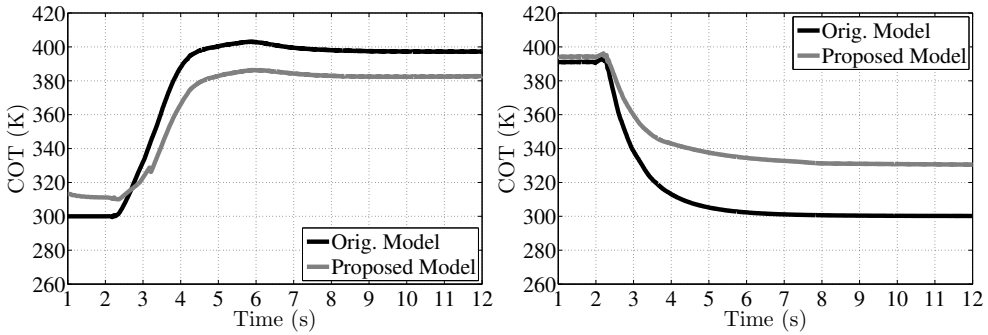


Figure 5.48: Compressor outlet temperature during tip in and tip out tests for T#1 at 1500 rpm

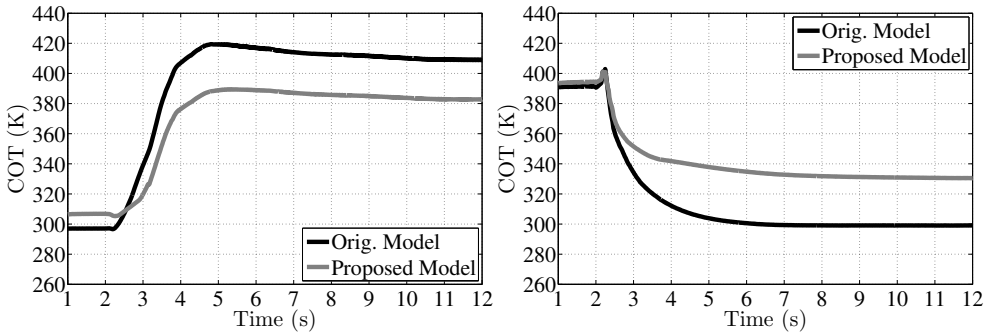


Figure 5.49: Compressor outlet temperature during tip in and tip out tests for T#2 at 1600 rpm

accumulated in the compressor case is released and the cooling down process is also slower.

For the turbine outlet temperature, during the tip in load tests (Figure 5.50 and Figure 5.51), despite of higher turbine inlet temperature, the proposed model provide a lower turbine outlet pressure. High temperature drop is predicted in the turbine due to the mechanical power produced and the heat power transferred.

The opposite effect is predicted during tip out load tests. During the deceleration, the gas receives heat from the turbocharger walls that are hotter due to thermal inertia of the material.

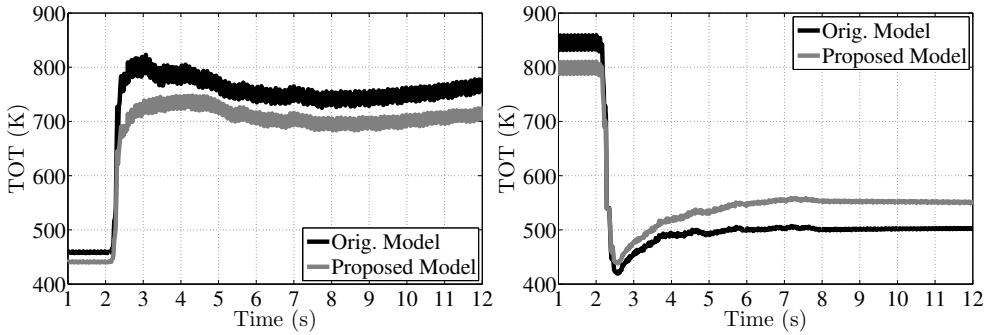


Figure 5.50: Turbine outlet temperature during tip in and tip out tests for T#1 at 1250 rpm

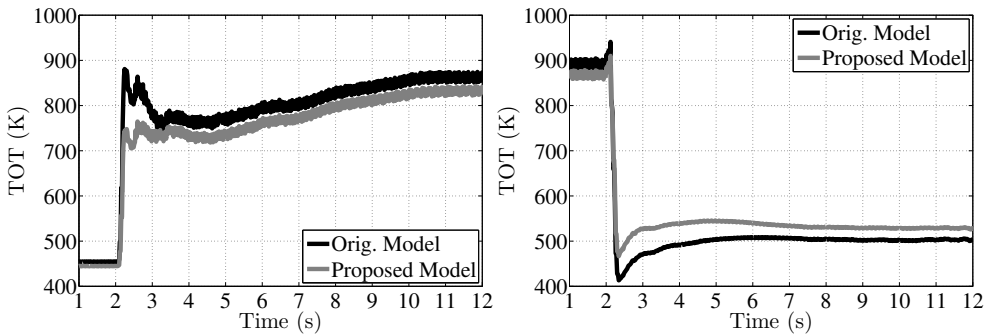


Figure 5.51: Turbine outlet temperature during tip in and tip out tests for T#2 at 2400 rpm

5.5 References

- [2] J. R. Serrano, P. Olmeda, F. Arnau, A. Dombrovsky, and L. Smith. “Analysis and Methodology to Characterize Heat Transfer Phenomena in Automotive Turbochargers”. In: *J. Eng. Gas Turbines Power* 137 (7) (2014). DOI: 10.1115/1.4028261 (cit. on pp. vii, 15, 55, 150, 160, 165).
- [26] Miguel Ángel Reyes-Belmonte. “Contribution to the Experimental Characterization and 1-D Modelling of Turbochargers for IC Engines”. PhD thesis. Universitat Poliècnica de València, 2013 (cit. on pp. 6, 26, 51, 52, 60, 66, 89, 91, 94, 98, 114, 145, 151, 153, 190).
- [47] D. Bohn, N. Moritz, and M. Wolff. “Conjugate Flow and Heat Transfer Investigation of a Turbo Charger: Part II — Experimental Results”. In:

- Proceedings of ASME Turbo Expo*. Vol. 3. ASME, 2003, pp. 723–729. DOI: 10.1115/GT2003-38449 (cit. on pp. 22, 98, 139, 164).
- [62] M. Cormerais, J. F. Hetet, P. Chesse, and A. Malboom. “Heat transfers characterisations in a variable geometry turbocharger: experiments and correlations”. In: *Proceedings of Spring Technical Conference of the ASME Internal Combustion Engine Division* (2006), pp. 53–64 (cit. on pp. 26, 70, 161).
- [63] M. Cormerais, P. Chesse, and J. F. Hetet. “Turbocharger heat transfer modeling under steady and transient conditions”. In: *International Journal of Thermodynamics* 12.4 (2010), pp. 193–202 (cit. on pp. 26, 162).
- [71] N. Baines, K. D. Wygant, and A. Dris. “The Analysis of Heat Transfer in Automotive Turbochargers”. In: *Journal of Engineering for Gas Turbines and Power* 132.4 (2010), p. 042301. DOI: 10.1115/1.3204586 (cit. on pp. 27, 138, 168).
- [89] J. R. Serrano, A. O. Tiseira, L. M. García-Cuevas, L. B. Inhestern, and H. Tartoussi. “Radial Turbine Performance Measurement Under Extreme Off-Design Conditions”. In: *Submitted to Energy* () (cit. on pp. 33, 147, 192).
- [131] C. Cuevas, D. Makaire, and P. Ngendakumana. “Thermo-hydraulic characterization of an automotive intercooler for a low pressure EGR application”. In: *Applied Thermal Engineering* 31.14–15 (2011), pp. 2474–2484. DOI: 10.1016/j.applthermaleng.2011.04.013 (cit. on p. 169).
- [132] M. Canakci. “Combustion characteristics of a DI-HCCI gasoline engine running at different boost pressures”. In: *Fuel* 96 (2012), pp. 546–555. DOI: 10.1016/j.fuel.2012.01.042 (cit. on p. 169).
- [133] J. M. Luján, V. Bermúdez, P. Piqueras, and Óscar García-Afonso. “Experimental assessment of pre-turbo aftertreatment configurations in a single stage turbocharged diesel engine. Part 1: Steady-state operation”. In: *Energy* 80.0 (2015), pp. 599–613. ISSN: 0360-5442. DOI: 10.1016/j.energy.2014.05.048 (cit. on p. 169).
- [134] V. Macián, J. R. Serrano, V. Dolz, and J. Sánchez. “Methodology to design a bottoming Rankine cycle, as a waste energy recovering system in vehicles. Study in a HDD engine”. In: *Applied Energy* 104 (2013), pp. 758–771. ISSN: 0306-2619. DOI: 10.1016/j.apenergy.2012.11.075 (cit. on p. 169).

- [135] J. M. Luján, H. Climent, P. Olmeda, and V. D. Jiménez. “Heat transfer modeling in exhaust systems of high-performance two-stroke engines”. In: *Applied Thermal Engineering* 69.1–2 (2014), pp. 96 –104. ISSN: 1359-4311. DOI: 10.1016/j.applthermaleng.2014.04.045 (cit. on p. 169).
- [136] J. Galindo, J. R. Serrano, H. Climent, and O. Varnier. “Impact of two-stage turbocharging architectures on pumping losses of automotive engines based on an analytical model”. In: *Energy Conversion and Management* 51.10 (2010), pp. 1958 –1969. ISSN: 0196-8904. DOI: 10.1016/j.enconman.2010.02.028 (cit. on p. 170).

Conclusions and Future Works

Contents

6.1	Introduction	190
6.2	Main contributions	190
	Heat transfer modelling	190
	Air flow modelling	192
6.3	Future works	194
	Heat transfer modelling	194
	Air flow modelling	194
6.4	References	195

Figures

6.1 Introduction

In the present thesis turbocharger heat transfer model have been improved compared to the previous works available in the literature as the work done by Reyes [26]. The improvements provide a more simple way of calculating heat transfer properties and the ability to compute the heat transfer with the ambient. Furthermore,

In order to develop the models experimental results from different tests benches at different conditions (hot exposed, adiabatic...) have been used. The models have been developed to be used coupled to 1D codes and have been validated using this type of simulation.

In the validation task the effect of turbocharger heat transfer models on the results provided by the whole engine 1D models have been analysed.

6.2 Main contributions

The main contributions of the thesis can be divided in two major categories heat transfer modelling and air flow modelling. The first category includes generalised heat transfer model, external heat transfer and effects of turbocharger heat transfer modelling on engine 1D modelling. The second category includes the VGT maps extrapolation model and the discharge coefficient prediction.

Heat transfer modelling

Traditionally, heat losses in small turbochargers has not been studied independently and the behaviour of the machine has been predicted by direct use of manufacturer maps. But at low loads, this energy transfer can reach values even higher than mechanical power.

In this thesis a general procedure to determine heat properties of automotive turbochargers is provided. The methodology is based on the usage of experimental information of eight different turbochargers, combining the information of [26] and new measurements. This experimental information includes conductive conductances and capacitances and convective conductances. With these experimental data generic correlations for conductive and convective conductances and capacitances have been obtained.

The turbocharger properties calculated by means of such correlations has been used coupled to a 1D model of a turbocharger test bench for validation. The results of the simulations show much better predictions in turbine outlet temperature compared to the original model without heat transfer modelling. Compressor outlet temperature prediction has been slightly improved, as well. It has been also proved for both variables that the precision of the generic

methodology is similar to the precision given by specific correlations based on empirical data of a given turbocharger.

It must be stated that the described methodology provides a general procedure for heat transfer account in turbochargers. The given correlations can be used on different automotive turbochargers requiring only a limited set of geometrical parameters as entry data. In that way, experimental characterisation of the turbocharger in several test rigs can be avoided without losing precision in compressor and turbine outlet temperature prediction.

This work also presents an external heat transfer model that takes into account radiation and convective phenomena and all the possible heat paths from turbocharger external surfaces. The model uses a simplified geometry, based on cylinders, of the whole turbocharger that is suitable to be used in whole-engine simulation software, requiring easy to obtain geometrical data (detailed turbocharger geometry is not necessary).

The adjusted and validated external heat transfer model has been used to perform an analysis of the different heat flows, showing that the most important external heat fluxes comes from turbine external surface, due to its higher temperature and its big areas. They can lead to be up to a half of turbine enthalpy drop. External heat fluxes at the central housing are negligible compared to the turbine enthalpy drop. In compressor side, external heat flow can be reversed, i.e. it can be lost or absorbed depending on the running conditions. In this side, the most important seems to be the heat radiated by the turbines side but the other paths cannot be neglected.

For validation purposes the heat transfer model has been used in 1D simulations of the turbocharger test bench and of a whole engine. Comparing simulations in standard one dimensional modelling software between traditional look up maps technique and the usage of turbocharger heat transfer model it has been concluded that both offer almost the same prediction for the main turbocharger variables at steady state conditions; except for turbine outlet temperature. Variables such as turbocharger speed or mass flow, present the same level of acceptance in both cases so no heat transfer model is needed if turbine outlet temperature is not a priority and a hot map, measured in similar conditions of the simulations, is available.

However, when the conditions to model are very different from those at which the map was obtained, the error using a look up map method can be considerable even for compressor outlet temperature prediction. In this case, using a heat transfer model, even with an adiabatic map, gives precise results whatever are the temperature conditions. In addition, using heat transfer model with adiabatic maps eventual problems that may arise during the turbocharger modelling task are avoided.

Finally, it has been stated in this work that the differences in turbine outlet temperature are about 25 K, even with moderate temperatures at turbine inlet

(about 600 K). The reason of this overprediction is in the definition of turbine efficiency used in the maps. In measured hot turbine maps it is common using ETE definition. The compressor and not turbine power is used in the numerator of such definition, what does not represent real turbine efficiency (because of mechanical losses).

In engine test bench full load tests for two different turbochargers have been simulated using a commercial 1D software and the results have been compared with the experimental data from an engine test bench. The main findings of this comparison lay in the fact that manufacturer maps in hot conditions are adequate in predicting all variables at engine full loads excepting COT and TOT. This fact shows the actual importance of using a heat transfer model for the turbocharger.

Compressor and turbine outlet temperatures are always well predicted using a heat transfer model without disturbing the prediction of the rest of engine parameters.

Contrary to the general view that heat transfer phenomena occurring in turbochargers are only important at partial loads and transient engine evolutions, in this work, it is shown that full load operating points are also affected by these phenomena. The compressor and turbine outlet temperatures are important variables to be predicted at these operating points. The importance is in inter-cooler design (or combustion process), after-treatment, exhaust energy recovery and two stage turbocharging modelling and design because accurately predicted boundary conditions can be used in each case.

The work also shows that turbo speed prediction is not affected by heat transfer when hot turbocharger maps in which compressor and turbine have been measured at the same time are used. The reason is the cancellation of compressor heat terms in this kind of maps. Only prediction of compressor and turbine outlet temperatures is improved by the heat transfer model, if they are compared to the model based on hot maps.

In partial load the same positive effects in the prediction of outlet temperatures are observed using turbocharger heat transfer model.

Air flow modelling

Regarding air flow modelling a method for extrapolating radial turbine performance in terms of VGT position, rotational speed and blade speed ratio has been developed. In order to fully validate the model, results from a special turbocharger gas stand have been used [89], which provides means for measuring at very high blade to jet speed ratio.

The method uses thirteen calibration coefficients which are fitted using a limited set of available turbine map data. Seven coefficients are fitted independently for the reduced mass flow and six for the efficiency. The reduced mass

flow calibration coefficients must be fitted in the first place since one of them, the quotient between the rotor and the stator discharge coefficients (coefficient 'c'), is used in the efficiency model equation.

The reduced mass flow and the efficiency variables are interrelated since the reduced mass flow appears in the efficiency equation and the efficiency appears in the mass flow equation. As both variables appear implicitly, after fitting the calibration coefficients, a system with the reduced mass flow and the efficiency equations must be solved, using an iterative procedure, for extrapolation purposes.

The model shows good agreement with the experimental data even when it is calibrated with a very limited set of data. Both mass flow and efficiency can be extrapolated beyond typical turbine map measured range in whatever variable, i.e. VGT position, reduced speed and blade to jet speed ratio.

One of the main advantages of the model is that it can be used easily for any radial VGT or FGT (fixed geometry turbine), as the geometrical parameters are easy to measure and the initial conditions and boundaries for the fitting procedure have been stated in the thesis. A good extrapolation is expected for any energy conversion system using radial turbines since model self calibration coefficients do not depend on turbine size and model is based on reduced or non-dimensional parameters for representing turbines performance. It is only necessary to have a standard turbine map measured in almost adiabatic conditions (or adiabaticized) and with at least two VGT positions to fit the necessary coefficients for reduced mass flow and efficiency extrapolation. Nevertheless, the higher the number of available VGT positions the better for the quality of the extrapolation model.

The accuracy of the extrapolation model regarding mass flow parameter is high in the intermediate expansion ratio range. At low expansion ratio the model is still able to reproduce the behaviour of most of the experimental points, even with negative turbine adiabatic efficiencies. The accuracy of the efficiency model is high in the intermediate σ range. At high σ the model curves cross most of the experimental points, mainly at intermediate turbine reduced speeds. Good results for both variables are also obtained when extrapolating turbine reduced speeds. Finally, the prediction of full VGT position maps is also accurate in the whole expansion ratio range.

The main limitation of this approach is that the model has to be calibrated for each turbine using turbocharger manufacturers map data or some operative points tested a priori to get model maximum predictability. Since there are 13 coefficients (7 for mass flow parameter and 6 for efficiency), at least 7 turbine operative points must be available for model self-fitting procedure. The higher the number of points the better the fitting results. If no data are available the predictions of the model will be less accurate but can still be possible by using average values of the proposed model coefficients.

Regarding discharge coefficient determination for two stage turbochargers an experimental methodology has been developed in this work to make possible a proper characterisation. The procedure is used to fit the discharge coefficient of the different valves to mathematical expressions in order to be used in 1D gas dynamic codes. The error in mass flow prediction using this procedure is small if compared with the experimental results.

6.3 Future works

The proposed future works have also been divided in the two categories used in the previous section.

Heat transfer modelling

Further research is needed to improve the resolution of the heat transfer model. For oil coking problem a model that does not neglect radial heat transfer in the housing must be developed. In the current state of the heat transfer model the capability to predict oil coking is limited since only axial heat transfer is considered. Furthermore a parametric study of the effect of each parameter of the model must be carried out. The effect of those parameters on the different turbocharger variables must be evaluated. In that way, the improvement in prediction can be done by improving the estimation of most sensible heat transfer parameters.

Some research is needed to make an improvement in the estimation of conductive conductances of the model using FEM simulation with detailed turbocharger geometry and material properties. In that way the thermohydraulic test bench characterization can be avoided with the reduction of costs.

The combined effect of VGT extrapolation tools and heat transfer model must be assessed in 1D engine simulations. The effect on engine variables such as torque and BSFC can be assessed.

Air flow modelling

One possible future work is to use a CFD approach in a similar way to the proposed in [137] in order to double check the validity of the proposed methods. Furthermore, available experimental off-design measurements can be used for validation.

Another way of improving the extrapolation model is developing a more physical model based on the different losses of the turbine. In that way the number of fitting coefficients can be reduced and less information may be required to fit the model with good precision.

Using similar experimental methodology to the one used for discharge coefficient determination can be used for twin entry turbine characterization. The flow distribution between the two branches of the turbine can be calculated using indirect measurements.

6.4 References

- [26] Miguel Ángel Reyes-Belmonte. “Contribution to the Experimental Characterization and 1-D Modelling of Turbochargers for IC Engines”. PhD thesis. Universitat Politècnica de València, 2013 (cit. on pp. 6, 26, 51, 52, 60, 66, 89, 91, 94, 98, 114, 145, 151, 153, 190).
- [89] J. R. Serrano, A. O. Tiseira, L. M. García-Cuevas, L. B. Inhestern, and H. Tartoussi. “Radial Turbine Performance Measurement Under Extreme Off-Design Conditions”. In: *Submitted to Energy* () (cit. on pp. 33, 147, 192).
- [137] G. Besagni, R. Mereu, P. Chiesa, and F. Inzoli. “An Integrated Lumped Parameter-CFD approach for off-design ejector performance evaluation”. In: *Energy Conversion and Management* 105 (2015), pp. 697 –715. ISSN: 0196-8904. DOI: 10.1016/j.enconman.2015.08.029 (cit. on p. 194).

Bibliography

- [1] **Payri, F., Olmeda, P., Arnau, F., Dombrovsky, A., and Smith, L.**
“External heat losses in small turbochargers: Model and experiments”
in: *Energy* 71 (2014), pp. 534–546. ISSN: 0360-5442. DOI: 10.1016/j.energy.2014.04.096 (cit. on pp. vii, 27, 60)
- [2] **Serrano, J. R., Olmeda, P., Arnau, F., Dombrovsky, A., and Smith, L.**
“Analysis and Methodology to Characterize Heat Transfer Phenomena in Automotive Turbochargers”
in: *J. Eng. Gas Turbines Power* 137 (7) (2014). DOI: 10.1115/1.4028261 (cit. on pp. vii, 15, 55, 150, 160, 165)
- [3] **Serrano, J. R., Olmeda, P., Arnau, F. J., Dombrovsky, A., and Smith, L.**
“Methodology to Characterize Heat Transfer Phenomena in Small Automotive Turbochargers: Experiments and Modelling Based Analysis”
in: *Proceedings of ASME Turbo Expo 2014* 2014 (cit. on pp. vii, 91)
- [4] **Serrano, J. R., Olmeda, P., Arnau, F. J., Dombrovsky, A., and Smith, L.**
“Turbocharger heat transfer and mechanical losses influence in predicting engines performance by using one-dimensional simulation codes”
in: *Energy* 86 (2015), pp. 204–218. DOI: 10.1016/j.energy.2015.03.130 (cit. on p. vii)
- [5] **Serrano, J. R., Arnau, F. J., García-Cuevas, L. M., Dombrovsky, A., and Tartoussi, H.**
“Development and validation of a radial turbine efficiency and mass flow model at design and off-design conditions”
in: *Energy Conversion and Management* 128 (2016), pp. 281–293. DOI: 10.1016/j.enconman.2016.09.032 (cit. on p. vii)

- [6] **Serrano, J., Olmeda, P., Arnau, F., and Dombrovsky, A.**
“General Procedure for the Determination of Heat Transfer Properties in Small Automotive Turbochargers”
in: *SAE Int. J. Engines* 8.1 (2015). DOI: 10.4271/2014-01-2857
(cit. on p. vii)
- [7] **Desantes, J. M., Galindo, J., Serrano, J. R., and Dombrovsky, A.**
“A comprehensive experimental procedure for turbochargers performance characterization”
in: *International Turbocharging Seminar* 2015 (cit. on p. vii)
- [8] **Sullivan, A., Brown, D., Eastwood, M., Green, J., Dombrovsky, A., and Arnau, F.**
“Development of a high temperature turbocharger for heavy duty applications”
in: *IMEchE International Conference on Turbochargers and Turbocharging* 2016 (cit. on p. viii)
- [9] **Suzuki, T.**
Romance of engines
ed. by Warrendale: Society of Automotive Engineers. Society of Automotive Engineers 1997 (cit. on p. 2)
- [10] **Sperling, D. and Gordon, D.**
Two Billion Cars: Driving Toward Sustainability
ed. by Oxford University Press. Oxford University Press 2009 (cit. on p. 2)
- [11] **Sturgeon, T., Van Biesebroeck, J., and Gereffi, G.**
“Value chains, networks and clusters: reframing the global automotive industry”
in: *Journal of Economic Geography* 8 (2008), pp. 297–321 (cit. on p. 2)
- [12] **World Energy Council**
Global Transport Scenarios 2050
tech. rep. WEC London 2011 (cit. on p. 2)
- [13] **Hartman, J.**
Turbocharging Performance Handbook
ed. by Motorbooks. Motorbooks 2007 (cit. on p. 3)
- [14] **Official Journal of the European Union**
REGULATION (EC) No 715/2007 OF THE EUROPEAN PARLIAMENT AND OF THE COUNCIL of 20 June 2007 on type approval of motor vehicles with respect to emissions from light passenger and commercial vehicles (Euro 5 and Euro 6) and on access to vehicle repair and mainte-

- nance information*
2007 (cit. on p. 4)
- [15] **Omer, A. M.**
“Energy, environment and sustainable development”
in: *Renewable and Sustainable Energy Reviews* 12.9 (2008), pp. 2265–2300. DOI: 10.1016/j.rser.2007.05.001 (cit. on p. 4)
- [16] **Turner, J., Popplewell, A., Patel, R., Johnson, T. et al.**
“Ultra Boost for Economy: Extending the Limits of Extreme Engine Downsizing”
in: *SAE Int. J. Engines* 7.1 (2014). DOI: 10.4271/2014-01-1185 (cit. on p. 4)
- [17] **Baines, N.**
Intake Boosting
Encyclopedia of Automotive Engineering. John Wiley & Sons, Ltd. 2014. DOI: 10.1002/9781118354179.auto126 (cit. on p. 5)
- [18] **Padzillah, M., Rajoo, S., and Martinez-Botas, R.**
“Influence of speed and frequency towards the automotive turbocharger turbine performance under pulsating flow conditions”
in: *Energy Conversion and Management* 80 (2014), pp. 416–428. DOI: 10.1016/j.enconman.2014.01.047 (cit. on pp. 5, 35)
- [19] **Burke, R., Vagg, C., Chalet, D., and Chesse, P.**
“Heat transfer in turbocharger turbines under steady, pulsating and transient conditions”
in: *International Journal of Heat and Fluid Flow* 52 (2015), pp. 185–197. DOI: 10.1016/j.ijheatfluidflow.2015.01.004 (cit. on pp. 5, 31)
- [20] **Chiong, M., Rajoo, S., Martinez-Botas, R., and Costall, A.**
“Engine turbocharger performance prediction: One-dimensional modeling of a twin entry turbine”
in: *Energy Conversion and Management* 57 (2012), pp. 68–78. DOI: 10.1016/j.enconman.2011.12.001 (cit. on p. 5)
- [21] **Barratta, M. and Spessa, E.**
Numerical Simulation Techniques for the Prediction of Fluid-Dynamics, Combustion and Performance in IC Engines Fuelled by CNG
Computational Simulations and Applications, InTech, Dr. Zhu Jianping (Ed.) 2011. DOI: 10.5772/25081 (cit. on pp. 5, 15)
- [22] **Andrés Omar Tiseira**
“Caracterización experimental y modelado de bombeo en compresores centrífugos de sobrealimentación”
PhD thesis. Universitat Poliècnica de València 2008 (cit. on p. 5)

- [23] **Carmen Cervelló Romero**
“Contribución a la caracterización experimental y al modelado de turbinas de geometría variable en grupos de sobrealimentación”
PhD thesis. Universitat Poliècnica de València 2004 (cit. on p. 5)
- [24] **Fajardo, P.**
“Methodology for the Numerical Characterization of a Radial Turbine under Steady and Pulsating Flow”
PhD thesis. Universitat Poliècnica de València 2012 (cit. on p. 5)
- [25] **Navarro, R.**
“A numerical approach for predicting flow-induced acoustics at near-stall conditions in an automotive turbocharger compressor”
PhD thesis. Universitat Poliècnica de València 2014 (cit. on p. 5)
- [26] **Miguel Ángel Reyes-Belmonte**
“Contribution to the Experimental Characterization and 1-D Modelling of Turbochargers for IC Engines”
PhD thesis. Universitat Poliècnica de València 2013
(cit. on pp. 6, 26, 51, 52, 60, 66, 89, 91, 94, 98, 114, 145, 151, 153, 190)
- [27] **Luis Miguel García-Cuevas González**
“Experiments and Modelling of Automotive Turbochargers under Unsteady Conditions”
PhD thesis. Universitat Poliècnica de València 2014
(cit. on pp. 6, 62, 113, 114, 118)
- [28] **Serrano, J., Olmeda, P., Páez, A., and Vidal, F.**
“An experimental procedure to determine heat transfer properties of turbochargers”
in: *Measurement Science and Technology* 21.3 (2010). DOI: 10.1088/0957-0233/21/3/035109 (cit. on pp. 7, 27, 52, 54, 89)
- [29] **Serrano, J. R., Olmeda, P., Tiseira, A., García-Cuevas, L. M., and Lefebvre, A.**
“Theoretical and experimental study of mechanical losses in automotive turbochargers”
in: *Energy* 55 (2013), pp. 888–898. DOI: 10.1016/j.energy.2013.04.042 (cit. on pp. 8, 27)
- [30] **Watson, N. and Janota, M.**
Turbocharging the Internal Combustion Engine
Macmillan Publishers, Ltd. 1982
(cit. on pp. 15, 18, 32, 113, 122, 123)

- [31] **Bohbot, J., Chryssakis, C., and Miche, M.**
“Simulation of a 4-Cylinder Turbocharged Gasoline Direct Injection Engine Using a Direct Temporal Coupling Between a 1D Simulation Software and a 3D Combustion Code”
in: *SAE Technical Paper 2006-01-3263* (2006) (cit. on p. 15)
- [32] **Vítek, O., Macek, J., and Polášek, M.**
“New Approach to Turbocharger Optimization using 1-D Simulation Tools”
in: *SAE Technical Paper 2006-01-0438* (2006) (cit. on p. 15)
- [33] **Jung, M., Ford, R. G., Glover, K., Collings, N., Christen, U., and Watts, M. J.**
“Parameterization and Transient Validation of a Variable Geometry Turbocharger for Mean-Value Modeling at Low and Medium Speed-Load Points”
in: *SAE Technical Paper 2002-01-2729* (2002) (cit. on p. 15)
- [34] **Shah, P. and Tan, C.**
“Effect of Blade Passage Surface Heat Extraction on Axial Compressor Performance”
in: *Journal of Turbomachinery* 129 (2007) (cit. on p. 15)
- [35] **Westin, F., Rosenqvist, J., and Ångström, H.-E.**
“Heat Losses from the Turbine of a Turbocharged SI-Engine - Measurements and Simulation”
in: *SAE Technical Paper* (2004) (cit. on p. 16)
- [36] **Sirakov, B. and Casey, M.**
“Evaluation of Heat Transfer Effects on Turbocharger Performance”
in: *ASME Journal of Turbomachinery* 135.2 (2012), p. 021011. DOI: 10.1115/1.4006608 (cit. on p. 16)
- [37] **Romagnoli, A. and Martinez-Botas, R.**
“Heat transfer analysis in a turbocharger turbine: An experimental and computational evaluation”
in: *Applied Thermal Engineering* 38 (2012), pp. 58–77. DOI: 10.1016/j.applthermaleng.2011.12.022 (cit. on pp. 16, 17, 24)
- [38] **Aghaali, H., Ångström, H.-E., and Serrano, J. R.**
“Evaluation of different heat transfer conditions on an automotive turbocharger”
in: *International Journal of Engine Research* 16.2 (2015), pp. 137–151. DOI: 10.1177/1468087414524755 (cit. on pp. 16, 25)

- [39] **Casey, M. V. and Fesich, T. M.**
“The Efficiency of Turbocharger Compressors With Diabatic Flows”
in: *Journal of Engineering for Gas Turbines and Power* 132 (7) (2012),
p. 072302. DOI: 10.1115/1.4000300 (cit. on pp. 16, 17)
- [40] **Shaaban, S. and Seume, J.**
“Analysis of Turbocharger Non-Adiabatic Performance”
in: *8th International Conference on Turbochargers and Turbocharging*.
Woodhead Publishing 2006. ISBN: 978-1-84569-174-5 (cit. on p. 18)
- [41] **Diango, A., Perilhon, C., Descombes, G., and Danho, E.**
“Application of exergy balances for the optimization of non-adiabatic
small turbomachines operation”
in: *Energy* 36 (2011) (cit. on p. 18)
- [42] **Diango, A., Perilhon, C., Danho, E., and Descombes, G.**
“Influence of Heat Transfer on Gas Turbine Performance”
in: *Advances in Gas Turbine Technology* (2011) (cit. on p. 18)
- [43] **Serrano, J. R., Olmeda, P., Arnau, F., Reyes-Belmonte, M., and
Lefebvre, A.**
“Importance of Heat Transfer Phenomena in Small Turbochargers for
Passenger Car Applications”
in: *SAE Int. J. Engines* 6.2 (2013), pp. 716–728. DOI: 10.4271/2013-01-
0576 (cit. on p. 19)
- [44] **Sidorow, A., Isermann, R., Cianflone, F., and Landsmann, G.**
“Comparison of a turbocharger model based on isentropic efficiency maps
with a parametric approach based on Euler’s turbo-machinery equation”
in: *18th IFAC World Congress* 2011 (cit. on pp. 20, 21)
- [45] **Lückmann, D., Schernus, C., Uhlmann, T., Höpke, B., and Nebbia,
C.**
“Friction and Heat Transfer Effects on Turbocharger Modeling”
in: *GT 2012 Conference* 2012 (cit. on p. 20)
- [46] **Porzig, D., Raetz, H., Schwarze, H., and Seume, J.**
“Thermal analysis of small high-speed floating-ring journal bearings”
in: *11th International Conference on Turbochargers and Turbocharging*.
Woodhead Publishing 2014. ISBN: 978-0-08-100033-5 (cit. on p. 22)
- [47] **Bohn, D., Moritz, N., and Wolff, M.**
“Conjugate Flow and Heat Transfer Investigation of a Turbo Charger:
Part II — Experimental Results”
in: *Proceedings of ASME Turbo Expo*. Vol. 3. ASME 2003, pp. 723–729.
DOI: 10.1115/GT2003-38449 (cit. on pp. 22, 98, 139, 164)

- [48] **Lüddecke, B., Filsinger, D., and Bargende, M.**
“On wide mapping of a mixed flow turbine with regard to compressor heat flows during turbocharger testing”
in: *10th International Conference on Turbochargers and Turbocharging*. Woodhead Publishing 2012. ISBN: 978-0-85709-209-0
(cit. on pp. 22, 25)
- [49] **Marelli, S., Marmorato, G., Capobianco, M., and Rinaldi, A.**
“Heat Transfer Effects on Performance Map of a Turbocharger Compressor for Automotive Application”
in: *SAE Technical Paper 2015-01-1287* (2015) (cit. on p. 22)
- [50] **Schinnerl, M., Seume, J., Ehrhard, J., and Bogner, M.**
“Heat Transfer Correction Methods for Turbocharger Performance Measurements”
in: *Proceedings of ASME Turbo Expo* 2016 (cit. on pp. 22–24)
- [51] **Muqem, M., Ahmad, M., and Sherwani, A.**
“Turbocharging of Diesel Engine for Improving Performance and Exhaust Emissions A Review”
in: *IOSR Journal of Mechanical and Civil Engineering* (2015)
(cit. on p. 23)
- [52] **Shaaban, S. and Seume, J.**
“Impact of Turbocharger Non-Adiabatic Operation on Engine Volumetric Efficiency and Turbo Lag”
in: *International Journal of Rotating Machinery* (2012) (cit. on p. 24)
- [53] **Cormerais, M., Hetet, J. F., Chesse, P., and Maiboom, A.**
“Heat Transfer Analysis in a Turbocharger Compressor Modeling and Experiments”
in: *SAE Technical Paper* (2006) (cit. on p. 24)
- [54] **Romagnoli, A. and Martinez-Botas, R.**
“Heat Transfer in an Automotive Turbocharger Under Constant Load Points: an Experimental and Computational Investigation”
in: *The 4th International Symposium on Fluid Machinery and Fluid Engineering* November 24-27, 2008, Beijing, China (2008)
(cit. on pp. 24, 30)
- [55] **Aghaali, H. and Ångström, H.-E.**
“Temperature Estimation of Turbocharger Working Fluids and Walls under Different Engine Loads and Heat Transfer Conditions”
in: *SAE Technical Paper 2013-24-0123* (2013). DOI: 710.4271/2013-24-0123
(cit. on pp. 24, 25, 30)

- [56] **Bohn, D., Heuer, T., and Kusterer, K.**
“Conjugate Flow and Heat Transfer Investigation of a Turbo Charger”
in: *J. Eng. Gas Turbines Power* 127 (2005) (cit. on p. 25)
- [57] **Bohn, D., Heuer, T., and Kusterer, K.**
“Conjugate Flow and Heat Transfer Investigation of a Turbo Charger:
Part I — Numerical Results”
in: *Proceedings of ASME Turbo Expo*. ASME 2003. DOI: 10.1115/GT2003-38449 (cit. on p. 25)
- [58] **Burke, R. D., Copeland, C., Duda, T., and Reyes-Belmonte, M. A.**
“Lumped Capacitance and 3D CFD Conjugate Heat Transfer Modelling
of an Automotive Turbocharger”
in: *Proceedings of ASME Turbo Expo* 2015 (cit. on p. 25)
- [59] **Aghaali, H.**
“On-Engine Turbocharger Performance Considering Heat Transfer”
PhD thesis. Royal Institute of Technology 2012 (cit. on p. 25)
- [60] **Aghaali, H. and Ångström, H.-E.**
“Improving Turbocharged Engine Simulation by Including Heat Transfer
in the Turbocharger”
in: *SAE Technical Paper 2012-01-0703* (2012) (cit. on p. 25)
- [61] **Shaaban, S., Seume, J., Berndt, R., Pucher, H., and Linnhoff, H.**
“Part-load Performance Prediction of Turbocharged Engines”
in: *8th International Conference on Turbochargers and Turbocharging*.
Woodhead Publishing 2006. ISBN: 978-1-84569-174-5 (cit. on p. 25)
- [62] **Cormerais, M., Hetet, J. F., Chesse, P., and Malboom, A.**
“Heat transfers characterisations in a variable geometry turbocharger:
experiments and correlations”
in: *Proceedings of Spring Technical Conference of the ASME Internal
Combustion Engine Division* (2006), pp. 53 –64
(cit. on pp. 26, 70, 161)
- [63] **Cormerais, M., Chesse, P., and Hetet, J. F.**
“Turbocharger heat transfer modeling under steady and transient condi-
tions”
in: *International Journal of Thermodynamics* 12.4 (2010), pp. 193 –202
(cit. on pp. 26, 162)
- [64] **Serrano, J., Arnau, F., Novella, R., and Reyes-Belmonte, M.**
“A Procedure to Achieve 1D Predictive Modeling of Turbochargers under
Hot and Pulsating Flow Conditions at the Turbine Inlet”
in: *SAE Technical Paper 2014-01-1080* (2014) (cit. on p. 26)

- [65] **Incropera, F., DeWitt, D., Bergman, T., and Lavine, A.**
Fundamentals of Heat and Mass Transfer
John Wiley & Sons 2007 (cit. on pp. 26, 98, 101, 110)
- [66] **Serrano, J. R., Olmeda, P., Arnau, F. J., Reyes-Belmonte, M. A., and Tartoussi, H.**
“A study on the internal convection in small turbochargers. Proposal of heat transfer convective coefficients”
in: *Applied Thermal Engineering* 89 (2015), pp. 587 –599. ISSN: 1359-4311 (cit. on pp. 26, 91)
- [67] **Lavagnoli, S., Paniagua, G., Maesschalck, C. D., and Yasa, T.**
“Analysis of the Unsteady Overtip Casing Heat Transfer in a High Speed Turbine”
in: *Journal of Turbomachinery* (2013) (cit. on p. 26)
- [68] **Burke, R. D., Olmeda, P., Arnau, F. J., and Reyes-Belmonte, M. A.**
“Modelling of turbocharger heat transfer under stationary and transient engine operating conditions”
in: *11th International Conference on Turbochargers and Turbocharging* 2014 (cit. on p. 26)
- [69] **Olmeda, P., Dolz, V., Arnau, F., and Reyes-Belmonte, M.**
“Determination of heat flows inside turbochargers by means of a one dimensional lumped model”
in: *Mathematical and Computer Modelling* 57.7 - 8 (2013), pp. 1847 – 1852. ISSN: 0895-7177. DOI: 10.1016/j.mcm.2011.11.078 (cit. on pp. 26, 91)
- [70] **Olmeda, P., Tiseira, A., Dolz, V., and García-Cuevas, L.**
“Uncertainties in power computations in a turbocharger test bench”
in: *Measurement* 59.0 (2015), pp. 363 –371. ISSN: 0263-2241. DOI: 10.1016/j.measurement.2014.09.055 (cit. on p. 27)
- [71] **Baines, N., Wygant, K. D., and Dris, A.**
“The Analysis of Heat Transfer in Automotive Turbochargers”
in: *Journal of Engineering for Gas Turbines and Power* 132.4 (2010), p. 042301. DOI: 10.1115/1.3204586 (cit. on pp. 27, 138, 168)
- [72] **Shaaban, S.**
“Experimental Investigation and Extended Simulation of Turbocharger non-adiabatic performance”
PhD thesis. Universität Hannover 2004 (cit. on p. 27)

- [73] **Burke, R. D.**
“Analysis and Modeling of the Transient Thermal Behavior of Automotive Turbochargers”
in: *J. Eng. Gas Turbines Power* 136 (2014) (cit. on p. 27)
- [74] **Tadesse, H., Rakut, C., Diefenthal, M., Wirsum, M., and Heuer, T.**
“Experimental Investigation of Steady State and Transient Heat Transfer in a Radial Turbine Wheel of a Turbocharger”
in: *Proceedings of ASME Turbo Expo* 2015 (cit. on pp. 27, 28)
- [75] **Mohd, I. A., Rajoo, S., and Darus, A. N.**
“Heat Distribution Study on Turbocharger Turbine’s Volute”
in: *Jurnal Mekanikal* 35 (2012), pp. 63–81 (cit. on p. 28)
- [76] **Hellstrom, F. and Fuchs, L.**
“Heat transfer effects on the performance of a radial turbine working under pulsatile flow conditions”
in: *48th AIAA Aerospace Sciences Meeting* (2010) (cit. on p. 28)
- [77] **Bet, F. and Seider, G.**
“Thermal Management of a Turbocharger for Unsteady Operation”
in: *STAR European Conference Noordwijk, March 22- 23* 2011 (cit. on p. 29)
- [78] **Diefenthal, M., Tadesse, H., Rakut, C., Wirsum, M., and Heuer, T.**
“Experimental and Numerical Investigation of Temperature Fields in a Radial Turbine Wheel”
in: *Proceedings of ASME Turbo Expo* 2014 (cit. on p. 29)
- [79] **Diefenthal, M., Rakut, C., Tadesse, H., and Wirsum, M.**
“Temperature Distribution in a Radial Turbine Wheel During Transient Operation”
in: *MTZ worldwide* 76.9 (2015), pp. 50–55. ISSN: 2192-9114 (cit. on p. 29)
- [80] **Gu, L., Zemp, A., and Abhari, R. S.**
“Numerical study of the heat transfer effect on a centrifugal compressor performance”
in: *Proc IMechE Part C: Journal Mechanical Engineering Science* 229.12 (2015), pp. 2207–2220 (cit. on p. 29)
- [81] **Heuer, T., Engels, B., and Wollscheid, P.**
“Thermomechanical Analysis of a Turbocharger Based on Conjugate Heat Transfer”
in: *Proceedings of ASME Turbo Expo* 2005 (cit. on pp. 29, 30)

- [82] **Verstraete, T., Alsalihi, Z., and Braembussche, R. A. V. den**
“Numerical Study of the Heat Transfer in Micro Gas Turbines”
in: *Journal of Turbomachinery* 129 (2007) (cit. on p. 29)
- [83] **Yamagata, A., Nagai, S., Nakano, K., and Kawakubo, T.**
“Prediction and measurement of Turbocharger compressor wheel temperature”
in: *8th International Conference on Turbochargers and Turbocharging*.
Woodhead Publishing 2006. ISBN: 978-1-84569-174-5 (cit. on p. 30)
- [84] **Chesse, P., Chalet, D., and Tauzia, X.**
“Impact of the heat transfer on the performance calculations of automotive turbocharger compressor”
in: *Oil & Gas Science and Technology Rev. IFP Energies nouvelles* 66.5 (2011), pp. 791–800. DOI: 10.2516/ogst/2011129 (cit. on p. 30)
- [85] **Burke, R. D., Copeland, C. D., and Duda, T.**
“Investigation into the assumptions for lumped capacitance modelling of turbocharger heat transfer”
in: *6th International conference on simulation and testing 2014-05-15 - 2014-05-16, Berlin* 2014 (cit. on pp. 31, 32)
- [86] **Moustapha, H., Zelesky, M., Baines, N., and Japikse, D**
Axial and radial turbines
Concepts NREC, Vermont 2003 (cit. on pp. 32, 113)
- [87] **Hiereth, H., Drexl, K., and Prenninger, P**
Charging the internal combustion engine
Springer 2007 (cit. on pp. 32, 113)
- [88] **Martin, G., Caillol, P. H. C., and Talon, V.**
“Implementing turbomachinery physics into data map-based turbocharger models”
in: *SAE technical paper 2009-01-0310* (2009) (cit. on p. 32)
- [89] **Serrano, J. R., Tiseira, A. O., García-Cuevas, L. M., Inhestern, L. B., and Tartoussi, H.**
“Radial Turbine Performance Measurement Under Extreme Off-Design Conditions”
in: *Submitted to Energy* () (cit. on pp. 33, 147, 192)
- [90] **Galindo, J., Serrano, J. R., Guardiola, C., and Cervelló, C.**
“Surge limit definition in a specific test bench for the characterization of automotive turbochargers”
in: *Experimental Thermal and Fluid Science* 30.5 (2006), pp. 449–462.
ISSN: 0894-1777. DOI: 10.1016/j.expthermflusci.2005.06.002
(cit. on p. 33)

- [91] **Romagnoli, A. and Martinez-Botas, R.**
“Performance prediction of a nozzled and nozzleless mixed-flow turbine in steady conditions”
in: *International Journal of Mechanical Sciences* 53.8 (2011), pp. 557–574. ISSN: 0020-7403. DOI: 10.1016/j.ijmecsci.2011.05.003
(cit. on p. 33)
- [92] **Baines, N.**
“A meanline prediction method for radial turbine efficiency”
in: *In: 6th International conference on turbocharging and air management systems. Proc. IMechE* C554-6 (1998), pp. 315–325 (cit. on p. 33)
- [93] **Dambach, R. and Hodson, H.**
“Tip leakage flow: a comparison between small axial and radial turbines”
in: *IMechE Sym S* 767 (2000) (cit. on p. 33)
- [94] **Payri, F., Serrano, J. R., Fajardo, P., Reyes-Belmonte, M. A., and Gozalbo-Belles, R.**
“A physically based methodology to extrapolate performance maps of radial turbines”
in: *Energy Conversion and Management* 55.0 (2012), pp. 149–163. ISSN: 0196-8904 (cit. on pp. 33, 113, 116, 118, 119, 121, 123)
- [95] **Eriksson, L.**
“Modeling and control of turbocharged SI and DI engines”
in: *Oil Gas Sci Technology-Revue de l'IFP* 62(4) (2007), pp. 523–538
(cit. on p. 33)
- [96] **Canova, M.**
“Development and validation of a control-oriented library for the simulation of automotive engines”
in: *Int J Engine Res* 5(3) (2004), pp. 219–228 (cit. on p. 33)
- [97] **Fang, X. and Dai, Q.**
“Modeling of turbine mass flow rate performances using the Taylor expansion”
in: *Applied Thermal Engineering* 30.13 (2010), pp. 1824–1831. ISSN: 1359-4311. DOI: 10.1016/j.applthermaleng.2010.04.016
(cit. on p. 33)
- [98] **Bozza, F. and Bellis, V. D.**
“Steady Modeling of a Turbocharger Turbine for Automotive Engines”
in: *J. Eng. Gas Turbines Power* 136 (2014) (cit. on p. 34)
- [99] **Sieros, G., Stamatis, A., and Mathioudakis, K.**
“Jet Engine Component Maps for Performance Modeling and Diagnosis”
in: *Journal of Propulsion and Power* 13.5 (1997) (cit. on p. 34)

- [100] **Zhugue, W., Zhang, Y., Zheng, X., Yang, M., and He, Y.**
“Zhugue W.-Development of an advanced turbocharger simulation method for cycle simulation of turbocharged internal combustion engines”
in: *Proc. IMechE Part D: J. Automobile Engineering* 223 (2009)
(cit. on p. 34)
- [101] **Zhu, S., Deng, K., and Liu, S.**
“Modeling and extrapolating mass flow characteristics of a radial turbocharger turbine”
in: *Energy* 87 (2015), pp. 628 –637. ISSN: 0360-5442. DOI: 10.1016/j.energy.2015.05.032
(cit. on p. 34)
- [102] **Baines, N.**
“Radial Turbines: An Integrated Design Approach”
in: *Proceedings of the 6th European Turbomachinery Conference, Lille, France 2005*
(cit. on p. 34)
- [103] **Chiong, M., Rajoo, S., Romagnoli, A., Costall, A., and Martinez-Botas, R.**
“Integration of meanline and one-dimensional methods for prediction of pulsating performance of a turbocharger turbine”
in: *Energy Conversion and Management* 81 (2014), pp. 270 –281. ISSN: 0196-8904. DOI: 10.1016/j.enconman.2014.01.043
(cit. on pp. 34, 35)
- [104] **Chiong, M., Rajoo, S., Romagnoli, A., Costall, A., and Martinez-Botas, R.**
“Non-adiabatic pressure loss boundary condition for modelling turbocharger turbine pulsating flow”
in: *Energy Conversion and Management* 93 (2015), pp. 267 –281. ISSN: 0196-8904. DOI: 10.1016/j.enconman.2014.12.058
(cit. on p. 34)
- [105] **Macek, J., Zak, Z., and Vitek, O.**
“Physical Model of a Twin-scroll Turbine with Unsteady Flow”
in: *SAE Technical Paper 2015-01-1718* (2015). DOI: 10.4271/2015-01-1718
(cit. on p. 34)
- [106] **Gugau, M. and Roclawski, H.**
“On the Design and Matching of Turbocharger Single Scroll Turbines for Pass Car Gasoline Engines”
in: *J. Eng. Gas Turbines Power* 136.12 (2014). DOI: 10.1115/1.4027710
(cit. on p. 35)
- [107] **Palfreyman, D. and Martinez-Botas, R.**
“The pulsating flow field in a mixed flow turbocharger turbine: an experimental and computational study”

- in: *Proceedings of the ASME Turbo Expo 2004* (2004), pp. 697–708
(cit. on p. 35)
- [108] **Avola, C., Copeland, C., Duda, T., Burke, R., Akehurst, S., and Brace, C.**
“Review of Turbocharger Mapping and 1D Modelling Inaccuracies with Specific Focus on Two-Stag Systems”
in: *SAE Technical Paper 2015-24-2523* (2015) (cit. on p. 35)
- [109] **Weber, O., Christmann, R., Gauckler, V., and Sauerstein, R.**
“R2S™ - modelling and consequences for the boost control”
in: *10th International Conference on Turbochargers and Turbocharging*.
Woodhead Publishing 2012 (cit. on pp. 35, 36)
- [110] **Heywood, J. B.**
Internal Combustion Engines Fundamentals
McGraw-Hill 1988 (cit. on p. 35)
- [111] **Douglas, J. F., Gasiorek, J. M., and Swaffield, J. A.**
Fluid Mechanics
Pearson Education Limited. 2005 (cit. on p. 36)
- [112] **Halder, M., Dash, S., and Som, S.**
“A numerical and experimental investigation on the coefficients of discharge and the spray cone angle of a solid cone swirl nozzle”
in: *Experimental Thermal and Fluid Science* 28.4 (2004), pp. 297–305.
ISSN: 0894-1777 (cit. on p. 36)
- [113] **Huang, S., Ma, T., Wang, D., and Lin, Z.**
“Study on discharge coefficient of perforated orifices as a new kind of flowmeter”
in: *Experimental Thermal and Fluid Science* 46 (2013), pp. 74–83
(cit. on p. 37)
- [114] **Serrano, J., Olmeda, P., Tiseira, A., García-Cuevas, L., and Lefebvre, A.**
“Importance of Mechanical Losses Modeling in the Performance Prediction of Radial Turbochargers under Pulsating Flow Conditions”
in: *SAE Int. J. Engines* 6.2 (2013), pp. 729–738. DOI: 10.4271/2013-01-0577
(cit. on p. 55)
- [115] **Society of Automotive Engineers**
“Supercharger Testing Standard”
in: *SAE SAE J1723* (1995) (cit. on p. 55)
- [116] **Society of Automotive Engineers Inc**
“Turbocharger Gas Stand Test Code”
in: *SAE SAE J1826* (1995) (cit. on p. 55)

- [117] **Joint Committee for Guides in Metrology**
Evaluation of measurement data – Guide to the expression of uncertainty in measurement
ed. by JCGM. JCGM 2008 (cit. on p. 58)
- [118] **Payri, F., Serrano, J. R., Olmeda, P., Páez, A., and Vidal, F.**
“Experimental Methodology to Characterize Mechanical Losses in Small Turbochargers”
in: *Proceedings of ASME Turbo Expo* 2010 (cit. on pp. 62, 77)
- [119] **Payri, F., Torregrosa, A. J., Broatch, A., and Brunel, J.**
“Pressure loss characterisation of perforated ducts”
in: *SAE Technical Paper 980282* (1998). DOI: 10.4271/980282
(cit. on p. 80)
- [120] **Payri, F., Olmeda, P., Martín, J., and García, A.**
“A complete 0D thermodynamic predictive model for direct injection diesel engines”
in: *Applied Energy* 88.12 (2011), pp. 4632–4641. ISSN: 0306-2619. DOI: 10.1016/j.apenergy.2011.06.005 (cit. on p. 80)
- [121] **Payri, F., Molina, S., Martín, J., and Armas, O.**
“Influence of measurement errors and estimated parameters on combustion diagnosis”
in: *Applied Thermal Engineering* 26.2 - 3 (2006), pp. 226–236. DOI: 10.1016/j.applthermaleng.2005.05.006 (cit. on p. 80)
- [122] **Benajes, J., Olmeda, P., Martín, J., and Carreno, R.**
“A new methodology for uncertainties characterization in combustion diagnosis and thermodynamic modelling”
in: *Applied Thermal Engineering* 71.1 (2014), pp. 389–399. ISSN: 1359-4311. DOI: 10.1016/j.applthermaleng.2014.07.010 (cit. on p. 80)
- [123] **Bornside, D. and Brown, R.**
“View factor between differing-diameter, coaxial disks blocked by a coaxial cylinder”
in: *J. Thermophys. Heat Transfer* 4.3 (1990), pp. 414–416
(cit. on p. 100)
- [124] **Sparrow, E., Miller, G., and Jonsson, V.**
“Radiative effectiveness of annular- finned space radiators, including mutual irradiation between radiator elements”
in: *J. Aerospace Sci.* 29.11 (1962), pp. 1291–1299 (cit. on p. 100)
- [125] **Shukla, K. and Ghosh, D.**
“Radiation configuration factors for concentric cylinder bodies”
in: *Indian J. Technology* 23 (1985), pp. 244–246 (cit. on p. 101)

- [126] **Churchill, S. W. and Chu, H. H.**
“Correlating equations for laminar and turbulent free convection from a horizontal cylinder”
in: *International Journal of Heat and Mass Transfer* 18.9 (1975), pp. 1049–1053. ISSN: 0017-9310. DOI: 10.1016/0017-9310(75)90222-7. URL: <http://www.sciencedirect.com/science/article/pii/0017931075902227> (cit. on p. 106)
- [127] **Churchill, S. W. and Bernstein, M.**
“A Correlating Equation for Forced Convection From Gases and Liquids to a Circular Cylinder in Crossflow”
in: *Journal of Heat Transfer* 99.2 (1977), pp. 300–306. DOI: 10.1115/1.3450685 (cit. on p. 107)
- [128] **Torregrosa, A., Arnau, F., Piqueras, P., Reyes-Belmonte, M., Knutsson, M., and Lennblad, J.**
“Acoustic One-Dimensional Compressor Model for Integration in a Gas-Dynamic Code”
in: *SAE Technical Paper*. SAE International Apr. 2012. DOI: 10.4271/2012-01-0834 (cit. on p. 113)
- [129] **Galindo, J., Tiseira, A., Navarro, R., Tarí, D., Tartoussi, H., and Guilain, S.**
“Compressor Efficiency Extrapolation for 0D-1D Engine Simulations”
in: *SAE Technical Paper*. SAE International Apr. 2016. DOI: 10.4271/2016-01-0554 (cit. on p. 113)
- [130] **Ahmed, F. S., Laghrouche, S., Mehmood, A., and Bagdouri, M. E.**
“Estimation of exhaust gas aerodynamic force on the variable geometry turbocharger actuator: 1D flow model approach”
in: *Energy Conversion and Management* 84 (2014), pp. 436–447. ISSN: 0196-8904. DOI: 10.1016/j.enconman.2014.03.080 (cit. on p. 115)
- [131] **Cuevas, C., Makaïre, D., and Ngendakumana, P.**
“Thermo-hydraulic characterization of an automotive intercooler for a low pressure EGR application”
in: *Applied Thermal Engineering* 31.14 - 15 (2011), pp. 2474–2484. DOI: 10.1016/j.applthermaleng.2011.04.013 (cit. on p. 169)
- [132] **Canakci, M.**
“Combustion characteristics of a DI-HCCI gasoline engine running at different boost pressures”
in: *Fuel* 96 (2012), pp. 546–555. DOI: 10.1016/j.fuel.2012.01.042 (cit. on p. 169)

- [133] **Luján, J. M., Bermúdez, V., Piqueras, P., and García-Afonso, Óscar**
“Experimental assessment of pre-turbo aftertreatment configurations in a single stage turbocharged diesel engine. Part 1: Steady-state operation”
in: *Energy* 80.0 (2015), pp. 599 –613. ISSN: 0360-5442. DOI: 10.1016/j.energy.2014.05.048 (cit. on p. 169)
- [134] **Macián, V., Serrano, J. R., Dolz, V., and Sánchez, J.**
“Methodology to design a bottoming Rankine cycle, as a waste energy recovering system in vehicles. Study in a HDD engine”
in: *Applied Energy* 104 (2013), pp. 758 –771. ISSN: 0306-2619. DOI: 10.1016/j.apenergy.2012.11.075 (cit. on p. 169)
- [135] **Luján, J. M., Climent, H., Olmeda, P., and Jiménez, V. D.**
“Heat transfer modeling in exhaust systems of high-performance two-stroke engines”
in: *Applied Thermal Engineering* 69.1–2 (2014), pp. 96 –104. ISSN: 1359-4311. DOI: 10.1016/j.applthermaleng.2014.04.045 (cit. on p. 169)
- [136] **Galindo, J., Serrano, J. R., Climent, H., and Varnier, O.**
“Impact of two-stage turbocharging architectures on pumping losses of automotive engines based on an analytical model”
in: *Energy Conversion and Management* 51.10 (2010), pp. 1958 –1969. ISSN: 0196-8904. DOI: 10.1016/j.enconman.2010.02.028 (cit. on p. 170)
- [137] **Besagni, G., Mereu, R., Chiesa, P., and Inzoli, F.**
“An Integrated Lumped Parameter-CFD approach for off-design ejector performance evaluation”
in: *Energy Conversion and Management* 105 (2015), pp. 697 –715. ISSN: 0196-8904. DOI: 10.1016/j.enconman.2015.08.029 (cit. on p. 194)